Preface

This report is created at Aalborg University's graduate study "Electro-Mechanical System Design" (EMSD). The project is devised according to the current regulations governing the education as stated in the study programme. The theme for this semester is *Electro Mechanical System Design.* The title of this project is *Adaptive control with self-tuning for center-driven web winders*.

Figures, tables and equations are numbered continuously throughout each chapter. E.g. Fig. 2.5 refers to the fifth figure in the second chapter. (4.6) refers to the sixth equation in the fourth chapter. The references are stated using the APA-method (Author, year) and further details about each source can be found in the back of the report. The report also contains a series of appendixes and attachments, which will be referred to throughout the report. The report is made to be read independent but the appendixes contain additional calculations and experiments.

Attached to the report is also a CD containing the report, appendixes, attachments, used MATLAB files, Simulink models and experiment data.

Contents

1. Nomenclature

Symbol	Description	Unit
θ	Vector of the parameters in the transfer function	-
ε_F	Filtered prediction error	-
$L()$	Filter operator	-
ε	Prediction error	-
$\hat{\theta}_N$	Estimated parameter	-
Z^N	Corresponding input and output	-
$V_N(,)$	Cost function	-
$\hat{y}(t\|\theta)$	Estimated output	-
φ^T	Regression vector	-
^	Estimated value	-
$\_1$	Parameter related to unwinder	-
$\_2$	Parameter related to winder	-
A	Area	m^2
a_1	Discrete simplified model constant relation to z^1	-
a_2	Discrete simplified model constant relation to z^0	-
APID	Adaptive PID-controller	-
b_1	Discrete simplified model constant relation to z^1	-
b_2	Discrete simplified model constant relation to z^0	-
B_d	Viscous friction of dancer	N·s/m
B_{M2}, B_m	Viscous friction constant of winder motor	Nm·s/rad
C	Damping ration of material	Pa/s
D	Dancer position	m
D(z)	Charataristic equation	-
$D_{1, 2, 3}$	Disturbance to the system	-
d_f	Filtered dancer position	m
$d_{interval}$	Dancer position by interval method	m
d_{ref}	Dancer reference	m
d_s	Simulated dancer position	m
E	Error signal	-
E	Young's modulus	Pa
F_{ini}	Initial force	N
$F_{t,1}$	Tension force in unwinder	N
G	Gear ratio	-
$G_{1..4}$	System	-
G_{sys}	The linear system	-
$H_{1, 2, 3}$	Feedback	-
J_{M2}, J_m	Rotor and coupling inertia of winder motor	$Kg·m^2$
K_0	Adjustable gain	-
K_{cr}	Critical gain	-
K_d	Spring constant in dampersystem	N/m
K_D	Derivative gain relating to PID controllers	-

K_I	Integral gain relating to PID controllers	-
K_P	Proportional gain relating to PID controllers	-
L	Length of un deformed material	m
L_c	Constant length	m
LTI	Linear time-invariant system	-
LTV	Linear time-varying system	-
L_v	Variable length	m
L_w	Length of web between un- and rewinder roll	m
M	Motor	-
M_d	Mass of dancer	Kg
N	Number of timesteps	-
$N_{G,}$ N_g	Gearing ratio	-
$p_{0,1}$	Parameter for PP controller	-
P_{cr}	Critical period	S
PE	Persistent excitation	-
PEA	Parameter Estimation Algorithm	-
PID1	Manual tuned PID-controller	-
PID2	Model based PID-controller	-
PP	Adaptive pole placement-controller	-
Q	Forward shift operator	-
$q_{0,1}$	Parameter for PP controller	-
R	Reference	-
r*	Reference after K_0	-
RLS	Recursive Least Square	-
S	Laplace operator	-
T	Torque	Nm
T_0	The systems sample time	Z
T_d	Derivative time	s
T_i	Integral time	s
T_m	Torque available to accelerate the motor inertia	Nm
TML	Torque minor loop	-
T_R	Rise time	s
T_s	Settling time	s
U	Controller output	-
V_1	Speed of unwinding	m/s
V_d	Speed of dancer	m/s
VLT	Frequency converter	-
W	Winder	-
A	Angular acceleration	rad/s^2
ε_1	Strain in unwind material	-
Λ	Parameter estimation forgetting factor	-
Λ	Pole	-
P	Density of un deformed material	Kg/m^3
ρ_1	Density of unwind material	Kg/m^3
σ_1	Stress in unwind material	Pa
T	torque	Nm
τ_{cou}	Coulomb friction	Nm
τ_{ref}	Torque reference	Nm
ω_{cr}	Critical frequency	rad/s

2. Introduction

Many industries require manufacturing with a continuous long piece of material. An example of this is the manufacturing of our daily newspaper. Here a long string of paper is feed to a rotating printing press. The paper is often unrolled from a large roll of paper and distributed through series of rollers and winders. The distributed paper is known as a web.

To produce the newspaper two processes are needed. One process is converting the web in the printing press and the other is handling the web. It is desirable to maximize the throughput of these combined processes and still maintaining the quality of the newspaper.

A certain tension in the web material is required to avoid slippage on the rollers and to avoid getting a blurry or otherwise unreadable text from printing process.

Other examples of web handling can be found in textile, plastic and steel industries. Common for all is that the tension in the web must be kept within certain threshold values. This raises the question on how to control the web handling process.

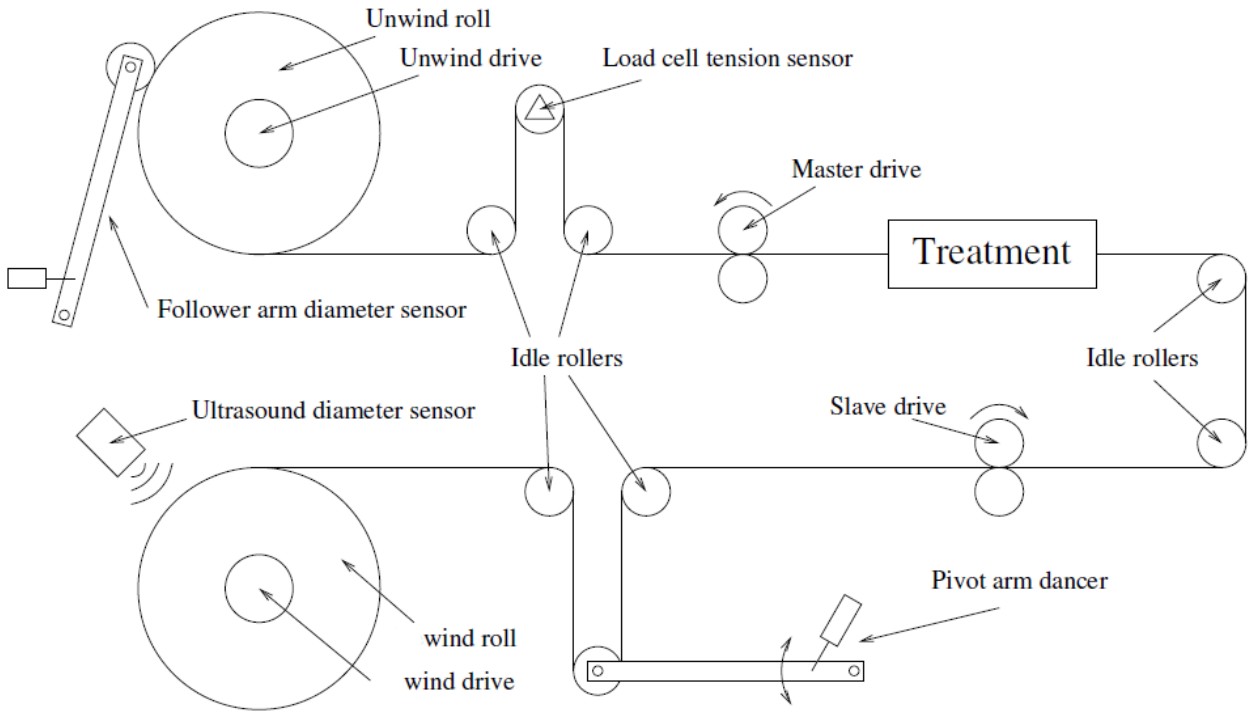

Fig. 2.1 Sketch of a web handling system with sensors and actuators included

A sketch of a web handling system is shown in Fig. 2.1. Here the speed of the combined process is determined by the master drive. To keep a certain tension in the upstream part the unwind drive is controlled with feedback from a load cell. Depending on the required accuracy this controller has to be altered due to changes in the unwind rolls diameter. A follower arm is used to measure the change in diameter. The control of tension downstream from the slave drive uses the same principle as explained for the upstream part. The process is just mirrored and uses different sensors.

The initial problem for this project can be stated as:

What influences the control of the web winder system?

The next step is to present the specific web winder system, then a model of the system is deduced and it is investigated, what parameters are decisive for the design of a given controller.

2.1 Project Objective

This thesis will focus on the tension control of the web material the from the slave drive to the winder.

In this project is no sensor is used to measure the changing roll diameter. A changing roll diameter will change both gearing and inertia felt by the actuator that turns the roll. This means that the transfer function from actuator to web tension changes.

Therefore the objective of this thesis is to develop an adaptive control which should be able to automatically determine the changing parameters of the web handling system and use this information to update the actuator control.

3. Problem Analysis

The purpose of this analysis is to describe and model the test bench, analyze the possible approaches to control the web. This will give the basis of the further control design and insights into the plants behavior.

3.1 Plant Description

The test bench used in this project is a downscaled center driven web winder delivered by Danfoss Drives. A picture of the web winder is shown in Fig. 3.1.

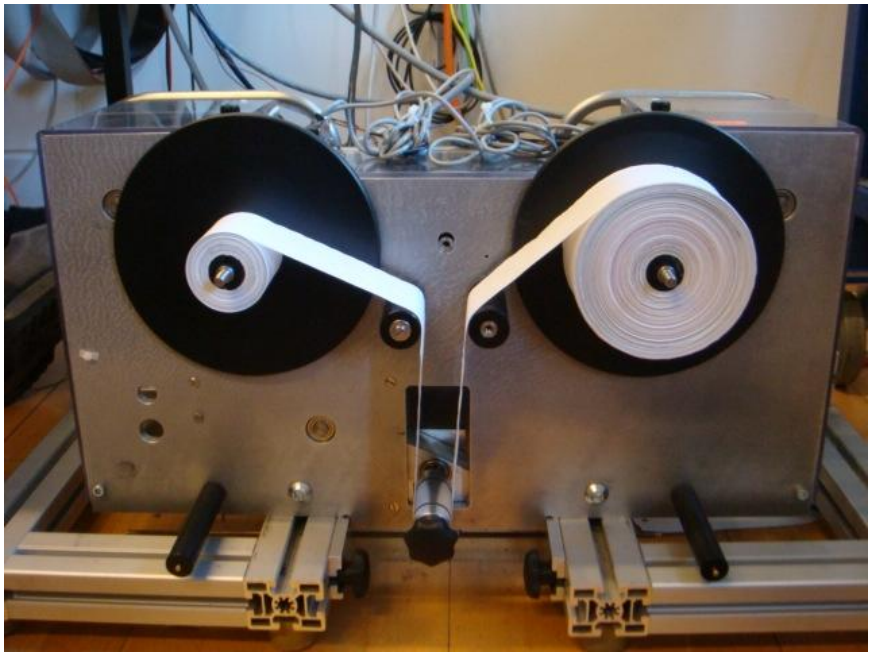

Fig. 3.1 Test bench

A sketch of the web handling system of this model is shown in Fig. 3.2. This system consists of an unwinder, two idle rollers, a dancer and a winder.

In this case the unwinder represents the slave drive on Fig. 2.1.

Two encoders are used, one for measuring the speed of the web and one for measuring the angular velocity of the motors rotor. A potentiometer is used to measure the position of the dancer.

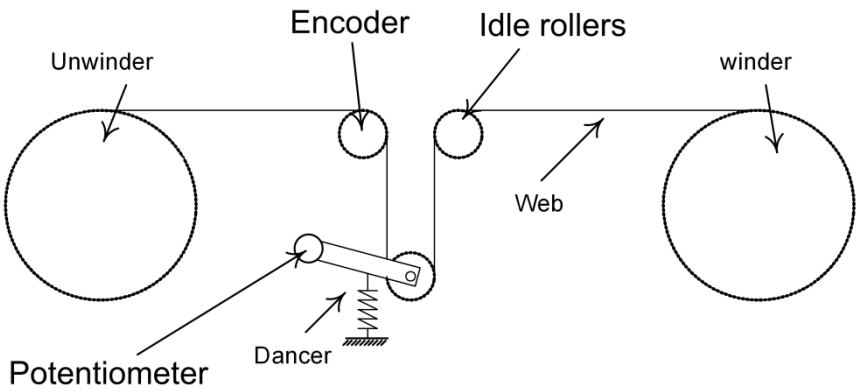

Fig. 3.2 Sketch of the web handling system

A known spring is attached to the dancer arm. This way an estimate of the tension in the web is available.

Each winder is connected to an induction motor through a transmission shown with a sketch in Fig. 3.3.

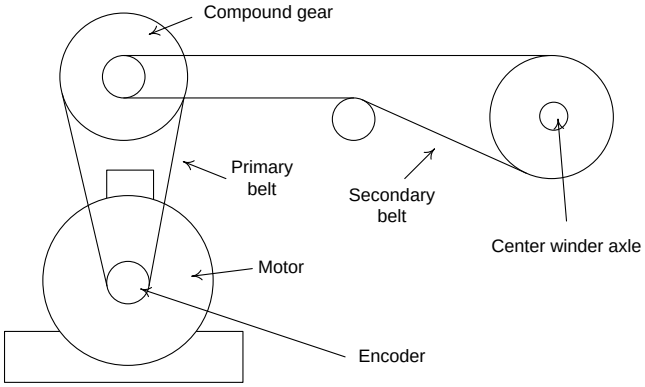

Fig. 3.3 Transmission from motor to winder roll

The transmission from motor to unwinder and motor to winder has a gearing ratio of 9.0:1 and 10.5:1 respectively. Both motors are from ATB and have a rated power output of 560 Watt.

The hardware set-up for the motor control is shown in Fig. 3.2

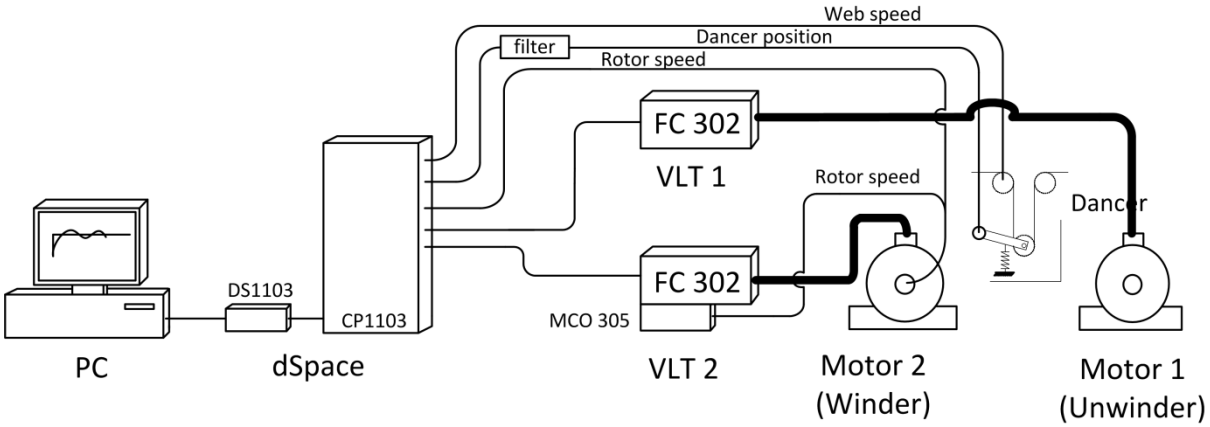

Fig. 3.4 Hardware setup for motor control

The motors are connected to two frequency converters (FC 302) delivered by Danfoss Drives. This type of converters is capable of controlling either speed or torque on the motor shaft with either scalar or field oriented control (FOC). This control can be done either with or without feedback depending on the desired accuracy.

Scalar speed control is used on the motor which drives the unwinder, because high precision is not required on this reel. But high precision is required on the winder. Therefore the winder motor is controlled with feedback from the encoder which measures the rotor position.

The feedback enters a programmable unit (MCO 305) which is attached and connected with FC 302. With MCO 305 it is possible to generate a set-point to the position or speed controller and calculate the reference to FC 302.

However in this project the set point generation and control will be done using a dSpace system. MCO 305 is only used as a link between the encoder and FC 302.

The dSpace system is a development environment, which enables fast implementation of MATLAB and SimuLink models in physical systems. This is achieved by a real-time processor (DS1103) communicating with the host PC and a connecting interface board (CP1103).

The work procedure is to develop a suitable Simulink model, using dSpace toolboxes. This enables a simple addressing of I/O ports on the connected interface board. When the model is ready for real-time implementation it is compiled to C-code using dSpace conversion libraries. This C-code is then downloaded to the real-time processor using the dSpace software called ControlDesk.

ControlDesk is also used to interface with the Simulink model as it runs on the real-time system. It is possible to create virtual instruments in ControlDesk which can change or display variables used in the model. ControlDesk is also used to record variables over time and hereby acting as a data acquisition system.

An in-depth explanation of the physical setup is described in appendix B, which includes port assignments, electrical diagrams and considerations about the setup.

3.2 Nonlinear Web Winder Model

The purpose of this section is to develop a model of the web winder that can be used for designing and testing controllers.

In Fig. 3.5 a sketch of the web winder is shown with the symbols used in the development of the model. The suffix 1 denotes the unwinding web material and the suffix 2 denotes the stretched and winding web material. The web material between the winders has an initial length (L) and a cross sectional area (A) which also constitutes a control volume.

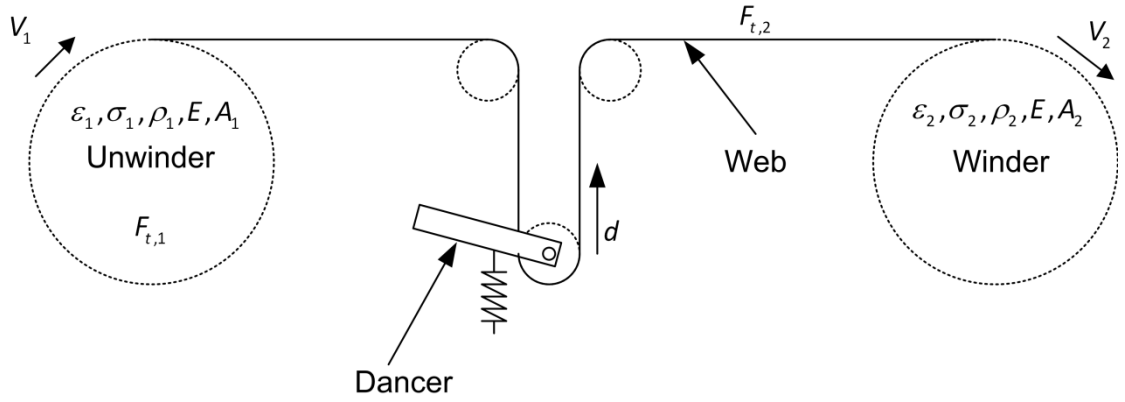

Fig. 3.5 Sketch of web winder. Suffix 1 and 2 denotes the unwinding web material and the winding stretched web material respectively.

When omitting the unwinder drive train the web winder consist of three subsystems.

- The web material
- The dancer
- The winder drive train

These systems are modeled separately before they are combined to form the complete combined model.

3.2.1 Assumptions

The following assumptions are used during the development of the model:

1. The paper velocity from the unwinder is constant
2. The cross section area of the web is uniform

   The web material on the test bench is a uniform roll of paper.
3. The strain is the length change divided by the unchanged length of the material and the strain << 1

   The definition of strain is normal and only small deformation is expected.
4. The deformation of the web material is elastic

   This assumption is used because plastic deformation is unwanted during the winding process and quite difficult to model.
5. The density of the web is unchanged
6. The speed of the dancer is negligible compared to the speed of the web $V_d << V_1$
7. The web material is very stiff, hence $V_1 \approx V_2$

   If assumption 6 is correct and the material is stiff the unwinder paper speed and the winder paper speed is approximately the same.

8. The dancer movement is negligible compared to the length of the web between the unwinder and the winder.

9. The dancer is only moving vertical

   The dancer is actually moving in a small arc but it is expected that the Dancer movement is small compared to the arc length.

10. The velocity of the dancer is the time derived of the displacement of the dancer

11. The tension in the previous section is constant.

12. The change of roll radius does not change the web length between the winders

    As one radius is increasing the other is decreasing therefore the changing radius is estimated to only having little influence on the web length and is therefore neglected.

13. The time delay caused by the time constants of the electrical circuits of the VLT can be neglected.

3.2.2 Web Material

The purpose in modeling the web material is to find an expression for the tension force development in the web material located between the winders. This requires a physical interpretation on how stress arises in the web material and how the stress is related to the winders tangential velocities V_1 and V_2.

In the following the Voigt model is used to explain arising stress and with the before mentioned assumptions, control volume analysis and continuum mechanics it is shown how the stresses are related to V_1 and V_2

The Voigt model consists of a viscous damper and an elastic spring in parallel as shown in Fig. 3.6

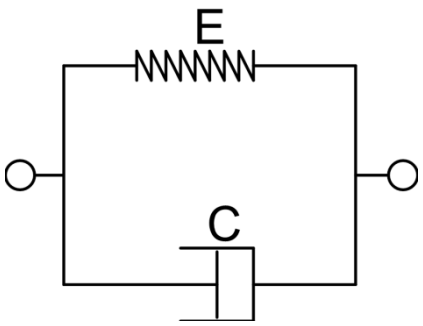

Fig. 3.6 Voigt model

With this model the stress in the web material is expressed as shown in (3.1)

$$\sigma = E\varepsilon + C\frac{d\varepsilon}{dt} = \frac{F_t}{A} \qquad (3.1)$$

The Laplace transformation of (3.1) the result can be seen in (3.2)

$$F_t = AE\varepsilon + AC\varepsilon s$$
$$F_t = \varepsilon \cdot (AE + ACs)$$
$$\varepsilon = \frac{F_t}{(AE + ACs)}$$

(3.2)

In order to relate the strain to the winder tangential velocities the following definitions are needed.

The definition of mass continuity states that stretching the material does not change mass of the stretched material. This is expressed as (3.3).

$$\rho \cdot A \cdot L = \rho_s \cdot A_s \cdot L_s$$

(3.3)

Where the suffix s denotes the stretched web material. With assumption 5 (3.4) is rewritten as shown in (3.4).

$$A \cdot L = A_s \cdot L_s$$

(3.4)

The strain is defined by (3.5).

$$\varepsilon = \frac{L_s - L}{L} = \frac{L_s}{L} - 1$$

(3.5)

By inserting (3.4) in (3.5) we get (3.6).

$$A_s = \frac{A}{1 + \varepsilon}$$

(3.6)

With assumption 3 (3.6) is rewritten in (3.7).

$$A_s = A \cdot (1 - \varepsilon)$$

(3.7)

The definition of mass conservation states that the change in mass of the control volume equals the difference between the mass entering and exiting the control volume. This is expressed in (3.8).

$$\frac{d}{dt}(\rho \cdot A \cdot L) = \rho_1 \cdot A_1 \cdot V_1 - \rho_2 \cdot A_2 \cdot V_2$$

(3.8)

With assumption 5 (3.8) is rewritten as seen in (3.9)

$$\frac{d}{dt}(A \cdot L) = A_1 \cdot V_1 - A_2 \cdot V_2$$

(3.9)

By inserting (3.7) in (3.9) we get (3.10).

$$\frac{d}{dt}\left(AL \cdot (1-\varepsilon_2)\right) = A \cdot (1-\varepsilon_1) \cdot V_1 - A \cdot (1-\varepsilon_2) \cdot V_2$$

(3.10)

The length L of the web is influenced by the movement of the dancer and the chancing radius of the winder rolls. With assumption 12 (3.10) is rewriting and is shown in (3.11).

$$\begin{aligned}
&\frac{d}{dt}\left((L_c - 2d) \cdot (1-\varepsilon_2)\right) = V_1 \cdot (1-\varepsilon_1) - V_2 \cdot (1-\varepsilon_2) \\
&-2V_d + 2V_d\varepsilon_2 + 2d\dot{\varepsilon}_2 - L_c\dot{\varepsilon}_2 = V_1 - V_1\varepsilon_1 - V_2 + V_2\varepsilon_2 \\
&(L_c - 2d) \cdot \dot{\varepsilon}_2 = V_2 - V_1 - 2V_d + V_1\varepsilon_1 - (V_2 - 2V_d) \cdot \varepsilon_2
\end{aligned}$$

(3.11)

By Laplace transformation of (3.11) and inserting (3.2) in (3.11) we get (3.12).

$$\begin{aligned}
&(L_c - 2L_d) \cdot \frac{F_{t,2}}{(A_2E + A_2Cs)}s = V_2 - V_1 - 2V_d + V_1\frac{F_{t,1}}{(A_1E + A_1Cs)} - (V_1 - 2V_d) \cdot \frac{F_{t,2}}{(A_2E + A_2Cs)} \\
&F_{t,2} \cdot \left(s + \frac{(V_2 - 2V_d)}{(L_c - 2L_d)}\right) = \frac{(A_2E + A_2Cs)}{(L_c - 2L_d)} \cdot (-V_1 + V_2 - 2V_d) + \frac{V_1 \cdot F_{t,1}}{(L_c - 2L_d)} \cdot \frac{A_2}{A_1}
\end{aligned}$$

(3.12)

With assumption 6,7 and 8 ($L_N \approx L_c - 2L_d$ and $V_1 \approx V_2 - 2V_d$) (3.12) can rewritten as shown in (3.13).

$$F_{t,2} \cdot \left(s + \frac{V_1}{L_N}\right) = \frac{A_2E + A_2Cs}{L_N} \cdot (-V_1 + V_2 - 2V_d) + \frac{V_1 \cdot F_{t,1}}{L_N}\frac{A_2}{A_1}$$

(3.13)

The input is considered to be $(-V_1+V_2-2V_d)$ and the output is $F_{t,2}$. The term at the outmost right in (3.13) is a constant due to assumption 11. This static contribution is omitted in further modeling of the web material and added later as an initial force. The transfer function for the tension force development in the web material is now expression for can be seen in (3.14).

$$\frac{F_{t,2}}{-V_1 + V_2 - 2V_d} = \frac{\frac{CA}{L_N}s + \frac{EA}{L_N}}{s + \frac{V_1}{L_n}}$$

(3.14)

The block diagram of the transfer function (3.14) is shown in Fig. 3.7.

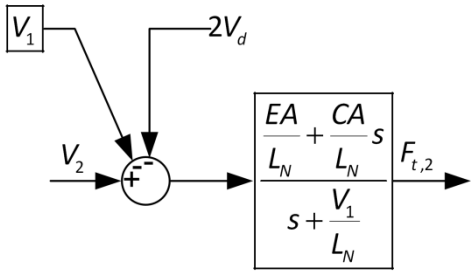

Fig. 3.7 Block diagram of tension force dynamics

Thus a model of the tension force related to the tangential velocities is accomplished.

3.2.3 Dancer

The mechanical model of the dancer is shown in Fig. 3.8.

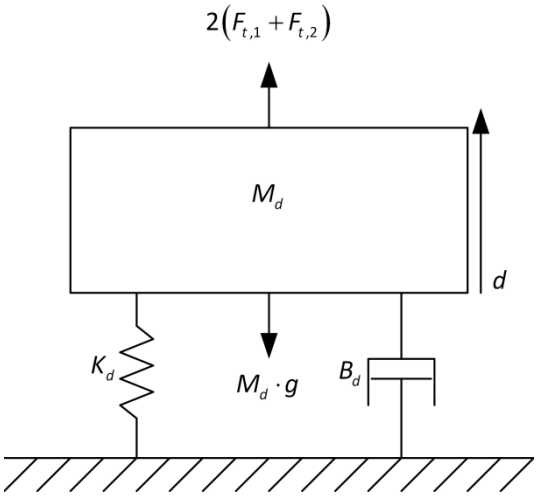

Fig. 3.8 Dancer as a mass-damper-spring system

The Dancer works as a pulley block. Therefore the constant $F_{t,1}$ and the varying $F_{t,2}$ are multiplied with 2.

The Dancer movement is modeled with Newton's second law of motion as shown in (3.15).

$$\sum F = M \cdot a$$
$$2(F_{t,2}+F_{t,1}) - M_d \cdot g = M_d \cdot a_d + B_d \cdot V_d + K_d \cdot d \quad (3.15)$$

The Laplace transformation of (3.15) is expressed as seen in (3.16).

$$2(F_{t,2}+F_{t,1}) - M_d g = (M_d s^2 + B_d s + K_d) d \quad (3.16)$$

The block diagram of (3.16) is shown in Fig. 3.9.

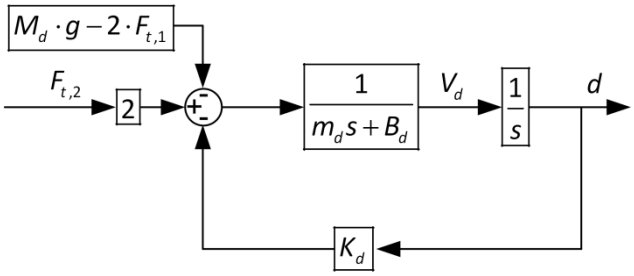

Fig. 3.9 Block diagram of dancer dynamics

Thus a model of Dancer position related to the tension force is accomplished.

3.2.4 Winder Drive Train

The drive train consists of the motor and a gearing which transmit the angular rotation of the motor rotor to web velocity.

With assumption 13 the motor can be modeled as only consisting of the mechanical part. This is done with Newton's second law of motion as seen in (3.17).

$$\Sigma \tau = \alpha_m J_m$$
$$\tau_m - \tau_{cou} - B_m \omega_m = \alpha_m J_m$$

(3.17)

By Laplace transformation of (3.17) we get (3.18).

$$\tau_m - \tau_{cou} = \left(J_m s + B_m\right) \cdot \omega_m$$
$$\frac{\omega_m}{\tau_m - \tau_{cou}} = \frac{1}{J_m s + B_m}$$

(3.18)

The inertia consists of the rotor inertia, the transmission inertia and the winded paper roll inertia. A calculation of the inertia is found in attachment A.

The gearing is modeled as (3.19).

$$\frac{V_2}{\omega_m} = \frac{R}{N_g}$$

(3.19)

The block diagram of the motor and gearing is shown in Fig. 3.10

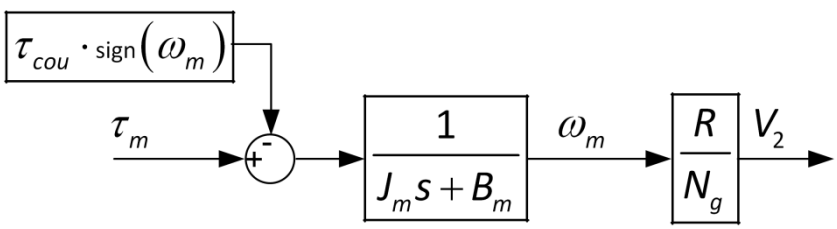

Fig. 3.10 Block diagram of drive train

Thus a model of Dancer position related to the tension force is accomplished.

3.2.5 Complete Web Winder model

By combining the block diagrams from Fig. 3.10, Fig. 3.9 and Fig. 3.7 we get the complete model of the web winder.

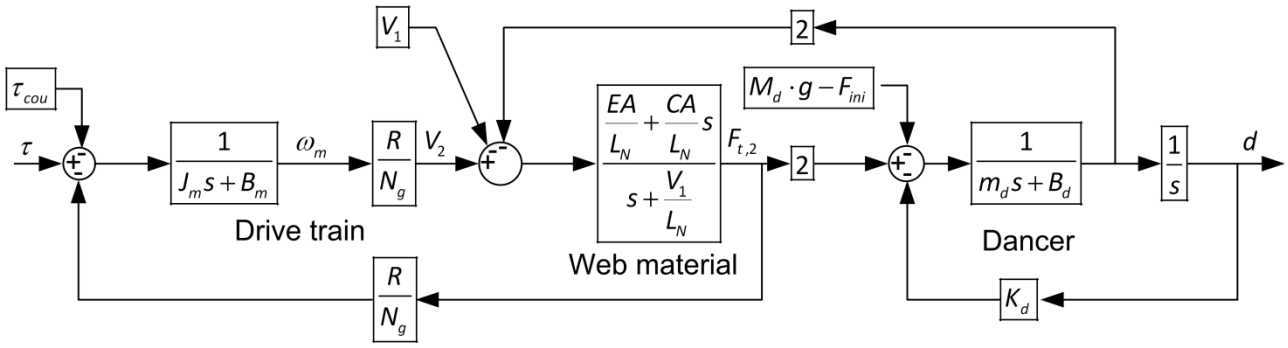

Fig. 3.11 The complete system of the web winding process

When combining the model the torque input is subtracted by the torque used for creating the tension force $F_{t,2}$.Hereby a complete model of the system consisting of the drive train, the web material and a dancer system.

3.3 Validation of Nonlinear Model

The reason for validating the web winder model is partly to find system parameters which are used as a starting point for further control design, partly to find out if the structure of the model is correct, and partly to debug the test bench setup.

3.3.1 Model Parameters

In Table 3.1 the model parameters are summarized.

Symbol	Value	Unit	Source
J_m	3.1 e-3	Kg·m^2	Calculated
B_m	0.55 e-3	Nm·s/rad	Estimated
τ_{cou}	85 e-3	Nm	Estimated
E	4 e9	Pa	Estimated
A	4.35 e-6	m^2	Estimated
L_N	0.61	m	Measured
R	57.3 e-3	m	Measured
N	10.5	-	Measured
K_d	1131	N/m	Measured
m_d	0.69	Kg	Measured
B_d	500	Nm·s/m	Estimated
F_{ini}	12	N	Estimated

Table 3.1 Model parameters

The inertia (J_m) is calculated in attachment A.

L_N is calculated in appendix J.

The coulomb and viscous friction ($\tau_{cou\,u}$, B_m) are estimated from spin down test as shown later.

The Young modulus of the paper is normally between 2 and 6 GPa (University of Cambridge, Department of Engineering). An estimate of 4 GPa therefore seems reasonable.

The cross sectional area is found by multiplying the known width of the paper by a measured average of the thickness.

The viscous friction of the Dancer and the initial load force is estimated during simulation of the web winder model.

3.3.1.1 Spin down test

The spin down test was done by accelerating the winder motor to a high speed (1400 RPM) and then switching off the VLT. The VLT is switched off by opening the connection between port 13 and 37 which acts as emergency switch off. This opens all the switches in the VLTs H-bridge. The motor will hereafter act as if all phase wires were cut simultaneously.

The experiment was repeated 3 times from 1400 RPM to standstill. By comparing with the theoretical model of the system an estimate of the two parameters should be possible. The model of the rotor is stated in equation (3.20)

$$J_m\alpha_m + B_m\omega = \tau - \tau_{cou} \qquad (3.20)$$

The model is implemented in Simulink as shown in Fig. 3.12.

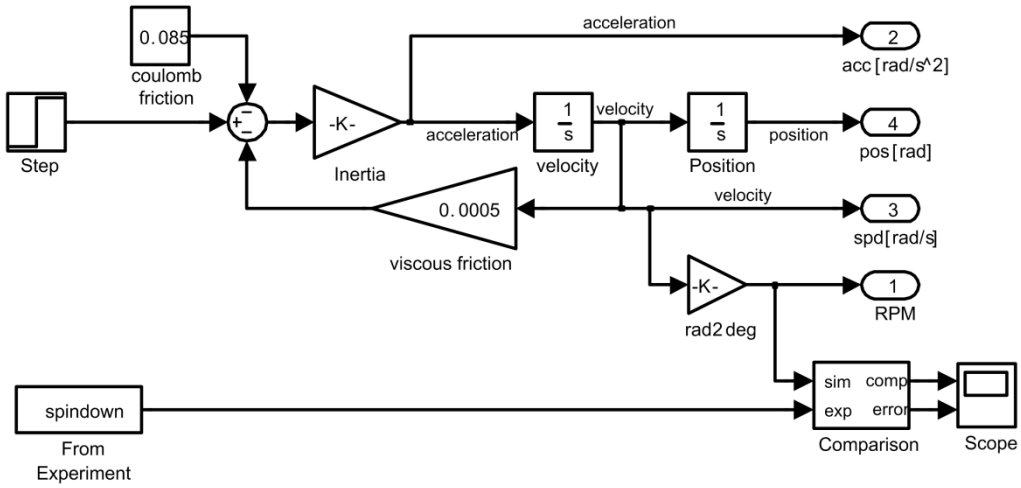

Fig. 3.12 SimuLink model of the rotor dynamics

By fitting the two parameters (B and F) manually through trial-and-error the result in Fig. 3.13 is obtained. The figure also contains an error graph showing the difference between the simulated and the measured values.

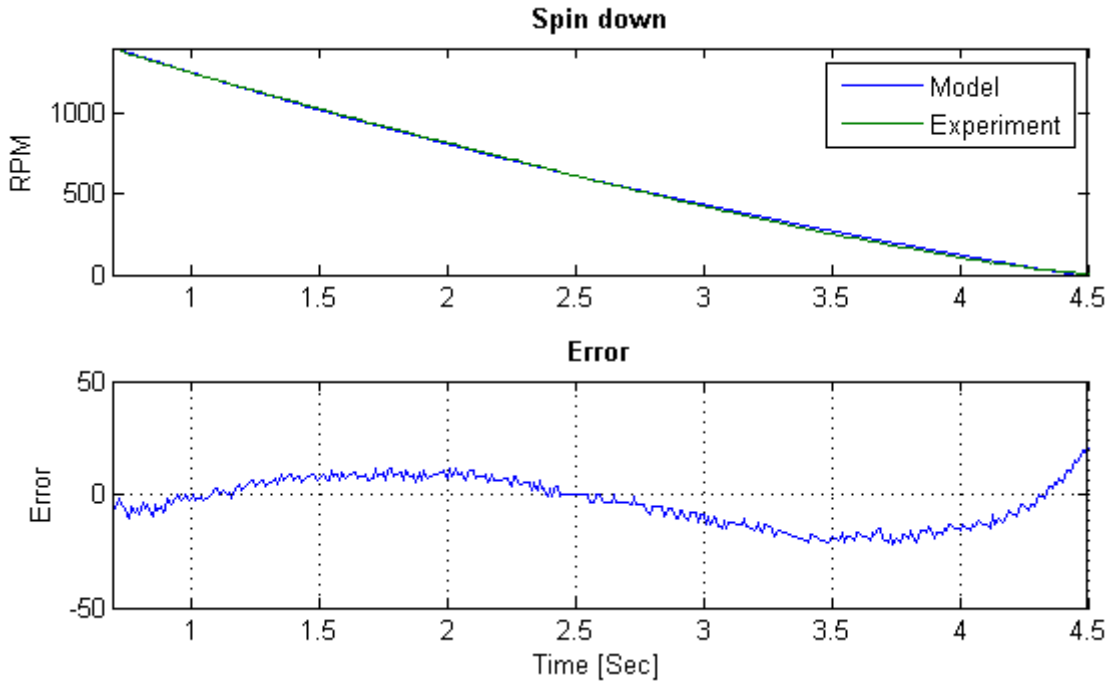

Fig. 3.13 Comparison between measured and simulated spin down experiments

Similar waveforms, and errors in the same range, were achieved with the two other experiments as well. The relative small deviation from the measured waveform is accepted as within the tolerable range.

3.3.2 Simulation and Test Bench Comparison

The purpose of this section is to investigate how well the model of the web winder corresponds with the test bench presented in section 3.1. The complete model of the test bench is represented in Fig. 3.14 Overview of the complete modelFig. 3.14.

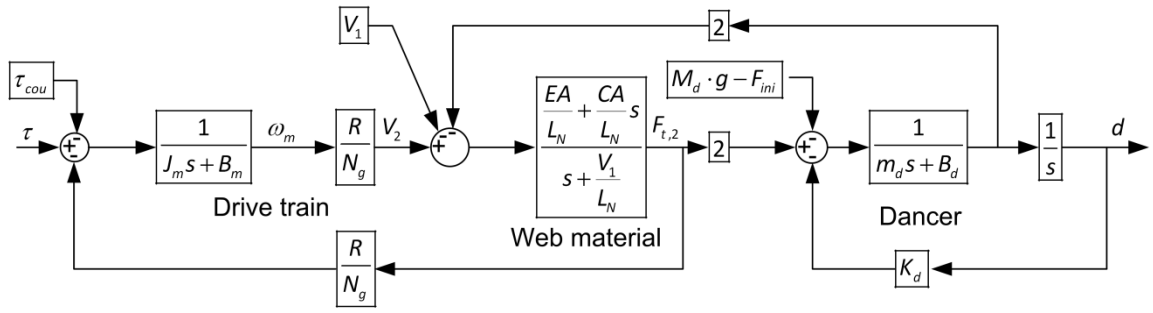

Fig. 3.14 Overview of the complete model

It is assumed that the damping is much smaller than the Young's modulus of elasticity E. Therefore the damping C is equaled 0 (Liu, 1998).

The preferable approach to validate the model is to isolate the subordinate transfer functions like the drive train, the web material block and the dancer block and compare each of them with the setup.

But because of difficulties measuring the tension force the web material and dancer are tried validating together. This is done by using measured shaft velocity from the setup as input to the model and then comparing the dancer position.

The comparison is shown in Fig. 3.13.

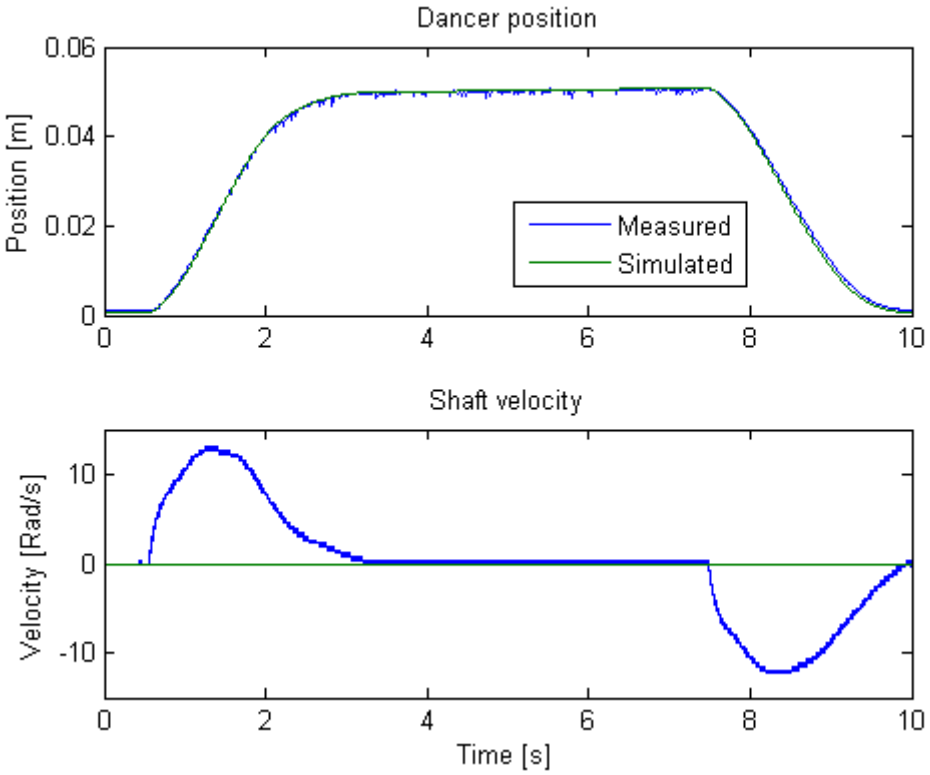

Fig. 3.15 Comparison of dancer position

Fig. 3.15 shows a well correspondence between the setup and the modeled web material and dancer.

The modeled drive train has been validated in the spin test. Here some slight deviation between the model and the test bench is shown. This possibly affects the overall system behavior as shown in Fig. 3.16. Here the measured torque step is applied to the complete model and the shaft velocity and dancer position are compared.

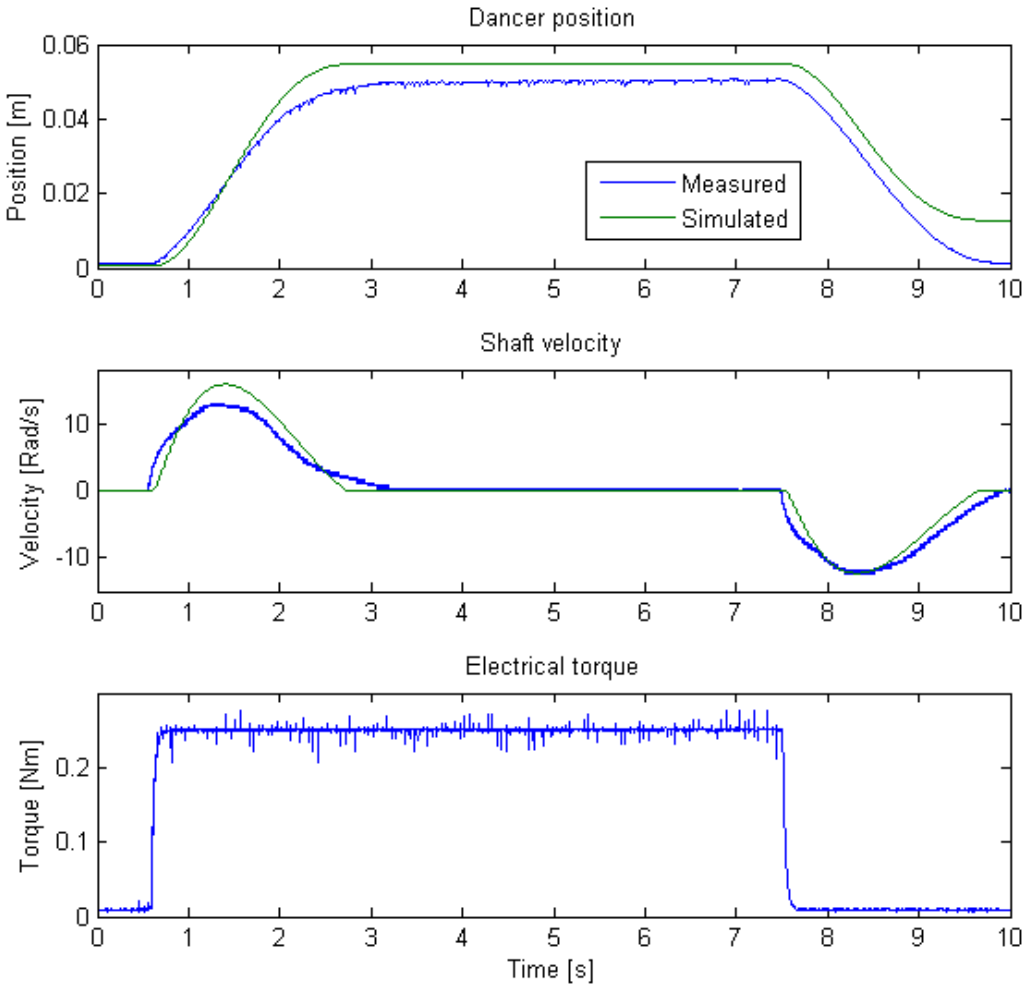

Fig. 3.16 Comparison of shaft velocity and dancer position

In Fig. 3.16Fig. 3.16 it is seen that the simulation approximately corresponds with the measured data.

There exits though a few differences. Firstly, from the data of the dancer position it seems that the simulation has less damping than the setup. The simulated dancer position rises faster and higher than the setup. Secondly, it seems that the friction in the simulation is too large since the dancer does not return to its original position when the torque is removed. A better fit could be achieved if the friction were corrected but this would not correspond to the spin down tests.

In appendix G is it investigated how well the simulated and measured data could fit if the viscous and coulomb frictions are changed. In this appendix the altered spindown test are also shown.

Thirdly, from the shaft velocity it seems that the setup possesses some unmodeled dynamics. The reason for this could be that the setup is moved from standstill were a difference between sticktion and coulomb friction exist. When the web winder is operating this will not be an issue and is therefore at first neglected.

3.4 Linear Web Winder Model

The purpose of this section is to deduce a linear model from the web winder model, to use for initial control design.

A parameter variation analysis is furthermore done to determining the most significant model parameters and to estimate how the web winder dynamics is expected to change as the paper is winding.

3.4.1 Transfer Function of the Web Winder Model

The complete web winder model from Fig. 3.11 in section 3.2.5 is represented in Fig. 3.17.

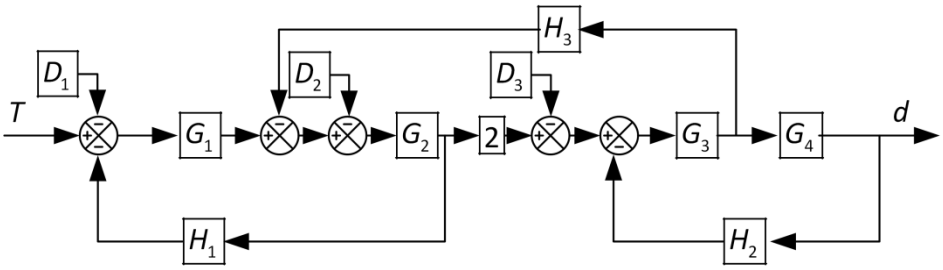

Fig. 3.17 Web winder model rewritten

Where each transfer function is substituted as in (3.21).

$$G_1 = \frac{R}{N_g\left(J_m s + B_m\right)} \quad G_2 = \frac{\frac{EA}{L_N}}{s + \frac{V_1}{L_N}} \quad G_3 = \frac{1}{m_d s + B_d} \quad G_4 = \frac{1}{s}$$

$$H_1 = \frac{R}{N_g} \qquad H_2 = K_d \qquad H_3 = 2$$

$$D_1 = \tau_{cou} \qquad D_2 = V_1 \qquad D_3 = m_d g - F_{ini}$$

(3.21)

The disturbances D_1, D_2 and D_3 are neglected in the linear model. This is assumed right because the disturbances only contribute with an offset. The disturbances are also placed within a feedback loop which also minimizes theirs effect on the overall system behavior.

The linear model is expressed with the block diagram shown in Fig. 3.18.

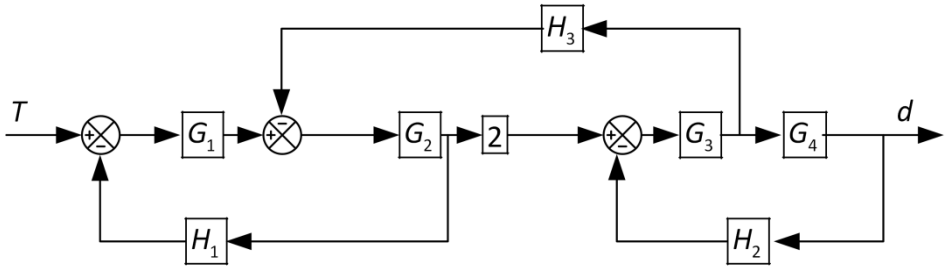

Fig. 3.18 Linear web winder model

In appendix F the loops are closed and (3.21) is inserted. This results in the linear transfer function of the web winder shown in (3.22).

$$G_{Total} = \frac{\frac{2REA}{L_N}}{\left(N_g J_m s^2 + \left(N_g B_m + N_g J_m \frac{V_1}{L_N}\right)\cdot s + \left(N_g B_m \frac{V_1}{L_N} + \frac{R^2 EA}{L_N N_g}\right)\right)\cdot\left(m_d s^2 + B_d s + K_d\right) + \frac{2REA}{L_N}\cdot\left(\frac{2N_g}{R} J_m s^2 + \frac{2N_g}{R} B_m s\right)} \quad (3.22)$$

From Fig. 3.18 and (3.22) it is seen that the linear web winder model consists of two second order system with a second order system in feedback.

The bodeplot of the linear model is shown in Fig. 3.19. This plot is made by using the parameters from Table 3.2.

Symbol	Value	Unit
J_m	$3.1\ 10^{-3}$	Kg·m
B_m	$0.55\ 10^{-3}$	Nm·s/rad
E	$4\ 10^{9}$	Pa
A	$4.35\ 10^{-6}$	m^2
L_N	0.61	m
R	$57.3\ 10^{-3}$	m
N_g	10.5	-
K_d	1131	N/m
m_d	0.69	Kg
B_d	500	Nm·s/m

Table 3.2 Values used for the linear model

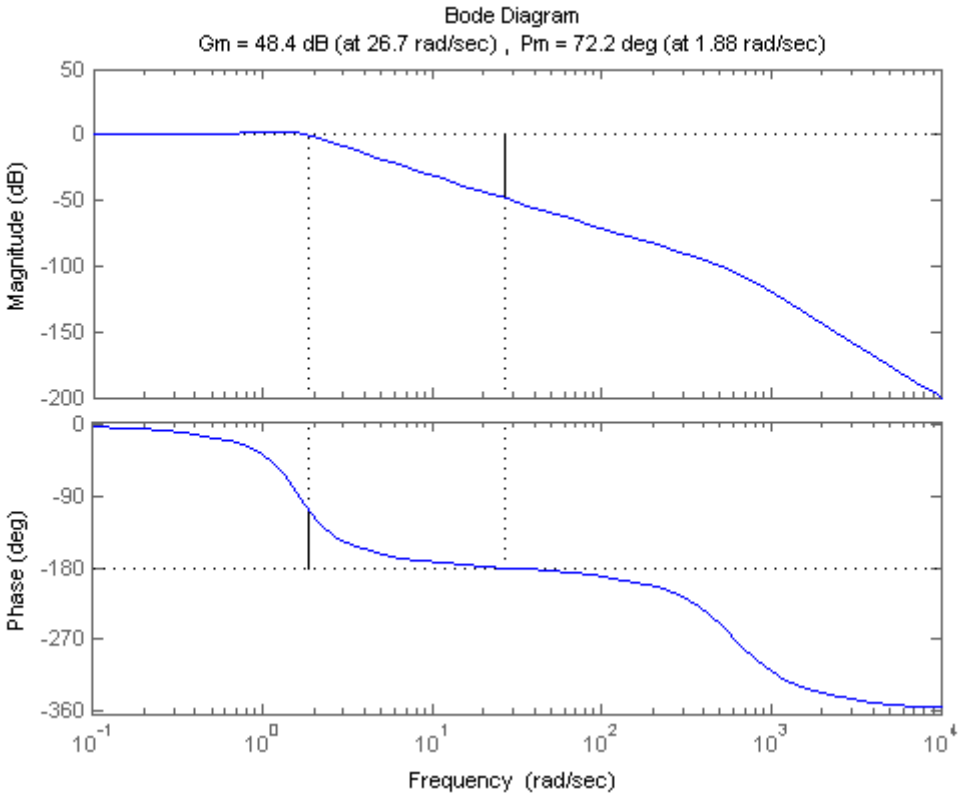

Fig. 3.19 Bode plot of linear system

The bode plot is made by multiplying (3.22) with the inverse of the steady state gain.

The steady state gain of the linear web winder model is found as the limit for s→0. The steady state gain is found in (3.23).

$$G_{\substack{Total \\ s\to 0}} = \frac{\frac{2REA}{L_N}}{\left(N_g B_m \frac{V_1}{L_N} + \frac{R^2 EA}{L_N N_g}\right)\cdot K_d} = \frac{2REA}{N_g B_m V_1 K_d + \frac{R^2 EA}{N_g}\cdot K_d}$$

(3.23)

When the values found in the nonlinear model is implement in (3.23) it can be seen that the second term in the numerator is much larger the first term there for the steady state gain can be simplified to (3.24).

$$G_{\substack{Total \\ s\to 0}} \approx \frac{2}{\frac{R}{N_g}\cdot K_d}$$

(3.24)

The nonlinear mode is reduced to a linear model and a steady state gain is found.

3.5 Validation of Linear Model

The linear web winder model is validated by a comparison with the nonlinear web winder model. The comparison is done in an operation point were the nonlinear model has settled to steady state after receiving a step input.

The parameter values used in the linear model are the same as used in the nonlinear model. The disturbance values used in the nonlinear model are shown in Table 3.3

Disturbance	Value
F_{cou}	85 10^{-3} Nm
$m_d g+F_{ini}$	18.8 N
V_1	0.2 m

Table 3.3 Disturbance values

At the operation point the linear and nonlinear model receives the same step. The step size is of 0.01 Nm.

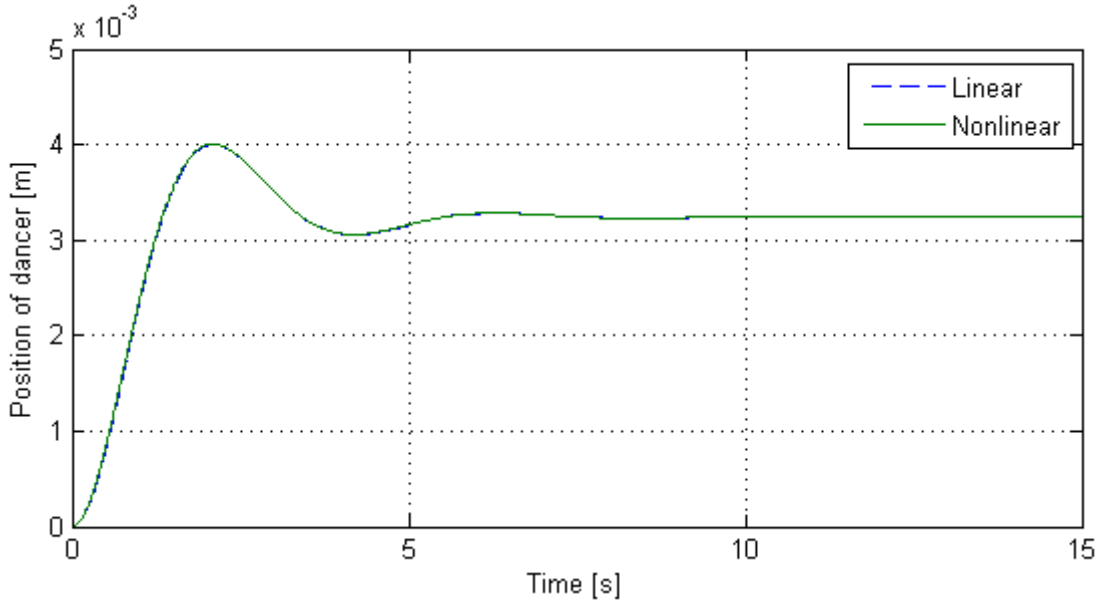

Fig. 3.20 Nonlinear and the linear model with small step

From the validation it is concluded that the linear model is a good approximation. There may be some nonlinear effects at startup where the linear model is not validated.

3.5.1 Parameter Variation Analysis

In this analysis it is investigated how variation in each parameter influence the natural frequency and damping of the linear model.

The parameters of interest are summarized in Table 3.4.

Description	Symbol
Radius	R
Inertia	J_m
Motor iscous friction	B_m
Young's modulus	E
Dancer spring constant	K_d
Dancer mass	m_d
Dancer viscous friction	B_d

Table 3.4 Parameter of interest

All parameters except the radius are varied $^{+}/_{-}$ 10 % from the value found in appendix E. The radius is varied from 13mm to 75mm which is the minimum and maximum value of the reel on the test bench.

3.5.1.1 Influence of Radius

In Fig. 3.21 it is seen that an increase in radius has a more significant impact on the linear model at the lower frequencies than at the higher frequencies. Thus, the change of radius influences the behavior of the dominant second order system.

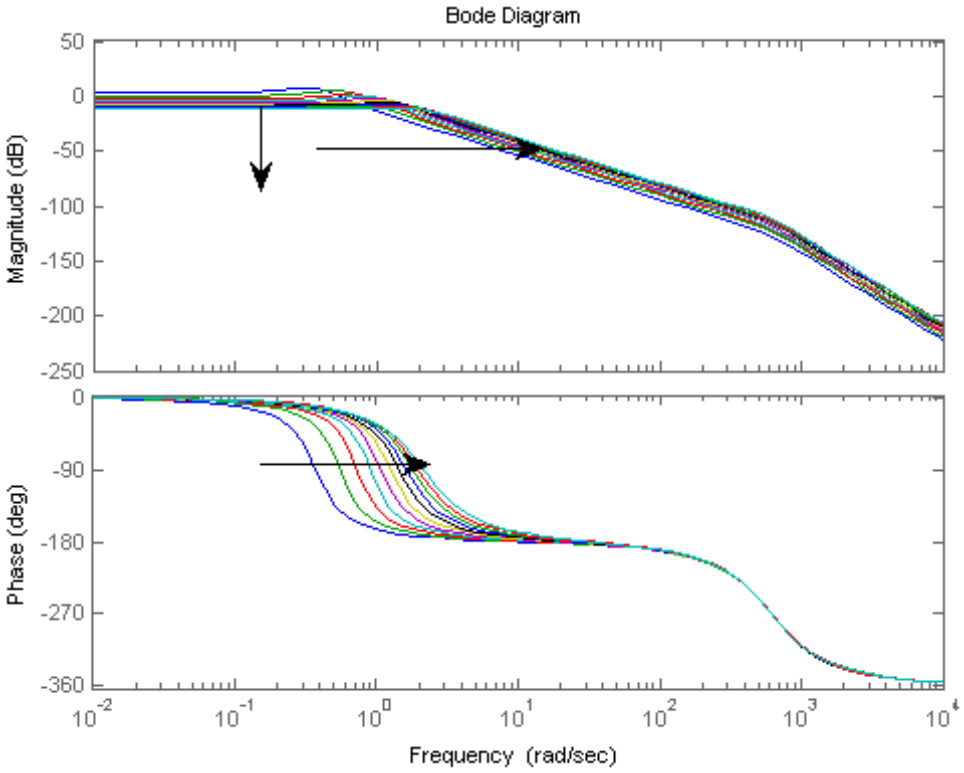

Fig. 3.21 Bode diagram while increasing the radius

In Fig. 3.22. the movement of one of the dominating complex poles is shown. The axis at the top and right represents the damping and natural frequency respectively.

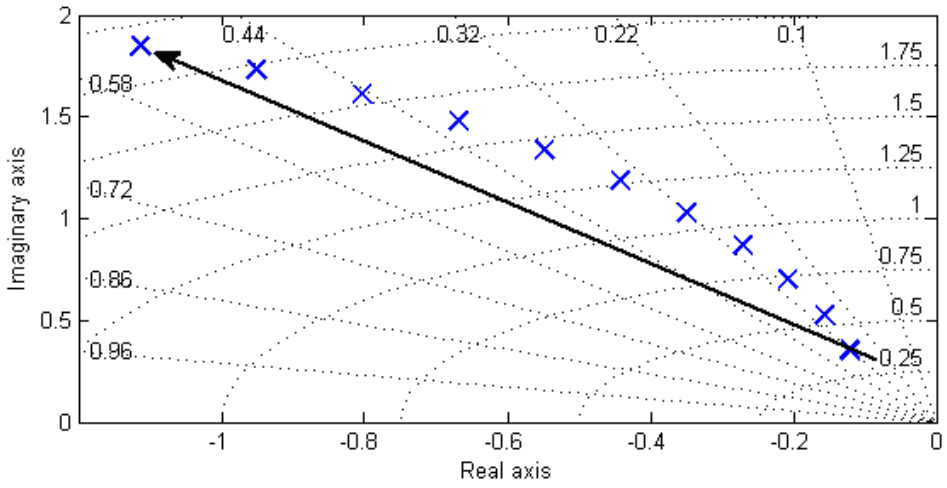

Fig. 3.22 Pole movement as radius increases

In Fig. 3.22 it is seen that as the radius increases both the natural frequency and damping of the dominant second order system.

3.5.1.2 Influence of Inertia

In attachment A the inertia is calculated to change only about 1.5 % though. But in the following the inertia is changed $^{+}/_{-}$ 10 %. Uncertainties when modeling the inertia is in this way accounted for.

In Fig. 3.23 the inertia is changed from 90 % to 110 %. It is seen in Fig. 3.23 that the change in inertia has more impact on the linear model at the lower frequencies than at the higher frequencies.

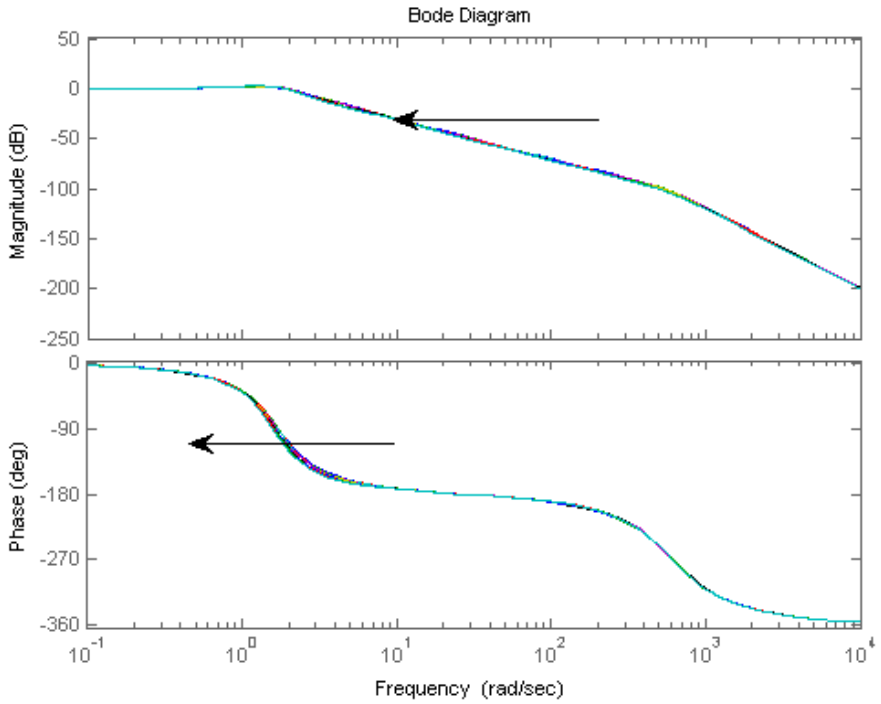

Fig. 3.23 Bode diagram while increasing inertia

In Fig. 3.24 the movement of one of the dominating complex poles is shown.

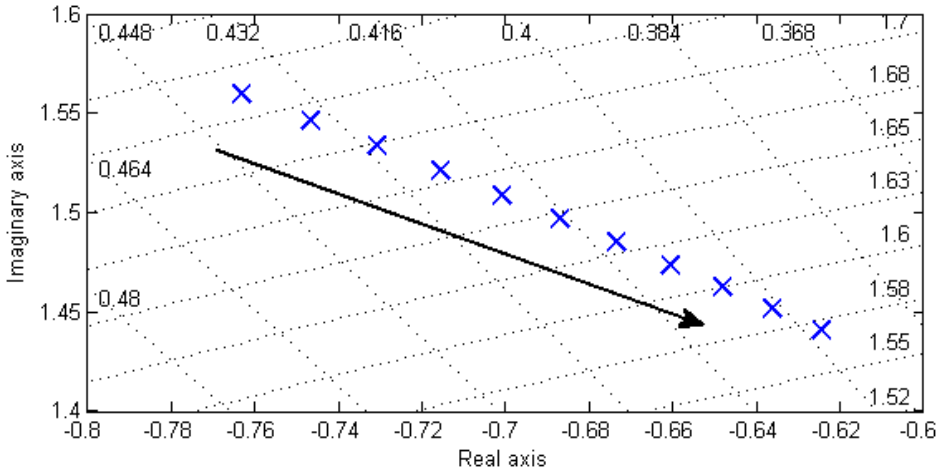

Fig. 3.24 Pole movement as inertia increases

Fig. 3.24 shows that as increasing the inertia decreases both the natural frequency and damping of the dominant poles

Comparing the influence of changing inertia with the influence of changing radius, it is seen that the change in inertia is insignificant.

But the significance of changing inertia would greatly increase if the width and diameter of the paper were several times larger. If this was the case the pole would move towards the imaginary axis and thereby reduce the stability of the system.

3.5.1.3 Influence of Motor Viscous Friction

Same analysis as above is done in appendix E for changing motor viscous friction. Here it is shown that the motor viscous friction has a larger influence at lower frequencies than at higher frequencies. The change in natural frequency and damping of the dominating poles is approximately 1 % when changing $^{+}/_{-}$ 10 %. This is properly because of the constants small value.

3.5.1.4 Influence of Elasticity

Same analysis as above is done in appendix E for changing elasticity. Here it is shown that the elasticity has a larger influence at higher frequencies than at smaller frequencies. The change in natural frequency and damping is less than 1 % when changing $^{+}/_{-}$ 10 %.

3.5.1.5 Influence of Dancer Spring

Same analysis as above is done in appendix E for changing dancer spring constant. Here it is shown that the changing spring constant has a larger influence at lower frequencies than at the higher frequencies. Changing the spring constant from 90 % to 110 % reduces the damping of the dominating poles with 50 % and increasing the natural frequency of the dominating poles with more than 100 %.

3.5.1.6 Influence of Dancer Viscous Friction

Same analysis as above is done in appendix E for changing dancer viscous friction. Here it is shown that the changing dancer viscous friction has equal influence at all frequencies. Changing the dancer viscous friction from 90 % to 110 % increases the damping of the poles with 20 % and decreasing the natural frequency of the poles with 8 %.

3.5.1.7 Influence of Dancer Mass

Same analysis as above is done in appendix E for changing dancer mass. Here it is shown that the changing dancer mass has larger influence at higher frequencies than lower frequencies. Changing the dancer mass from 90 % to 110 % decreases the damping of the faster poles with 10 % and decreasing the natural frequency of the faster poles with 10 %.

3.5.1.8 Summary

The influences of the changing parameters on the slower dominating poles are summarized in Table 3.5.

Increased Parameter	Symbol	Natural frequency	Damping
Radius	R	Increasing	Increasing
Inertia	J_m	Decreasing	Decreasing
Motor viscous friction	B_m	No significant effect	No significant effect
Young's modulus	E	No significant effect	No significant effect
Dancer spring constant	K_d	Increasing	Increasing
Dancer viscous friction	B_d	Decreasing	Increasing
Dancer mass	M_d	No significant effect	No significant effect

Table 3.5 Main points from parameter variation

The tendencies from Table 3.5 are later used for obtaining a conservative tuned PID control.

From the analysis it is concluded that the most influential parameter is the changing radius. The analysis shows that the natural frequency is expected to increase at least 600 % and that the damping is expected to double as paper is winded.

3.6 Simplified Web Winder Model

The linear model and the nonlinear model have several parameters that influence the systems dynamic behavior, to reduce the amount of parameters that have to be estimated a simpler model is preferred. In (Liu, 1999) the model of the web material and the dancer can be estimated as shown in (3.25).

$$\frac{d}{(V_2 - V_1)} = \frac{1}{2s} \qquad (3.25)$$

From (Liu, 1999) it is found that (3.25) is sufficient to describe the dynamic behavior of dancer and web system in most industrial applications.

An intuitive understanding of (3.25) could be to see the equation a mass continuity equation. This is more obvious if (3.25) is rewritten as shown in (3.26).

$$V_2 - V_1 = 2 \cdot d \cdot s \qquad (3.26)$$

From (3.26) it can be seen that a difference between the paper entering the web handling system (V_1) and the paper leaving the web handling system (V_2) will result in a change in dancer velocity. The reason why the dancer velocity is multiplied by 2 is due to the web winders pulley-arrangement. It is hereby assumed that the dynamic of the dancer is much faster than the dynamics of the drive train.

From section 3.5.1 it is shown that the system contains 2 conjugated complex poles with a low bandwidth, and 2 complex conjugated poles with a high bandwidth, this supports the claim that the system contains two systems with large difference in bandwidth. In section 3.5.1 it is also found that the bandwidth of the slow dominating poles are affected by the inertia of the system, but the mass of the dancer have no significant effect, this implies that the slow poles originates primarily from the drive train. The simplified model (3.25) of the system is hereby found plausible.

When (3.25) is combined with the model of the drive train, the simplified on Fig. 3.25 is achieved

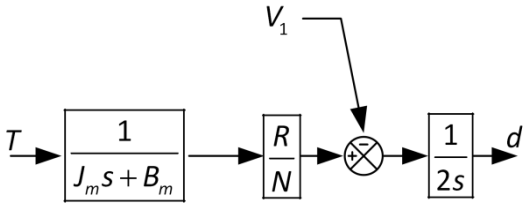

Fig. 3.25 Simplified model of the system

The simplify model of the system is hereby deduced, and will later be employed as foundation for the parameter estimation.

3.7 Control Approach

With the web handling system described above it is possible to set up 2 different control approaches.

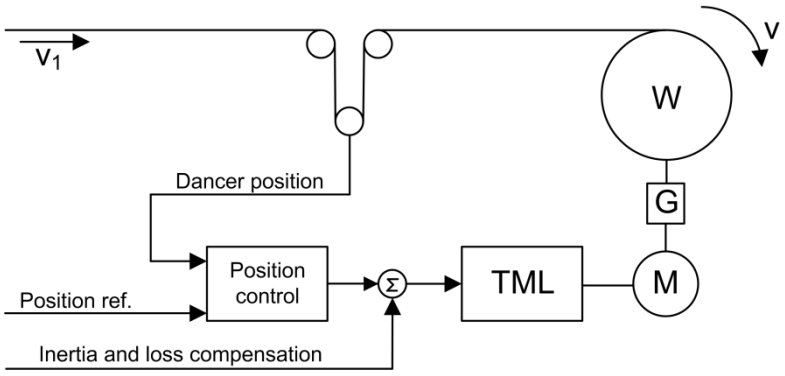

Fig. 3.26 Torque regulated position controlled

The first approach is shown in Fig. 3.26. Here the tension is torque regulated position controlled. This means that a torque reference is determined by the position control and feed to the torque minor loop (TML) on the FC302. Additionally when accelerating the web inertia and friction compensation is needed.

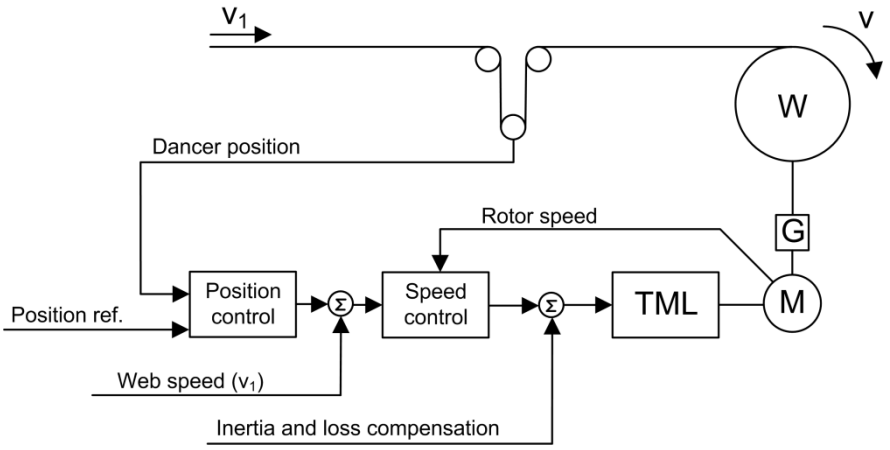

Fig. 3.27 Speed regulated position controlled

The second approach is shown in Fig. 3.27. Here the tension is speed regulated position controlled. This means that the position control and the measured web speed determine a speed reference which is feed to the speed control which determines the correct torque. Also here inertia and friction compensation is needed when accelerating the web.

The second approach has experienced high control performance when the inertia of the system is limited. By high performance it means that the control approach give fast tension and speed responses and thus have high response to load change or other disturbances. But as the inertia increases the speed loop bandwidth decreases. This results in poorer performance(Liu, 1999).

Better performance for systems with high inertia is achieved with the first approach (Liu, 1999).

4. Problem Statement

In the problem analysis it is found that the web winder model can be explained by a 4^{th} order system of type 0. This system has two dominating poles. This knowledge and the assumption that the motor is the dominating subsystem are used to simplify the system to a 2 order system of type 1.

The most influential parameter is the radius which dramatically increases natural frequency by more than 600 % and doubles the damping. The inertia has less importance on the test bench. But in other systems with potential for much larger increase in inertia the system could destabilize.

Since the inertia does not change significant a suitable control strategy for the test bench is the speed regulated position control.

For better performance this control needs to adapt to the changing system caused by the changing radius. This problem analysis leads to the following problem statement:

How is it possible to utilize adaptive control for the given web winder system ?

4.1 Field of Interest

The interest of this thesis is to investigate how indirect adaption could be used. This means how to develop an algorithm that automatic estimate the changing system parameters and uses these estimates to adapt the control law.

The aim is to develop an algorithm that is also suitable to other web winders with larger inertia influence.

Two controller structures are investigated, a PID-controller and a pole placement-controller. The performance of these controllers with and without adaption are evaluated by their ability to hold a dancer position reference while the web winder is subjected to disturbances

4.2 Limitation

Several different parameter estimation methods exist. In this thesis only the recursive least square method is investigated.

As mentioned above the speed regulated position controlled approach fits the test bench. However in development of the adaptive control the torque regulated position controlled approach is used because it is found easier or faster to test, implement and evaluate.

- Inertia and loss compensation is not investigated.
- Other web materials are not considered.
- The limit on torque input is set to $^{+}/_{-}$ 1 Nm.
- The default reference for position control is set to 35 mm.
- The systems sample time is set to 0.01 s.

4.3 Procedure

The remaining of the thesis is approached by the procedure shown in Fig. 4.1.

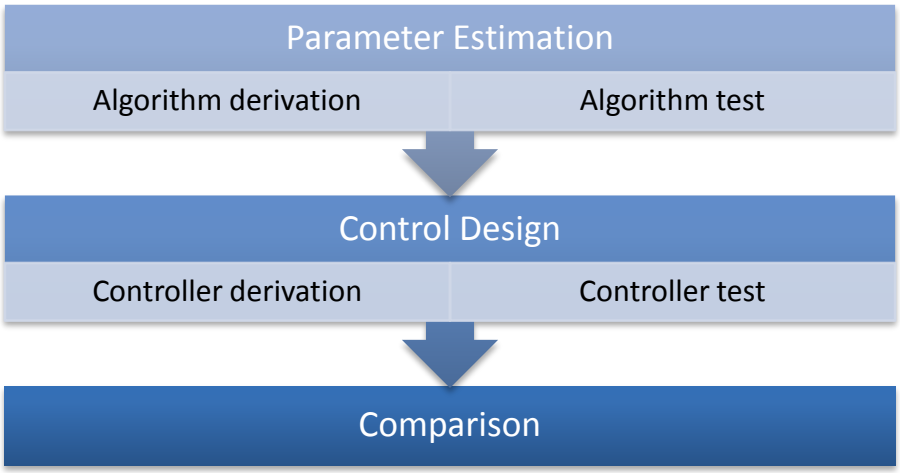

Fig. 4.1 Thesis structure

Each step in Fig. 4.1 is explained in the following.

4.3.1 Parameter Estimation

This step presents the parameter estimation principle and how recursive least square originates from this principle. While doing this the derivation of the method is done and the conditions for convergence are discussed.

The algorithm is tested in a simulation both on an ideal system and with data from the test bench.

4.3.2 Control Design

For comparison reasons a conservative non-adaptive PID controller is derived and tested both in simulation.

If the parameter estimation system seems plausible then the adaptive controllers are designed. Based on the estimation an algorithm is derived for determining the controller parameters for both the PID and the pole placement controller. The adaptive controllers are tested in simulation on an ideal system.

4.3.3 Control Comparison

Each controller's performance is finally evaluated using the test bench.

5. Parameter Estimation

To achieve the adaptive controllers stated in the problem statement, this chapter has the purpose of determine a suitable parameter estimation algorithm. This algorithm will serve as the basis for the later adaptive controllers being derived in the next chapter, by continuously estimating the plants behavior.

In Fig. 5.1 the structure of adaptive control with parameter estimation is shown. Here the process input and output is feed to an algorithm which estimates the parameters that characterizes the process dynamics. The parameters are then feed to an algorithm which designs a control that meets certain requirements.

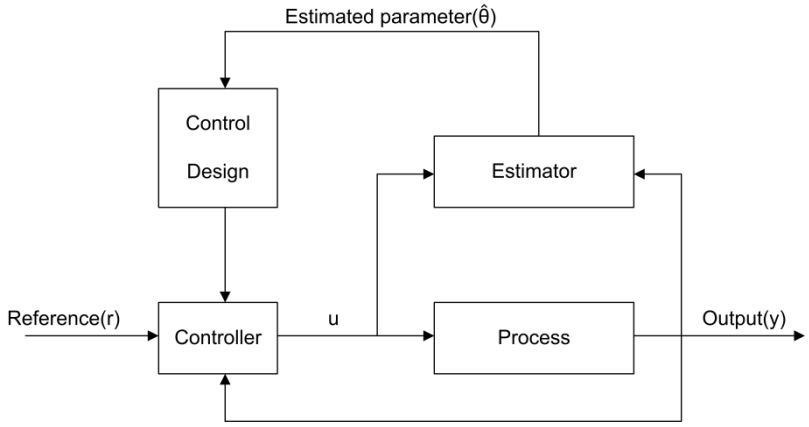

Fig. 5.1 Control structure of adaptive control with parameter estimation

This chapter explains the estimation principle, the used estimation method and how this method is implemented on the test bench. The theory explained in this chapter is based on (Ljung, 1999) and (Ljung, et al., 1983).

5.1 Estimation Principle

The guiding principle of parameter estimation is that given a set of past corresponding inputs and outputs (Z^N), selects the systems parameters (θ) in order to minimize the difference between the models predictions ($\hat{y}(t|\theta)$) and the systems output ($y(t)$) as much as possible.

This principle can be expressed with the following expression.

$$\hat{\theta}_N = \hat{\theta}_N\left(Z^N\right) = \arg\min V_N\left(\theta, Z^N\right) \tag{5.1}$$

Where $V_N\left(\theta, Z^N\right)$ is the cost function or the structure of how the difference between predictions and systems output is minimized. This function is expressed with.

$$V_N(\theta, Z^N) = \frac{1}{N}\sum_{t=1}^{N} \ell(\varepsilon_F(t,\theta))$$

(5.2)

Where $\ell(\varepsilon_F(t,\theta))$ is the norm which can be chosen in many ways. Obviously the task is to find a norm that enables a reasonable estimate within a certain time span.

$\varepsilon_F(t,\theta)$ is the filtered error between the model prediction and the systems output. The error is expressed with the following two equations.

$$\varepsilon_F(t,\theta) = L(q)\cdot\varepsilon(t,\theta)$$

(5.3)

$$\varepsilon(t,\theta) = (y(t) - \hat{y}(t|\theta))$$

(5.4)

The filter $L(q)$ can be used to enhance or suppress signals in certain frequency ranges. For example it could counteract slow drift terms, high frequency noise or enhance signals in the systems bandwidth.

5.1.1 Model Prediction

In appendix A is the discrete expression of the simplified model is derived. The linear difference equation of this expression is given by.

$$y(t) = -a_1 y(t-1) - a_2 y(t-2) + b_1 u(t-1) + b_2 u(t-2)$$

(5.5)

With (5.6) the predicted output $\hat{y}(t|\theta)$ is found with Auto Regression with eXogenous variables (ARX).

The regression vector is given by.

$$\varphi(t) = \left[-y(t-1) - y(t-2) + u(t-1) + u(t-2)\right]^T$$

(5.6)

And the parameter vector is given by.

$$\theta = \left[a_1\ a_2\ b_1\ b_2\right]^T$$

(5.7)

The model prediction is now expressed with (5.8).

$$\hat{y}(t|\theta) = \varphi^T(t)\theta$$

(5.8)

By using the ARX model it is assumed that the measurement noise in system, which it is applied to, is white noise with zero mean.

5.1.2 Least Squares Method

A commonly used estimation method is the Least Square Method (LSM). With this method the norm is given by (5.9) (Ljung, 1999).

$$\ell\left(\varepsilon_F(t,\theta)\right)=\frac{1}{2}\cdot\varepsilon_F^2(t,\theta)$$

(5.9)

Inserting (5.9) in (5.2) and disregarding filtering, by letting $L(q)$ equal 1, (5.10) is found.

$$V_N\left(\theta,Z^N\right)=\frac{1}{N}\sum_{t=1}^{N}\frac{1}{2}\cdot\varepsilon^2(t,\theta)=\frac{1}{N}\sum_{t=1}^{N}\frac{1}{2}\cdot\left(y(t)-\varphi^T(t)\theta\right)^2$$

(5.10)

Then to find the minimum we equal the derivative of (5.10) with zero, shown in (5.11) to derive the final estimate $\hat{\theta}_N$.

$$0=\frac{d}{d\theta}\left(V_N\left(\theta,Z^N\right)\right)=\frac{d}{d\theta}\left(\frac{1}{N}\sum_{t=1}^{N}\frac{1}{2}\cdot\left(y(t)-\varphi^T(t)\theta\right)^2\right)$$

$$\sum_{t=1}^{N}\varphi(t)y(t)=\sum_{t=1}^{N}\varphi(t)\varphi^T(t)\theta$$

$$\hat{\theta}_N=\left[\sum_{t=1}^{N}\varphi(t)\varphi^T(t)\right]^{-1}\sum_{t=1}^{N}\varphi(t)y(t)$$

(5.11)

If the inverted matrix $\left[\sum_{t=1}^{N}\varphi(t)\varphi^T(t)\right]^{-1}$ exists then the parameters can be found analytically.

The procedure for parameter identification given in (5.11) is also called batch or offline identification.

5.1.3 Recursive Least Square

In order to obtain online identification a recursive algorithm of the least squares method is derived from the offline least square estimation presented in section 5.1.2.

This estimate is represented in (5.12).

$$\hat{\theta}_N=\left[\sum_{t=1}^{N}\varphi(t)\varphi^T(t)\right]^{-1}\sum_{t=1}^{N}\varphi(t)y(t)$$

(5.12)

The derivation starts with denoting (5.13).

$$\bar{R}(t)=\sum_{k=1}^{t}\varphi(k)\varphi(k)^{T}$$

(5.13)

Inserting (5.13) in (5.12) and sum up to (t-1) (5.14) is found.

$$\sum_{k=1}^{t-1}\varphi(k)y(k)=\bar{R}(t-1)\hat{\theta}(t-1)$$

(5.14)

From (5.13) is (5.15) found.

$$\bar{R}(t-1)=\bar{R}(t)-\varphi(t)\varphi(t)^{T}$$

(5.15)

With (5.13) to (5.15); (5.12) can be rewritten as (5.16).

$$\begin{aligned}\hat{\theta}(t)&=\bar{R}^{-1}(t)\left(\sum_{k=1}^{t-1}\varphi(k)y(k)+\varphi(k)y(k)\right)\\&=\bar{R}^{-1}(t)\left(\bar{R}(t-1)\hat{\theta}(t-1)+\varphi(k)y(k)\right)\\&=\bar{R}^{-1}(t)\left(\bar{R}(t)\hat{\theta}(t-1)+\varphi(k)\left(y(k)-\varphi(k)^{T}\hat{\theta}(t-1)\right)\right)\\&=\hat{\theta}(t-1)+\bar{R}^{-1}(t)\varphi(k)\left(y(k)-\varphi(k)^{T}\hat{\theta}(t-1)\right)\end{aligned}$$

(5.16)

The expression (5.16) is a recursive estimate of the parameters when using least squares. This expression is often not suited for computation, since the matrix $\bar{R}(t)$ needs to be inverted in each time step. Therefore we define the following.

$$P(t)=\bar{R}^{-1}(t)$$

(5.17)

By inserting (5.17) in (5.15) is (5.18) found.

$$P(t)=\left(P^{-1}(t-1)+\varphi(t)\varphi(t)^{T}\right)^{-1}$$

(5.18)

To rewrite the expression (5.18) we use the following lemma (Ljung, et al., 1983).

Let A, B, C and D be matrices of compatible dimensions, so that the product BCD and the sum A + BCD exist. Then,

$$\left(A+BCD\right)^{-1}=A^{-1}-A^{-1}B\left(DA^{-1}B+C^{-1}\right)^{-1}DA^{-1}$$

(5.19)

By defining A = $P(t)$, B = $\varphi(t)$, C = 1 and D = $\varphi(t)^T$ (5.20) is found

$$P(t)=P(t-1)-P(t-1)\varphi(t)\left(\varphi(t)^T P(t-1)\varphi(t)+1\right)^{-1}\varphi(t)^T P(t-1)$$

$$P(t)=P(t-1)-\frac{P(t-1)\varphi(t)\varphi(t)^T P(t-1)}{\varphi(t)^T P(t-1)\varphi(t)+1}$$

(5.20)

With (5.20) only the inverse of a scalar now needs to be computed. The algorithm for estimating with recursive least square is summarized with two equations in (5.21).

$$\hat{\theta}(t)=\hat{\theta}(t-1)+P(t)\varphi(k)\left(y(k)-\varphi(k)^T\hat{\theta}(t-1)\right)$$

$$P(t)=P(t-1)-\frac{P(t-1)\varphi(t)\varphi(t)^T P(t-1)}{\varphi(t)^T P(t-1)\varphi(t)+1}$$

(5.21)

The initial values for P and $\hat{\theta}$ can be calculated from (5.17), (5.13) and (5.12) at the time step $t_0=\dim(\theta)$ or by choosing $P(0)=C\cdot I$ where C is a constant, I is the identity matrix and $\theta(0)=\theta_{Initial\,guess}$.

5.1.4 Weighting and Forgetting Factor

With (5.11) and (5.21) the estimated parameter is based on observed data from the first time step. If the parameters in the system changes with time, the data from the earlier time steps would give a wrong picture of the present system. It is therefore discussed, how the estimating algorithm should neglect data from earlier time steps. This feature is referred to as *forgetting*.

The minimizing criterion with a forgetting profile is given by (5.22).

$$V_N\left(\theta,Z^N\right)=\sum_{t=1}^{N}\overline{\beta}(N,t)\varepsilon^2(t,\theta)$$

(5.22)

A common choice for the forgetting profile $\overline{\beta}(N,t)$ given by (5.23).

$$\overline{\beta}(N,t)=\overline{\lambda}^{N-t}$$

(5.23)

With $\overline{\lambda}<1$ but close to 1, (5.24) is applied.

$$\overline{\lambda}^{t}=e^{t\cdot\ln(\overline{\lambda})}=e^{t\cdot\ln(\overline{\lambda}-1+1)}\approx e^{t(\overline{\lambda}-1)}$$

(5.24)

This gives an exponential-decay time of T_0 time steps as shown in (5.25).

$$T_0=\frac{1}{1-\overline{\lambda}}$$

(5.25)

Which means that values older than T_0 samples get a weight less than $e^{-1}\approx 37\%$ of present values. By using (5.23) and performing the steps from (5.9) to (5.21) is (5.26) found.

$$\hat{\theta}(t)=\hat{\theta}(t-1)+P(t)\varphi(k)\left(y(k)-\varphi(k)^{T}\hat{\theta}(t-1)\right)$$
$$P(t)=\frac{1}{\lambda(t)}\left[P(t-1)-\frac{P(t-1)\varphi(t)\varphi(t)^{T}P(t-1)}{\varphi(t)^{T}P(t-1)\varphi(t)+\lambda(t)}\right]$$

(5.26)

Where $\lambda(t)=\overline{\lambda}$

From (5.26) it is seen that smaller values of λ(t) increases the gain of the present predicted error. Therefore the choice of the forgetting factor λ(t) becomes a tradeoff between tracking ability and noise sensitivity.

If the frequency range of the system is known then some of the noise disturbance can be reduced with a filter as presented in (5.3).

5.1.5 Persistent Excitation

The estimated parameters in equation (5.26) or (5.21) will only converge if the input signal excites all modes of the system and that the excitation is detectable in the output. This condition is known as persistent excitation (PE).

The definition of PE corresponds to the requirement of no singularity mentioned in section 5.1.2.

When the system has 2n parameters then it has n possible modes of excitation. Therefore the input signal should at least possess n distinct frequencies. This could be achieved with superposing the input signal with n sinusoids, a pulse function or a pseudo random binary sequence (PRBS).

As mentioned above the superposed input signal needs to have a detectable influence on the output. Therefore the superimposed input signal needs to be larger than noise input and the influence on the output has to be detectable from the measurement noise.

Normally the amplitude of the sinusoids or a pulse function is at least as large as the noise variance. And the frequency of the sinusoids or the pulse function is around the systems bandwidth.

5.2 Testing the Parameter Estimation Algorithm

This chapter has the purpose of evaluating whether the recursive least square algorithm is suitable for estimation of the web winders system parameters. This will be examined through simulations the first half of this chapter before, if successful, being implemented in the actual system in the last part of the chapter. The algorithm is tested through the steps outlined here.

- Model definition
- Offline test based on Simulink
    - Test of parameter convergence against ideal model
    - Test of parameter convergence against ideal model with injected noise
    - Test of parameter convergence against varying model
    - Test of parameter convergence against varying model with injected noise
- Online test performed on the web winder machine
    - Test with various estimation filters
    - Test with different excitation signals

The argumentation for choosing theses steps is to gradually test the estimation algorithms ability to estimate accurate. Each of these steps will be discussed through the chapter. The recursive least square algorithm will through the chapter commonly be referred to as the *parameter estimation algorithm* (PEA).

Through this chapter the word *test* will refer to the testing of an overall system modification, e.g. the implementation of a filter. Each test may be divided into several *experiments* which refers to either practical experiments with the actual web winder in the laboratory or simulations in Simulink. In either case is experiments used to either support or discard proposed tests.

5.3 Definition of the model

This chapter will derive the model used for the least square algorithms estimations. The model is based upon the simplified model explained in chapter 3.6, and will discussed how the system model is revised and interpreted by the estimation algorithm. The simplified model links torque input to the system, with the dancer position as shown in Fig. 5.2.

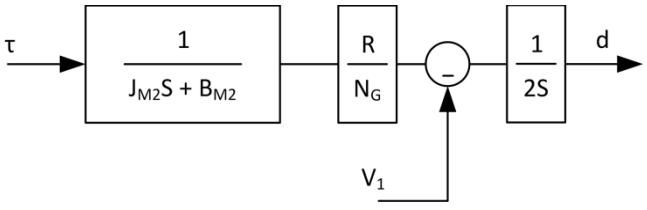

Fig. 5.2 Block diagram of the simplified model

As shown on Fig. 5.2, is the simplified model primarily governed by the motor model, the gearing ratio, and the velocity of the paper as it comes of the unwinder roll (V_1). The difference in paper velocity is related to the dancer position through an integrator block.

It poses a problem that the model, from torque input to dancer position, is not linear due to the subtraction of paper speed (V_1). If the change in V_1 is assumed slow compared to the speed of the estimation algorithm, the subtraction of V_1 can be seen as a constant which causes an offset in the estimation. This assumed constant offset will have no influence on the estimation of the systems dynamic behavior and will therefore be neglected. Based on this assumption a collected model from input torque to dancer position (d) is given by (5.27).

$$d = \frac{R}{S \cdot (2 \cdot N_G \cdot J_{M2} \cdot S + 2 \cdot N_G \cdot B_{M2})} \cdot \tau$$

(5.27)

The continuous model in (5.27) is through appendix A transformed into a discrete model which is given by (5.28).

$$d = \frac{b_1 \cdot z + b_2}{z^2 + a_1 \cdot z + a_2} \cdot \tau$$

(5.28)

To test if the found discrete model represents the continuous model, a step response comparison is shown in Fig. 5.3. The comparison is based on the found system parameters from the model validation section in chapter 3.3. And the discrete model constants are calculated on basis of the Z-transformation of the model in appendix A. The discrete sample time is by the project group selected to 0.01 s. this sample time will be used for all further analysis and implementation in the test bench.

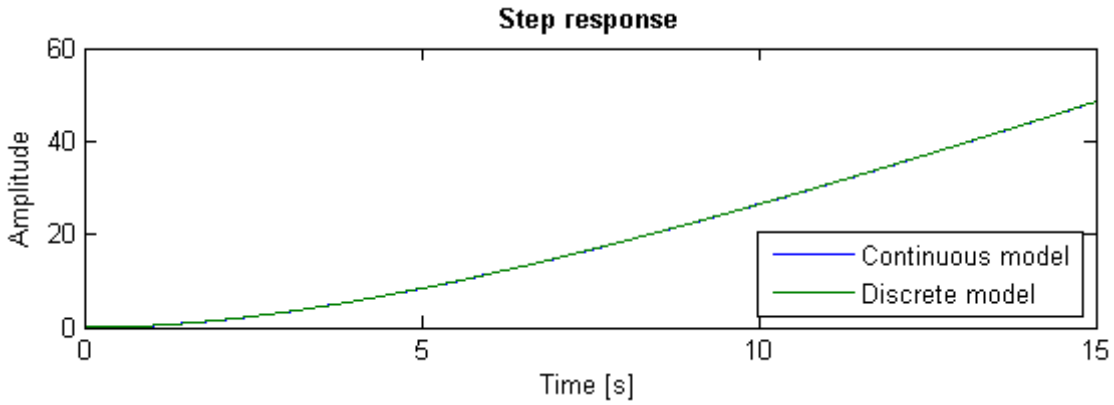

Fig. 5.3 Step response comparison between continuous and discrete model

The step comparison shows identical behavior between the two models whereby the discrete model is found to represent the continuous model.

From (5.28) it is seen that the discrete model contains two numerator constants (b_1 and b_2) and two changing denominator constants (a_1 and a_2). By following the recursive least square algorithm explained in section 5.1.3 this renders a 4x1 θ-vector (5.29), a 4x4 covariance matrix P (5.30) and a 1x4 φ vector (5.31).

$$\theta = \begin{bmatrix} a_1 \\ a_2 \\ b_1 \\ b_2 \end{bmatrix}$$

(5.29)

$$P = \begin{bmatrix} 1 & 0 & 0 & 0 \\ 0 & 1 & 0 & 0 \\ 0 & 0 & 1 & 0 \\ 0 & 0 & 0 & 1 \end{bmatrix}$$

(5.30)

$$\varphi(t) = \begin{bmatrix} -d(t-1) \\ -d(t-2) \\ \tau(t-1) \\ \tau(t-2) \end{bmatrix}$$

(5.31)

The recursive least square algorithm contains a forgetting factor which enables the algorithm to weight new estimates higher than older, or weigh all estimates equal depending the setting of the forgetting factor λ. Equation (5.32), also explained in section 5.1.4, relates the lambda factor to the amount of samples remembered by the estimation algorithm.

$$T_0 = \frac{1}{1-\lambda}$$

(5.32)

The forgetting factor is iteratively set by the project group on basis of initial testing. The selection is a weighting between relative slow and stable estimation (large λ) and fast adaptation to changes (low λ). The project group has found a values of 0.999 suitable, which by (5.32) enables the algorithm to weight the last 1000 estimations highest and base its new estimations on this memory. With a system sample time of 0.01 s, this will be equivalent to 10 s of memory. Data older than 10 s will be exponential decayed.

In order to determine whether the PEA is working plausible a set of success criteria is employed from which the results can be compared. The project group has chosen the following criteria on basis of initial intuitive testing:

- 3% tolerance on estimated numerator constants b_1 and b_2
  - The estimated parameters have to be within an acceptance band of $^{+}/_{-}$ 3 % of ideal value to keep estimated models response at acceptable amplitude and phase shift.
- 1‰ tolerance on estimated denominator constants a_1 and a_2

  - The estimated parameters have to be within an acceptance band of $^{+}/_{-}$ 1‰ of the ideal values for the estimated models response to be of the correct type.
- Parameters has to settle within 10 seconds
  - The system algorithm should be fast, therefore correct estimation values should be found quickly. Especially for the LTI systems. A parameter is found settled if its value enters the acceptance band and stays within this band.
- 10 % tolerance on natural frequency and zero placements
  - With the parameters sufficiently exact it, is also important to check that the dynamic behavior of the estimated parameters also are within in a acceptance band of $^{+}/_{-}$ 10 %.

The criteria are chosen by the project group as a base for comparison of multiple simulations. The criteria will primarily be used for the simulation tests where the correct parameters are known. The comparison method for later test bench experiments will be explained in section 5.8.

As a discrete model representing the system is found in this section, it is possible to test whether the least square algorithm can estimate the parameters sufficiently enough to be used as parameter estimation in the final system.

5.4 Simulation Test with LTI Model

The principle of this test is to validate whether the least square algorithm works and is able to estimate parameters in a model as shown in Fig. 5.4. To achieve this, two sets of constants is employed. First the constants found in the model validation chapter 3.3. These constants are assumed to represent the actual system and referred to as the *ideal constants* in this section. The second set of constants is chosen in the vicinity of the ideal constants by the project group to make them deviate from the ideal constants. These chosen constants will act as the least square algorithms initial values.

The goal is having the least square algorithm estimate the correct values (ideal constants) of this LTI system on basis of the chosen initial values. If this succeeds it is plausible that the algorithm can estimate the actual parameters on basis of the constants found in the validation chapter (Chapter 3.3). Table 5.1 contains both the set of ideal constants and the set of chosen initial constants.

	Ideal (s)	Chosen (s)
J_{m2}	0.0031	0.0025
B_{m2}	$5.5 \cdot 10^{-4}$	$5 \cdot 10^{-4}$
R	0.0573	0.06
N_G	10.5	10.5
	Ideal (z)	**Chosen (z)**
a_1	-1. 999822	-1.998001
a_2	0. 999822	0.998001
b_1	$4.414902 \cdot 10^{-7}$	$5.710478 \cdot 10^{-5}$
b_2	$4.414640 \cdot 10^{-7}$	$5.706672 \cdot 10^{-5}$

Table 5.1 Ideal and chosen parameters used for the estimation test

The chosen constants are within a reasonable range from the ideal parameters, in order to emulate the deviation between the ideal parameters and the actual physical parameters found in the web winder test bench. The z-parameters in Table 5.1 are the discrete representation of the continuous S-function made from the S-parameters in Table 5.1. The model which is sought estimated is shown on Fig. 5.4

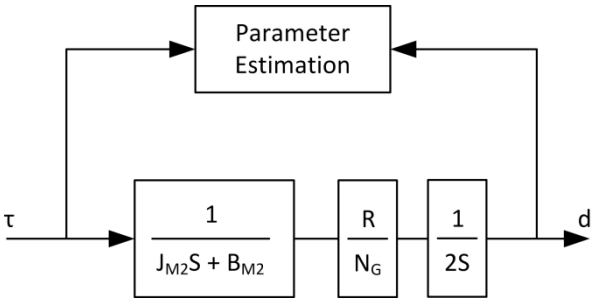

Fig. 5.4

The inputs to the parameter estimation block are motor torque (τ) and the dancer position (d). The first step is to see how well the guessed system represents the ideal system. This is compared on Fig. 5.5. In order to achieve this, a square wave input is used as τ, which also is shown on Fig. 5.5. This input is chosen for its similarity to steps, which can be used to excite as much dynamic behavior as possible. The signal is also chosen to have a mean value of 0, whereby both positive and negative signals occurs. This is chosen as the ideal system is of type 1 and therefore would rise fast and positively, negative signals will help to keep the response low and induce a response more similar to a type 0 systems step response. As the least square algorithm should converge fast, a 10 seconds simulation is chosen as sufficient.

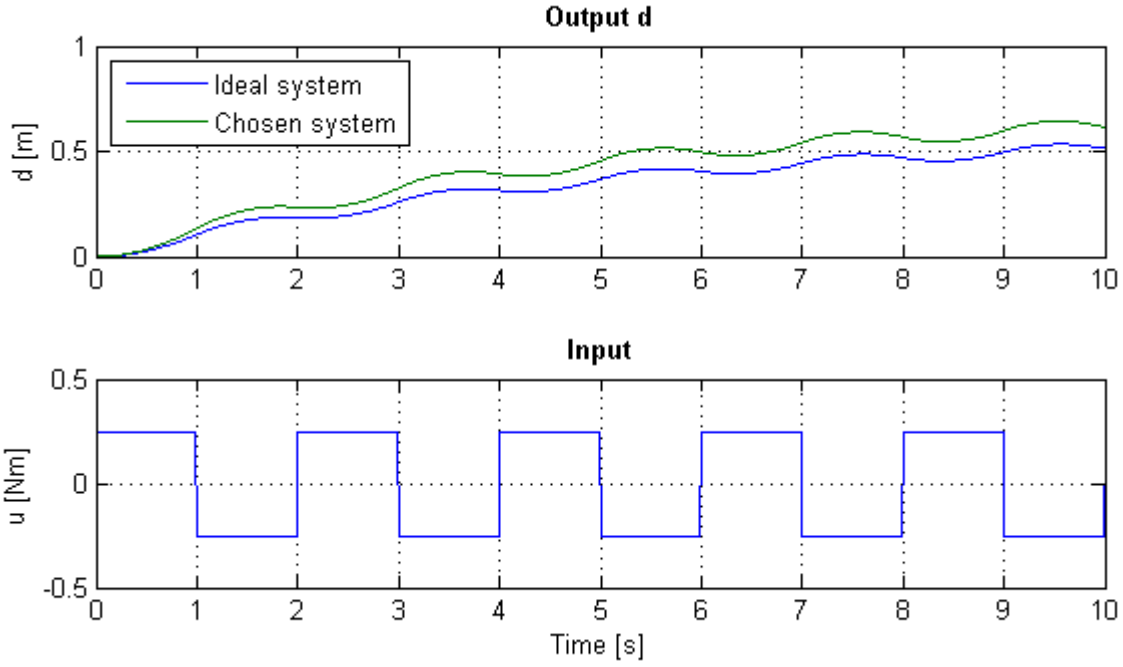

Fig. 5.5 Position comparison between system with ideal and chosen constants

The guessed system does not represent the ideal system very well seen from the comparison. This can be seen in the two graphs divergent behavior. This is obviously anticipated as the chosen system deliverable is selected to be a bit off.

The next step is to let the recursive least square algorithm estimate the parameters on basis of the guessed values. The simulation is again run for 10 seconds and the found parameters are shown in Table 5.2.

Parameter	a_1	a_2	b_1	b_2
Estimated value	-1.998002	0.998001	$4.539611 \cdot 10^{-5}$	$4.548749 \cdot 10^{-5}$
Deviation	<1‰	<1‰	-2.9%	-3.1%

Table 5.2 Estimated parameters after 10 s simulation

By comparing the results with the ideal parameters, it can be seen that the parameters are estimated closely but with deviations of up to 3.1%. But that does not exclude the parameters from still representing the system. Therefore a simulation is run where the found estimated parameters (shown in Table 5.2) does constitute an estimated model and the behavior is compared with the ideal system as shown on Fig. 5.6 based on the same input signal mentioned earlier.

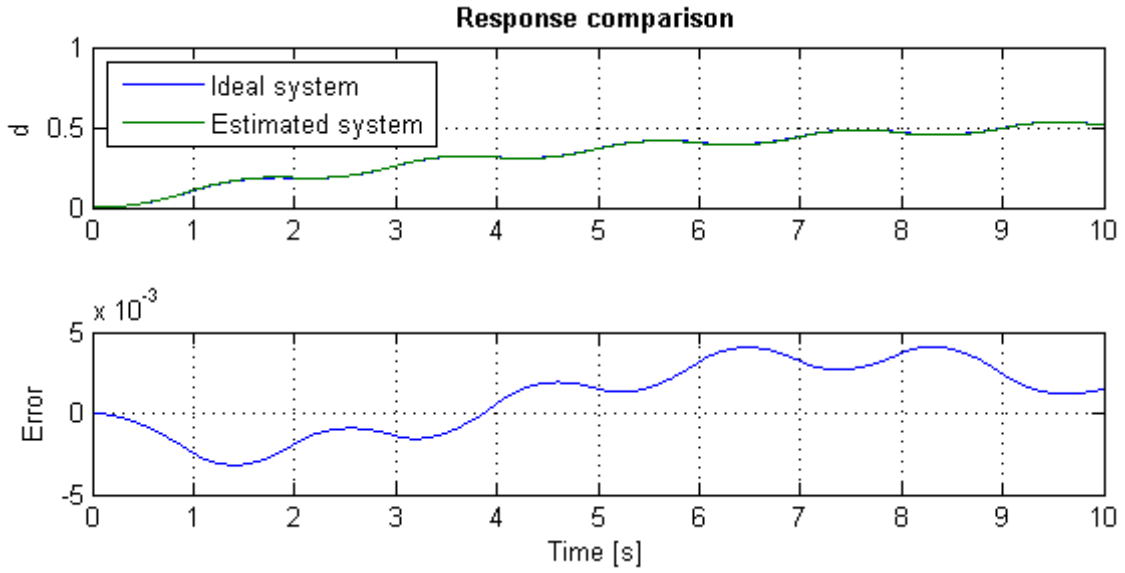

Fig. 5.6 Response comparison between ideal and estimated system when both are excited with the same square wave input

The response comparison shows that the estimated system with the found parameters behaves as the ideal system with small deviations in the order of 0.01 m, measured as the difference between the lowest and highest error. the response and accuracy is found acceptable but further analysis of the parameter accuracy is performed.

By analyzing the found parametera, and the parameters sought it can be seen that the numerator parameters are very small, in the order 10^{-5}. This suggest that any errors between the found and the ideal parameters also are very small. As this error is squared, it is plausible that it becomes so small that numerical rounding errors in MATLAB have influence. To get bigger parameters it is therefore examined if a gain of 1000 inserted on the estimation signal can give plausible results. The principle is shown on Fig. 5.7.

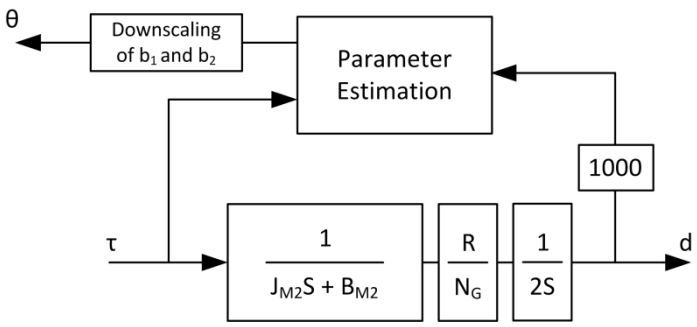

Fig. 5.7 Sketch of estimation system with inserted gain and downscaling of the θ-parameters

The output from the system is hereby scaled by 1000 but the input to the parameter estimation block is not, this gives larger outputs and hereby larger estimated parameters in the numerator, which previously contained very small numbers. Due to the system being linear the estimated numerator parameters will be 1000 times larger, is afterwards downscaled to have the correct values. The value of 1000 is chosen by the project group to test whether higher gains enhances the estimation performance. A 10 second simulation is again run and the estimated parameters are shown in Table 5.3.

Parameter	a_1	a_2	b_1	b_2
Estimated value	-1.998214	0.998214	$4.407705 \cdot 10^{-5}$	$4.366071 \cdot 10^{-5}$
Deviation	<1‰	<1‰	1‰	9‰

Table 5.3 Estimation results after 10 s of simulation

By comparing with the ideal values in Table 5.1, it is clear that the higher gain-solution has improved the results and that these parameters are very close to the ideal. A simulation with the estimated parameters is run and the result is compared to the ideal systems as shown on Fig. 5.8.

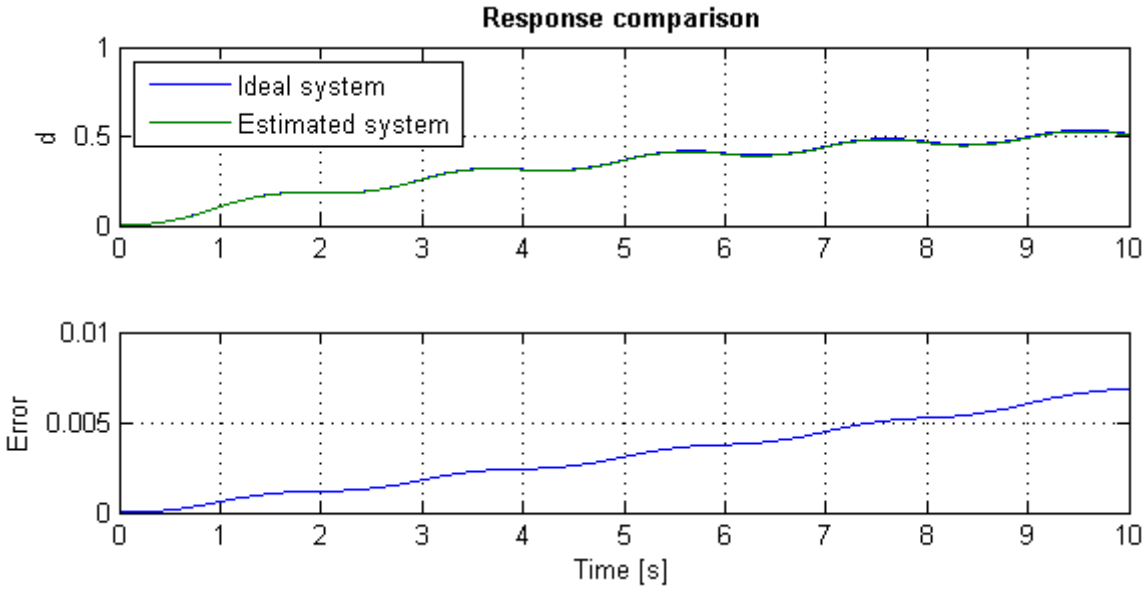

Fig. 5.8 Response comparison between ideal and estimated system when estimated using a gain of 1000

From Fig. 5.8 it is not possible to distinguish the two position graphs, same results as before the gain was implemented, and the response error is still in the range of 0.01 m. The main difference is more accurate parameters with deviations of only up to 9 ‰, which is considered a success.

The next step is to see if the parameters during simulation converge against a fixed value or if they cycle and the found solution only fits by accident. A plot of the θ-parameters is shown on Fig. 5.9.

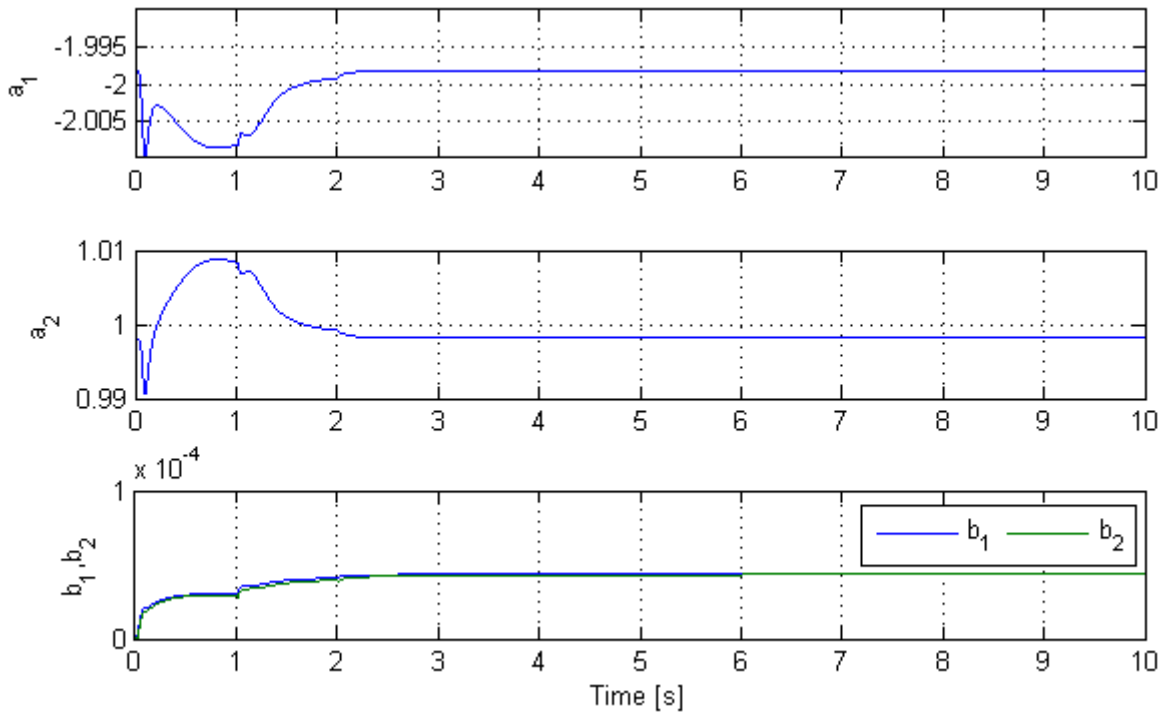

Fig. 5.9 Developments of the θ-parameters though the estimation simulation

From Fig. 5.9 it can be seen that all parameters have fixed values after 2.5 seconds. It can therefore be concluded that the system converges and find constant parameter values for the LTI system, which is also expected. It can also be concluded that the parameters need to be of a certain size or the signals need to be large, in order to achieve better accuracy. This is emulated by addition of the 1000 gain. The recursive least square algorithm seems plausible on basis of this simple test.

5.5 Simulation Test with LTI Model and Added Noise

As seen previous, the system converges fast and accurately to the ideal LTI system. But as the system also should work in a practical application, the next step is to test whether the system still converges when noise is present.

To simulate realistic noise in the simulation, a section of noise is recorded from the dancer signal, which is the primary source of noise in the system. This recording is made while the two motors both run at 400 RPM and the shielding around the dancer cable is connected to the earth potential as described in appendix B. The recording is made while the dancer is kept stationary at a position of 35 mm as stated in the project limitations. The measured signal is shown in Fig. 5.10.

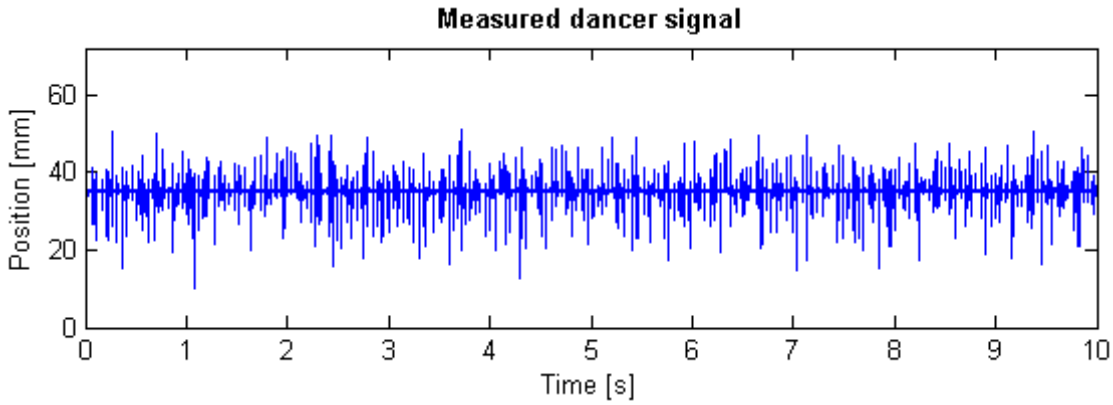

Fig. 5.10 Snip of measured dancer signal with dancer at 35 mm

In order to isolate the noise, the mean value (the dancer position) is calculated and subtracted the signal. The resulting signal has a zero bias with respect to zero, by moving the noise from the 35 mm position down to 0 mm position. This noise signal can later be added to other signal as a source of noise.

By comparing the noise levels in Fig. 5.10 with the total range of the dancer (0 – 72 mm) it is clear the noise levels are very large with peaks of $^{+}/_{-}$ 15 mm. But to check whether the estimation algorithm still can estimate even though noise is present, the simulation sketched in Fig. 5.11 is conducted.

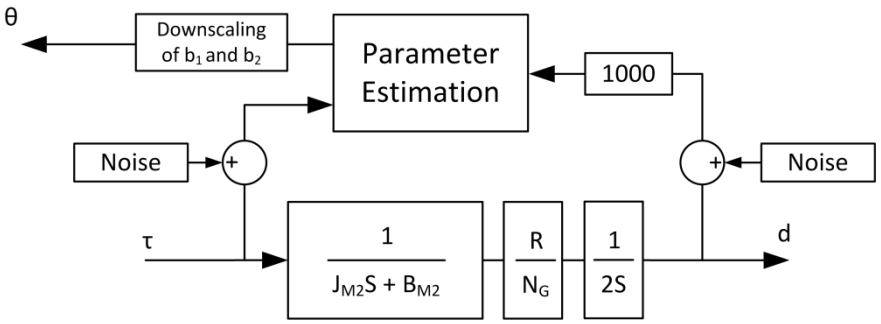

Fig. 5.11 Simulation of parameter convergence with injected noise and signal scaling of 1000

The reason why the noise is added to both estimation signals is derived from Fig. 5.12 which shows the test bench's position loop. The zero bias noise found earlier, is on Fig. 5.12 added to the dancer signal to indicate this signal as being the main source of noise.

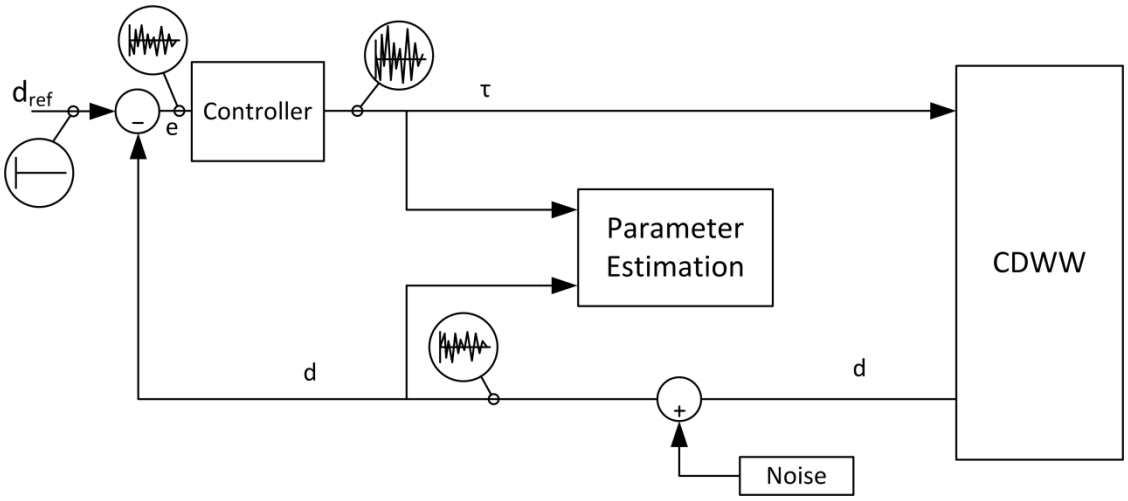

Fig. 5.12 Illustration of the noise's influence on the system

If noise is added, to the presumably ideal system, the noise will of course first influence the dancer signal. If the position loop reference (d_{ref}) in this derivation is assumed constant and zero; the noise will influence the error signal (e) to the controller. The purpose of this project is to continuously find a suitable controller, therefore it is not possible to determine the controllers influence on the error signal other than the noise must be changed and presumable be larger. But in this analysis it is assumed as equivalent to the noise added at the dancer signal. The estimation algorithm might estimate the behavior of the noise signal if the same signal is added to both the τ- and the d signal. The noise added to the τ signal is therefore delayed slightly to avoid correlation.

The system estimated is this test is the same LTI system as in the previous section 5.4, and the d signal is still multiplied by a 1000 as seen earlier improving the algorithm. The measured zero biased noise is then added to the parameter estimation input signals.

The section has the purpose of testing whether the algorithm still can estimate the parameters even when noise is present. The noise measured and explained earlier is added to the estimation signals as explained on Fig. 5.11. This is done through a simulation and the results are presented in Fig. 5.13 which shows the algorithms capability to estimate the parameter after 25 seconds. The simulation time is elongated from 10 seconds to 25 seconds due to the disturbance from the noise creates longer parameter settling time. The model is excited by at square wave signal with amplitude of $^{+}/_{-}$ 0.25 Nm and a period of 2 seconds. The square wave signal is chosen to excite as much dynamic behavior as possible.

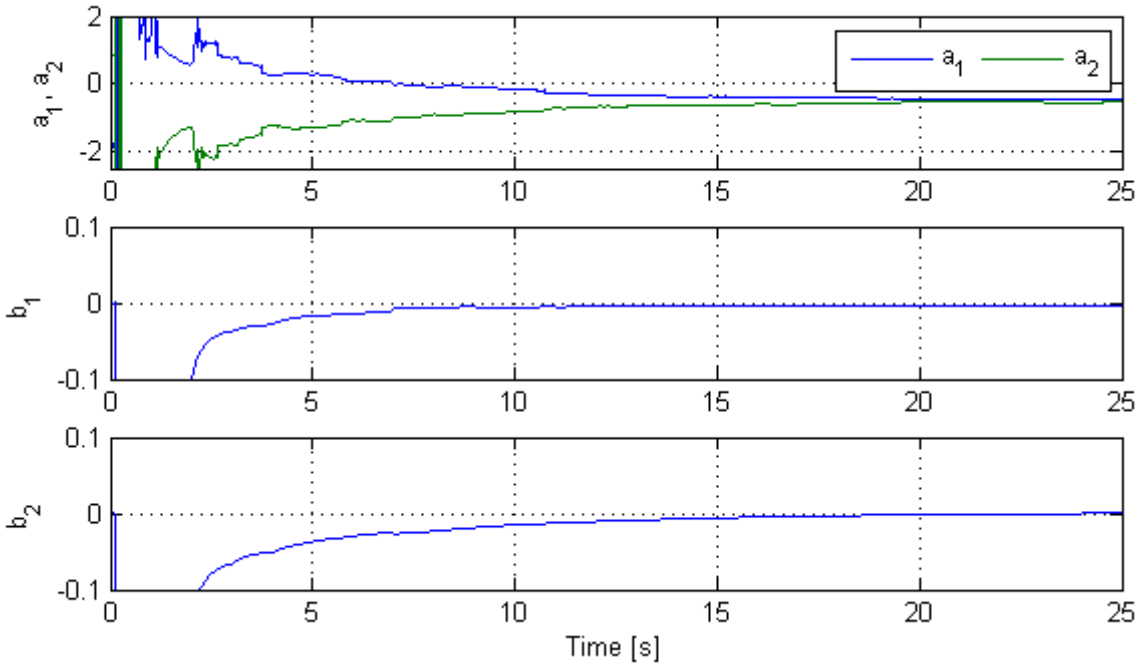

Fig. 5.13 Plot of estimated parameter values through simulation with injected noise

It seems at first sight, that the system converges and that b_1 and b_2 is estimated after 15 seconds. But as Table 5.4 shows, the algorithm does not converge to the right values. Table 5.4 contains the found estimates and the respectively deviation from the ideal values in percent.

Parameter	a_1	a_2	b_1	b_2
Estimated value	-0.464003	-0.536207	$-3.242398 \cdot 10^{-3}$	$0.355021 \cdot 10^{-3}$
Deviation	77 %	154 %	7450 %	-700 %

Table 5.4 Estimation results after 25 s of simulation

These deviations are very large and unacceptable, which is also being underlined by a comparison plot on Fig. 5.14 which compares the ideal models response to the estimated systems response to the same square wave input.

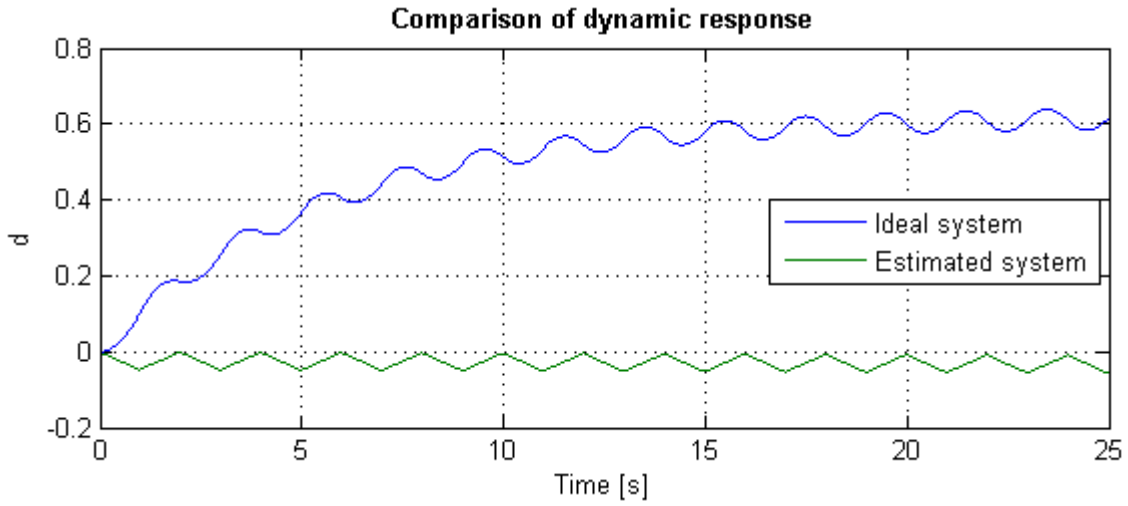

Fig. 5.14 Position comparison of the estimation results after introduction of noise in the estimation system

As the only difference between this test and the previous LTI test is the injected noise, the noise must be the cause for the bad convergence. The following section will therefore explore various means to reduce the noise to a level where, if possible, the algorithm can converge.

5.5.1 Measures to Reduce Noise

There are different ways to perform noise reduction. One possibility is to shield the cables and make sure these cables does not run near noise sources. This have been implemented on the machine in such a way that the signal cables shielding is connected to the earth potential and the signal wire is wound with the neutral wire. The cables are placed as far from the motors as possible. And an analog anti aliasing filter is implemented as described in appendix B. But the noise shown in Fig. 5.10 is still present.

An experiment is run using the model in Fig. 5.11 to see how much the noise should be reduced if the algorithm where to converge. The reduction is made by scaling the noise using a scalar stated in the Gain-column in Table 5.5 The parameters accuracy is calculated and stated in Table 5.5 as well.

Gain	a_1	a_2	b_1	b_2	Settles?
0.1	-1.643772	0.643725	-0.689866	$0.837858 \cdot 10^{-5}$	No
	21 %	55 %	-106 %	95 %	
0.02	-1.979976	0.979974	$9.393016 \cdot 10^{-6}$	$8.166813 \cdot 10^{-5}$	No
	9 ‰	2 %	370 %	46 %	
0.01	-1.993625	0.993624	$3.644893 \cdot 10^{-5}$	$5.237780 \cdot 10^{-5}$	No
	2 ‰	4 ‰	21 %	-15%	
0.002	-1.998036	0.998036	$4.416304 \cdot 10^{-5}$	$4.399803 \cdot 10^{-5}$	Yes
	<1‰	<1‰	<1‰	2‰	18 sec
0.001	-1.998173	0.998173	$4.423981 \cdot 10^{-5}$	$4.390863 \cdot 10^{-5}$	Yes
	<1‰	<1‰	2‰	4‰	9 sec

Table 5.5 Estimation results after 25 s of simulation with scaled noise introduced in the estimation system

The “Settles?” column tells whether the values enter the acceptance band and stays within it until the end of the simulation or whether the parameter diverges or cycles. The time stated for those who settle are the time from the simulations start and until the parameters cross the acceptance limits for the last time before staying within these limits.

From Table 5.5 it can be concluded that a noise reduction of a factor 500 is needed to make the system estimate within the acceptance band. But the convergence is first settled at around 18 seconds. This is a long time for the system compared to the success criteria. But a reduction factor of a 1000 is needed just to get the settling time under 10 seconds. But at noise reduction of a factor 1000 is not realistic as the system is presented today where the signal cables already are shielded and kept as far away from the motors and frequency converters as possible.

Therefore a physical solution does not seem plausible. Instead it seems interesting to test filters. Especially as the noise consists of a small portion of what seems to be white noise and a few large spikes. These spikes can be drastically reduced by implementing a low pass filter on the signal.

It is therefore chosen to implement a second order low pass filter on the noise before adding it to the model as earlier. A second order filter is chosen as it has a steeper frequency response decline above the filter frequency. The same comparison table is made with filters in steps of 2 Hz.

Filter frq.	a_1	a_2	b_1	b_2	Settles?
2 Hz	-1.998226	0.998226	$4.412269 \cdot 10^{-5}$	$4.404194 \cdot 10^{-5}$	Yes
	<1‰	<1‰	<1‰	1‰	4 sec
4 Hz	-1.998192	0.998192	$4.420150 \cdot 10^{-5}$	$4.409126 \cdot 10^{-5}$	Yes
	<1‰	<1‰	-2‰	<1‰	4 sec
6 Hz	-1.998087	0.998087	$4.427191 \cdot 10^{-5}$	$4.405289 \cdot 10^{-5}$	Yes
	<1‰	<1‰	-3 ‰	1‰	4.5 sec
8 Hz	-1.997994	0.997994	$4.428383 \cdot 10^{-5}$	$4.390360 \cdot 10^{-5}$	Yes
	<1‰	<1‰	-3‰	4‰	6 sec
10 Hz	-1.997921	0.997922	$4.417993 \cdot 10^{-5}$	$4.378377 \cdot 10^{-5}$	Yes
	<1‰	<1‰	-1 ‰	7‰	12 sec
12 Hz	-1.997842	0.997842	$4.382761 \cdot 10^{-5}$	$4.384178 \cdot 10^{-5}$	No
	<1‰	<1‰	7‰	6‰	
14 Hz	-1.997738	0.997738	$4.307943 \cdot 10^{-5}$	$4.422909 \cdot 10^{-5}$	No
	<1‰	<1‰	2 %	-2‰	
16 hz	-1.997599	0.997599	$4.181150 \cdot 10^{-5}$	$4.509408 \cdot 10^{-5}$	No
	<1‰	<1‰	5 %	-2 %	

Table 5.6 Estimation results after 25 s of simulation with added noise being filtered

From this table it is clear that, the lower filter frequency is, the better the algorithm convergences and the settling time reduces. It can be seen that a filter of at least 10 Hz is needed to make the system settle at a constant value. But with a 10 Hz filter this takes 12 seconds. The obvious choice would be to select the lowest possible filter, but this has consequences as a lower filter gives a higher phase shift or delay in the signal, which could be a problem later in the control part as the signal is artificial delayed. Therefore the best choice of filter must be a balancing between settling time and phase shift. The project group therefore chooses the filter with the highest frequency while settling under 5 seconds. The filter which can achieve this seems to be the 6 Hz filter. This filter is therefore chosen for the further analysis.

Fig. 5.15 shows the parameters convergence based on simulation with the 6 Hz filter implemented.

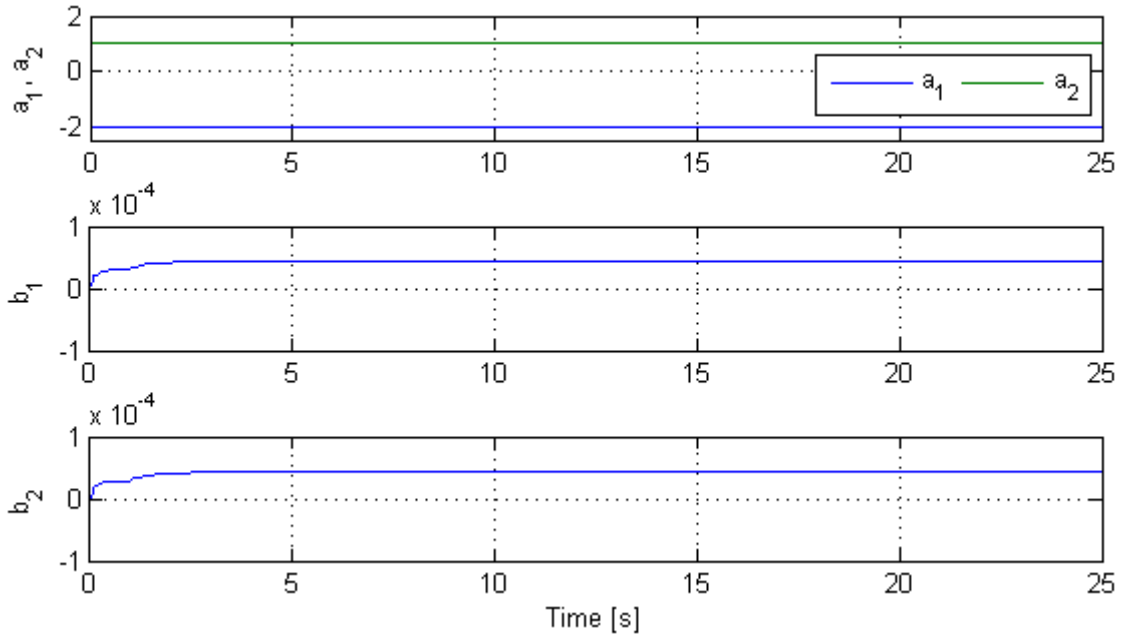

Fig. 5.15 Plot of estimated parameter values through simulation with injected noise filtered at 6 Hz

The scaling of the plot in Fig. 5.15 is especially made in such a way that if a parameter moves outside the acceptance limits it would show as a change in the graph, any changes within the acceptance band would only show as a straight line. In this way it is visually possible to see that the parameters converges and keeps at constant values, with respect to the tolerance limits.

Fig. 5.16 shows the noise before and after the filtering using the 6 Hz filter. This filtered noise signal is then added both τ and d signals to the PEA. The second graph on Fig. 5.16 shows the original models response compared to the models response based on the estimated parameters found and the square wave input signal.

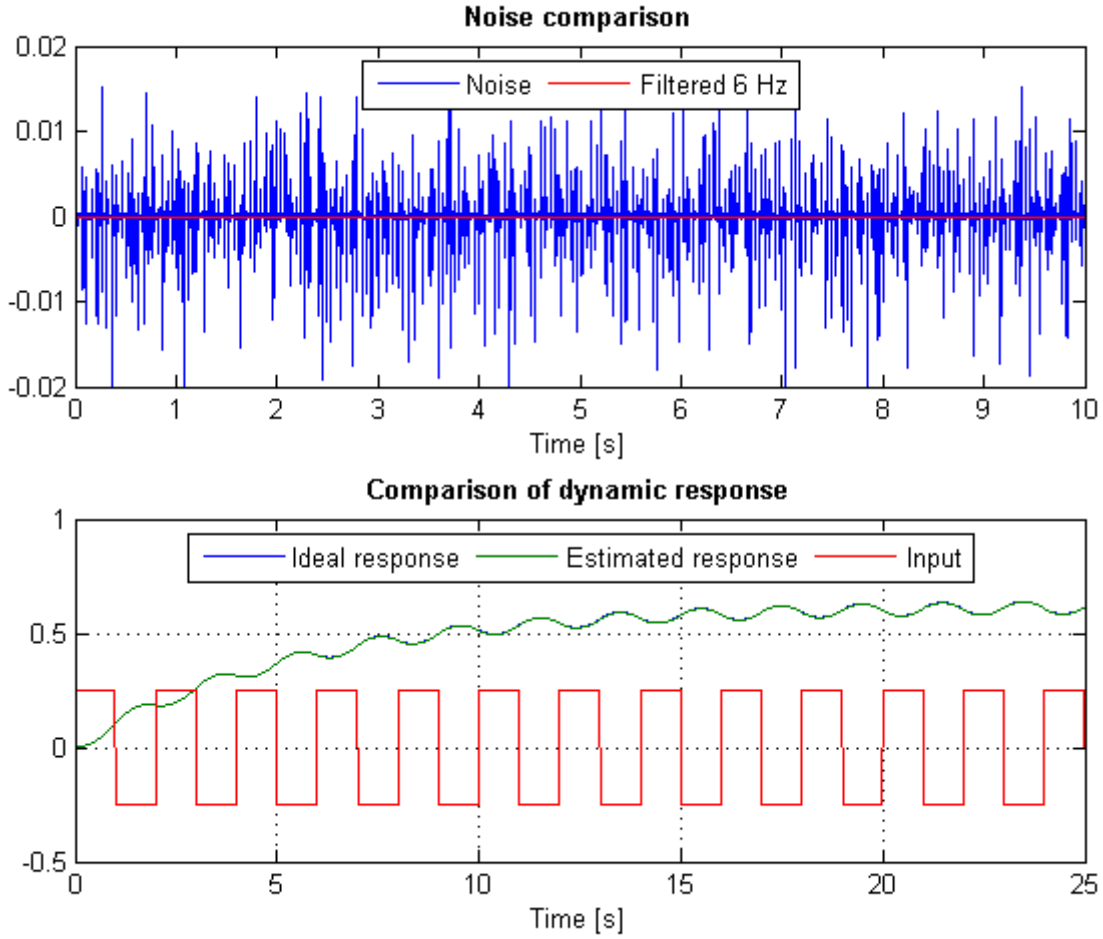

Fig. 5.16 Top graph displaying the added noise signal. Bottom graph dispaying the position comparison and the input signal

It is clear that the two responses are very much alike and is a better fit than the comparison made in Fig. 5.14. To further investigate the accuracy of the estimation, the estimated systems natural frequency and the placements of the systems zeros are calculated using MATLABs *damp* and *zero* functions and the result is compared with the ideal models properties. The zeros are in all cases, due to the models structure, placed on the real axis. The comparison is therefore based on the zeros location compared to the ideal systems on the real axis.

A comparison of the two models natural frequency as the simulations is run is shown on Fig. 5.17.

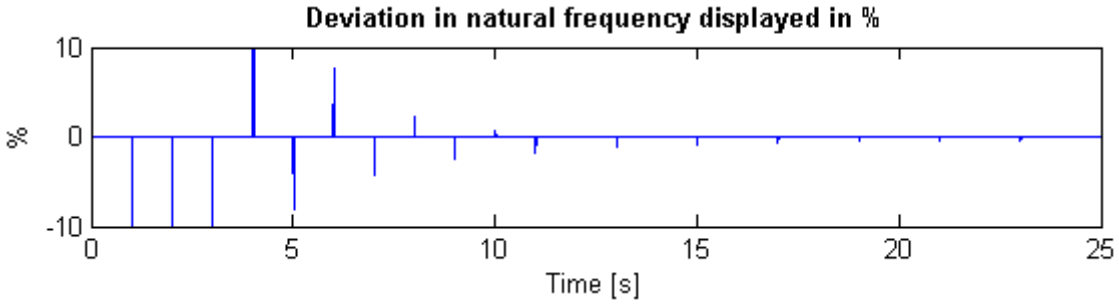

Fig. 5.17 Comparison of natural frequency between the ideal and the estimated system

The comparison shows large deviations peaks the first 5 seconds which gradually decreases as the simulation develops. The peaks are coincident with the input square waves rising and falling edges, but the deviations are immediately detected by the algorithm and suppressed.

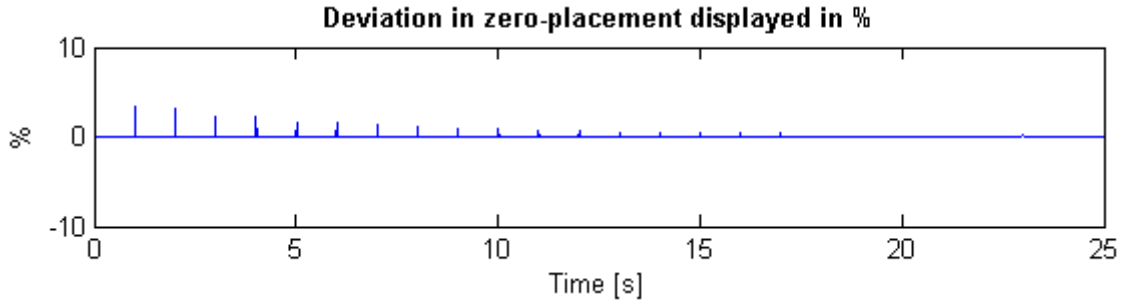

Fig. 5.18 Comparison of zero placements between the ideal and the estimated system

Fig. 5.18 compares the zero placements which shows the same tendencies as the natural frequency comparison. This tendency is relatively large deviation peaks at start which is gradually reduced as the estimation is getting better.

It can therefore be concluded that the algorithm seems plausible, as long as the noise in the system is reduced. This could for instance be done by the application of a 6 Hz filter on the dancer signal.

5.6 Simulation Test with LTV Model

The next step is to investigate how the algorithm estimates changing parameters. This will be examined by varying the ideal models parameters realistic over time and compare the estimation result to determine if the estimation algorithm detects the changes as they actually are made. The system is sketched on Fig. 5.19, where the arrows across the motor and gearing model indicates that these models have time changing behavior in this test.

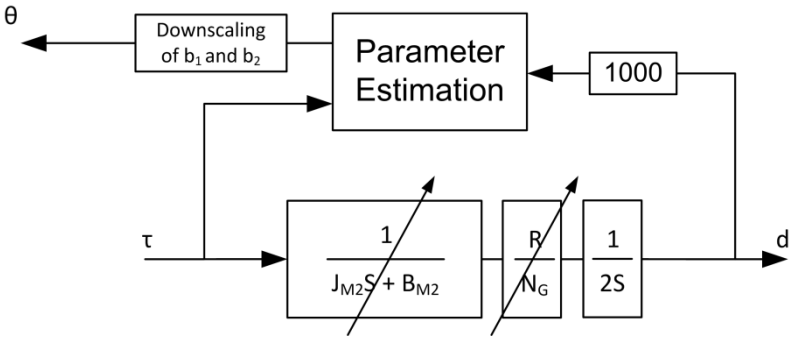

Fig. 5.19 Model of the estimation system with time varying parameters and scaling of d

Table 5.7 shows the physical parameters which constitute the time varying ideal model. This model is sought estimated as correctly as possible during the simulation. The table also contains the variations of the parameters from start simulation and until finish. The simulation is run for 15 minutes as this is a realistic time for the paper to be winded from one reel to another.

	Start value at t=0 s	End value at t = 900 s
R	13 mm	72 mm
J_{M2}	0.00309	0.00325 (+5 %)
N_G	10.5	10.5
B_{M2}	0.00055	0.00055 (sine $^{+}/_{-}$ 25%)

Table 5.7 start and end values for time varying parameters

All the parameters change linearly except the friction B_{M2}, which is varied using a sine function in such a manner that the value will have changed $^{+}/_{-}$ 25 % at the end of the simulation (1 sine cycle). A sine pattern is chosen for this parameters as it is the only which cannot be determined wheter rises or falls during experiments. The radius and inertia on the other hand is known to rise as more paper is wound and time progresses.

Fig. 5.20 shows the new discrete ideal model parameters as they vary over time. These parameters are calculated continuously based on the changes in Table 5.7 and employing the discretazation of the model in appendix A. The goal is to estimate these as exact as possible using the recursive least square estimation algorithm implemented in Simulink.

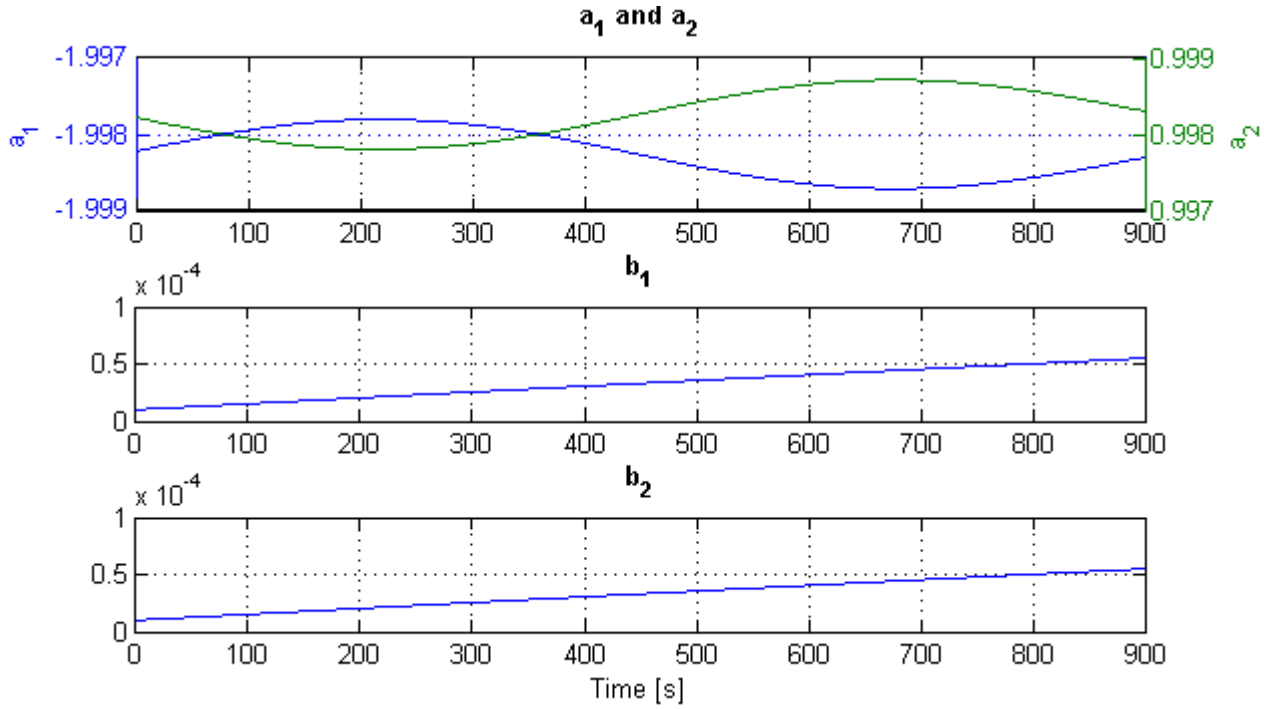

Fig. 5.20 development of ideal model parameters during the experiments

The next step is to test whether the PEA can estimate these changing parameters without noise present. This will test if the algorithm ideally can estimate the parameters acceptable. Fig. 5.21 shows the comparison between the ideal parameters (also shown on Fig. 5.20) and the estimated parameters found through the simulation.

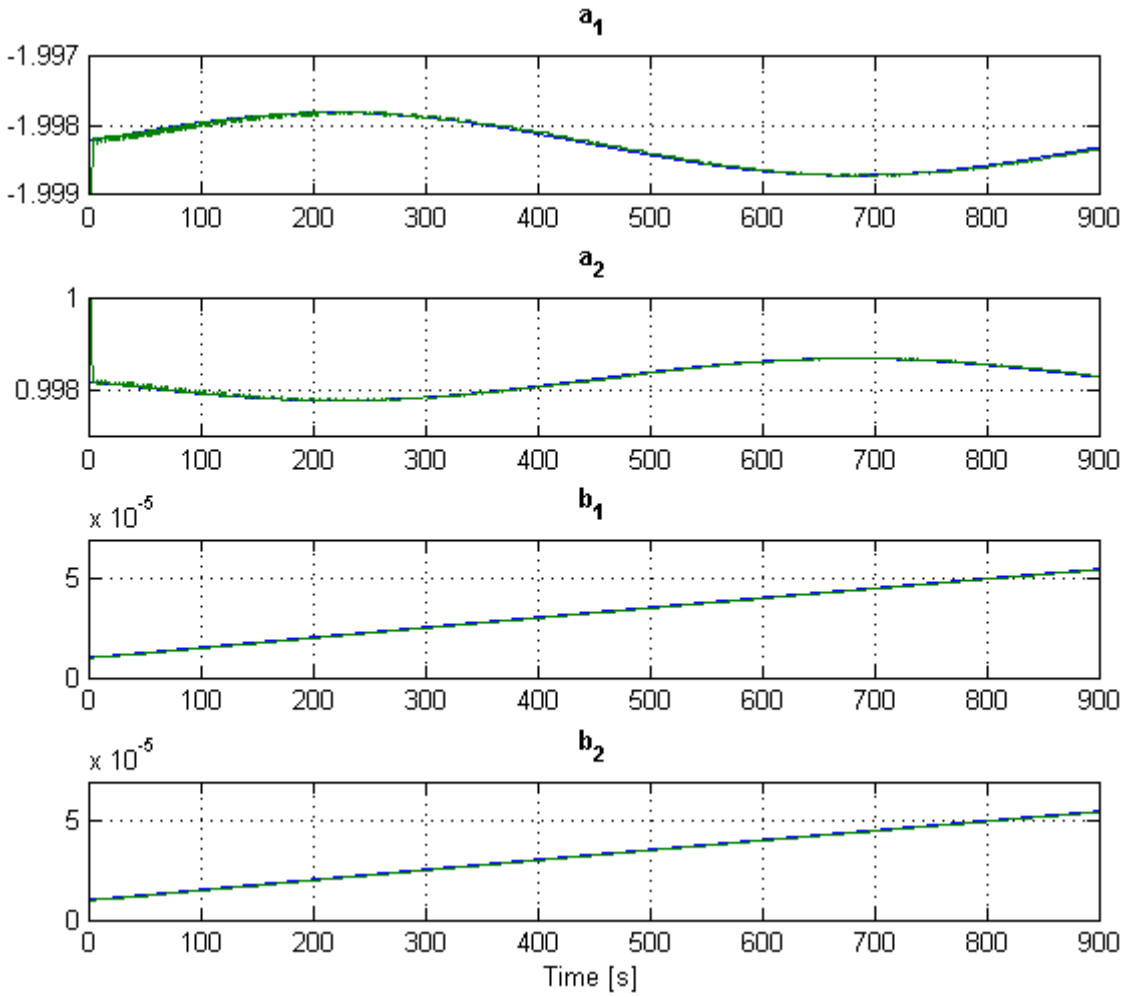

Fig. 5.21 Comparison between ideal (blue) and estimated (green) parameters during simulation

By looking at the graphs in Fig. 5.21 it seems that the algorithm converges fast and continuously estimates the correct values. But to quantify the results Table 5.8 has been made. This table shows the largest peak deviation and the mean deviation throughout the simulation. The first 5 seconds is ignored as the algorithm initially settles here, this is also supported by the results presented in Table 5.6.

	a_1	a_2	b_1	b_2
Peak	<1‰	<1‰	4%	5%
Mean	<1‰	<1‰	1.8 %	1.9%

Table 5.8 Parameter deviation through estimation simulation

The deviation can be analyzed graphically by observing Fig. 5.22 which shows the instant deviation between the ideal parameters and the estimated parameters as the simulation is progressing.

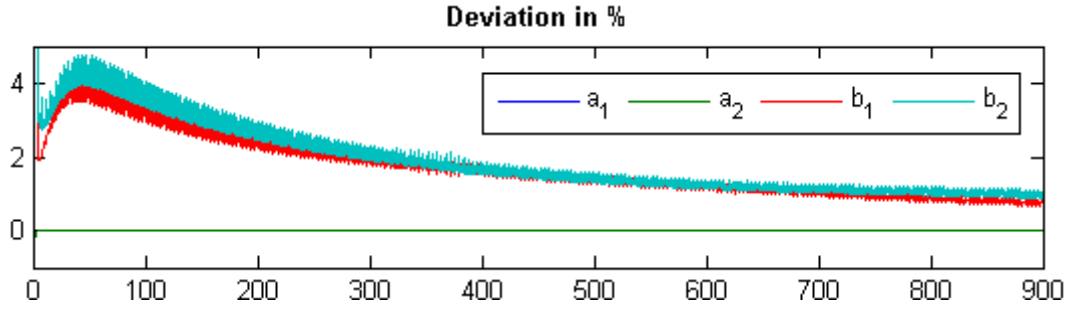

Fig. 5.22 Instantaneous deviation between ideal and estimated parameters in percentage.

To check the dynamic behavior of the system, the ideal systems natural frequency is compared to the estimated systems. This is shown on Fig. 5.23. The comparison is made using MATLABs *damp* and *zero* functions.

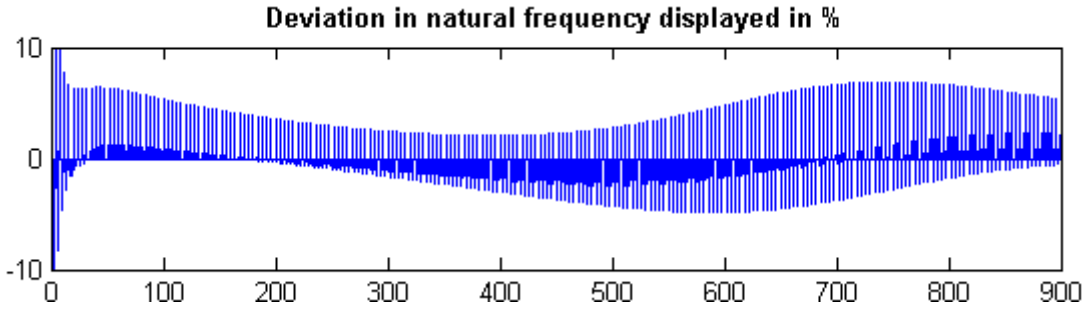

Fig. 5.23 Deviation in natural frequency compared to ideal system

From this comparison it seems that even though the parameters are estimated very correctly the system still experiences relatively high deviations in natural frequency of up to 8 %. A comparison of the systems zero-placement is shown on Fig. 5.24.

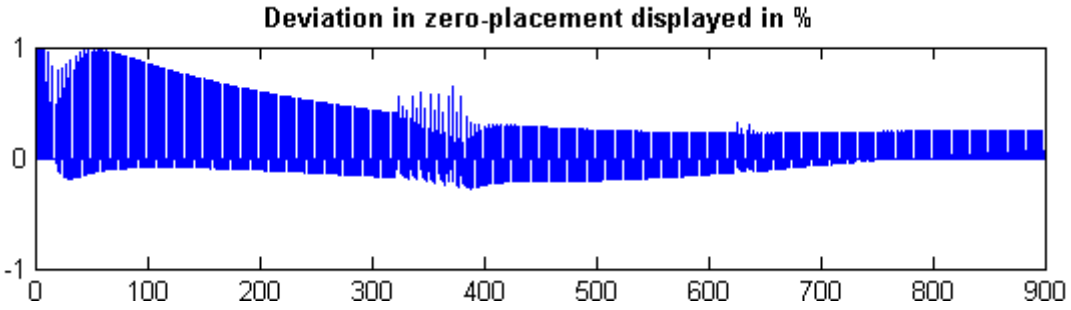

Fig. 5.24 Deviation in zero-placement compared to ideal system

The zero-placements only deviate by up to 1 %. Based on this analysis it seems that the algorithm can estimate the parameter sufficiently but may experience minor deviation peaks in the estimation results. It also seems that even though the parameters are closely estimated, the natural frequency still deviates up to 8 %. This can have influence on the systems dynamic behavior.

5.7 Simulation Test with LTV Model and Added Noise

This final test has the purpose of examining whether the algorithm converges when the system parameters changes and noise is present. The same parameter wave forms are employed as in the last test, and the noise is again filtered using the second order low pass filter.

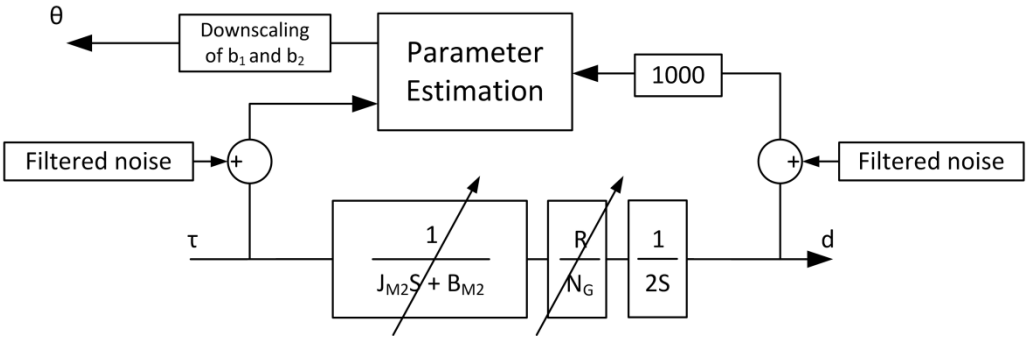

Fig. 5.25 Estimation system with time varying model parameters and added filtered noise

The test is only run up to 8 Hz as earlier tests shown that higher filter frequencies deteriorates the algorithms performance. The results of the tests are shown in Table 5.9.

Filter frq.		a_1	a_2	b_1	b_2
2 Hz	Peak	<1‰	<1‰	4.5 %	5%
	Mean	<1‰	<1‰	1.8 %	1.9 %
4 Hz	Peak	<1‰	<1‰	6.5 %	6.5 %
	Mean	<1‰	<1‰	1.5 %	2 %
6 Hz	Peak	<1‰	<1‰	11 %	11 %
	Mean	<1‰	<1‰	1.1 %	2.4 %
8 Hz	Peak	<1‰	<1‰	14 %	14.5 %
	Mean	<1‰	<1‰	0.7 %	2.8 %

Table 5.9 Parameter deviation comparison through the simulation

The mean deviation is calculated over the time interval of 5-900 seconds. From Table 5.9 it is again clear that the denominator parameter a_1 and a_2 are precisely found, but the numerator parameters b_1 and b_2 have larger deviations. This test actually shows the 8 Hz filter having one of the smallest mean deviations. But the 8 Hz filter also has the largest peak deviations. The 6 Hz filter is again chosen for further analysis, as being the one with the best performance and highest filter frequency, hence lowest phase shift. It should be noted that in these simulations, only the mean deviation can be kept within the acceptance band.

The further analysis will focus on the 6 Hz filter. Fig. 5.26 shows the parameter deviation as it develops through the simulation.

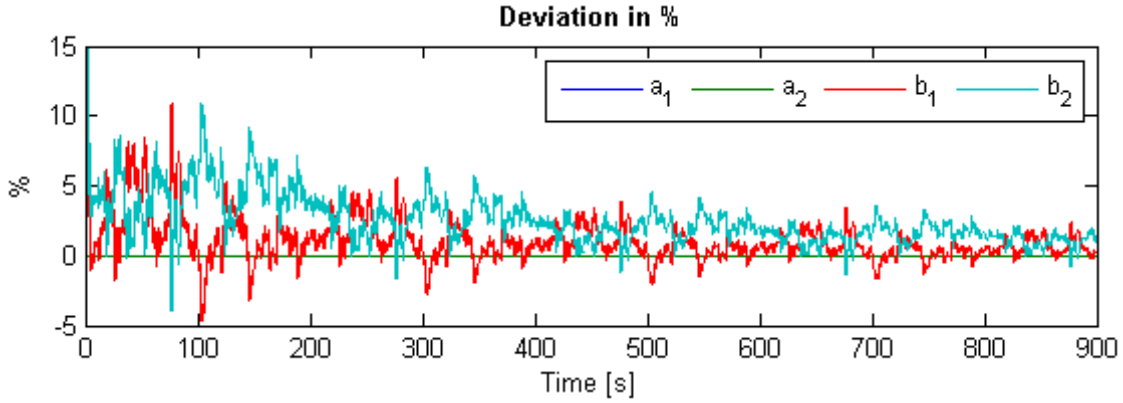

Fig. 5.26 Parameter deviation in % through simulation with added noise, filtered at 6 Hz

On notable thing is that it seems the deviations are getting smaller as the simulation run, even though the noise is the same repeated signal throughout the simulation, and the ideal parameters change uniformly. Fig. 5.27 shows the parameter estimation plotted against the ideal values.

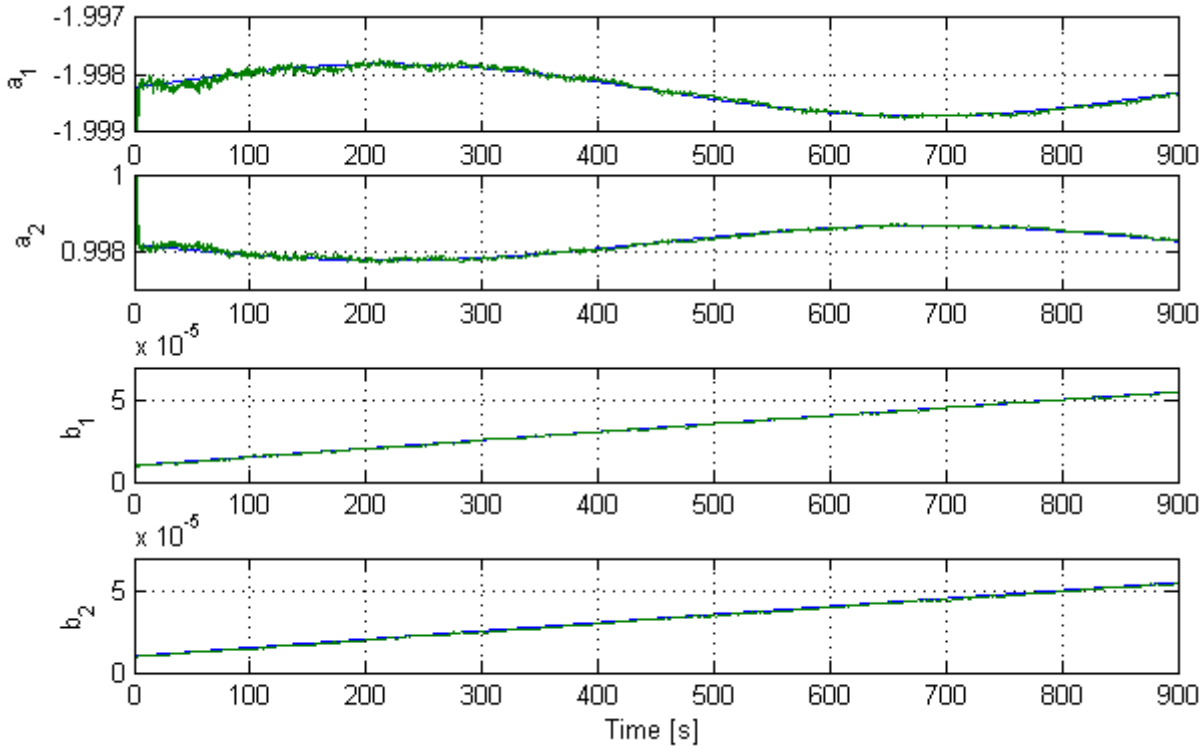

Fig. 5.27 Parameter estimations plotted with ideal parameters for comparison. The added noise is filtered with a 6 Hz filter

The estimation does seem to follow the ideal parameter very well but also seems very noise and changing. In order to quantify whether this estimation is accurate; the estimated system and the ideal systems natural frequency is compared on Fig. 5.28.

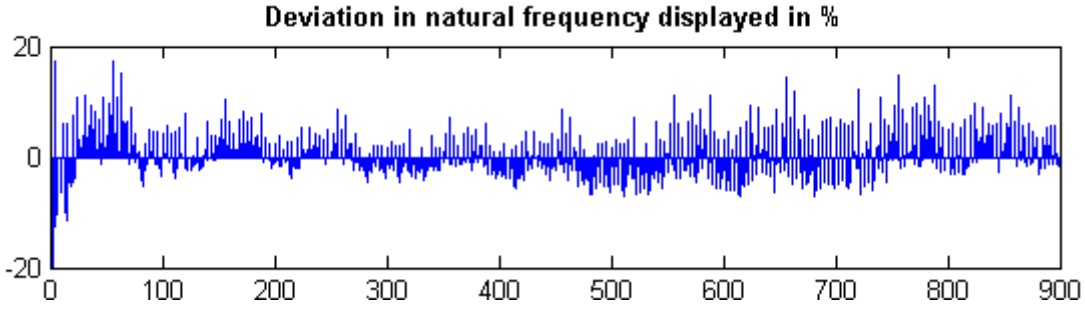

Fig. 5.28 Deviation in natural frequency compared to ideal system

The comparison is made in percentage and tells how big a deviation the estimated system has at a certain point in time. It seems the estimation at multiple points have deviations of up to 18 %. But the mean deviation of the graph (5-900 secods) is <1 ‰. The same comparison is made to check the systems zero-placement. This comparison is made as the zero placements are important for the system response also.

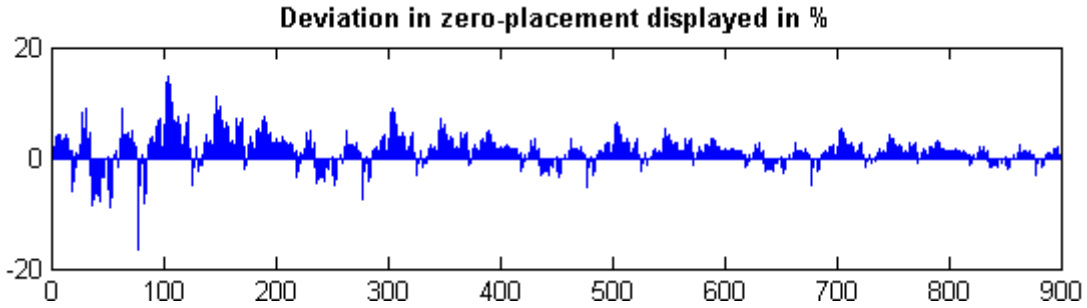

Fig. 5.29 Deviation in zero placement compared to ideal system

Again peaks of up to 15 % is present while the graph only has a mean deviation of <1 ‰. To examine whether these large peaks are acceptable and to make a visual representation, the two systems response is plotted against each other in Fig. 5.30.

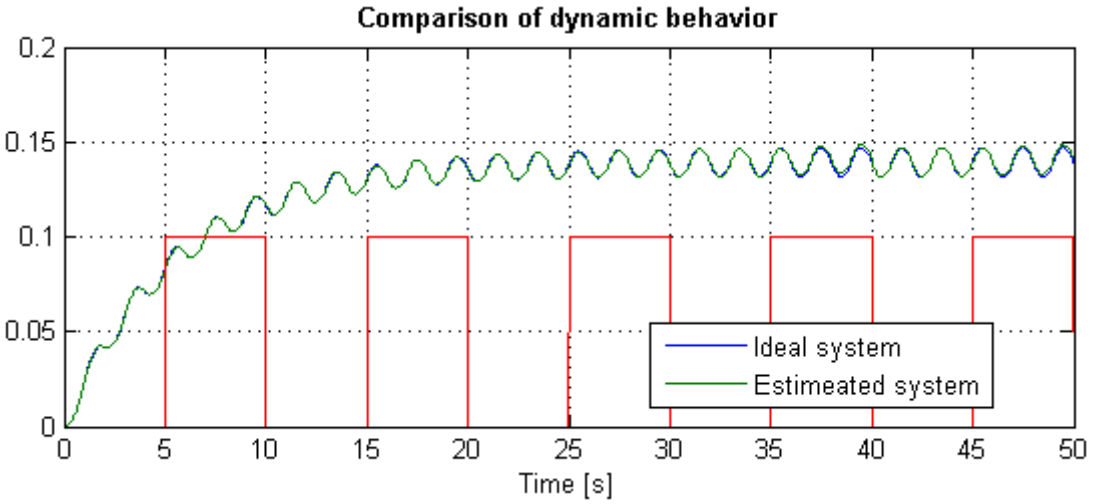

Fig. 5.30 Comparison of dynamic behavior using two plot methods

Fig. 5.30 also contains a square waveform. This waveform determines how the estimated systems response is plotted as described in Table 5.10.

Signal state	Plot method
High Value	The system is plotted using the equation: $\hat{d}(t) = b_1(t) \cdot \tau(t-1) + b_2(t) \cdot \tau(t-2) - a_1(t) \cdot \hat{d}(t-1) - a_2(t) \cdot \hat{d}(t-2)$ Hereby is the next estimated position a function of the last calculated position, the estimated parameters in the θ-vector and the excitation inputs. Hereby is the dynamic behavior tested. If the system has the same response during a longer interval the found parameters can be seen as representing the ideal system sufficiently.
Low value	The system is plotted using the equation: $\hat{d}(t) = b_1(t) \cdot \tau(t-1) + b_2(t) \cdot \tau(t-2) - a_1(t) \cdot d(t-1) - a_2(t) \cdot d(t-2)$ Hereby is the next estimated position a function of the last ideal systems position (d), the estimated parameters in the θ-vector and the excitation inputs (τ). This plot method check whether the θ-values are correct estimated.

Table 5.10 Plot methods used to examine dynamic behavoir

Both equations in Table 5.10 are derived from the simplified discrete model presented in (5.28). The input signal is the same square wave input signal as used in previous simulations.

As both graphs on Fig. 5.30 follow each other very close despite the change between the plot methods it must be concluded that the deviation in natural frequency is acceptable. It can therefore be concluded that noise in the dancer signal will disturb the algorithm too much to find suitable parameters. But a 6 Hz (or less) second order low pass filter seems plausible to make the algorithm converge.

The systems bandwidth is earlier found to 2 rad/s, at this frequency the 6 Hz filter will have a phase shift of -4 degrees which is found acceptable.

5.8 Estimation Tests with Web Winder

This section has the purpose of testing the RLS algorithm when implemented on the web winder. The algorithm is implemented in the dSpace system as illustrated on Fig. 5.31. In order to make the web winder function a controller needs to be implemented, which in these tests are done using a PID controller with the following gains:

- $k_P = 20$
- $k_I = 2$
- $k_D = 2$

This controller aims to wind the paper with a constant tension throughout the experiments. The gains are found by manually tuning the PID in such a way that it is able to regulate the winder through a full roll of paper. The manually tuned regulator does not necessarily have good performance, because this is

not the goal in this test, the goal is to validate whether the parameter estimation algorithm can converge sufficiently accurate. Therefore the PID regulator tuning will not be discussed further. In all the experiments the winder contains at least 200 meters of paper. The amount may vary above 200 meters due to paper replacements following paper failures. The experiments are run at a constant reference of 35 mm, while the unwinder accelerates from 50 RPM to 1000 RPM at 2 RPM/s.

The sections is based on the Simulink implementation of the parameter estimation algorithm as sketched on Fig. 5.31.

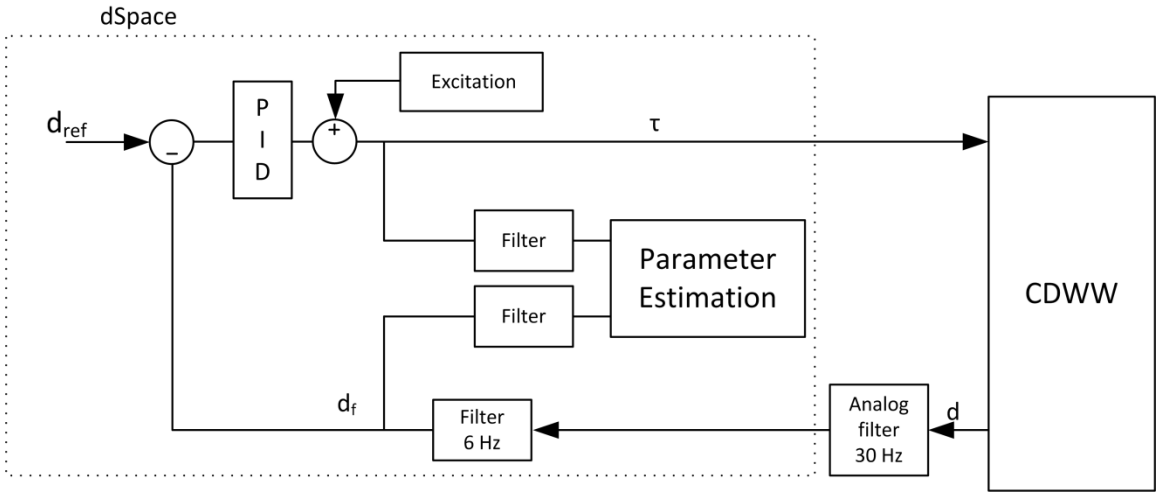

Fig. 5.31 Sketch of Simulink implementation in dSpace

The figure contains two unknown block elements, the excitation block and the filter blocks inserted on the estimation signals. The contents of these blocks will be the subject of the further analysis.

A 6 Hz second order low pass filter is also inserted, to filter the dancer position. This choice is based on the analysis in section 5.5 which found that a noise reduction is needed. It was found that a 6 Hz filter is necessary to make the system converge. It is also found that this filter gives a small and acceptable phase shift. This filtered position labeled d_f on Fig. 5.31 will in this section be referred to as the dancer position. The estimation filters are implanted on both the d_f and the τ signal as any noise present in the d_f also is assumed be present in the τ signal, due to the controllers P-term and if the reference is kept constant, which is the case through all the experiments.

The purpose of the following sections is to test various combinations of parameter estimation input filters, labeled *Filter* on Fig. 5.31, and excitation signals, labeled *Excitation* on Fig. 5.31, to find a combination which makes the parameter estimations as accurate as possible.

The estimation result will be refered to as *estimed parameters* or *the* θ*-vector*, which contains the four estimated parameters a_1, a_2, b_1 and b_2.

The results of the experiments are compared on basis of deviation between the measured dancer position (d_f) and the estimated position based upon the estimated model parameters. The d_f signal and the τ signal are therefore logged along with the estimated parameters during each experiment. When the experiment is finished, the parameters are evaluated offline.

The parameters are used to construct a time varying linear system which is excited with the measured τ signal from the experiment using Simulink. The comparison is made using the following three methods:

- **Continuous method**
  - Compares the position error when the parameters are updated continually
  - Tests the algorithms ability to estimate the position correctly based on the measured τ and d_f signal. This position error is equivalent to the parameter estimation error e.

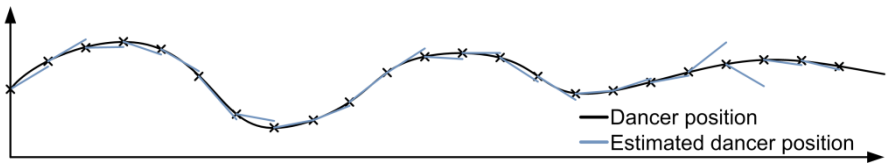

Fig. 5.32 graphical illustration of continuous method, X marks θ updates.

- **Interval method**
  - Compares the position error when the θ-parameters are sampled every 10 seconds and held constant until next sample.
  - Tests the algorithms ability to estimate the position correctly based on the measured τ signal and its own output during 10 seconds intervals. This method can generate excess errors if the parameters are sampled simultaneously with a deviation in the parameter estimations when the next 10 seconds is based on this value.

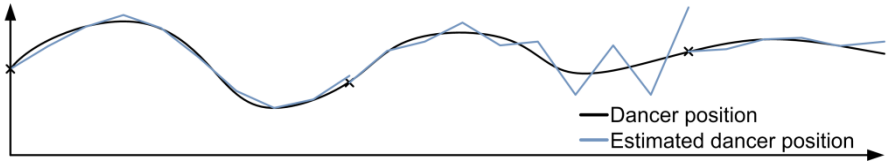

Fig. 5.33 graphical illustration of the interval method, X marks θ updates.

- **Interval method with mean**
  - Compares the position error when the parameters are sampled every 10 seconds, based on a 5 seconds mean value, and held constant until next sample
  - The method does essentially the same as the previous but calculates a mean values based on the 5 seconds before the parameters are sampled and held. This should remove the problem with unfortunate parameter samples.
- **Largest oscillation**
  - When signal excitation is employed the system is disturbed by this signal which in some cases is large enough to make the dancer oscillate. As oscillations are unwanted this comparison show much the excitation disturbs the system.

If the estimated parameters are correct, the deviation should be zero. If the parameters are wrong, and the estimated model is excited with the same input signal as the winder is, the estimated position should deviate largely.

5.9 Estimation Test with Various Filters

The test has the purpose of evaluating whether the web winders dynamic behavior can be estimated correctly using the parameter estimation algorithm and various filters. Ideally should the algorithm work without filters but based on the experience gathered in section 5.7 the system suffers from noise in the dancer measurements which disturbs the estimation. The filters are implemented as illustrated on Fig. 5.34, where the arrows across the filter blocks, indicates that the filters are varied between each experiment.

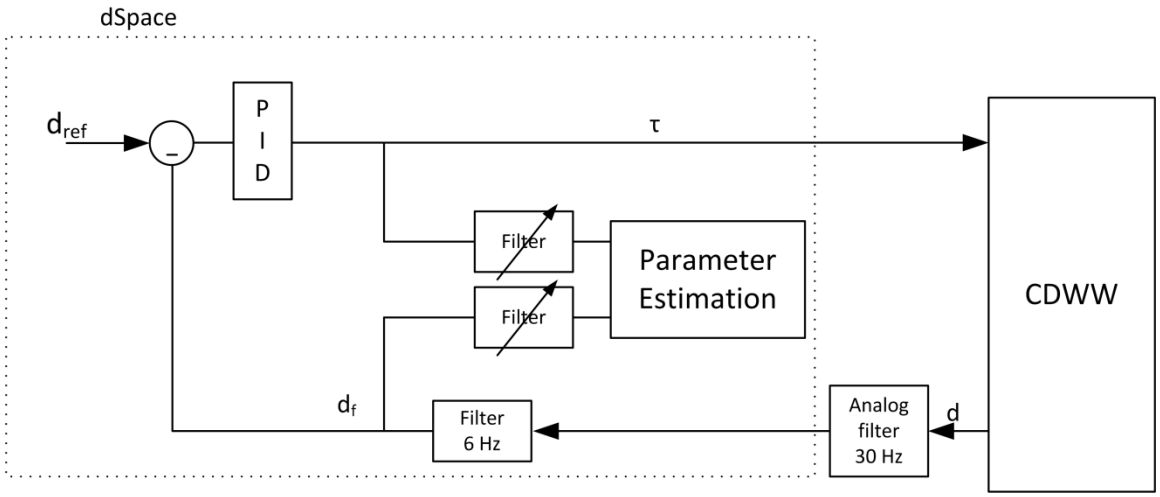

Fig. 5.34 Sketch of estimation test with varying filters

The test is divided into 4 experiments with 4 different filters. First a test without filters, then three experiments with second order low pass filters with filter frequencies of 2, 4 and 6 Hz. The four experiments are stated in Table 5.11.

	Filter	Continuous	Interval		Interval with mean		Osc.
		RMS [%]	Peak [%]	RMS [%]	Peak [%]	RMS [%]	[mm]
Exp1	No filter	4 ‰	-	-	-	-	-
Exp2	2 Hz	<1 ‰	20/-18	2.9	20/-19	2.9	1.5
Exp3	4 Hz	<1 ‰	17/-17	3	17/-17	3.1	1.5
Exp4	6 Hz	<1 ‰	68/-56	7	52/-52	7	1.5

Table 5.11 Estimation results with different estimation filters

Experiment 1 does not converge at all and produces extreme deviation, which renders this solution not working. The three filter experiments agrees that the lower filter frequency, the lower RMS deviation. The peak deviations are also small for the 2 and 4 Hz filter compared to the 6 Hz filter. The deviation of 1.5 mm is normal for the web winder and is mainly consisting of filtered noise signals.

The 2 Hz filter is chosen for further analysis as this is the filter which generates the smallest deviations while still having a good dynamic performance. This is concluded by comparing the three filter experiments which is shown in appendix H.

The results from the 2 Hz experiment is commented in the following, starting by displaying the estimated θ-parameters on Fig. 5.35.

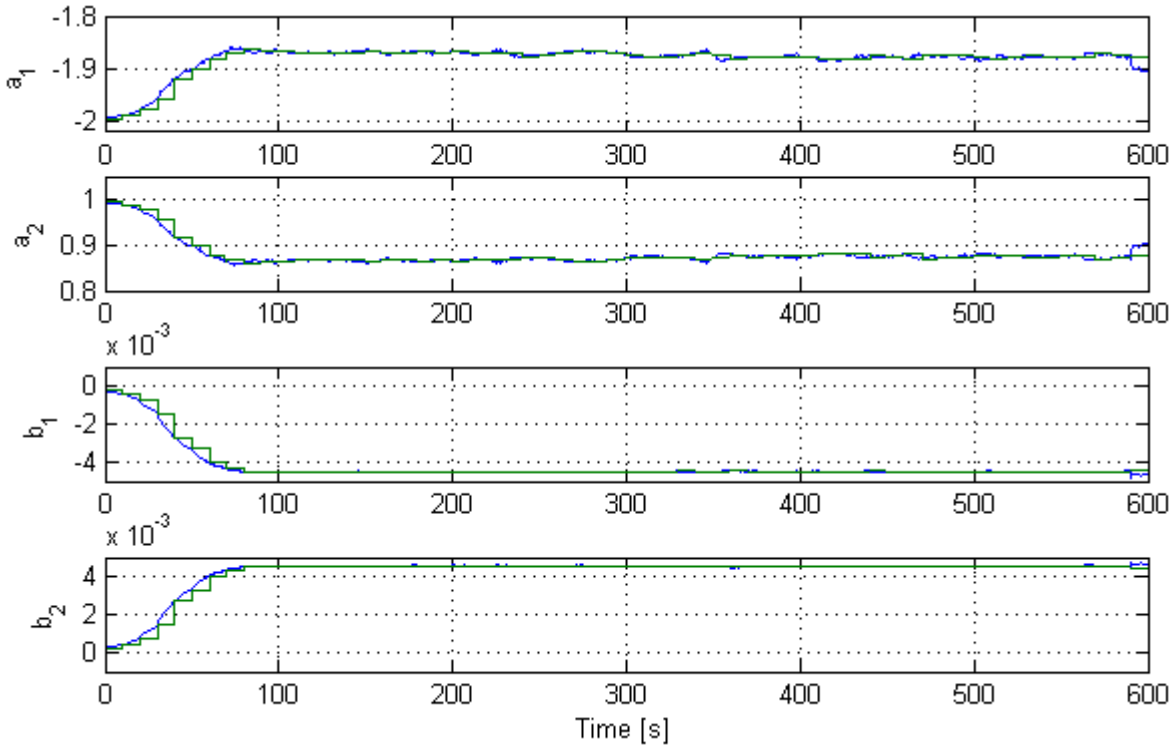

Fig. 5.35 Estimated parameters (blue) and sampled parameters (green) during experiment 2.

Other than the estimated θ-parameters, Fig. 5.35 also display the sampled θ-parameters used to the interval comparison. This comparison is made to show that these two set of parameters does not deviate from each other. The θ-parameters used for the interval comparison *with mean* is left out as these parameters are very close to the plotted interval-parameters.

To show whether the estimated parameters seem correct, is the deviation between the output from the interval comparison and the measured dancer position plotted in percentage in Fig. 5.36.

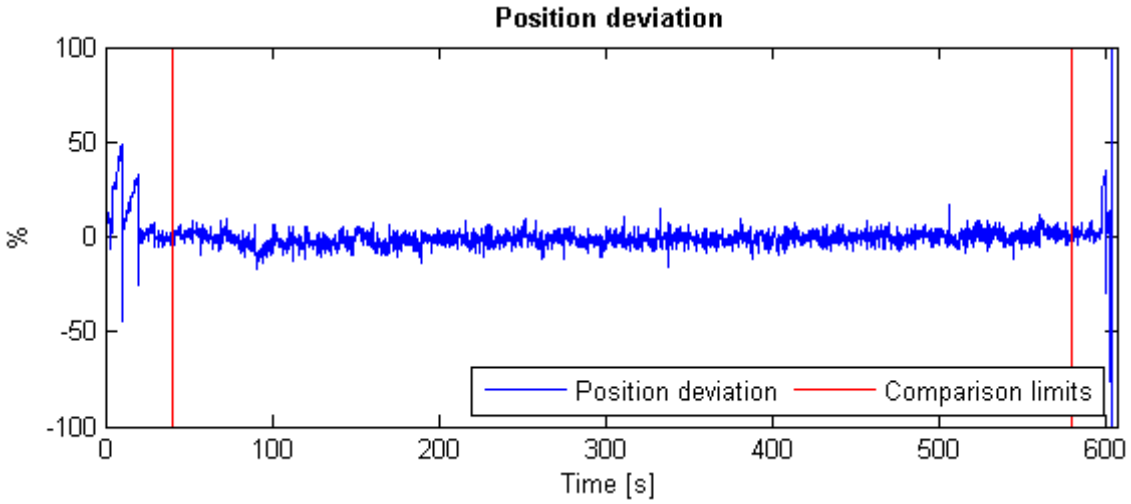

Fig. 5.36 Dancer position deviation based on the interval method, in percentage during experiment 2

The comparison on Fig. 5.36 has small deviations but it should be noted that this comparison method only compares the actual dancer position with the theoretical position based on the estimation values.

This test does only partly indicate whether the dynamic behavior is accurate. It is also seen that the position deviation is small at e.g. 50 s. but the θ-parameters at this point is not at their settled level yet.

The red vertical lines indicates the section within which the RMS and peak deviation results in Table 5.11 are determined. The sections before and after are neglected as the algorithm needs time to converge at start, and that not all experiments takes equal time to conduct. Therefore are these limits introduced to create an equal comparison basis between experiments.

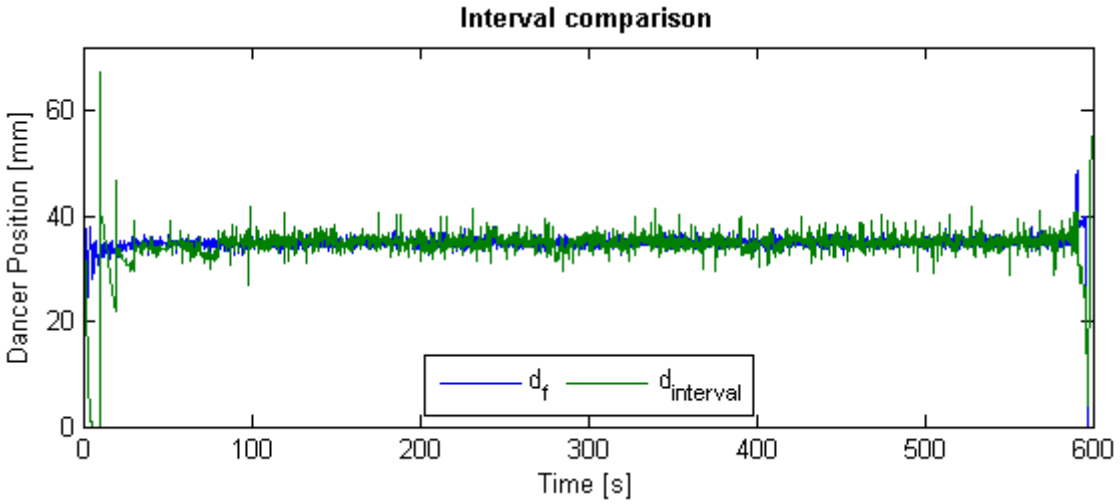

Fig. 5.37 Dancer position comparison made using the interval method during experiment 2

Fig. 5.37 shows the comparison between estimated dancer position and the measured dancer position. This comparison is essentially the same as the on Fig. 5.36, istead of percentage it is compared in dancer position, which enables graphical comparison of the dynamic behavior for the reader.

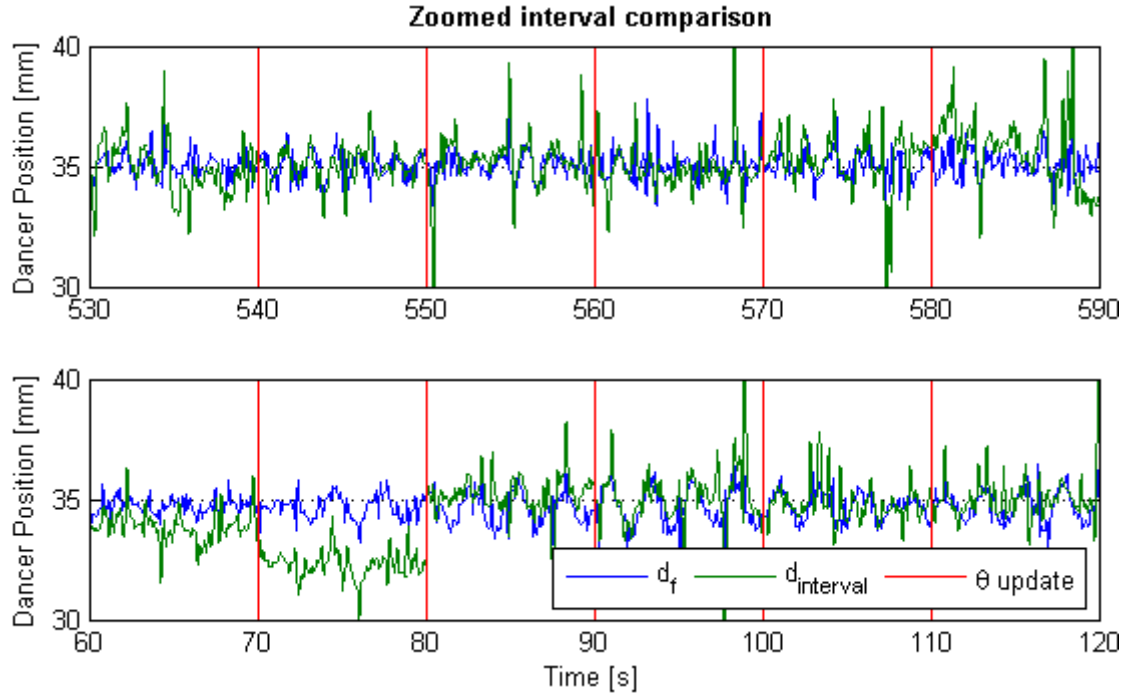

Fig. 5.38 Shows a zoomed comparison of dancer position using the interval method

To better estimate the dynamics visually, a zoom comparison is made on Fig. 5.38 where zoomed section of the data already displayed in Fig. 5.37 is displayed. The plot is divided into two subplots, the top plot is the section of the experiment which the project group estimates as the best fit. The bottom graph is the section which the project group finds most diverting.

At first glance does the zoom comparison does seem good, with accurate signal frequency, phase and amplitude. But with the exception of large spikes, and some sections offset errors in the worst case plot.

But it should be noted that the theory in section 5.1.5 states the estimation algorithm should estimate poorly when the system is in steady state, as no signals excites the system dynamic behavior. This is the case in this experiment as the system is in steady state with the dancer held at a constant position. The only signals present to excite the dynamics is the induced noise and the PID controllers attempts to counter act noise and disturbances.

With this in mind the zoomed comparison actually only shows the algorithms ability to correctly estimate the systems steady state gain and the dynamics of its noise. It is therefore too early to conclusively decide whether the algorithm works. But these experiments show that the smaller filter frequencies the smaller errors. But dynamic behavior in the range of $^{+}/_{-}$ 1.5 mm around the reference could as easily be noise as actual dancer movement.

5.10 Estimation Test with Added Square Wave Signal

This test has the purpose of testing whether the addition of an excitation signal can improve the estimation accuracy by exciting the systems dynamics. From section 5.1.5 it is suggested that excitation is necessary in order to make the algorithm estimate the system dynamic behavior correctly. A square wave signal is chosen because this signal excites maximum dynamic behavior.

Fig. 5.39 shows a sketch of the estimation system as implemented in dSpace. The square wave excitation signal is added between the PID controller and the estimation algorithms τ-measurement point. The found filter value of 2 Hz is implemented before the parameter estimation block.

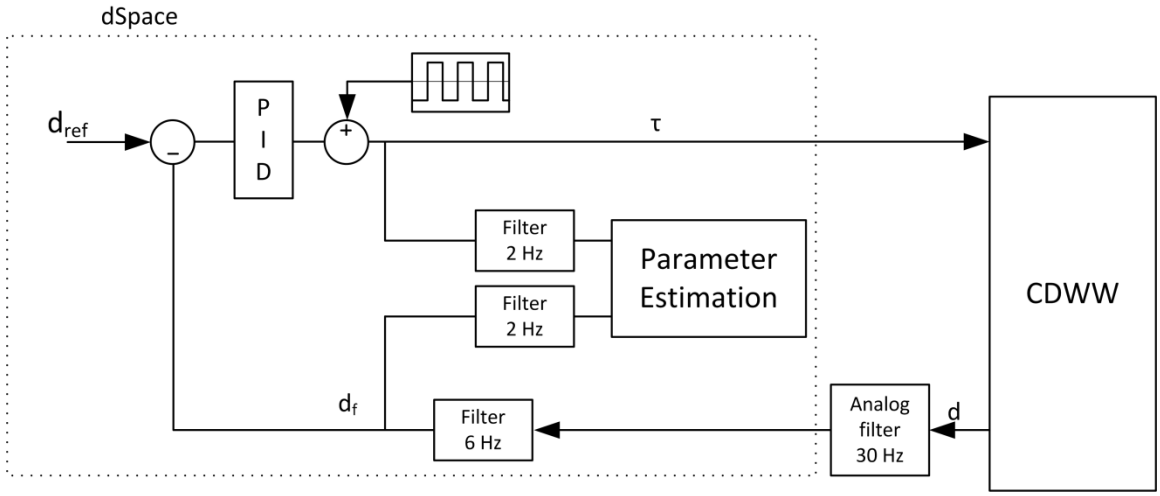

Fig. 5.39 Sketch of the dSpace program

The experiment is run at a constant reference, while the unwinder accelerates from 50 RPM to 1000 RPM at 2 RPM/s. the PID controller is the same as used in previous experiments with k_P = 20, k_I = 2 and

k_D = 2. Every experiment is stopped after at least 180 meters of paper has been wound. The complete roll contains 200 meters of paper but 10 meters at each end is used as buffer, so the paper does not roll off the unwinder roll.

Nine experiments are conducted based on 3 different square wave amplitudes and 3 different periods. The square wave period is the time from one rising edge and until the next.

In order to compare the different test result numerically a result table has been made, shown on Table 5.12 which also shows the excitations signals period and amplitude in each experiment. The three periods and amplitudes are estimated by the project group on basis of initial tests which showed these intervals interesting.

	Signal		Continuous	Interval		Interval with mean		Osc .
	Period [s]	Amp [Nm]	RMS [%]	Peak [%]	RMS [%]	Peak [%]	RMS [%]	[mm]
Exp5	1s	0.025	<1 ‰	55/-60	8.8	85/-84	9.5	1.5
Exp6	1s	0.05	<1 ‰	32/-73	6.5	32/-73	6.4	1.5
Exp7	1s	0.075	<1 ‰	34/-111	8.8	27/-106	8.3	2
Exp8	2s	0.025	<1 ‰	180/-177	16.7	112/-152	12.7	7
Exp9	2s	0.05	<1 ‰	85/-140	10	65/-120	8.9	10.5
Exp10	2s	0.075	<1 ‰	56/-85	11.4	73/-95	12.4	22
Exp11	3s	0.025	<1 ‰	185/-153	14.7	151/-72	10.4	5
Exp12	3s	0.05	<1 ‰	39/-133	12.2	37/-135	12	10
Exp13	3s	0.075	<1 ‰	58/-108	11.5	57/108	11.3	12

Table 5.12 Excitation signal properties and experiment results

From the table, the following relations can be observed:

- Longer excitation period produces larger RMS deviations
- Higher deviations in general compared to no excitation

From the deviations point of view, this excitation signal is not improving the estimation as the RMS deviations is higher than the deviation in the unexcited experiments. But in fact, as later discussed at Fig. 5.43, the dynamic behavior is improved.

Based on the results in Table 5.12 no clear detectable pattern is found, the best results is therefore based on the interval test method to detect which excitation signal gives the best estimation result. Appendix H contains all the experiment plots which is the foundation for this experiment. If a true pattern where to be detected a lot more experiments where to be conducted, but as the purpose of this test is to show that excitation in fact improves the estimation performance experiment 6 is chosen as the best excitation signal using square waves.

To see how much the excitation improves the estimation, the experiment with the worst result (experiment 12) is displayed. Later will the best experiment (experiment 9) be displayed to show how a variation of the excitation signals period and amplitude affect the estimation results.

Fig. 5.40 shows the development in θ-parameters during experiment 12. Besides the θ-parameters is the sampled θ-parameters used for the interval comparison also plotted in order to show that these does not deviate largely from the original θ-values. The θ-parameters used for the interval comparison *with mean* is left out as these parameters are very close to the interval-parameters.

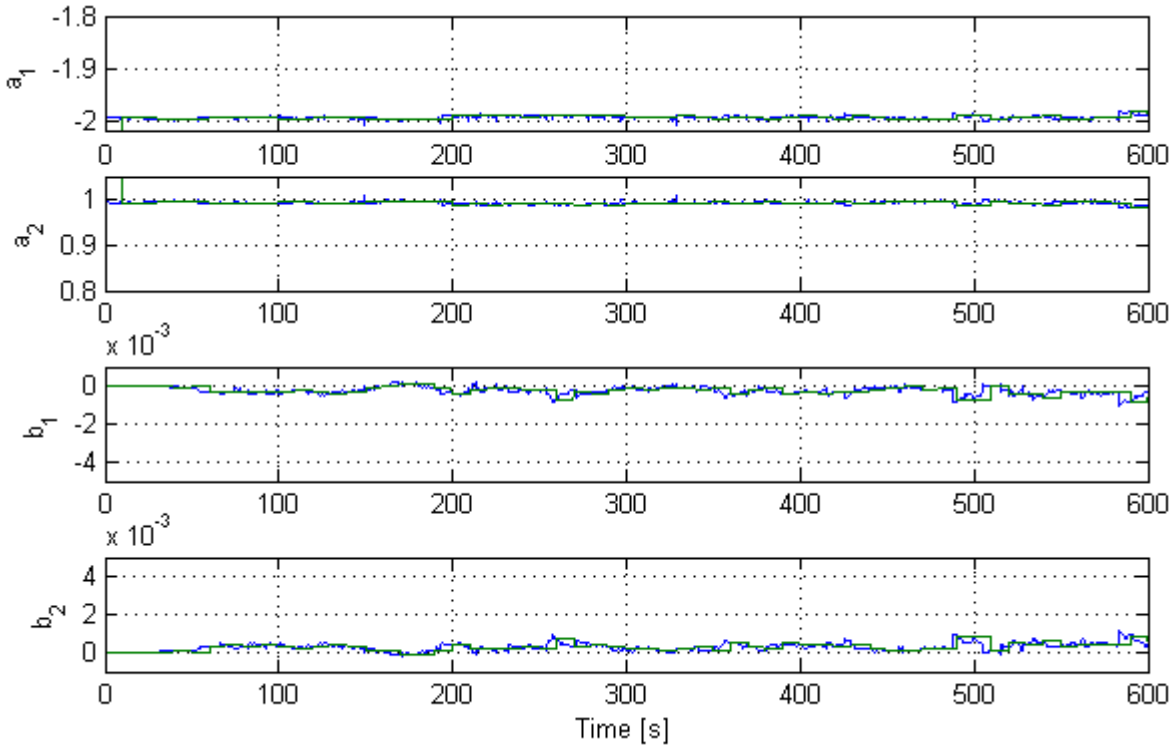

Fig. 5.40 Estimated parameters during experiment 12. Blue indicates the estimated values, green is the sampled and held values.

Fig. 5.40 shows the parameters being stable and over all continuous, but with small glitches or spikes. These spikes are unwanted as they later will cause the adaptive regulators to act as if the system suddenly changes behavior.

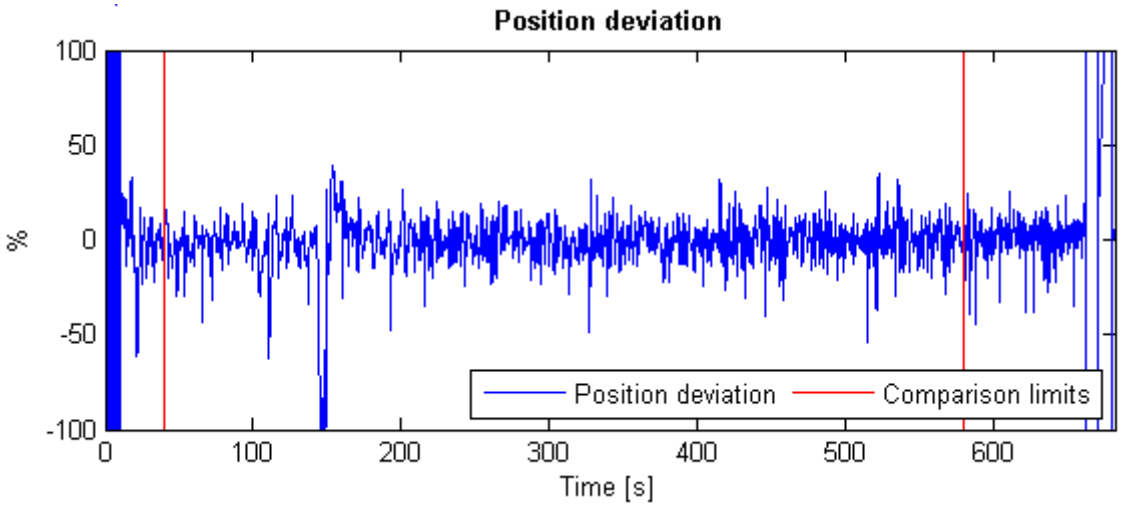

Fig. 5.41 Dancer position deviation based on the interval method, in percentage during experiment 12

Fig. 5.41 shows the comparison between the estimated dancer position based on the interval method and the actual measured dancer position. The interval method is based on sampling the found θ-values every 10 seconds and using these as parameters in the system model. The model with these parameters is then excited with the measured torque input which the Web winder also experienced during the experiment. The peak error and RMS error in Table 5.12 is based on Fig. 5.41.

The first 40 seconds and the data beyond 600 seconds are discarded in the comparison. The reason for this is the estimation algorithms need to initial settle, and the variation in unwinder speed in comparison to later experiments making later experiments shorter. Therefore data beyond 600 seconds is discarded to make the comparison most fair.

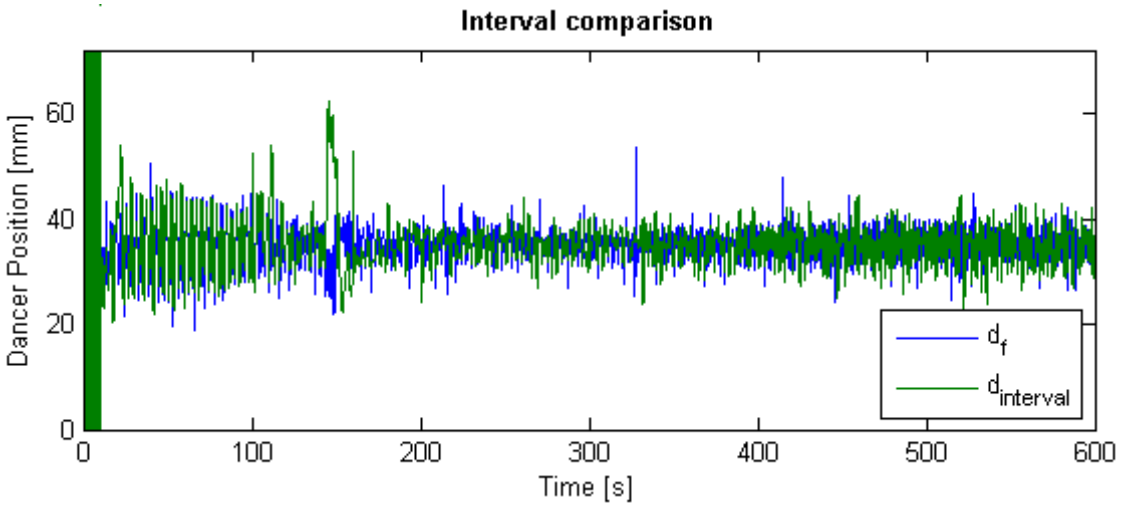

Fig. 5.42 Comparison between dancer position and estimated dancer position using interval method during experiment 12

Fig. 5.42 compares the estimated dancer position using the interval method with the actual dancer position. This plot essential shows the same comparison as Fig. 5.41 but in position instead of percentage. In this plot is possible to estimate the accuracy of the estimated systems dynamic behavior.

Fig. 5.43 shows zoomed sections of the data presented on Fig. 5.42 for better visual comparison.

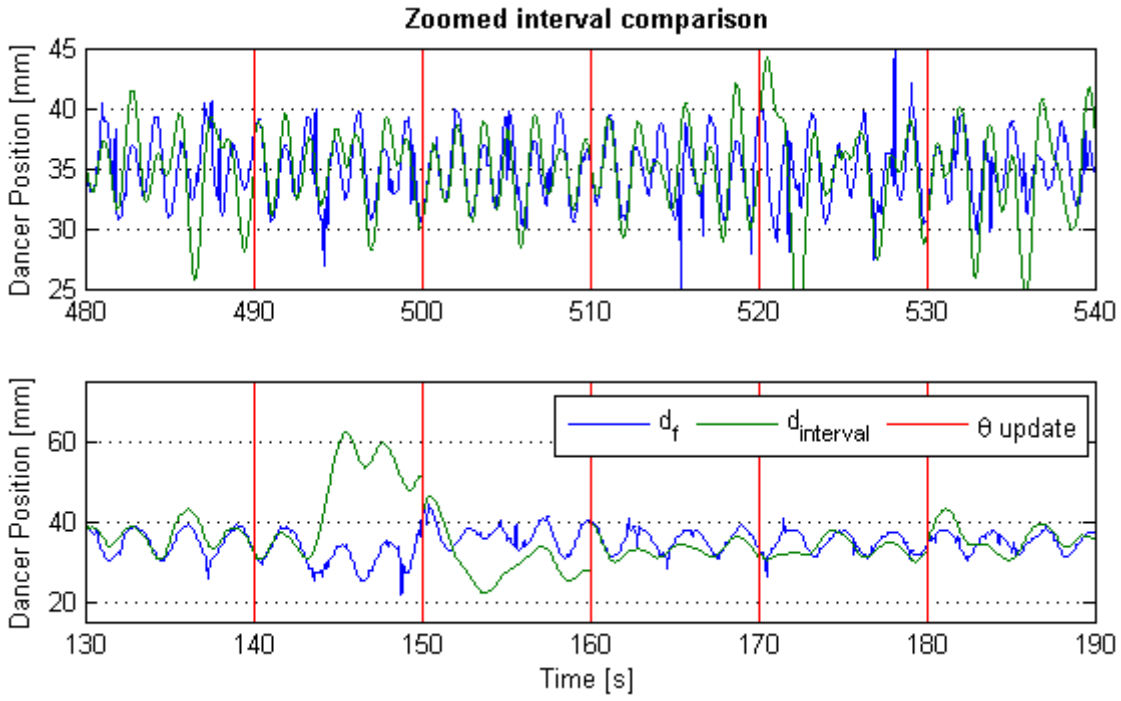

Fig. 5.43 Zoomed dancer position comparison using the interval method, during experiment 12

The top graph of Fig. 5.43 shows a portion of the experiment where the dancer position is best estimated. The bottom graph show a portion where the estimated behavior is worst. The sections are chosen by the project group. The vertical lines indicate where the θ-values are sampled and renewed.

I should be noted that the frequency and phase shift fits in both best and worst case. But the amplitude is deviating multiple places. In the following is the same graphs presented for experiment 9 for comparison. Experiment 6 is the experiment in the square wave test with the smallest deviation.

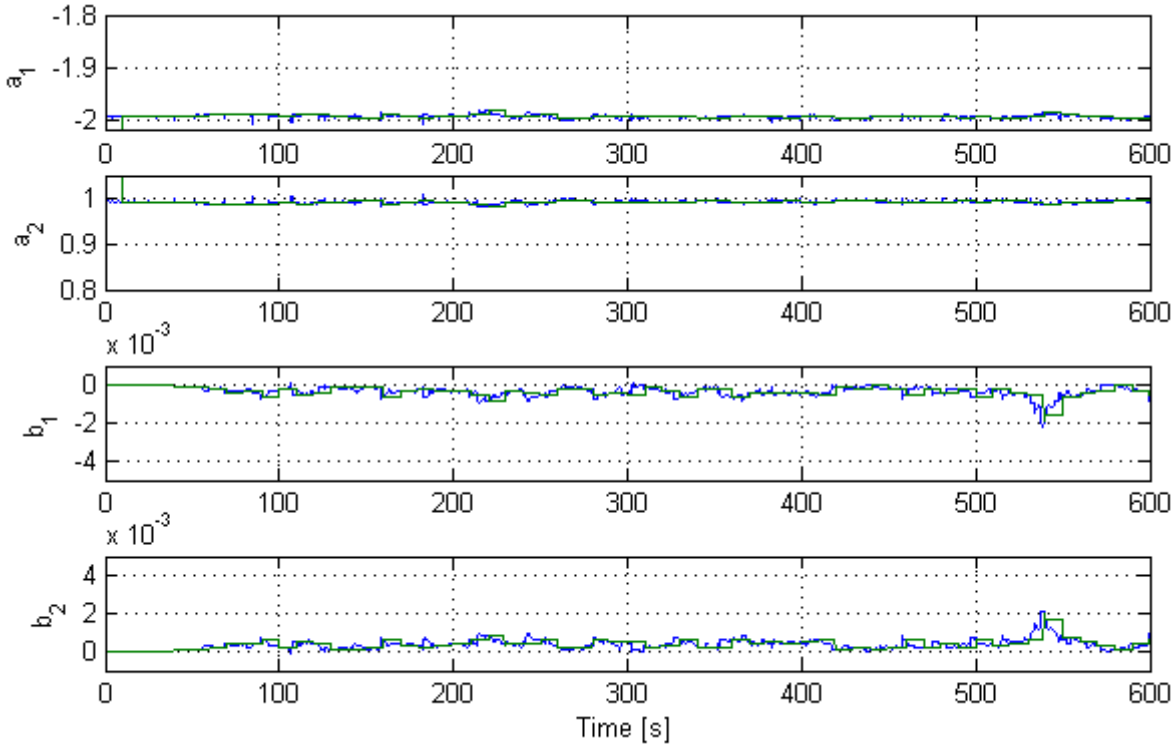

Fig. 5.44 Estimated parameters during experiment 9. Blue indicates the estimated values, green is the sampled and held values.

The estimated parameter looks like the parameters from experiment 12 in the sense that they keep a steady level but experiences glitches and sudden changes.

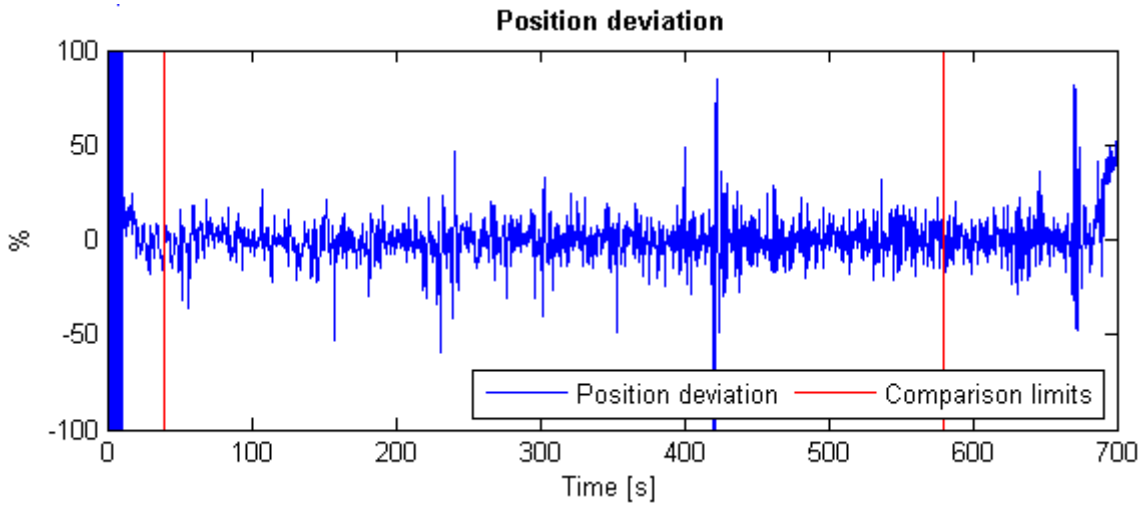

Fig. 5.45 Dancer position deviation based on the interval method, in percentage during experiment 9

The position deviation is smaller than experiment 12, with exception of an error at around 420 seconds. But the experiment still has the lowest RMS deviation in the test.

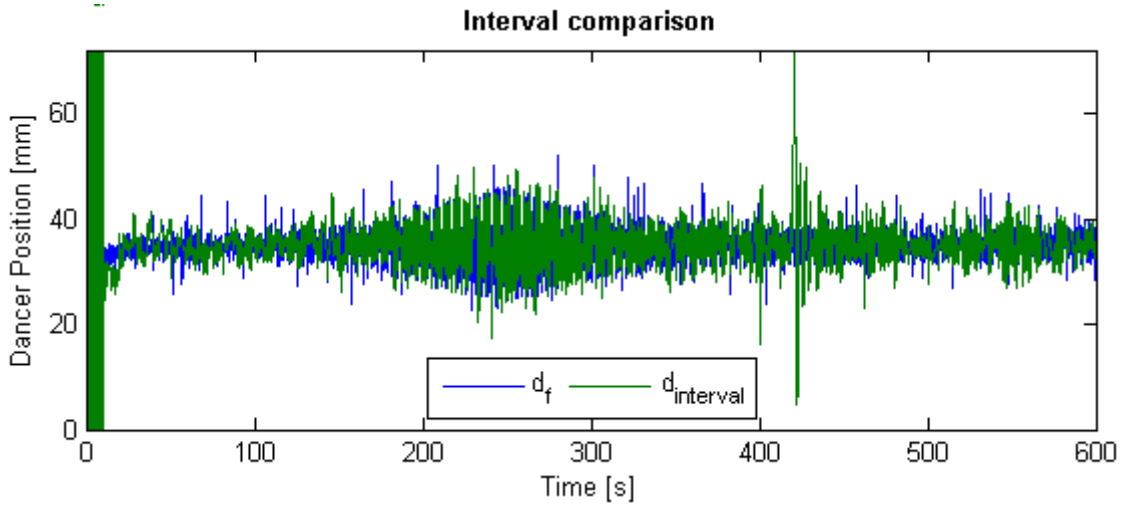

Fig. 5.46 Comparison between dancer position and estimated dancer position using interval method during experiment 9

From the position comparison on Fig. 5.46 it seems that the algorithm estimates most like the measured data if the dancer position experiences large oscillations, as the case is from 200 to 300 seconds.

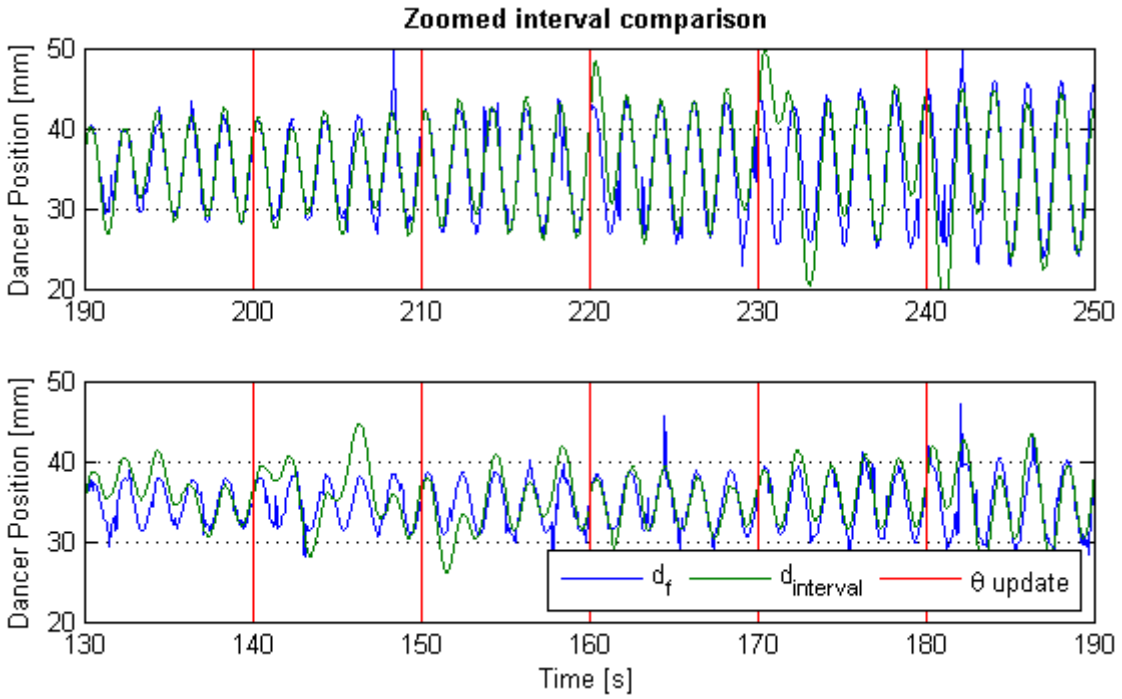

Fig. 5.47 Zoomed dancer position comparison using the interval method during experiment 6

Fig. 5.47 shows zoomed sections of the dancer position comparison. The top graph is the best case the bottom case shows a portion of the data which the project group has chosen as the worst case. Both best and worst case sections have matched the frequency and phase shift in the dancer signal almost perfectly. In the best case the amplitude is correct except for the time immediately following the last

three θ-updates. The worst case has general amplitude problems throughout the graph. But in each case the model quickly converges against the actual behavior.

Over all does the excitation using square waves improve the parameter excitation as the estimated dynamic behavior is improved in comparison to the unexcited tests performed in section 5.9. But the estimated parameters seem to suffer from sudden changes and glitches. And the deviations have large peaks. It is therefore tested if other signals might improve the performance further.

5.11 Estimation Test with Added Sine Signal

This section has the purpose of testing whether a sine signal does improve the performance of the parameter estimation algorithm. A sine signal is chosen for its simplicity and being a continuous signal. This may be an advantage as the estimation signals (d_f and τ) both are being filtered before the estimation block as shown on Fig. 5.48. A sine signal will have the same form after passing the filters whereas the square wave signal will experience "ramping". And hereby will the estimation algorithm and the web winder receive significant different signals.

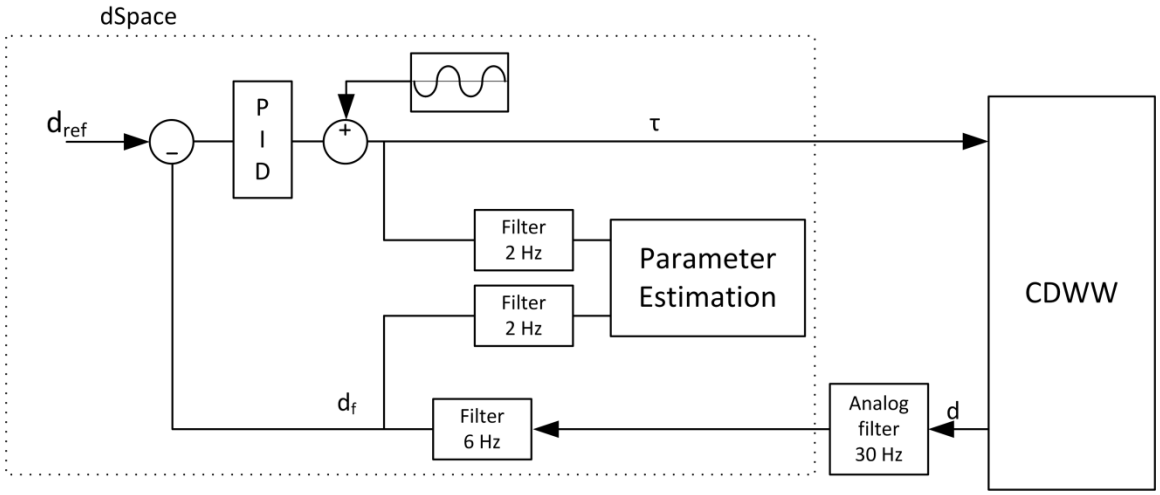

Fig. 5.48 Sketch of the dSpace program with added excitation

This test is divided into two sections. First is 4 different sine signals tested, by adding them as the excitation signal as shown on Fig. 5.48. Each of the four signals has the same frequency but different amplitudes as shown in Table 5.13. The best amplitude will be chosen for at later test where the amplitude is held constant and the frequency is varied.

A set of initial test is conducted by the project group in order to asses 4 $^{rad}/_{s}$ as a good initial frequency for the amplitude test. The results of the tests are shown in Table 5.13.

	Excitation		Continuous	Interval		Interval with mean		Osc.
	Freq	Amp	1 ‰	Peak	RMS	Peak	RMS	
Exp14	4 rad	0.5	1 ‰	37/-37	3.1%	46/-46	3.1	13 mm
Exp15	4 rad	0.03	1 ‰	14/-21	2.8	14/-21	2.8	8.5 mm
Exp16	4 rad	0.02	1 ‰	14/-17	2.6%	14/-17	2.6	6 mm
Exp17	4 rad	0.01	1 ‰	13/-12	2.6%	12/-12	2.5	3 mm

Table 5.13 Results from experiments with different sine amplitudes added as excitation signal

The comparison is made on basis of the same three methods as the square wave signal. The continuous plot method which tests the estimated dancer accuracy on basis of the estimated θ-parameters, and the d_f and τ signal measured during the experiment. The interval plot method; which samples the θ-values every 10 seconds and plots the estimated response and plot the estimated dancer position on basis of these estimated θ-values and the τ signal measured during the experiment. The interval plot method with mean; this method is essentially the same as the *interval method*, the only difference is that a mean θ-values is calculated on basis of 5 seconds preceding data.

And finally the largest position deviation from the reference is stated in the results table to indicate how much the added signal disturbs the system.

By first comparing the results in Table 5.13 with the results found from using square wave signal as excitation (Table 5.12) it appears that the sine signal has reduced both the deviation peaks and the RMS errors significant.

From Table 5.13, a relation between higher amplitude and larger error can be observed, which makes an amplitude of 0.01 Nm preferable, but by comparing the dynamic behavior graphically (see appendix H) experiment 17 has tendencies resembling the tests without excitation stated in section 5.9. Here the position error was shown to be small but the dynamic behavior was governed by noise. This indicates that 0.01 might be too small a signal to influence the estimation positively, as it does not create significant dancer output.

An amplitude of 0.02 is therefore chosen for further analysis. Experiment 16, which tests this amplitude, has the smallest error and still an acceptable estimation of the dynamic behavior. This is also the experiment with the smallest oscillations as seen from Table 5.13. The results from experiment 16 are shown on Fig. 5.49, Fig. 5.50, Fig. 5.51 and Fig. 5.52.

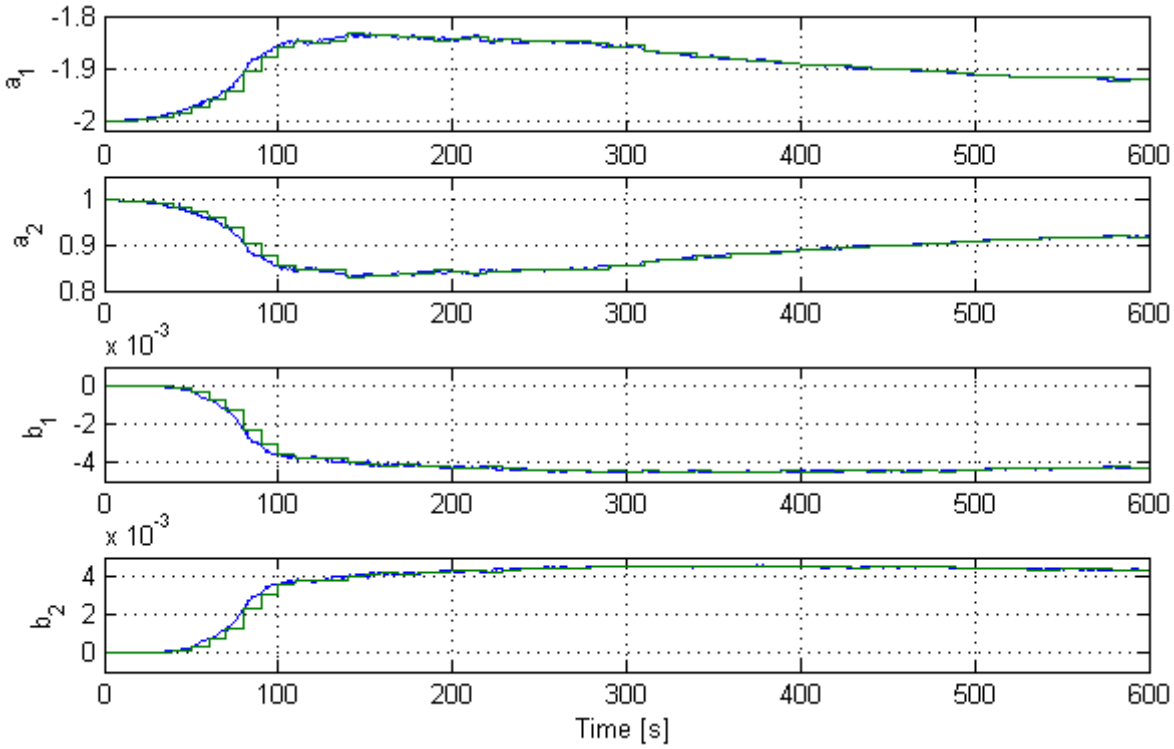

Fig. 5.49 Estimated parameters during experiment 16. Blue indicates the estimated values, green is the sampled and held values

The sine signal has, compared to the square wave signal, drastically reduced the glitches in the parameters. The parameters now seem to change smoother.

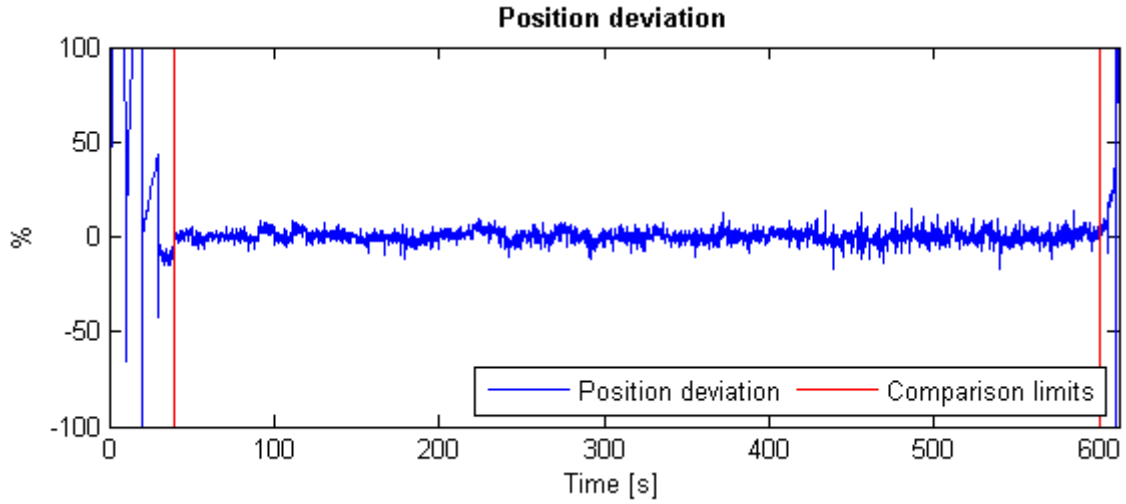

Fig. 5.50 Dancer position deviation based on the interval method, in percentage during experiment 16

The position deviation is also very small and without large peaks.

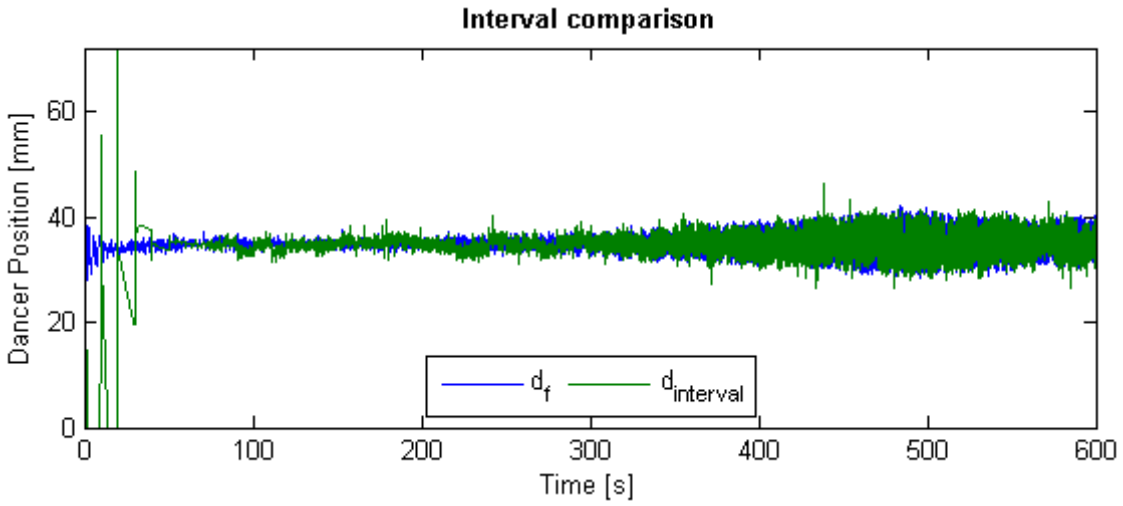

Fig. 5.51 Comparison between dancer position and estimated dancer position using interval method during experiment 16

The position plot on Fig. 5.51 indicates good estimates from around 90 seconds and until the end. But the system does not seem to estimate correct from 40 seconds and up to 90 seconds. A zoomed comparison is made on Fig. 5.52

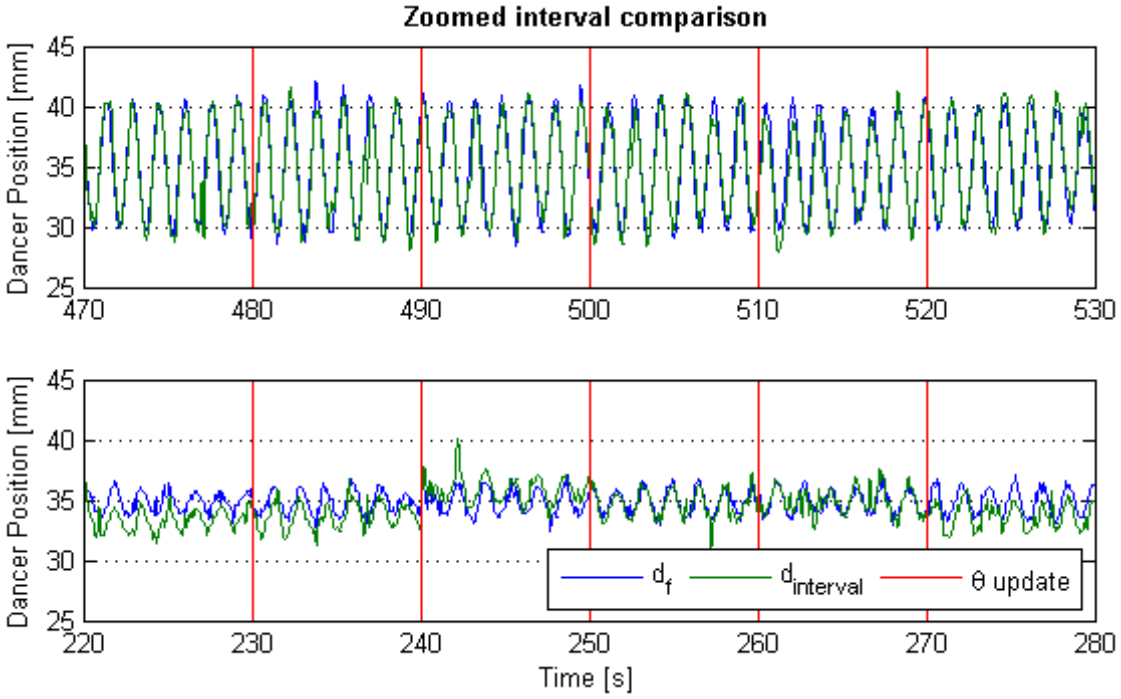

Fig. 5.52 Zoomed dancer position comparison using the interval method during experiment 16

The top graph in Fig. 5.52 show the portion of the comparison with the best accuracy. The bottom graph shows the section with the worst accuracy. Both intervals are chosen by the project group.

Both graphs on Fig. 5.52 have correct frequency and phase. The amplitude on the top graph deviates only slightly from the measured data. But the amplitude on the bottom graph seems to suffer from small offsets, but the estimate is still exact and found acceptable. The amplitude of 0.02 is therefore chosen for the further analysis of varying excitation frequency.

Table 5.14 contains 5 experiments with the same amplitude of 0.02 Nm but varying frequency in steps of 2 rad/s.

	Excitation		Error		Error with 5 s mean		Osc.
	Freq	Amp	Peak	RMS	Peak	RMS	
Exp18	2 rad	0.02	23/-34	4.5	23/-34	4.5	8 mm
Exp19	4 rad	0.02	27/-30	4.6	27/-30	5	5 mm
Exp20	6 rad	0.02	15/-17	2.9	15/-18	2.9	2.2 mm
Exp21	8 rad	0.02	15/-25	4	23/-29	4.3	1.5 mm
Exp22	10 rad	0.02	12/-15	3.2	12/-15	3.3	1.5 mm

Table 5.14 Results from experiments with different sine frequencies added as excitation signal

The experiments are compared in the same way as the previously excitation tests.

From Table 5.14 the lowest RMS and peak deviation occur at 6 rad/s, but the smallest dancer oscillation occurs at 8 and 10 rad/s.

By analyzing experiment 21 and 22 it is found that the dynamic behavior is poorly estimated, as seen earlier in the unexcited experiments. 6 rad/s and 2 Nm is therefore found as the best excitations signal in this badge of tests. A small amount of dancer oscillation will be accepted in favor of better estimation of dynamic behavior.

The rest of the analysis will concern the test results from experiment 20.

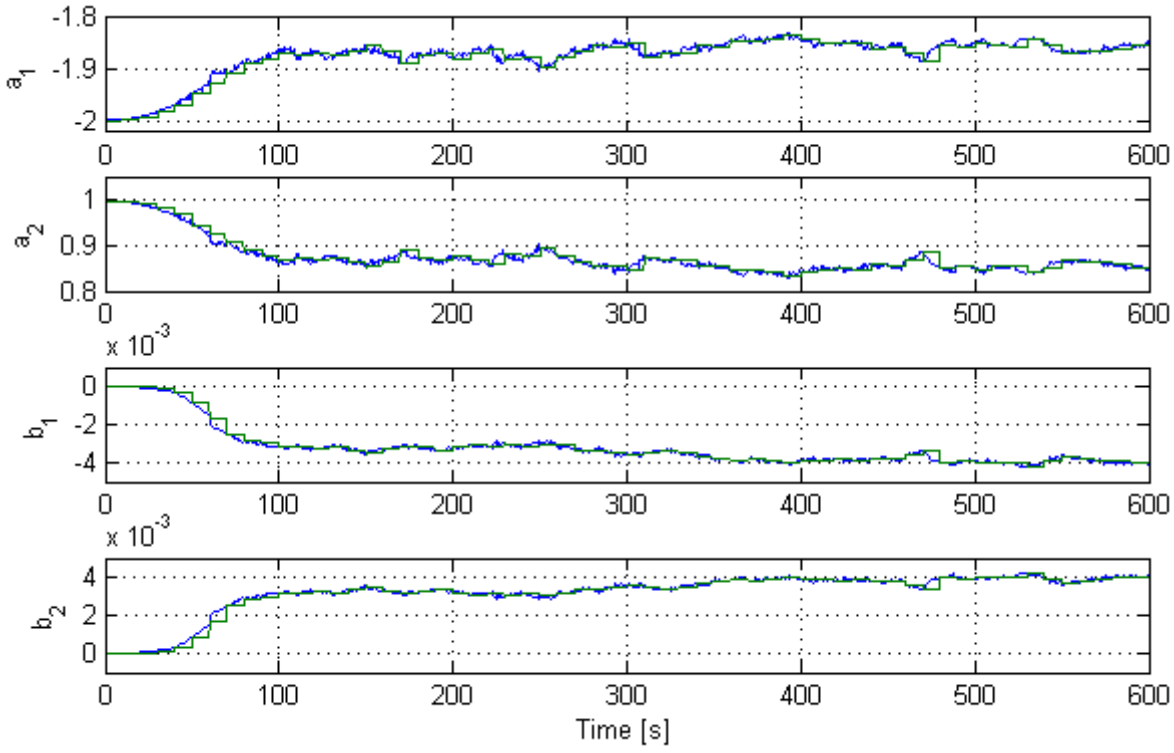

Fig. 5.53 Estimated parameters during experiment 20. Blue indicates the estimated values, green is the sampled and held values

The estimated parameters seem to fluctuate a bit more than in experiment 16 but still seem more continuous than when excited with square wave signals.

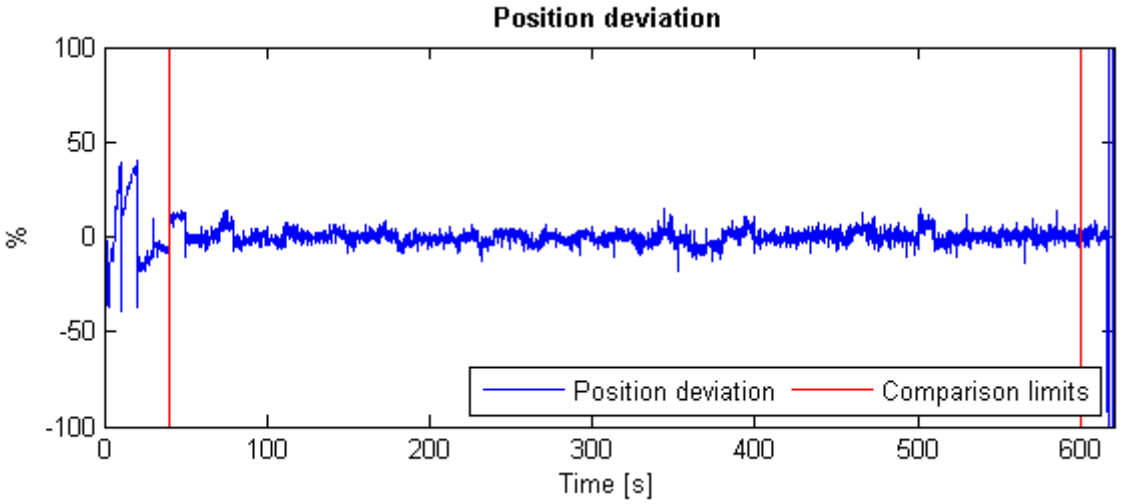

Fig. 5.54 Dancer position deviation based on the interval method, in percentage, during experiment 20

The positions deviations are very small which is also reflected in the low RMS value in Table 5.14

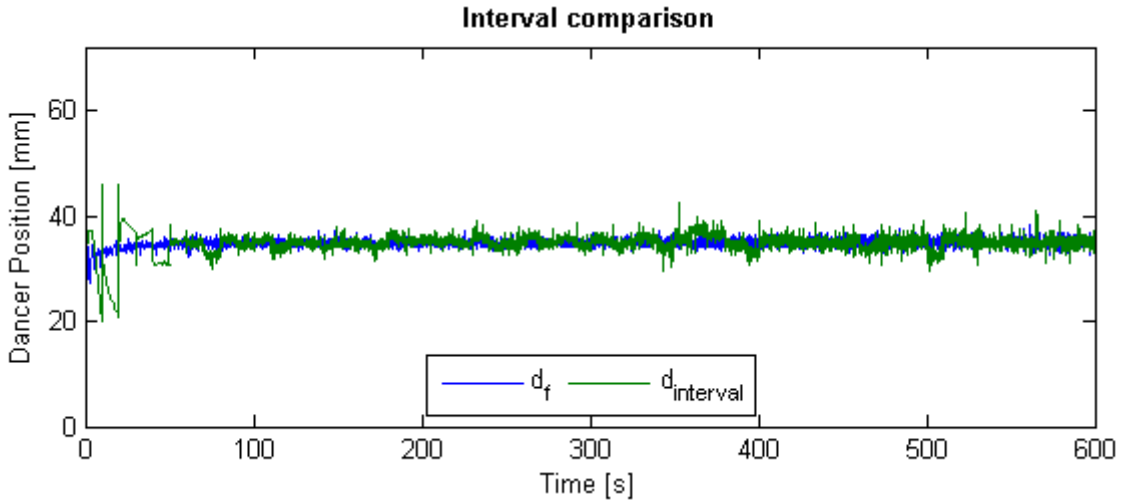

Fig. 5.55 Comparison between dancer position and estimated dancer position, using interval method, during experiment 20

From Fig. 5.55 it can be seen that unwanted oscillations are reduced. The estimation lags though at the start and until 80 seconds into the experiment. This section is plotted on Fig. 5.56 for further analysis. The estimation seems to follow the measurements acceptable over all but with deviations at 360 seconds and 500 seconds.

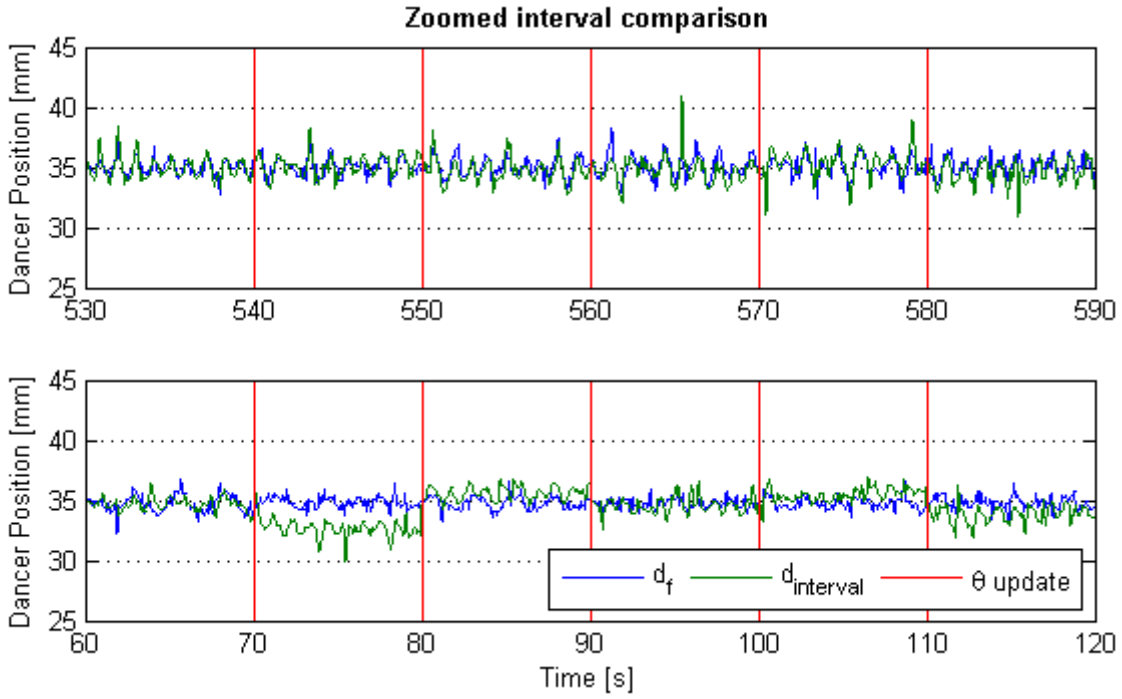

Fig. 5.56 Zoomed dancer position comparison using the interval method during experiment 20

The zoomed comparison on Fig. 5.56 is as previously divided into a best case, the upper graph, and a worst case, the lower graph. In both cases is the frequency of the compared signals correct. But the worst case lags correct amplitude and offset at some section. But overall is the estimation accepted because this experiment is the one which induces the smallest dancer oscillation while still estimating the dancers' dynamics very closely.

5.12 Summary of Parameter Estimation

This chapter has proposed a parameter estimation algorithm and it is found working in both simulations and practical implementation. The PEA is based on the recursive least square method. It Is found that persistent excitation is needed for accurate parameter estimation. A forgetting factor fo 0.999 was also found suitable.

The recursive lest square algorithm was first tested to be able to estimate the parameters in a LTI system using Simulink. It was found that a gain of 1000 improves the estimation accuracy.

Noise resembling the actual noise in the Web Winder was introduced which caused the algorithm to fail. Measures were made to reduce this noise, it was first tested whether simple noise reduction was plausible but this would require an unrealistic reduction of a factor 1000.

Filters were therefore introduced and it was found that a second order low pass filter of 6 Hz is plausible. But the lower filter frequency is, the better response, unless it would cause too high phase shift or signal distortion.

The same experiments were conducted with a time varying system in Simulink. It was found that a gain still is necessary to improve the accuracy. Noise was introduced and a filter was found necessary based on the conclusion from the LTI tests. Again a filter frequency of 6 Hz was found plausible.

With the algorithm found plausible theoretically, both ideal and with added noise, the algorithm was implemented in the actual web winder and tests were performed.

It was found that filters are essential because of the signal noise. But with only filters the dynamics were not estimated plausible. Excitation was therefore introduced and tested with both a square wave signals and sine signals.

The square wave signal improves the estimation of θ-parameters. These parameters are found representing the test bench dynamics, but suffer from large deviation peaks and sudden changes in estimation parameters. A sine signal is tested and found reducing the deviation peaks, smoothing the estimation parameters and reducing the dancer oscillations.

From the experiments it seems that the dancer needs to be disturbed and oscillate unwanted in order to make estimation of the dynamic behavior correct. This is also anticipated from the theory. It should be noted that all the practical experiments were conducted with a PID controller implemented which is manually tuned to be used throughout the whole paper roll. A more aggressive controller might reduce the oscillations from the excitation signal.

Another experience from conducting the experiments in praxis using the test bench is that the estimation algorithm seems to converge faster at higher paper speeds. This is observed when the unwinder roll is started at higher speeds and may explain why many of the experiments require around 80 seconds before finding acceptable estimates. This fits with all the previous experiments are based on a slow rising unwinder speed ramp.

But overall the recursive least square algorithm is found working, it does perform acceptable results in both theoretical and practical situation. But for successfully implementing in the web winder, noise filters and excitation signals is found necessary.

6. Controller Design

This chapter has the purpose of describing and dimensioning suitable controllers for the web winder. The controller is a key component in the web winder as it seeks to keep a constant tension in the web through operation. The previous chapter sought to develop an algorithm which could determine the web winders model parameters at each instant. This is a power full feature as it enables the possibility of change the controller as the plant changes behavior. This chapter will aim to develop a controller algorithm which uses the estimated systems to online adapt its behavior.

But before the introduction of adaptive controllers, traditional controllers based on constant parameters will be discussed. The four different controllers which the project group has chosen to explore are:

- Manual tuned PID controller (PID1)
- Model based PID controller (PID2)
- Adaptive PID controller tuned via parameter estimation (APID)
- Pole placement controller tuned via parameter estimation (PP)

The manually tuned PID controller is found by changing the PID parameters intuitively during multiple tests until a suitable result was obtained. The manually tuned PID controller does share structure with the calculated PID controller (PID2) but does inherently not contain any derivation concerning its parameters.

The PID2 will be tuned by utilizing the knowledge about the stability of the system describe in chapter 3.5.1, and the purpose is to design a conservative controller that is able to function as the system changes characteristics during the winding process. This will be achieved by showing how the PID is designed for the worst case scenario and it performance in this parameter region. The tuning strategy that is used is Ziegler-Nichols method.

The APID and the PP controller are different from the PID1 and PID2 by the fact that these continually are updated with new estimates of the systems behavior. To test if these controllers work, a linear time varying (LTV) model will be employed. The same model as in chapter 5.6. The model emulates the actual systems changing behavior over time. The advantage by using a model is that the controllers' performance can be estimated in Simulink using model simulations. The time varying model parameters will be referred to as the θ-*values* where θ is the vector containing the a_1, a_2, b_1 and b_2 parameters. The LTV model will in each test be fed the same known time varying parameters. The θ-parameters sent to the controller will be changed according to the three stages detailed below.

1. The controller is fed the known time varying parameters
2. The controller is fed estimated parameters found using the parameter estimation algorithm
3. The controller is fed estimated parameters found using the parameter estimation algorithm but noise is added to emulate the actual web winder

The philosophy behind the stages is to start simple and gradually add to the complexity of the tests until the controller is found acceptable for implementation in the machine. Stage 1 is illustrated in Fig. 6.1.

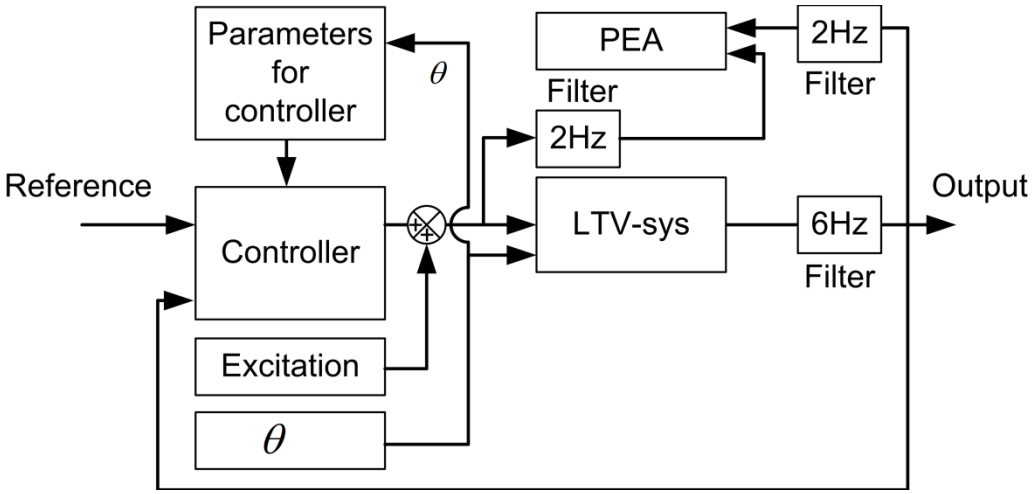

Fig. 6.1 Stage 1 LTV-system with design via the parameters in the LTV system

The first stage shows the controllers ability to control the system with varying parameters if the estimation of the system is perfect. The excitation is in all 3 stages a sine signal with a frequency of 6 rad/s and a amplitude of 0.02. Stage 2 is illustrated in Fig. 6.2

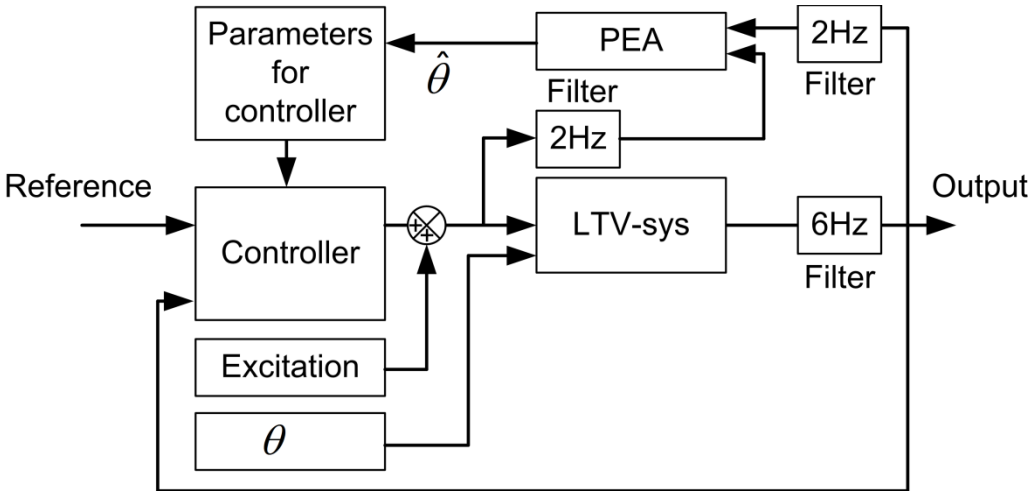

Fig. 6.2 LTV system with design via the estimated parameters in the LTV system

The purpose of the second stage is to test if the system is able to control the output of the system when the system parameters are estimated using the parameter estimation algorithm (PEA). Stage 3 is shown in Fig. 6.3.

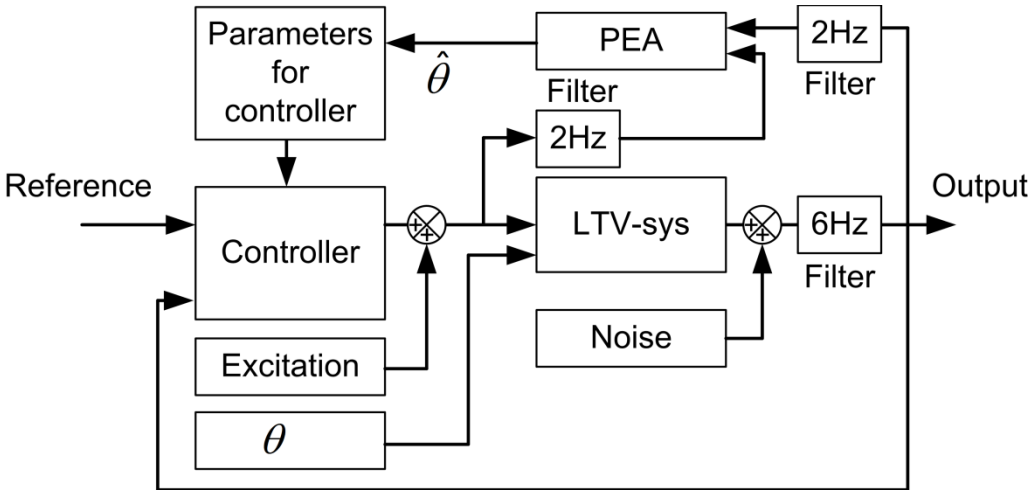

Fig. 6.3 LTV-system with design via the estimated parameters in the LTV system and with noise added

The third stage is to show how the system is able to cope with noise added on the output of the LTV-system; this is done to show the robustness to noise in the system. The stage is otherwise identical to stage two.

The PID1 and PID2 controllers are not tested to the same degree. PID1 is designed manually and therefore inherently will be working. PID2 is tested on the nonlinear model of the system and is not dependant on the estimation of the parameters as the case with APID and PP.

The basis for the comparison of the simulated controllers will be an initial step on the reference from 0 mm to 35 mm. From this initial step the overshoot, the rise time, the settling time and steady state error will be compared. The tolerances of the settling time are $^{+}/_{-}$ 5% of the reference.

6.1 Manual Tuned PID-controller

The main purpose of this controller is to make a functioning controller in such way that it is possible to conduct an entire winding process without changing the control parameters. This controller will act as a base line which represents the performance achievable by simply changing the controller intuitively through trial and error. This controller was used during the test of the parameter estimation algorithm in chapter 5.

This controller is tuned by changing the parameter in a PID controller, shown in Fig. 6.4, until a satisfying result is achieved.

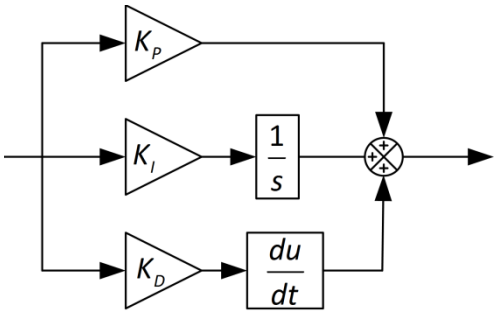

Fig. 6.4 PID controller as implemented in Simulink

The controller parameters are found as in Table 6.1

K_P	20
K_I	2
K_D	2

Table 6.1 Manual tuned PID parameters

Further variation of the control parameters might have revealed a better controller, but this setup is able to conduct an entire winding process. It will later in chapter **Fejl! Henvisningskilde ikke fundet.** be shown that the controller is robust against large disturbances.

6.2 Model Based PID-controller

On the basis of chapter 3.4 will a PID controller be designed to work in the whole range of the system. It will be designed using the Ziegler-Nichols tuning rules (Ogata, 2002).

The most conservative values for all the parameters are chosen to make the controller function in all operation points. This means that the controller will be designed using the smallest paper radius, because it was found to be the most significant changing parameter during operation. The inertia does also change during operation but only a little compared to the radius, which changes approx. a factor 5.5.The effect of the varying parameters can be found in chapter 3.5.1. The different value for the parameters are shown in Table 6.2.

Symbol	Value	Unit	Deviation from validated value
J_{M2}	$3.1\ 10^{-3}$	Kg·m	0
B_{M2}	$0.55\ 10^{-3}$	Nm·s/rad	0
E	$4\ 10^{9}$	Pa	0
A	$4.35\ 10^{-6}$	m^2	0
L_N	0.61	m	0
R	$13\ 10^{-3}$	m	-77%
N_G	10.5	-	0
K_d	1018	N/m	-10%
m_d	0.69	Kg	0
B_d	450	Nm·s/m	-10%

Table 6.2 Parameters used for worst case

The PID-controller will act as position control of the dancer. The structure is shown in Fig. 6.5. A PI and a P controller will besides the PID controller also be tested for comparison.

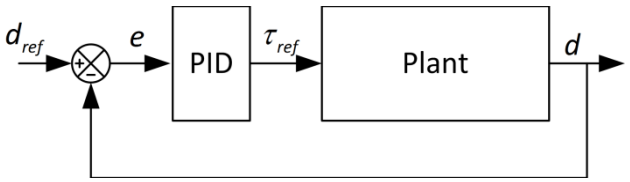

Fig. 6.5 Control structure for the static PID

The dancer position, *d,* is another way to express the tension in the web in steady state. Therefore the desired tension can be converted into a desired position of the dancer if desired, but the position will be used as reference in this chapter.

The position controller will be implemented in dSpace, where the controller output is a torque reference that is sent to the winder VLT. The VLT has internal control structures, which it utilizes to get the motor to deliver the wanted torque. The internal torque control is based on feedback flux-orientated control. Torque from the motor is then actuating the rest of the plant with rotor inertia, paper, dancer etc.

6.2.1 The Ziegler-Nichols Method

When the plants critical gain (K_{cr}) and the critical period time (P_{cr}) are found using the root-locus, the parameters for the P, PI and PID-controller can be determined by means of Table 6.3 (Ogata, 2002).

Controller type	K_p	T_i	T_d
P	0.5 K_{cr}	∞	0
PI	0.45 K_{cr}	1/1.2 P_{cr}	0
PID	0.6 K_{cr}	0.5 P_{cr}	0.125 P_{cr}

Table 6.3 Ziegler-Nichols tunings rule based on critical gain K_{cr} and critical period P_{cr}

The critical gain and the critical period are determined by Routh's stability criterion. This criterion investigates if there are unstable roots in the characteristic equation of transfer function, without having to solve the equation. This is done by examine the constants in front of the different orders of S. The constants have to fulfill different condition this is clarified in appendix C, the result is shown in Table 6.4.

System	K_{cri}[-]	P_{cri} [s]
G_{sys}	802	0.5927

Table 6.4 The critical values for the two systems

This operation point is selected to have the lowest bandwidth. The Ziegler Nichols tuning method can be used for P, PI and PID controllers. Depending on the controller different controller constants can be calculated using (6.1). This calculation gives the controller constants displayed in Table 6.5.

$$K_I = \frac{K_p}{T_i} \qquad K_D = K_p T_d \tag{6.1}$$

Type of controller	K_P	K_I	K_D
P	401	0	0
PI	360.9	730.7	0
PID	481.2	974.3	35.65

Table 6.5 Values for the controllers.

These values are implemented and tested on the linear model to investigate if they have appropriate properties.

6.2.2 Implementation in Model

The controller structure is implemented in the system as shown in Fig. 6.6.

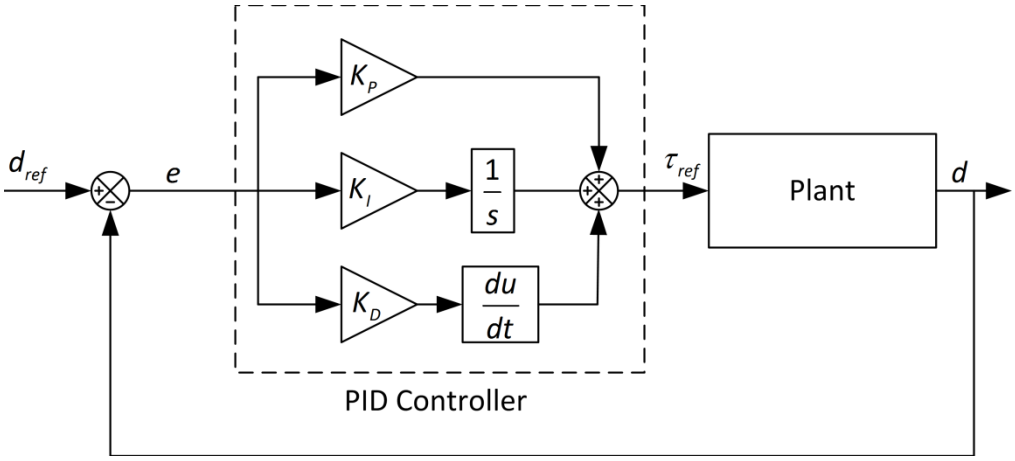

Fig. 6.6 Structure of the PID-regulator

A simulation result of the implementation with the linear model as plant is shown in Fig. 6.7. The simulations are run using a reference (d_{ref}) of 0.035 m and a initial dancer position of 0 m at the time 0.

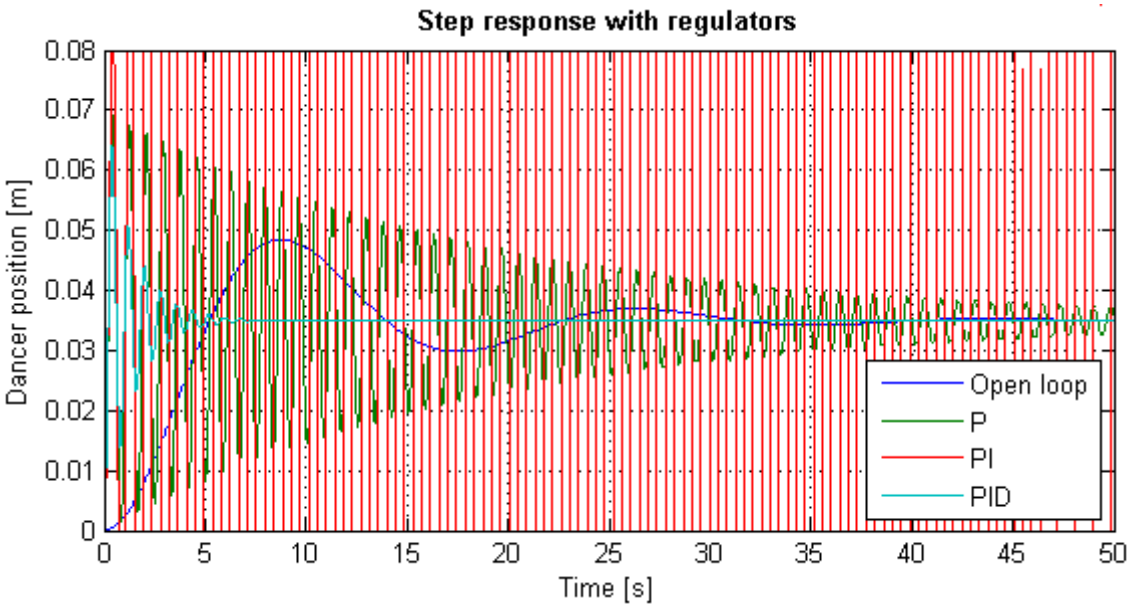

Fig. 6.7 Comparison of different regulators based on the ZN method

From Fig. 6.7 it can be seen that the parameters found from the Ziegler-Nichols tuning rules for the P- and the PI-controller is performing poorly. The P-controller has a very long settling time and the PI-controller is unstable. This result is in accordance with (Liu, 1999) where it is pointed out, that some difficulties occur with the use of a PI-controller. A PID-controller or a lead compensator is needed.

It should be noted that the Ziegler-Nichols tuning method only gives an estimate of suitable controller parameters. The P- and the PI-controller are improved by iteration and the new value values are shown in Table 6.6. There was not found new values for the PID-controller since the iteration did not improve the performance of the system. With the P-regulators proportional gain of 60 the steady state value is within 2% of the value.

Type of controller	P	I	D
P	60	0	0
PI	50	2	0
PID	481.2	974.3	35.65

Table 6.6 The improved values for P- and PI-controllers

A new simulation was run using the parameters from Table 6.6 and the results are compared in Fig. 6.8

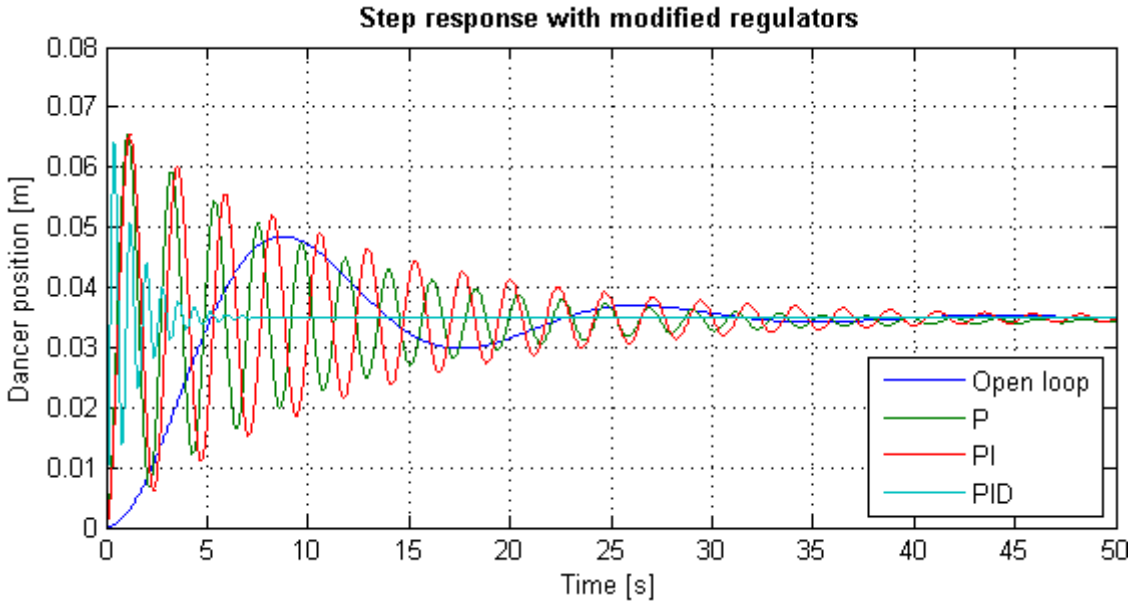

Fig. 6.8 Improved regulators in the linear model

From Fig. 6.8 it can be seen that the system with the PI-regulator is stable now, this is because the oscillation decays to a level around the reference. The P-controller is improved but the steady state error is bigger than with the Ziegler-Nichols parameters but still within 5 %. The best controller is found to be the PID-controller since it is much faster to find the steady state than the others, but there might be some problems with implementing in the real system due to the use of the time derivative which can make the controller noise sensitive.

The values from the manual tuned PID controller was smaller than the parameters found in Table 6.1 this indicates that this controller based on the linear model is much too aggressive to work properly. A practical test showed that the paper broke repeatedly during start-up and therefore no more testing was conducted. It was decided to design a new controller based on the nonlinear model because this should be able to handle some of the nonlinearities better, and therefore the controller would supposedly have a better performance. This is supported by the knowledge that it is during the start-up that the nonlinearities are very determining of the behavior of the system.

6.2.3 Design Based on the Nonlinear Model

High controller parameters were initially found using the non-linear model also. When this phenomenon occurred it was decided to introduce noise in the position feedback in order to emulate the actual system as closely as possible. The test was also made because it earlier has been found that high amounts of noise in the position measurements poses a problem. The noise is introduced as it is done in the parameter estimation chapter 5.5, by adding noise measured on the actual web winder. This noise is then filtered using a 6 Hz second order low pass filter as found suitable in the estimation chapter 5.7 before adding it to the models feedback.

With the noise implemented in the feedback from the dancer the gain in a P-controller is increased until the system have a sustained oscillation. This resulted in a smaller gain than without noise.

Under normal circumstances a critical gain would be found by raising the gain until the system experiences a sustained oscillation, and where a larger gain would result in an unstable system.

A problem observed is that the nonlinear model have a large overshoot even with low gains, when this large initial overshot is completed, the system still have some sustained oscillations but at a lower amplitude than the first overshoot. When these sustained oscillations are emerged, the gain can be raised further without the system becomes unstable; the amplitude just becomes larger. The lowest gain, where the oscillation is sustained, is 40 as it can be seen from Fig. 6.9 which show a step reference test at 0.035 m with only a P-regulator implemented. Fig. 6.10 show a zoomed section of the simulation for better comparison and observation of critical period.

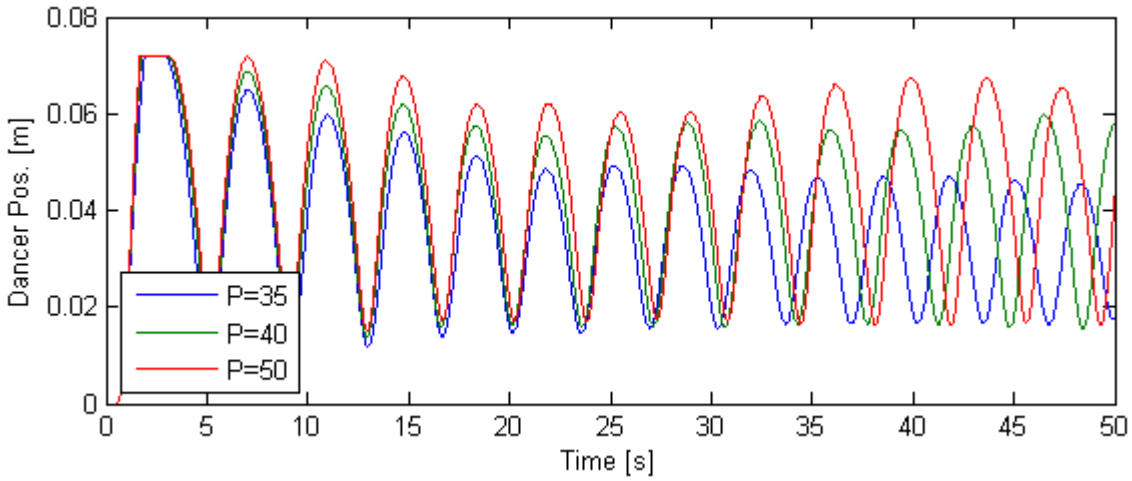

Fig. 6.9 The step response of the nonlinear system

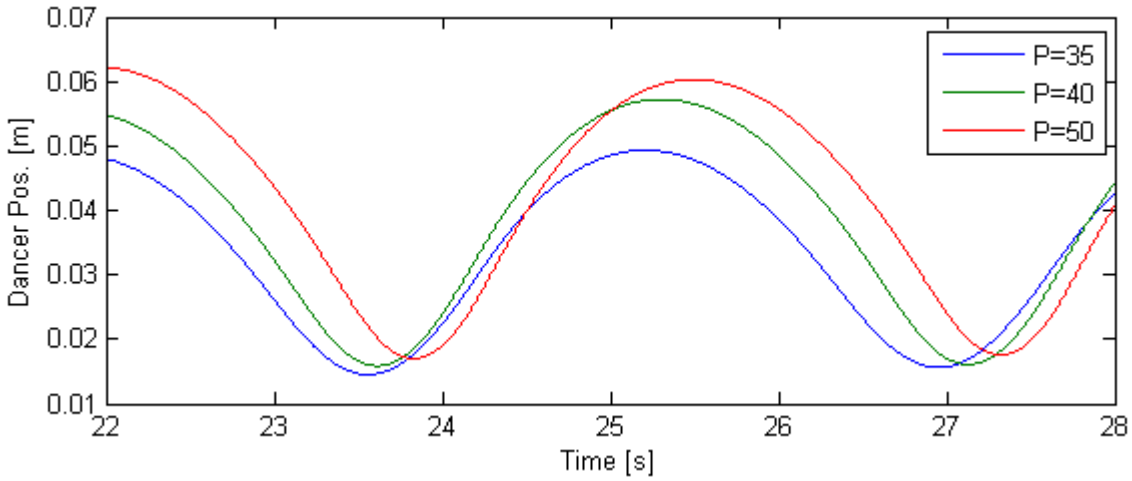

Fig. 6.10 Zoom on the step response of the non-linear system

The critical gain is chosen to 40 because this is the lowest proportional gain where there is a sustained oscillation is achieved. The critical period is approx 3 s. The values for the different controllers are calculated using Table 6.3 and (6.1). The found parameter constants are displayed in Table 6.7.

	K_P	K_I	K_D
P	20	0	0
PI	18	7.2	0
PID	24	9	16

Table 6.7 Controller parameters from the nonlinear model

A PID controller is chosen as the PI controller previously is described as not giving good results and as the PID controller eliminates possible steady state errors, a capability the P-controller lacks. It is chosen only to test the PID controller on the nonlinear model. The controller will later be tested on the test bench also. A step response of the nonlinear model with the found PID controller is shown in Fig. 6.11, the step size is 0.035 m.

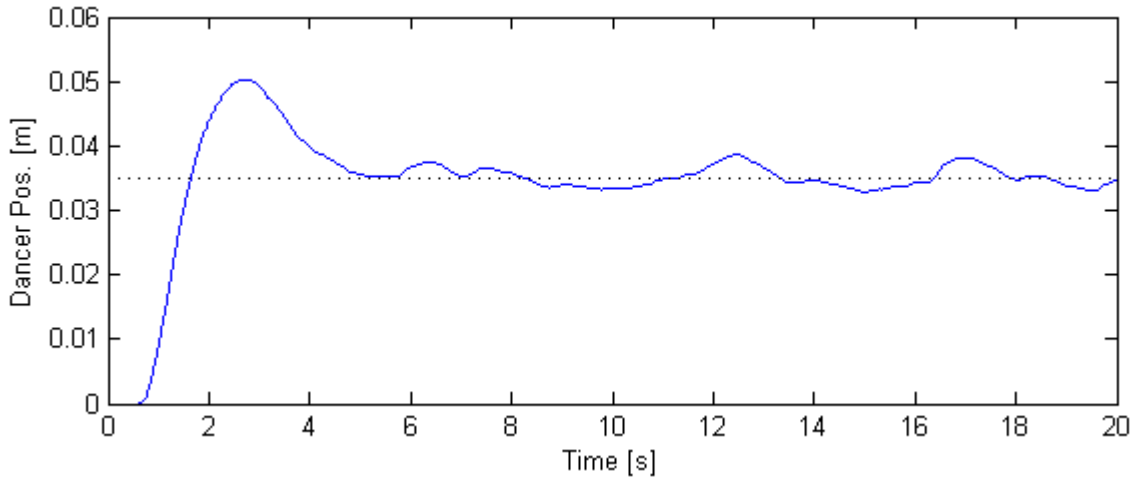

Fig. 6.11 A step response of the nonlinear model with PID controller

It can be seen from Fig. 6.11 that the step response of the system settles after 5 s, the rest of the oscillation is due to noise from the feedback, if the same controller is used and the noise is removed from the simulation, the position is maintained at the reference. Based on this analysis is the static PID controller found plausible and will be used for further testing on the actual web winder.

6.3 Adaptive PID-controller

The purpose of this section is to discuss and determine a suitable PID controller algorithm which can be updated as the web winder changes behavior. The adaptive PID controllers main purpose is therefore to continuously be able to control the plants output based on a desired referece, a feedback mearuements, and knowledge about the system gained from the parameter estimation algorithm earlier discussed.

As the estimated parameters constitutes a discrete transfer function which is assumed adequate representing the actual web winders behavior, it is reasonable to keep the further analysis in the discrete domain.

The design plan for this section is as stated below:

- Derive a discrete equivalent model of the PID controller

- Adapt a tuning method which on basis of the systems parameters can dimension the controller parameters
- Test whether the found solution seems plausible through simulation tests

When all the sections are completed, it should be possible to estimate whether the solution seems plausible for implementation in the actual web winder machine.

6.3.1 Discrete PID-controller

This section derives the discrete PID structure which will be used for later implementation of the algorithm. The derivation is based on theory from (Ogata, 1995). The general control structure is shown in Fig. 6.12.

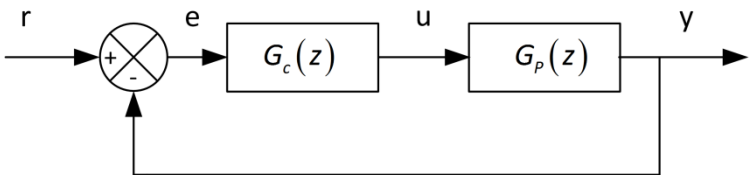

Fig. 6.12 Generel control structure

The PID controller in the Laplace domain is given by (6.2).

$$G_C(s)=\frac{U(s)}{E(s)}=K\left(1+\frac{1}{T_i s}+T_d s\right) \tag{6.2}$$

The discrete PID controller is initially derived by approximating the integral term with trapezoidal summation and the derivative term with a two point difference, which gives (6.3).

$$G_C(z)=K\left(1+\frac{T}{2T_i}\frac{1+z^{-1}}{1-z^{-1}}+\frac{T_d}{T}\left(1-z^{-1}\right)\right) \tag{6.3}$$

With the constants defined in (6.4) it is possible to revise the controller to the form given in (6.5).

$$K_P=K-\frac{K_I}{2} \quad , \quad K_I=\frac{KT}{T_I} \quad , \quad K_D=\frac{KT_D}{T} \tag{6.4}$$

$$G_C(z)=K_P+\frac{K_I}{1-z^{-1}}+K_D\left(1-z^{-1}\right) \tag{6.5}$$

Equation (6.5) is commonly referred to as the *position-form* PID. With this form each part of the controller is multiplied with the error signal.

When the process is starting up or changed from manual to automatic the reference signal changes rapidly and therefore the output of the proportional and derivative part often becomes larger than the

saturation limit. This is commonly known as the *kicking* phenomena. To avoid the kicking phenomena the *velocity-form* PID is used (Ogata, 1995).

$$G_C(z) = \frac{K_P\left(1-z^{-1}\right)+K_I+K_D\left(1-z^{-1}\right)\left(1-z^{-1}\right)}{\left(1-z^{-1}\right)}$$

(6.6)

Hereby is two discrete PID structures proposed. The structure in (6.6) will be used for further analysis due to its better performance in adaptive environments as the case is in this project. The structure of the selected adaptive PID controller can be seen in Fig. 6.13.

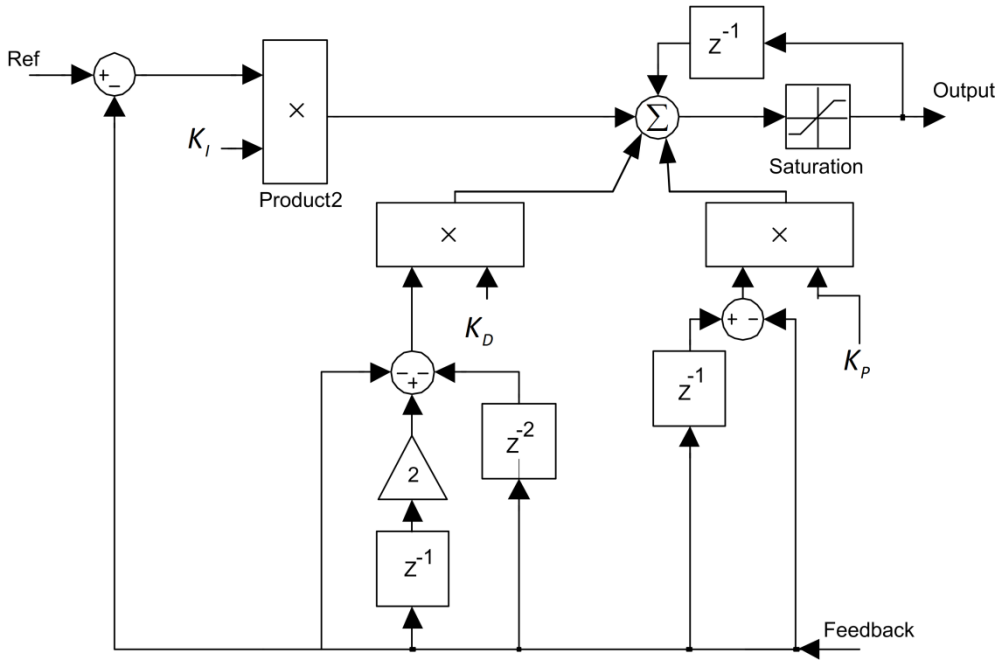

Fig. 6.13 The implementation of the adaptive PID

The type of PID controller is selected and it is prepared for implementation in the web winder system. The next step is to tune the different gains in the controller by means of the estimated parameters.

6.3.2 Tuning of a Discrete PID-controller

The purpose of this section is to determine the discrete PID controllers parameters, as the system parameters changes during operation. One design approach is to determine the critical gain K_{cr} and the critical period T_{cr}. When these two parameters are found; a modified Ziegler-Nichols tuning algorithm for discrete systems can be employed as the case with the static PID. The theory stated in this section is adapted from (Bobal, et al., 1999). In a continuous system the critical gain and period is found when the systems poles are placed on the imaginary-axis of the s-plane. In a discrete system the critical poles is placed on the unit circle. There are two possible places the poles can be placed on the unit circle to make the system unstable:

1. There is a pair of complex conjugate pole $z_{1,2}=\alpha\pm j\beta$.
2. There are real poles $\alpha=-1,\beta=0$, for $\alpha=1$ there will not be a oscillation of the system.

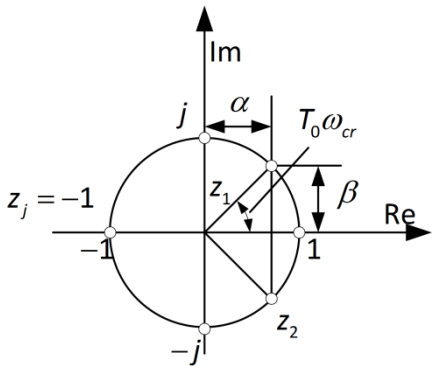

Fig. 6.14 Placements of critical poles on the unit circle

A simple SISO system will have the structure in discrete domain as shown in (6.7)

$$G_p(z) = \frac{Y(z)}{U(z)} = \frac{z^{-d}B(z^{-1})}{A(z^{-1})} \tag{6.7}$$

Where Y(z) and U(z) are the z-transforms of the controller output and the process output. d is the time delay as a multiple of the sample period. A and B are n-degree polynomial defined by (6.8)

$$A(z^{-1}) = 1 + \sum_{i=1}^{n} a_i z^{-i} \quad B(z^{-1}) = \sum_{i=1}^{n} b_i z^{-i} \tag{6.8}$$

The structure of the system with the controller can be seen in Fig. 6.15.

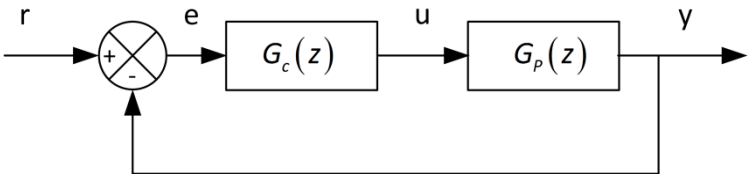

Fig. 6.15 The controller and the plant

The controller in the system is at this point a pure P-controller, the idea is to find the critical gain by raising the value of the gain until the system becomes unstable. The P-controller have the structure shown in (6.9)

$$G_c(z) = \frac{U(z)}{E(z)} = K_p \tag{6.9}$$

Where E(z)= R(z)-Y(z) is the z-transform of the error. R(z) is the Z-transform of the reference signal. With a combination of the controller and the system the discrete transfer function will have the form of the closed loop system as shown in (6.10).

$$G_{cl}(z)=\frac{Y(z)}{R(z)}=\frac{z^{-d}K_pB(z^{-1})}{A(z^{-1})+z^{-d}K_pB(z^{-1})}$$

(6.10)

The characteristic polynomial D(z) of (6.10) is (6.11).

$$D(z)=z^{n+d}\left[A(z^{-1})+z^{-d}K_pB(z^{-1})\right]$$

(6.11)

To have complex conjugated poles on the unit circle, D(z) must contain a quadratic three-term as shown (6.12)

$$C_1=z^2-2\alpha z+1$$

(6.12)

To have real poles at α=-1, D(z) must include *j*-terms as shown in (6.13).

$$C_j(z)=(z+1)^j,\ j=1,2,...$$

(6.13)

The idea is to separate D(z) in components consisting of terms made of complex poles and terms made of real poles. The complex poles are found in (6.14) and the real poles are found in (6.15).

$$z^{n+d}\left[A(z^{-1})+z^{-d}K_p(T_0)B(z^{-1})\right]=(z^2-2\alpha z+1)z^{n+d-2}E(z^{-1})$$
$$\text{where } E(z^{-1})=1+\sum_{i=1}^{n+d-2}e_iz^{-i}$$

(6.14)

$$z^{n+d}\left[A(z^{-1})+z^{-d}K_p(T_0)B(z^{-1})\right]=(z+1)^j z^{n+d-j}F(z^{-1})$$
$$\text{where } F(z^{-1})=1+\sum_{i=1}^{n+d-j}f_iz^{-i}$$

(6.15)

There are basically three and two unknown parameters in each of the equations K_p , α and e_i in equation (6.14) and K_p and f_i in equation (6.15). The solutions to the real roots are simpler, than the solution of the complex roots.

A pole at α=-1, which is the only unstable real pole, forms a unstable component which corresponds to a continuous function $\cos(\pi/T_0)t$ with critical period $T_{cr}=2T_0$. This is due to the definition of z in the z-transform:

$$z=e^{j\omega T_0}=\cos(\omega T_0)+j\sin(\omega T_0)$$

(6.16)

For z=-1 the critical frequency can found as $\omega_{cr}=2\pi/T_{cr}(T_0)= \pi/T_{cr}$. And the maximum gain in the open loop is given by (6.17).

$$K_{cr}\left(T_0\right)=-\frac{1}{G_p\left(-1\right)}$$

(6.17)

The term in (6.12) have a denominator with $z^2-2\cos(\omega T_0)z+1$ of the Z-transform of the harmonic functions cos(ωt) or sin(ωt) the real component of the pole can then be expressed as shown in (6.18).

$$\alpha=\cos\left(\omega_{cr}T_0\right)=\cos\left(2\pi T_0/T_{cr}\left(T_0\right)\right)$$

(6.18)

When the real component is know, the critical period can be derived as shown in (6.19)

$$T_{cr}\left(T_0\right)=\frac{2\pi T_0}{\cos^{-1}\left(\alpha\right)}$$

(6.19)

The next step is to investigate how this theory can be utilized on the simplified discrete plant model, shown in (6.20). This model is a second order model, which parameters should be continuously updated using the estimation algorithm.

$$G_P\left(z\right)=\frac{b_1\cdot z+b_2}{z^2+a_1\cdot z+a_2}$$

(6.20)

The method to find the ultimate gain is described in (Bobal, et al., 1999). If there is no time delay in the system the characteristic polynomial can be written as (6.21).

$$D\left(z\right)=z^2+\left(a_1+b_1K_P\right)z+\left(a_2+b_2K_P\right)$$

(6.21)

By comparing (6.21) to (6.14) it is possible to find any complex poles. With n=2 and d=0 inserted (6.14) equation (6.22) is found.

$$z^{2+0}\left[A\left(z^{-1}\right)+z^{-0}K_{p1}\left(T_0\right)B\left(z^{-1}\right)\right]=\left(z^2-2\alpha z+1\right)z^{2+0-2}E\left(z^{-1}\right)$$
$$z^2\left[1+a_1z^{-1}+a_2z^{-2}+K_{p1}\left(T_0\right)\left(b_1z^{-1}+b_2z^{-2}\right)\right]=\left(z^2-2\alpha z+1\right)$$

(6.22)

To solve this equation the coefficient with the same power of z is compared:

$$\begin{aligned} z^2: &\quad 1 = 1 \\ z^1: &\quad a_1 + K_{p1}(T_0) b_1 = -2\alpha \\ z^0: &\quad a_2 + K_{p1}(T_0) b_2 = 1 \end{aligned}$$

(6.23)

By solving the equation relating to z^0 it is possible to determine the ultimate gain as shown in (6.24)

$$K_{p1}(T_0) = \frac{1 - a_2}{b_2}$$

(6.24)

The real part of the complex conjugated poles can be found by combining (6.24) and the equation for z^1 as shown in (6.25).

$$\alpha = \frac{a_1 + K_{p1}(T_0) b_1}{2}$$

(6.25)

From this real part the critical period can be calculated by means of (6.19).

To find the critical gain if the system has 2 real poles (6.15) is used with n=2,d=0 and j=1 it becomes (6.26).

$$\begin{aligned} & z^{n+d}\left[A\left(z^{-1}\right) + z^{-d} K_{p2}(T_0) B\left(z^{-1}\right)\right] = (z+1)^j z^{n+d-j} F\left(z^{-1}\right) \\ & z^2\left[1 + a_1 z^{-1} + a_2 z^{-2} + K_{p2}(T_0)\left(b_1 z^{-1} + b_2 z^{-2}\right)\right] = (z+1)^1 z^1 \left(1 + f_1 z^{-1}\right) \\ & z^2\left[1 + a_1 z^{-1} + a_2 z^{-2} + K_{p2}(T_0)\left(b_1 z^{-1} + b_2 z^{-2}\right)\right] = (z+1)(z+f_1) \\ & z^2 + \left(a_1 + K_{p2}(T_0) b_1\right) z + \left(a_2 + K_{p2}(T_0) b_2\right) = z^2 + (1+f_1) z + f_1 \end{aligned}$$

(6.26)

As in (6.23) the coefficient in front of the same powers of z compared and (6.27) is arised.

$$\begin{aligned} z^2: &\quad 1 = 1 \\ z^1: &\quad a_1 + K_{p2}(T_0) b_1 = 1 + f_1 \\ z^0: &\quad a_2 + K_{p2}(T_0) b_2 = f_1 \end{aligned}$$

(6.27)

By substituting the expression for f_1 found in the equation for z^0 in the equation for z^1 we get (6.28).

$$a_1 + K_{p2}(T_0)b_1 = 1 + a_2 + K_{p2}(T_0)b_2$$
$$a_1 - a_2 - 1 = K_{p2}(T_0)b_2 - K_{p2}(T_0)b_1$$
$$\frac{a_1 - a_2 - 1}{b_2 - b_1} = K_{p2}(T_0)$$

(6.28)

To ensure the there are complex conjugated poles when the equation is solved the discriminant from (6.21) has to be negative. This is tested in (6.29).

$$d = b^2 + 4ac \le 0$$
$$\left(a_1 + b_1 K_{p2}(T_0)\right)^2 - 4\left(a_2 + b_2 K_{p2}(T_0)\right) < 0$$

(6.29)

The complete controller design process is summerazied in Fig. 6.16. Where the algorithm is shown as it later wille be implemented in the controller software.

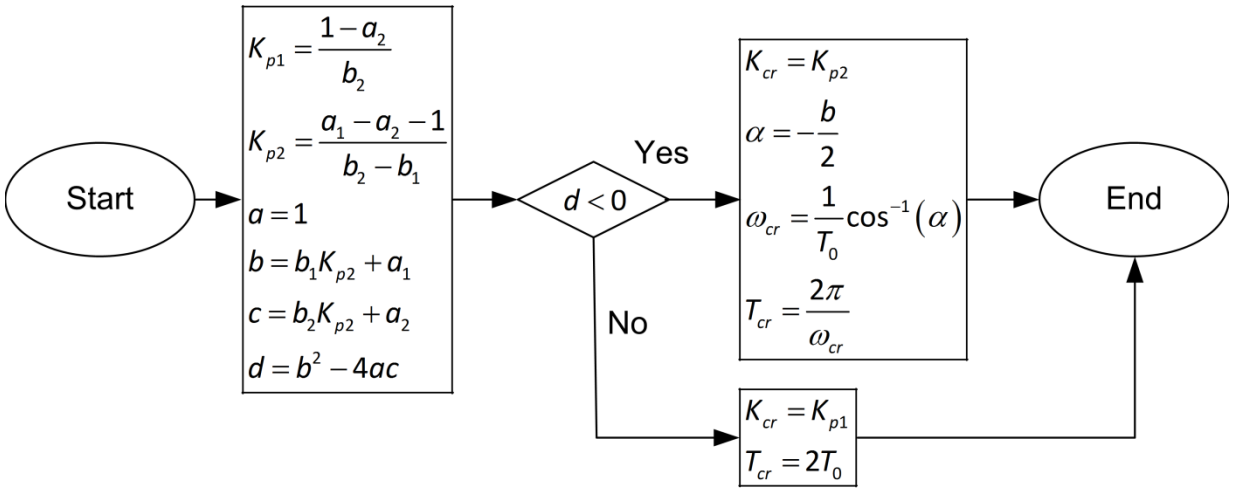

Fig. 6.16 Flow diagram for a second order system

When the critical gain and period is found these can be utilized in a modified Ziegler-Nichols design approach to find suitable controller parameters. Hereby is an algorithm found which on basis of the found system parameters (a_1, a_2, b_1 and b_2) can find the critical gain and period which is needed to tune the controller using a modified Ziegler-Nichols method.

When using a discrete plant the control parameters has to designed in another matter than in the continuous case (Bobál, 2005). Due to this the Ziegler-Nichols method have to be modified, the modified equation for the different gains are shown in (6.30).

$$K_P = 0.6K_{cr} - \frac{K_I}{2} \quad K_I = 1.2\frac{K_{cr} \cdot T_0}{T_{cr}} \quad K_D = \frac{3 \cdot K_{cr} \cdot T_{cr}}{40 \cdot T_0}$$

(6.30)

Here by it is possible to implement the velocity PID describe (6.6) and use the estimated parameters to calculate the controller parameters.

6.4 Simulation Test Of Adaptive PID-controller

The adaptive PID controller is the first adaptive controller that is tested. The performance of the controller is evaluated through three stages as detailed in this chapter's introduction. Each stage is represented by a separate Simulink model, which can be found on the attached CD. The known θ-parameters in each experiment are the same as being used in the parameter estimation chapter.

6.4.1 Stage 1

In this stage the controller will be tested with the known system parameters, as input to the calculation of control parameters. A reference step test is conducted with a reference of 0.035 m at t=0, and an initial dancer position of 0 m. The result of the test with the implemented adaptive controller is shown on Fig. 6.17.

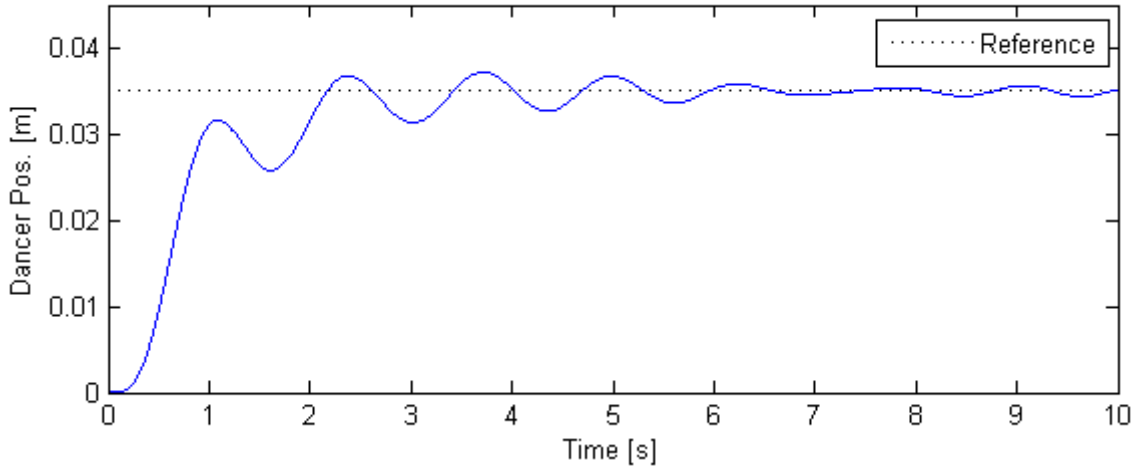

Fig. 6.17 The first 10 seconds of the step response

To quantify the results for better comparison with later experiments Table 6.8 is presented.

	Value
Overshoot [mm]	2.17
Settling time [s]	4.51
Rise time [s]	2.17
Steady state error [mm]	0

Table 6.8 The characteristic for the first stage

Table 6.8 shows the results for the first 10 s which covers the initial start-up response. But the LTV model changes behavior over a significant longer time span in which the controller also should be able to hold the reference value. Fig. 6.18 shows the output of the system over a longer time span.

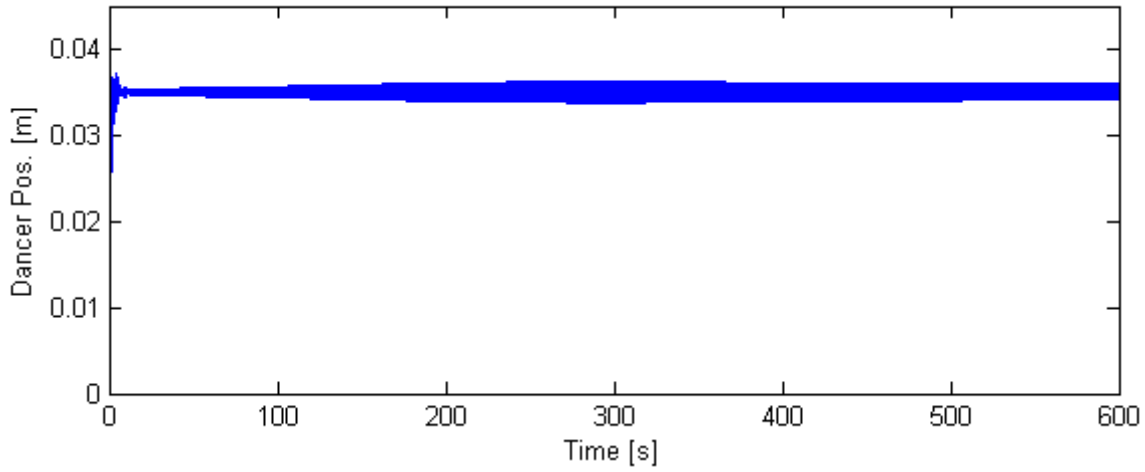

Fig. 6.18 System response throughout the simulation

In Fig. 6.18 it can be seen that the amplitude actually grows in size. The maximum error is though within $^{+}$/-5 %. From Fig. 6.18 it can be difficult to see that the amplitude is oscillating with the same frequency of 6 rad/s as the sinusoidal signal used for excitation. Fig. 6.19 show the output from the PID controller to the plant through the simulation.

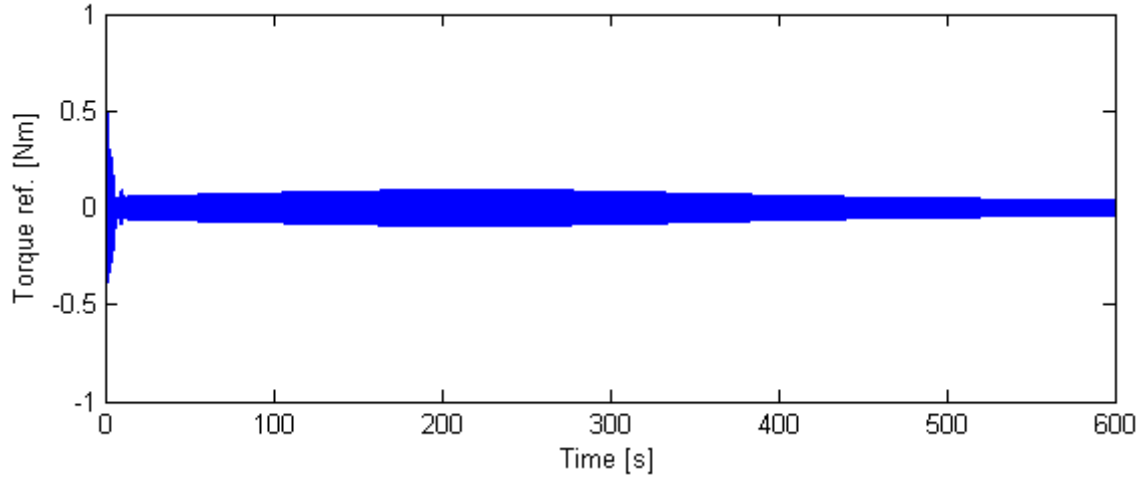

Fig. 6.19 The torque reference from the controller

It can be seen from Fig. 6.19 that the controller only does a large control effort in the beginning. But this descends fast to a level around +/- 0.05 [Nm]. A zoom of the reference torque signal is shown in Fig. 6.20.

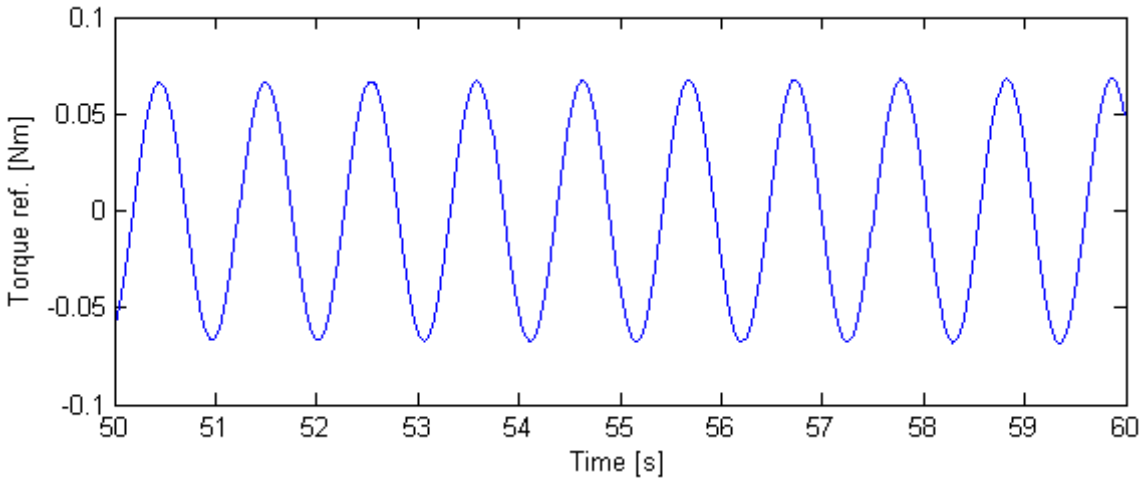

Fig. 6.20 The torque reference from the controller in the interval from 50 to 60 s.

The added sinusoidal excitation signal have amplitude of 0.02 Nm, which is a smaller than the size of the torque reference signal shown in Fig. 6.20 but the frequency of the excitation signal and the controllers output signal is approximately the same. This indicates that it is the excitation signal which creates the oscillations.

To test whether the estimation algorithm can estimate the system parameters correctly with a PID controller in the system, the output from the estimation block is examined. This is already found plausible in the practical estimation experiments in chapter 5.6, but is again tested in this ideal simulation. This comparison can be seen in Fig. 6.21 and Fig. 6.22.

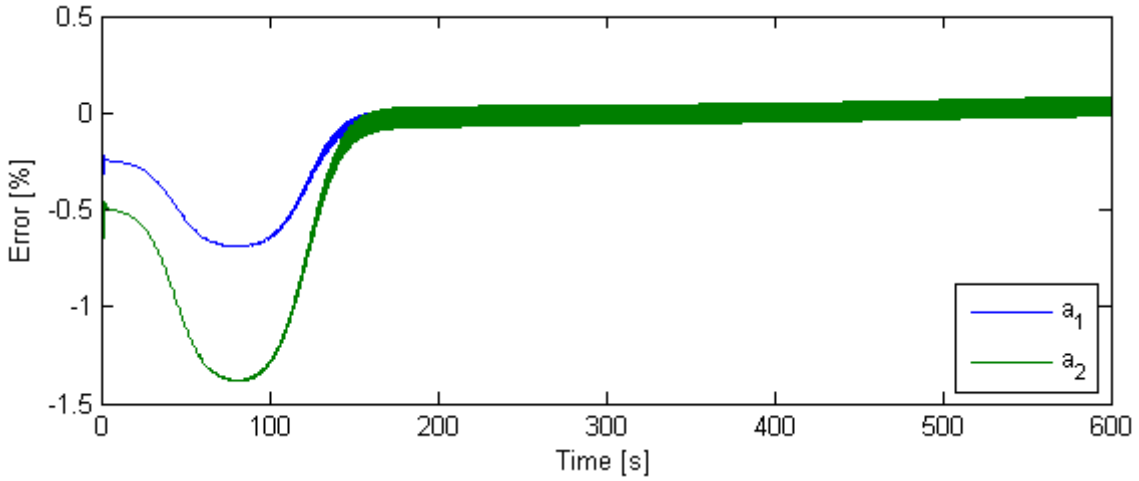

Fig. 6.21 The estimations error of a_1 and a_2

It can be seen in Fig. 6.21, that the system with this controller implemented is able to estimate a_1 and a_2 with in very small tolerances within 1.5%. This is not the case for b_1 and b_2 as it can be seen in Fig. 6.22.

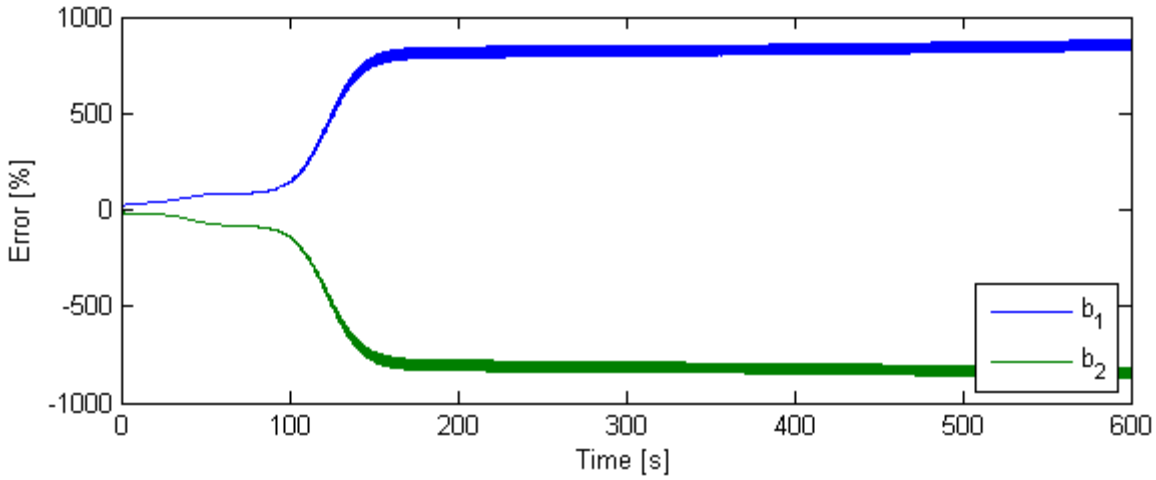

Fig. 6.22 The estimation of b_0 and b_1 for the hold periode

From Fig. 6.22 it can be seen that b_1 and b_2 have and error of approx. 800 %, after 150 s, this could imply that the estimation of the systems dynamics becomes wrong even with the added sinusoidal signal.

By comparing the dynamics of the found parameters, see Fig. 6.23, it can be seen that the found parameters deviates from the sought but the solution is still valid. This can be seen by the parameters in dynamic comparison is able to closely mimic the behavior of the dancer. This indicates that the found parameters still represents the system even though the exact sought parameters are not achieved. This might indicate that the PEA simple have found a different solution.

The dynamic behavior of the estimated θ-values are tested by means of the interval method described in chapter 5.8.

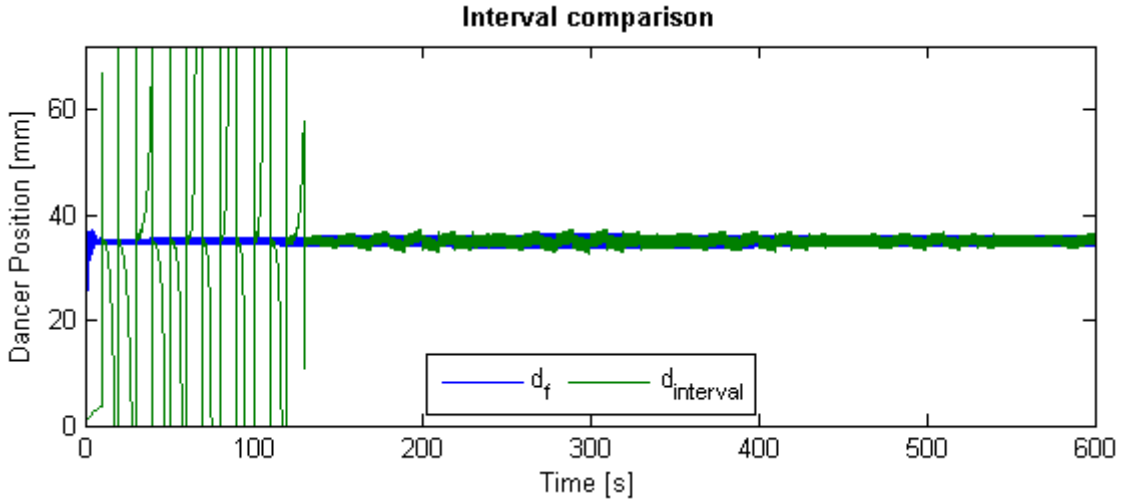

Fig. 6.23 The dancer position

Fig. 6.23 shows large deviations in the beginning. The large deviation disappear when the parameters for b_1 and b_2 is settled. This would imply that the parameters found in the estimation displays the same dynamic behavior. To show the difference to a time period where the parameters are settled, a zoom is shown on Fig. 6.24.

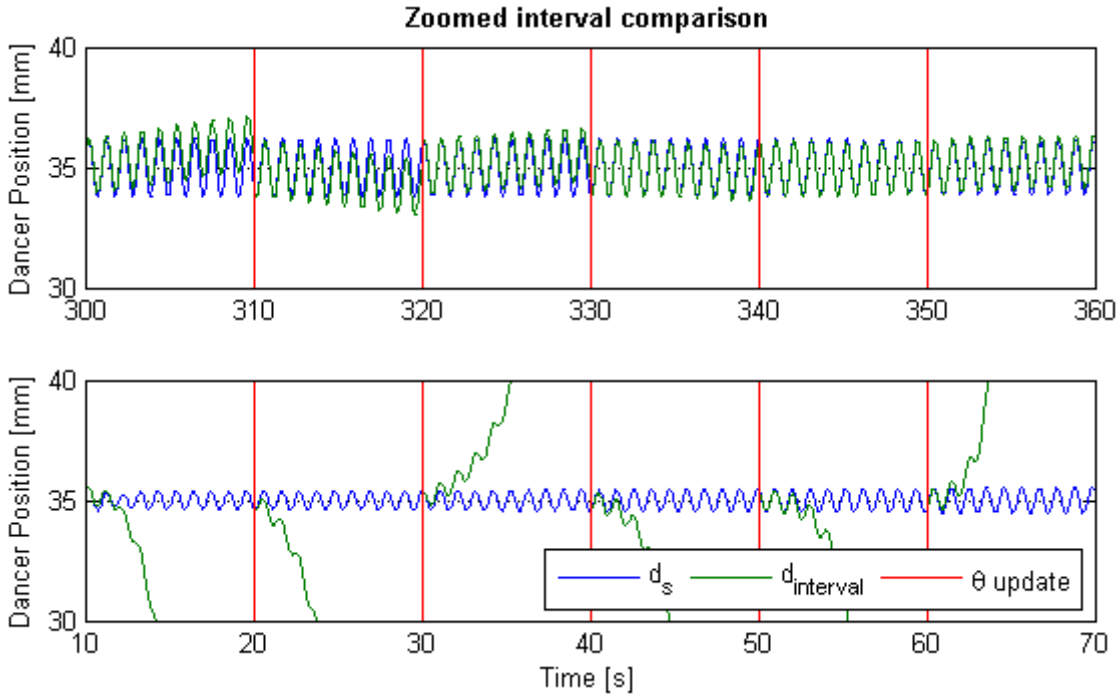

Fig. 6.24 A zoomed interval comparison of the dancer position

The top graph of Fig. 6.24 show a period where the parameters are settled, it can be seen that the frequency and amplitude of the signal is correct, but some of them have ascending value besides the fast over-laying frequency. But the overall behavior is very alike.

The bottom graph of Fig. 6.24 show a period from the beginning of the test, where the estimation have not found a settling point. It can be seen that the estimated parameters ($d_{interval}$) gives the same the same dancer position but only at the first peaks. Then the dancer position based on the interval method ($d_{interval}$) will be very diverging from the simulated dancer position (d_s).

Due to the coherence between the estimated parameters and the dynamic of the simulated LVT system, it is concluded that the values found by the estimation algorithm describe the system sufficient to be able to be used to design a controller. This test also indicates that the PEA-solution is not unique, as a different solution provides a response very alike the ideal LTV systems.

The controller parameters found in the APID simulation is shown in Fig. 6.25.

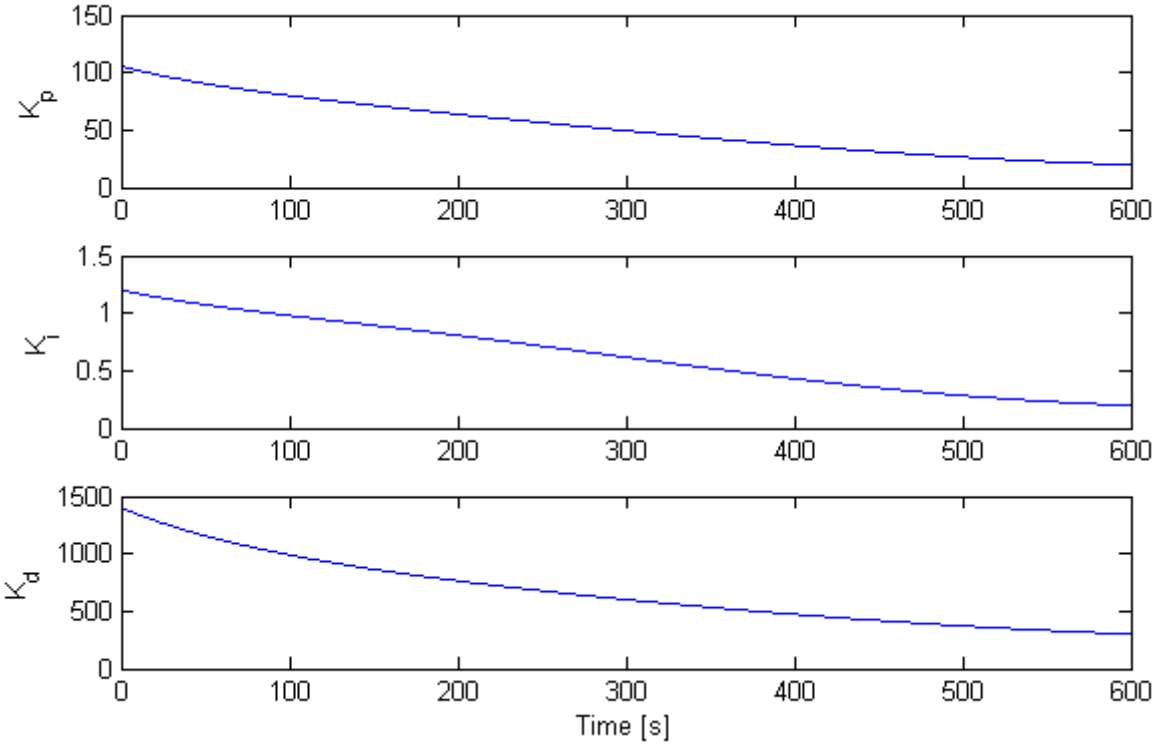

Fig. 6.25 The parameters for the PID-controller

All the parameters in Fig. 6.25 decreases through the simulation, this is function of the critical gain which also decreases as shown on Fig. 6.26. As the critical gain has influence on the control parameters these will also decrease.

The controller parameters for the APID are is not directly comparable to the controller parameters for the PID1 and PID2 because these are designed and implement as continuous controllers, whereas the APID is designed on basis of discrete model parameters.

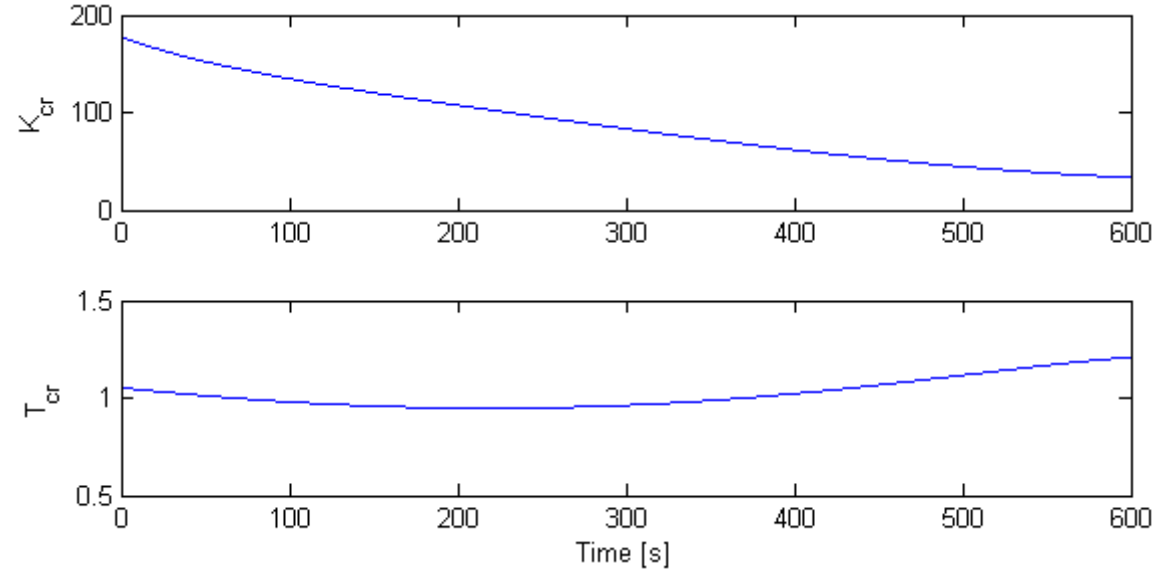

Fig. 6.26 The critical gain and critical period

As it can be seen does the critical gain decreases with time which implies that the system become more unstable as radius of the winder reel is increases. This is contradicting the observations made in chapter 3.5.1, where it is shown that and increase in radius would increase the damping of the system which should make it relatively more stable.

This is affecting all the 3 parameters K_P, K_I and K_D to decrease. The critical period of the system is oscillating slowly. This oscillation properly origins from the method used to simulate the system, as the simulated systems damping of the motor is also oscillating with one cycle/900 s as shown in chapter 5.6 on Fig. 5.20.

6.4.2 Stage 2

In this stage the controller will be tested by its ability to control the LVT system. But in this test is the system parameters fed to the controller is found via the parameter estimation algorithm. This test is primary conducted to estimate whether this loops might create unwanted phenomena. If this test proves successful the adaptive algorithm is one step closer implementation. A reference step is again tested and display on Fig. 6.27.

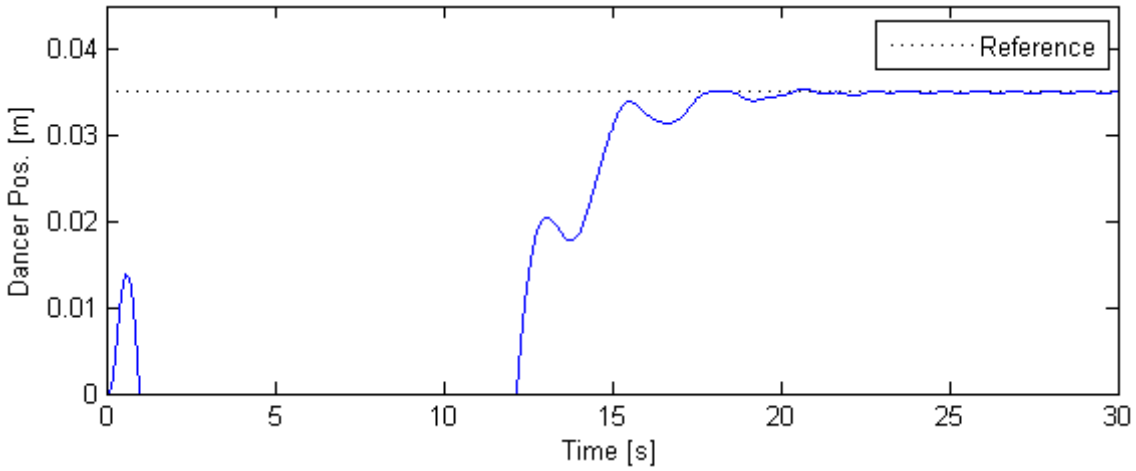

Fig. 6.27 The first 30 seconds of the step response

The step has an amplitude of 0.35 m at t=0 the results from the test is quantified in Table 6.9.

	Value
Overshoot [mm]	-1211
Settling time [s]	17.34
Rise time [s]	17.91
Steady state error	0

Table 6.9 The characteristic for the second stage

Table 6.9 represent the result of the first 30 s. The large overshoot is a result of the PEA not having estimated suitable system parameters, which renders a bad controller performance.

Fig. 6.18 show the output of the system as the LTV model changes parameters.

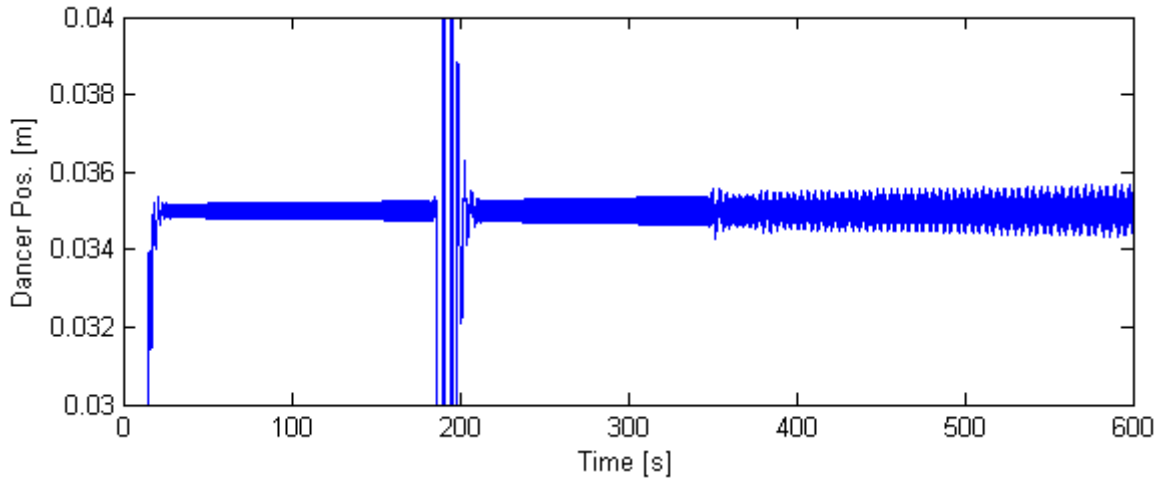

Fig. 6.28 A close up of around the reference in the hole period

From Fig. 6.28 it can be seen that the oscillating phenomena for the previous stage also occurs in this test. Though at this experiment the oscillations are larger, but still within 5% for the main part of the experiment, with exception of the period around 190 s. As shown later in Fig. 6.31, does the estimation algorithm also make large deviations at this point. It is difficult to determine whether it is the estimations which initialize a deviation which affects the controller or whether it is the controller which suddenly outputs a large peak and throws off the estimation. The debugging is difficult due to the closed loop nature of the estimation algorithm and controller block.

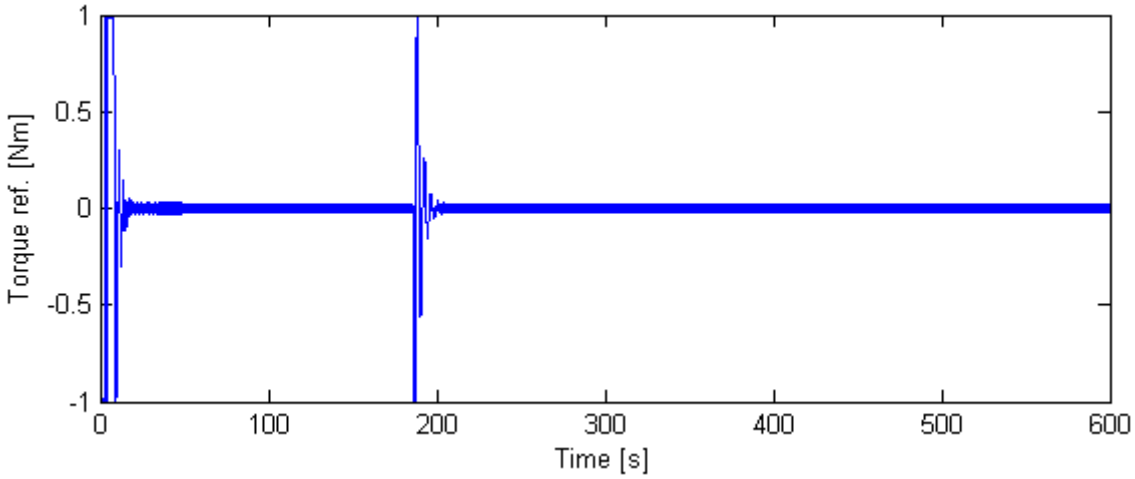

Fig. 6.29 The torque reference from the controller

It can be seen from Fig. 6.29 that the control effort still is small in the system, except for the period around 190 s.

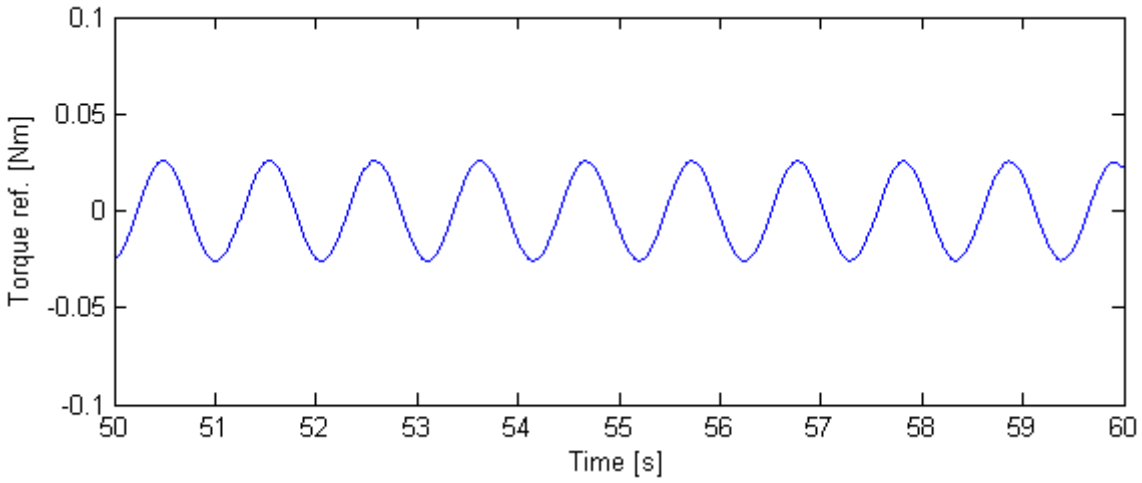

Fig. 6.30 The torque reference from the controller in the interval from the 50 to the 60 s.

It can be seen from Fig. 6.30 that there still is an oscillation in the control signal. It is still larger than the added sinusoidal signal but a lot smaller than in stage 1.

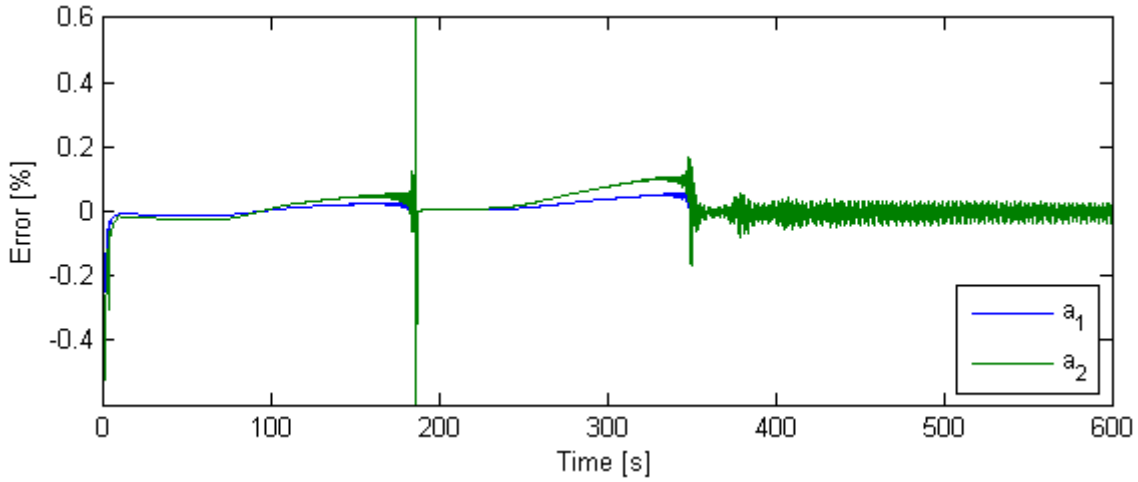

Fig. 6.31 The estimations error of a_1 and a_2

The error of the estimates for a_1 and a_2 can be seen in Fig. 6.31. the estimation is better than the estimates in stage 1, here the error of a_1 and a_2 is within +/- 0.2 %, with the exception of around 190 s and at the beginning. The bad estimates in the beginning could explain why the controller have a large overshoot, the estimates of the system is not good enough to make a reasonable controller to the system.

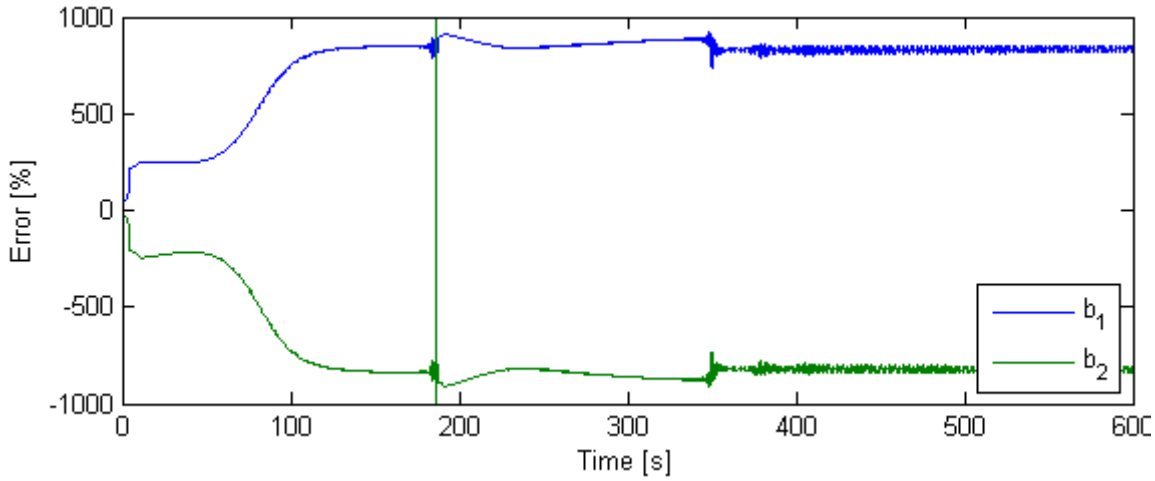

Fig. 6.32 The estimations error of b_1 and b_2

Fig. 6.32 shows the estimation of the parameters b_1 and b_2 are just as poor as the estimation in stage 1. But it is noteworthy that the estimates are very alike the estimates from stage 1. This indicates that the combination of adaptive PID controller and parameter estimation does have a positive influence on each other. This can be seen from the a-parameters are found better, and the b-parameters are found with similar deviation compared to stage 1. The exception is the large error at 190 s. The parameters reach a level of around 800 % over and under the correct value.

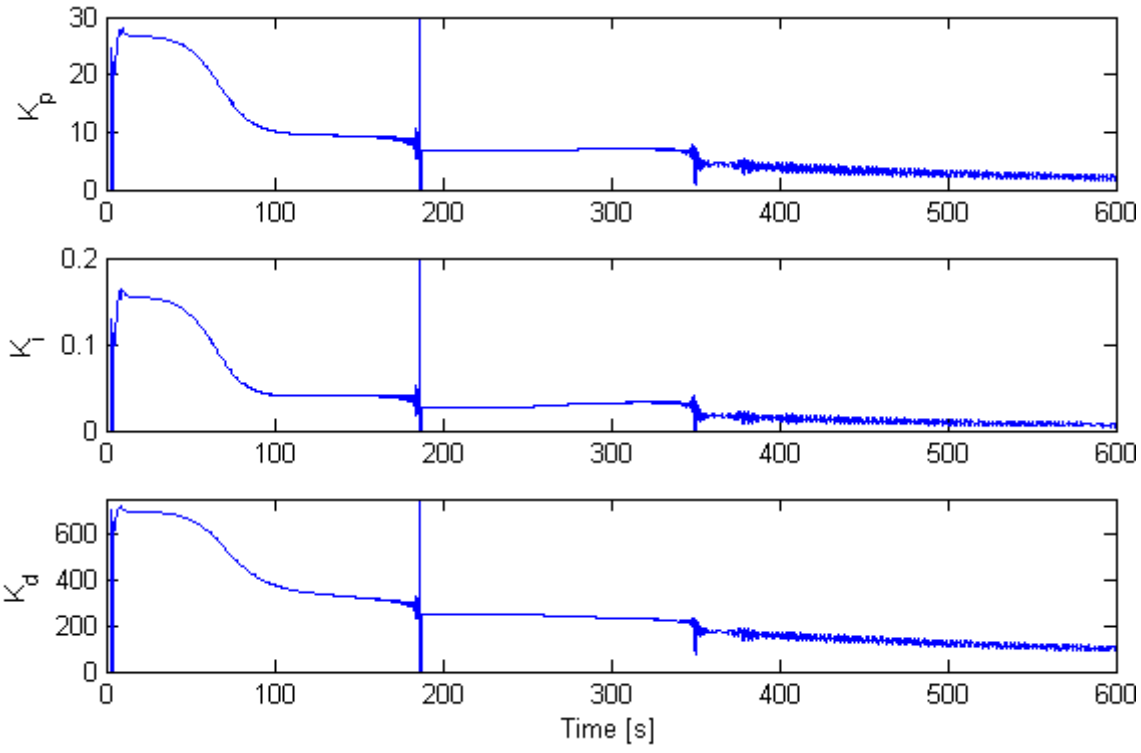

Fig. 6.33 The parameters for the PID-controller

The gains for the PID-controller shown on Fig. 6.33 finds a level for the first 70 seconds, when this period is completed all the parameters drops to a level below the values found in stage 1. The ratio between the found values are 1:3 between stage 2 and stage 1. It can also be noted that in stage 1 the parameters for the controller was decreasing steady, but here in stage 2 after approx 350 s the parameters begins to oscillate.

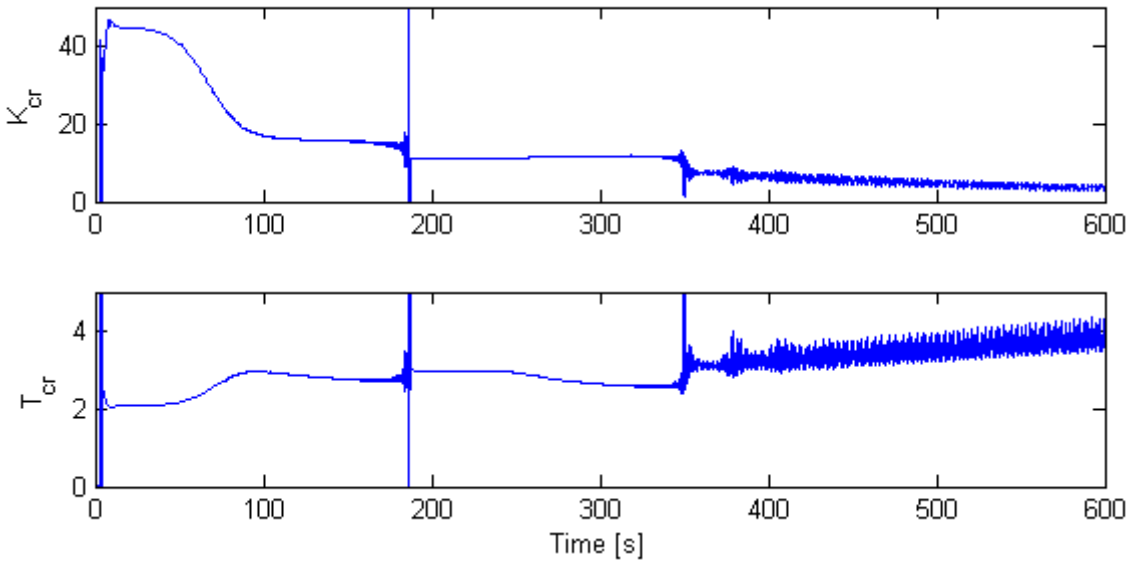

Fig. 6.34 The critical gain and critical period

From Fig. 6.34 it is seen that the critical period does not display the sinusoidal behavior as in stage 1. It has a tendency to maintain a constant level for a period e.g. from 190 to 250 s. The critical gain also experiences almost flat level from 190 s to 350.

From stage 2 it can be seen that system does not perform as wanted all the time, but it is able to handle large deviation from the correct parameters.

6.4.3 Stage 3

In this stage the controller will be tested in the same way as stage 2, by controlling a system which parameters are continuously being estimated, but with noise introduced into the output of the LTV system. The concept is displayed in the introduction to this chapter. This is to show that the system is able to control the system even when it does not use the correct parameters due to noise added to the system. The noise employed is the same as used in the parameter estimation chapter to investigate the PEAs robustness.

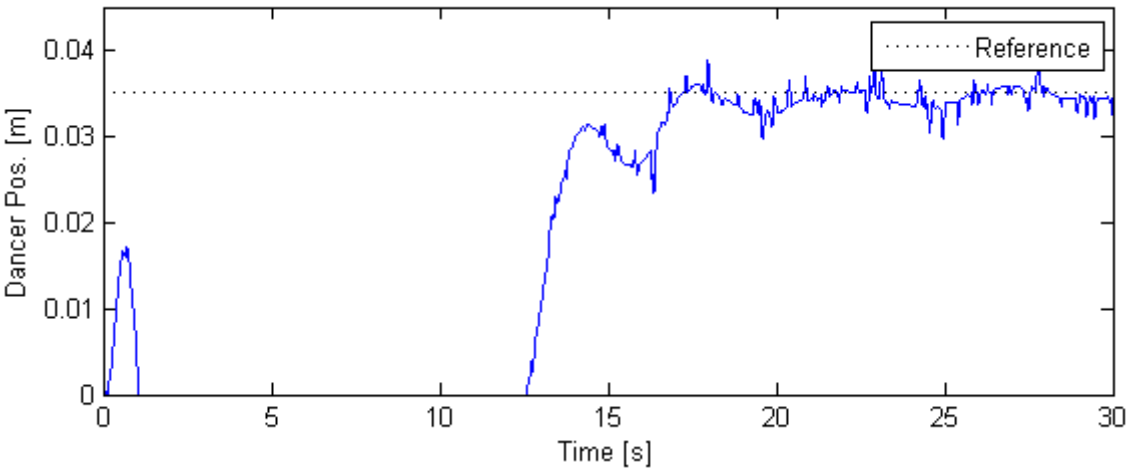

Fig. 6.35 The first 30 s of the step response

	Value
Overshoot [mm]	-825.6
Settling time [s]	>30
Rise time [s]	16.82
Steady state error	0

Table 6.10 The characteristic for the third stage

It should be noted that the high settling time is a result of the noise, on the signal as it can be seen in Fig. 6.35 the noise is visible as small peaks on the position. It is difficult to find a settling time due to the fact that the measurements are larger than 5 % of the reference.

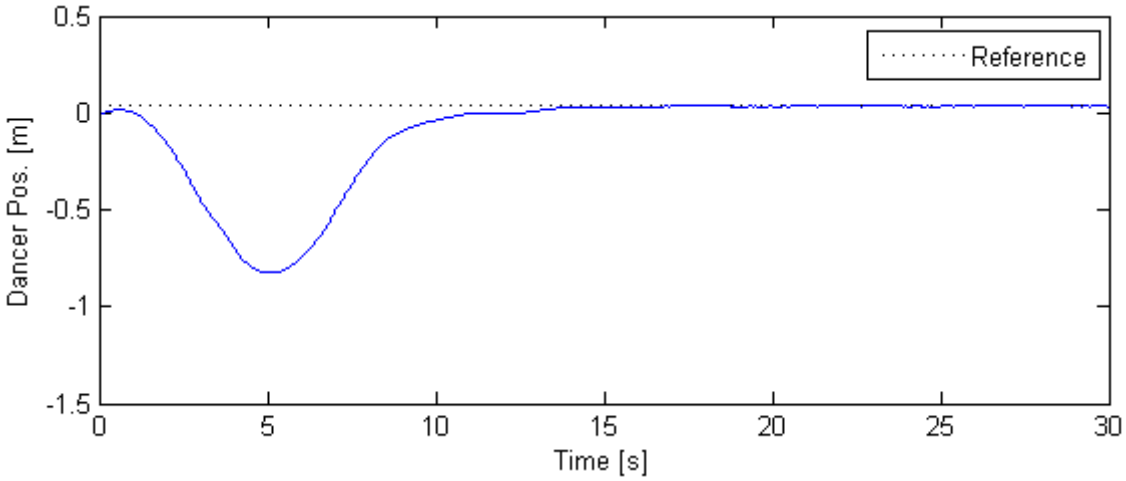

Fig. 6.36 The whole signal of the first 30 s of the step response

In Fig. 6.36 it can be seen that the system have a large overshoot but it is able to have 0 steady state error.

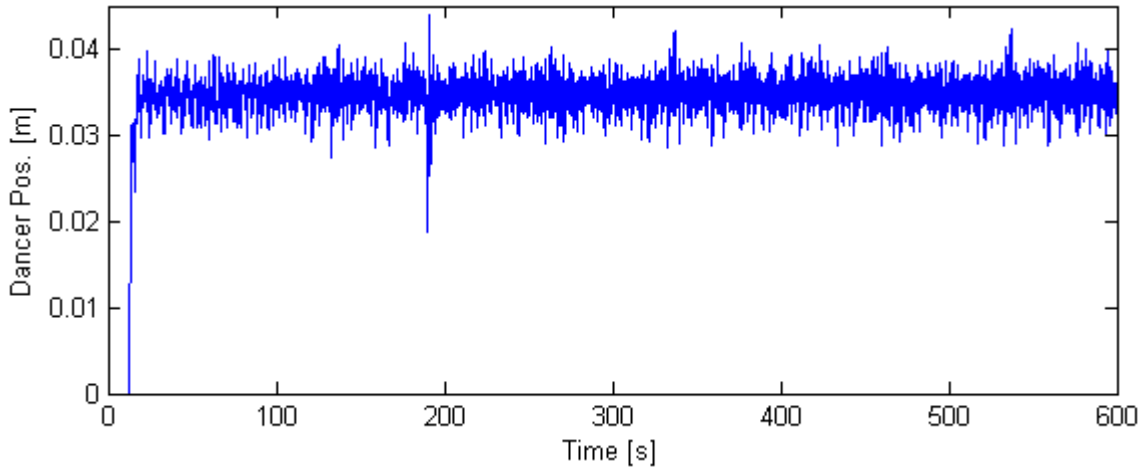

Fig. 6.37 The whole period of the step response

Fig. 6.37 the system is unstable in some periods e.g. approx 190 s. This is nearly the same time as in stage 2 here the large step in position occurred after 186.4 s. In stage 3 a similar error occurs after 188.5 s. This could imply that the system have an unstable behavior in this region. But the error at this point is less extreme and is faster reduced in stage 3 compared to stage 2.

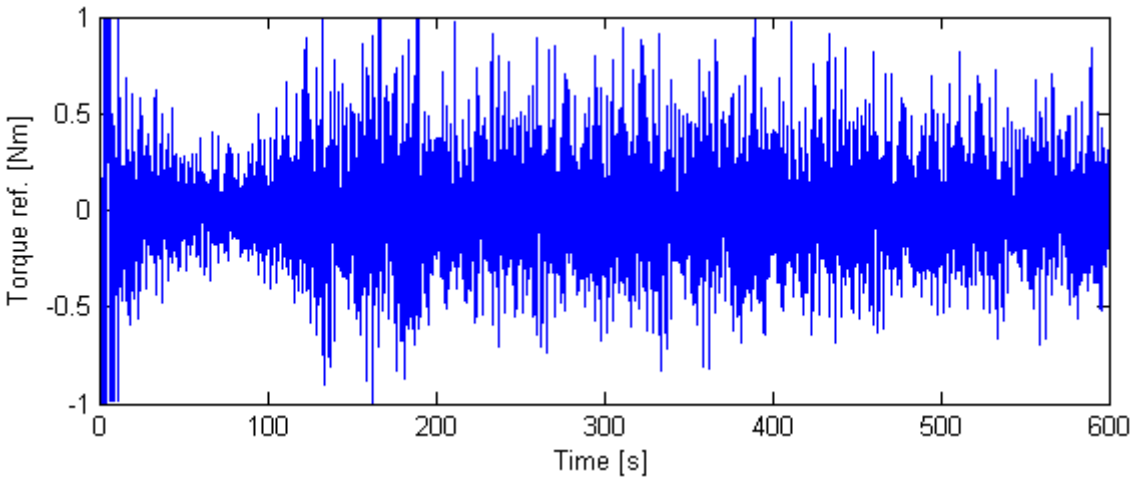

Fig. 6.38 The torque reference from the controller

Fig. 6.38 shows that opposed to stage 2, the torque demanded through the experiments has large peaks, some of them are reaching the limitation of the system.

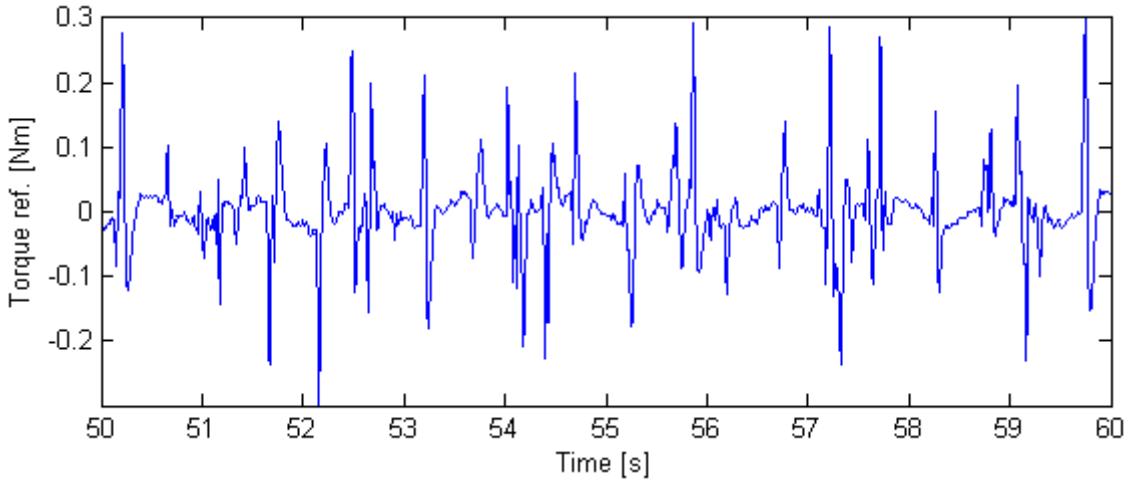

Fig. 6.39 The torque reference from the controller in the interval from 50 to 60 s

The torque signal in Fig. 6.39 seems to consist of only a few peaks that have the high values and a smaller signal just above 0. The sinusoidal excitation disturbance is also less obvious than in stage 2 and can hardly be seen.

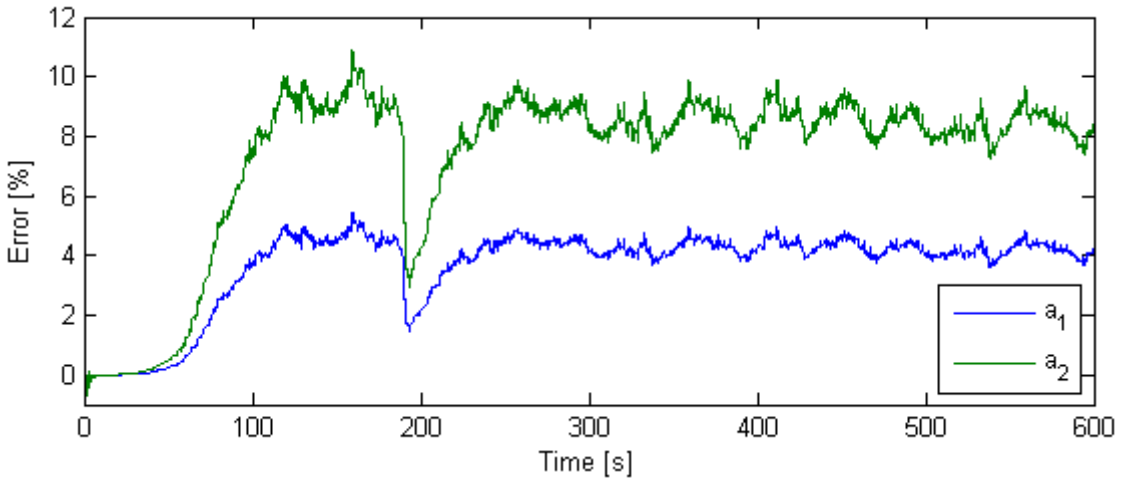

Fig. 6.40 The estimations error of a_1 and a_2

Fig. 6.40 shows the estimation error of the a_1- and a_2-parameters. The errors has a maximum values of 11.3, but is kept at a level of approx. 9 % for a_1 and approx. 4 % for a_2 through most of the simulation. This error is larger than in stage 2, but the error peak at around 190 s is reduced.

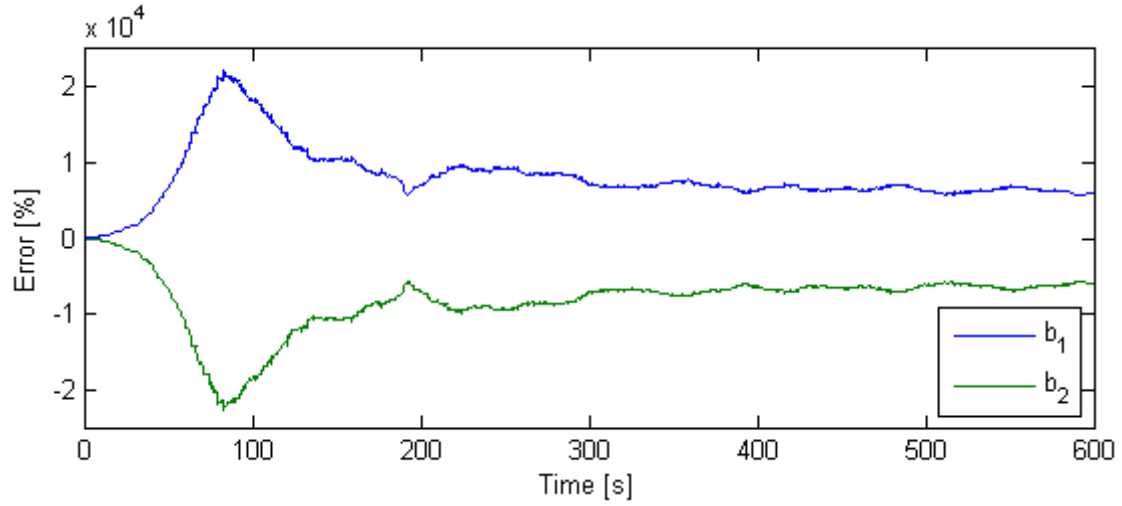

Fig. 6.41 The error of b_1 and b_2

The estimation error of b_1 and b_2 has a large peak error around 90 s, but the error is for the most approximately 1000 % as seen in Fig. 6.41. This is approximate the same size as in stage 2 and stage 1. The difference in the estimation between stage 1,2 and 3 is, that stage 3 has high error values of 20000 % whereas the error in stage 1 and 2 is about 1000 % before the errors levels out.

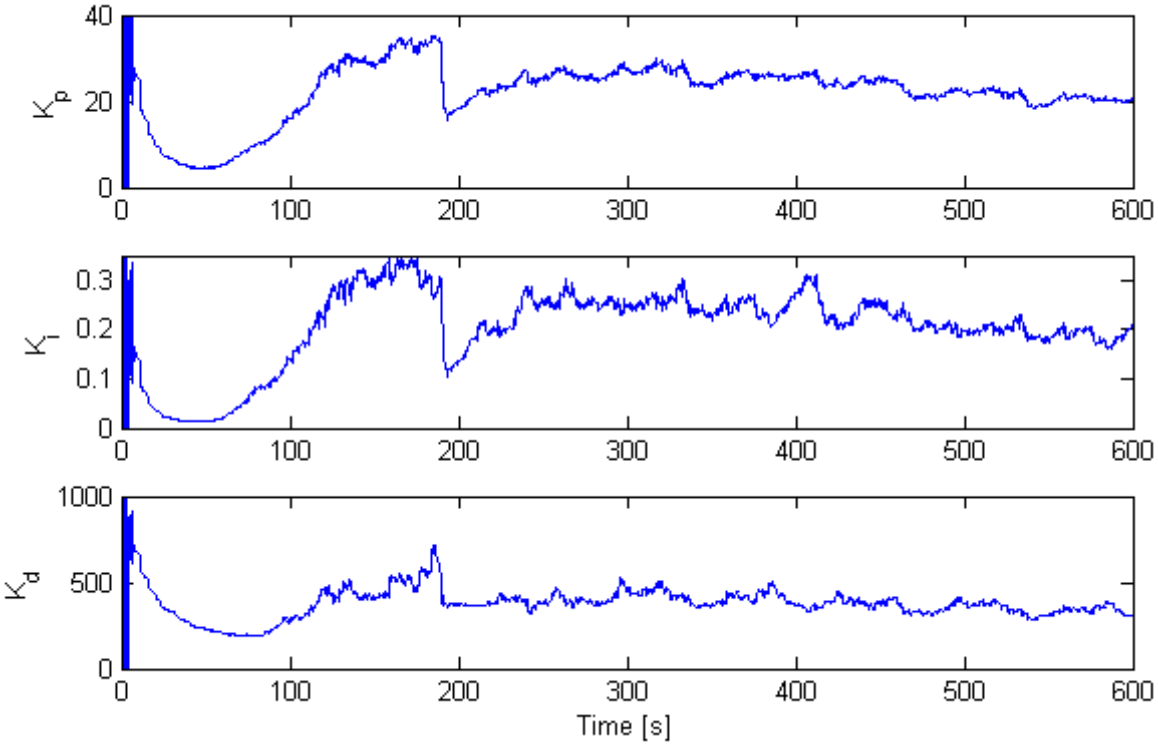

Fig. 6.42 The parameters for the PID-controller

By studying Fig. 6.42 it can be seen that the controller parameters first find a tendency after the error peak around 190 s. This effect can also be seen in Fig. 6.43 where the critical gain and period is shown.

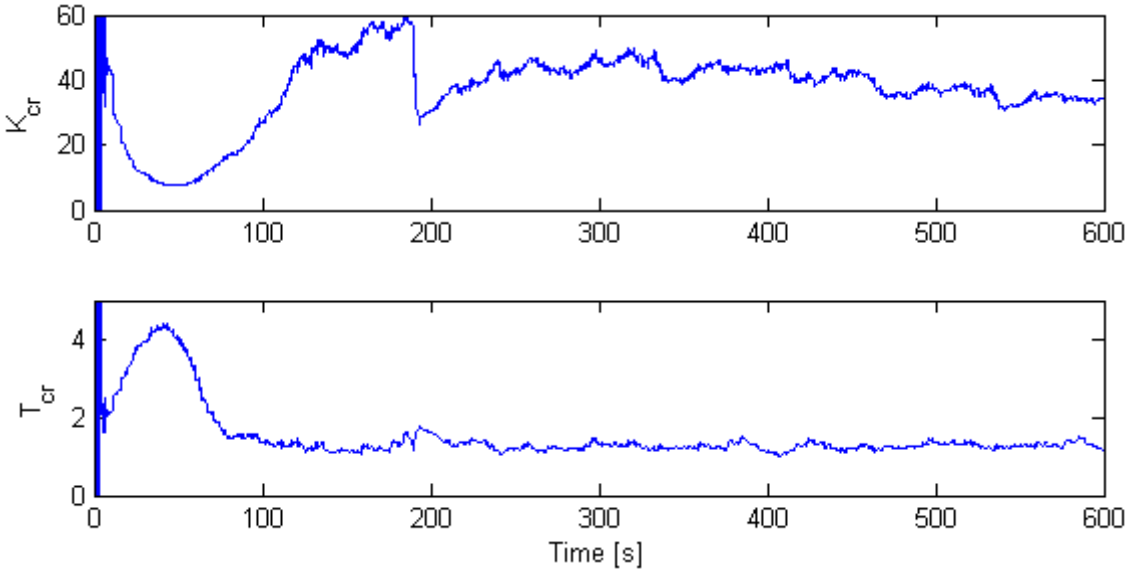

Fig. 6.43 The critical gain and critical period

6.4.4 Summary of APID-controller simulations

The characteristic for the step respond for the 3 different stages are shown in Table 6.11.

	Stage 1	Stage 2	Stage 3
Overshoot [mm]	2.17	-1211	-825.6
Settling time [s]	4.51	17.34	>30
Rise time [s]	0.0216	17.91	16.82
Steady state error [mm]	0	0	0

Table 6.11 The characteristic for the 3 step resonses

From Table 6.11 it can be seen that controller shown poor performance when the controller parameters is determined by the estimated parameters, this is properly because the estimation is very poor in the beginning where the step is executed. It is found that the controller is able to handle some noise in the system. The noise have some positive effect on the system because the estimation of the parameters do not have large steps in the values. Over all does the performance of the regulator not seem convincing, as the dancer oscillates and the system parameters are poorly estimated. But this should be seen in the light of the regulation being constantly disturbed by the excitation signals which induces the oscillations. It should also be remarked that the system parameters aren't estimated as anticipated, but as test shows, do they still represent the systems dynamics good.

Tendencies to positive synergy can also be detected from stage 2 where the parameter estimation was improved by the controller-estimation feedback loop. The adaptive PID controller should therefore be implemented in the real system, but the parameter estimation should be allowed to estimate for some time to find good estimates, before the APID controller is allowed to run the web winder.

6.5 Pole Placement Controller

This section will describe how a pole placement controller is designed and implemented in the web winder system. Starting with some general consideration on how to design a system with a pole placement controller, later it is shown how the theory is applied to the web winder system and how the specific discrete transfer function for the system is applied.

The idea of a pole placement controller is to move the poles of a system to a desired location where the system performance will be better. This could e.g. be achieved by changing the damping or the bandwidth of the system. The fundamental basis of arbitrary pole placement is exact knowledge about the systems transfer function. This is assumed known through the application of the PEA algorithm.

The closed loop poles of a given system can be found as the roots in the characteristic polynomial. If the open loop transfer function is changed, this will also affect the closed loop system. The principle of the controller is to change the systems transfer function until the wanted poles are obtained. The theory applied in this section is based upon (Cheok).

The controller has the structure shown in (6.31), for a discrete second order system, used to represent the web winder .

$$\frac{E(z)}{U(z)}=\frac{Q(z)}{P(z)}=\frac{q_1 z+q_2}{p_1 z+p_2}$$

(6.31)

When the order of the system is raised the order of the controller also has to be raised to be able to control all the poles.

The controller Q(z)/P(z) and the system B(z)/A(z) is illustrated in Fig. 6.44.

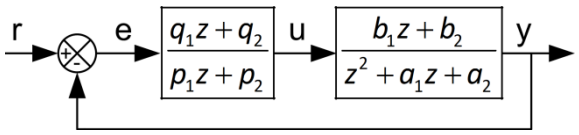

Fig. 6.44 The system with feedback

When the system and the controller is combined the transfer function from *r* to *y* can be seen in (6.32).

$$\frac{Y(z)}{R(z)}=\frac{1}{1+\frac{Q(z)}{P(z)}\frac{B(z)}{A(z)}}=\frac{P(z)A(z)}{P(z)A(z)+Q(z)B(z)}$$

(6.32)

The characteristic polynomial will be as shown in (6.33)

$$A(z)P(z)+B(z)Q(z)=D(z)$$

(6.33)

The characteristic equation is determining the behavior of the closed loop system. The characteristic equation has the structure shown in (6.34), where λ is a pole.

$$D(z)=(z-\lambda_1)(z-\lambda_2)(z-\lambda_3)\ldots(z-\lambda_n)$$
$$D(z)=d_0 z^n+d_1 z^{n-1}+d_2 z^{n-2}\ldots d_n z^0$$

(6.34)

For n=3 in this systems case, the three poles will give the equations in (6.35) for d_0 to d_1.

$$
\begin{aligned}
d_0 &= 1 \\
d_1 &= -\lambda_1 - \lambda_2 - \lambda_3 \\
d_2 &= \lambda_1\lambda_2 + \lambda_1\lambda_3 + \lambda_2\lambda_3 \\
d_3 &= -\lambda_1\lambda_2\lambda_3
\end{aligned}
$$

(6.35)

By comparing the power of z in (6.33) in combination with right side of (6.34) as shown in (6.36) it is possible to determine d_1 to d_3.

$$
\left(z^2 + a_1 z + a_2\right)\left(p_1 z + p_2\right) + \left(b_1 z + b_2\right)\left(q_1 z + q_2\right) = d_0 z^3 + d_1 z^2 + d_2 z + d_3
$$

(6.36)

By selecting the wanted poles λ_1 to λ_3 it is possible to calculate d_1 to d_3 by means of (6.35). To make the calculation of p_1, p_2,q_1 and q_2 more transparent equation (6.36) can be rewritten into the matrix form shown in (6.37).

$$
\begin{bmatrix} 1 & 0 & 0 & 0 \\ a_1 & 1 & b_1 & 0 \\ a_2 & a_1 & b_2 & b_1 \\ 0 & a_2 & 0 & b_2 \end{bmatrix} \begin{bmatrix} p_1 \\ p_2 \\ q_1 \\ q_2 \end{bmatrix} = \begin{bmatrix} d_0 \\ d_1 \\ d_2 \\ d_3 \end{bmatrix}
$$

(6.37)

With exception of $p_1=d_0=1$ the rest of coefficients will be found using Cramer's rule, this is shown in appendix D. The result of the calculations for p_1 to q_2 can be seen in (6.38). Equation (6.38) is expressed as fractions with several constants instead of matrix equations. This form is chosen for its simplicity to later implementation in non-matrix compatible hardware on the test bench

$$
\begin{aligned}
p_1 &= d_0 \\
p_2 &= \frac{d_1\left(b_2 \cdot b_2 - 0 \cdot b_1\right) + b_1\left(b_1 \cdot d_3 - d_2 \cdot b_2\right) - d_0\left(b_2 \cdot \left(a_1 \cdot b_2 - b_1 \cdot a_2\right)\right)}{b_2 \cdot b_2 + b_1\left(b_1 \cdot a_2 - a_1 \cdot b_2\right)} \\
q_1 &= \frac{\left(d_2 \cdot b_2 - b_1 \cdot d_3\right) + d_1 \cdot \left(b_1 \cdot a_2 - a_1 \cdot b_2\right) + d_0\left(a_1 \cdot \left(a_1 \cdot b_2 - b_1 \cdot a_2\right) - a_2 \cdot b_2\right)}{b_2 \cdot b_2 + b_1\left(b_1 \cdot a_2 - a_1 \cdot b_2\right)} \\
q_2 &= \frac{\left(b_2 \cdot d_3\right) + b_1\left(d_2 \cdot a_2 - a_1 \cdot d_3\right) + d_1\left(-b_2 \cdot a_2\right) - d_0\left(a_2\left(b_1 \cdot a_2 - a_1 \cdot b_2\right)\right)}{b_2 \cdot b_2 + b_1\left(b_1 \cdot a_2 - a_1 \cdot b_2\right)}
\end{aligned}
$$

(6.38)

These equations are the basis for calculating the pole placement regulator parameters illustrated on Fig. 6.44.

6.5.1 Adjustable Gain

The systems characteristic equation changes when using a pole placement controller, there is therefore a risk that the steady-state gain also changes. To compensate for effect, a adjustable gain K_0 can be implemented on input to the system as shown in Fig. 6.45 (Ogata, 1995).

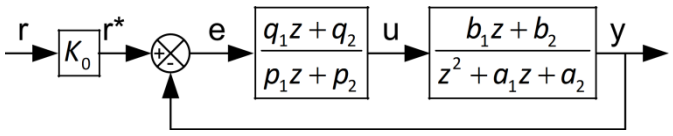

Fig. 6.45 The system with adjustable gain implemented

K_0 will be selected to be the inverse of the steady-state gain of the closed loop with the controller and model. The steady-state gain can be found by substituting z with 1 in the transfer function for the closed loop, shown in (6.39).

$$G_{\substack{cl \\ z=1}} = \frac{(q_1 z + q_2)(b_1 z + b_2)}{(p_1 z + p_2)(1 + a_1 z + a_2)} \longrightarrow \frac{(q_1 + q_2)(b_1 + b_2)}{(p_1 + p_2)(1 + a_1 + a_2)}$$

(6.39)

By selecting $K_0 = 1/G_{cl}$ for z=1 it is possible to have unity gain from input to output. This gain has to be adjusted each iteration. By adjusting the gain every iteration the system is able to take care of the change in the systems DC-gain as the radius of the reel is increased during the winding process. The complete controller function and gain is shown in Fig. 6.46.

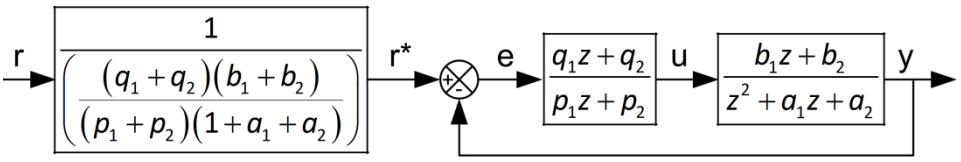

Fig. 6.46 Complete PP controller with adjustable gain

To be able to vary the controller parameters, the implementation cannot be as a simple transfer function in Simulink. These are rewritten in (6.40) to become a function of z^{-1}.

$$\frac{u}{e} = \frac{q_1 z + q_2}{p_1 z + p_2} = \frac{q_1 + q_2 z^{-1}}{p_1 + p_2 z^{-1}}$$
$$u \cdot \left(p_1 + p_2 z^{-1}\right) = e \cdot \left(q_1 + q_2 z^{-1}\right)$$
$$u \cdot p_1 = e \cdot q_1 + e \cdot q_2 z^{-1} - u \cdot p_2 z^{-1}$$

(6.40)

The controller will be implemented as illustrated in Fig. 6.47 with output saturation limits of $^{+}/_{-}$ 1 Nm. The parameter for p_1 is 1 and is implemented as a gain.

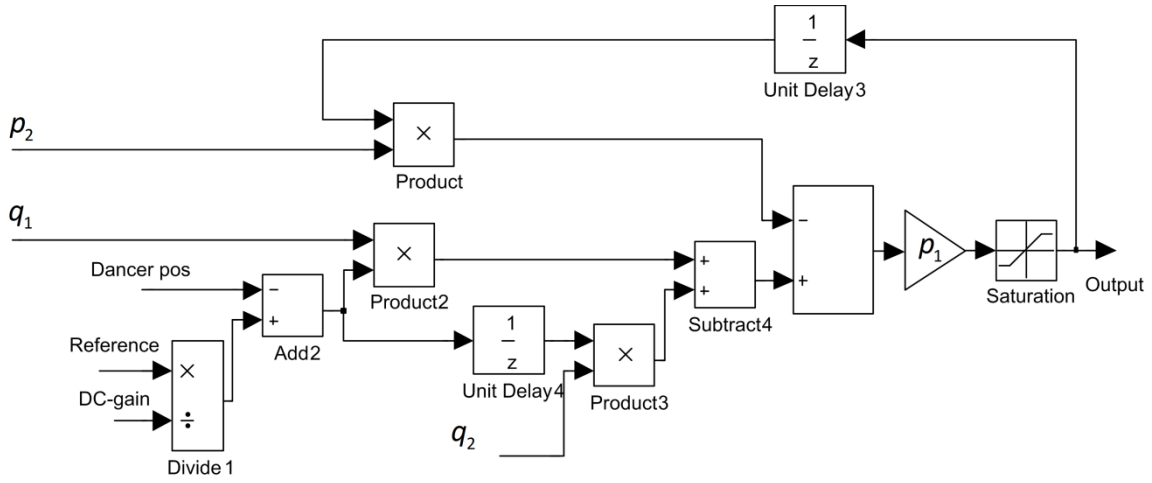

Fig. 6.47 The implementation of the pole placement controller

It is described how it is possible to implement a pole placement controller, consisting of a parameter calculation in (6.38) a DC-gain compensator and how the controller is implemented in Fig. 6.47.

6.5.2 The Selection of Poles

The wanted poles can be found by selection a damping ratio ζ and a bandwidth ω of the system. The poles with a given bandwidth and damping ratio can be found via a root locus.

When selecting new poles for the system, it should be considered how much power the new poles require (Ogata, 2002). If the new poles are much faster than the old problems could occur with actuator limitation, which would demand larger actuators. The effect of different poles location in the Z-plane can be seen in Fig. 6.48. The bandwidth of the system is written on the periphery of the unit circle, and the damping ratio is written as number from 0.1 to 0.9 inside the unit circle, the dotted line is in both cases the curve of the given bandwidth or damping ratio.

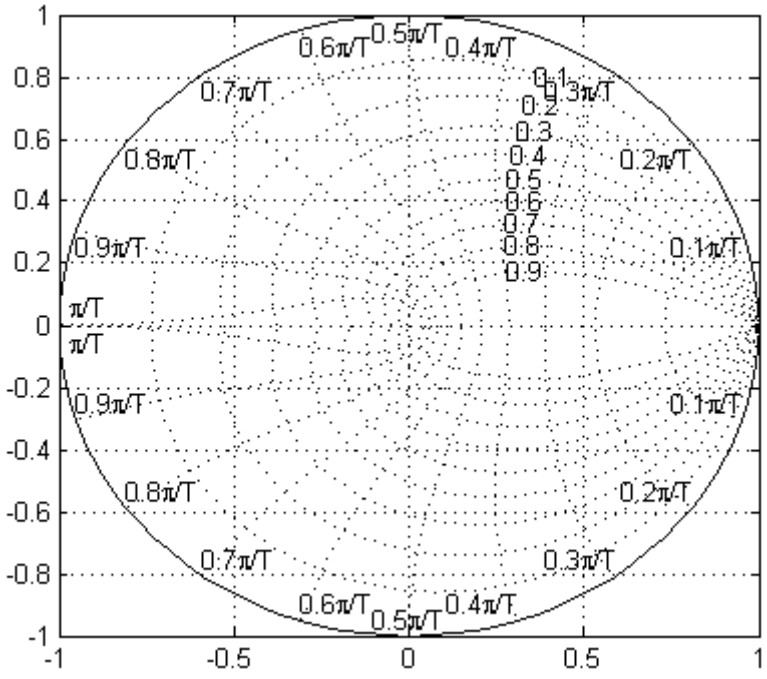

Fig. 6.48 The effect of placement of different poles

A given pole's damping and bandwidth in the Z-plane can be found by means of (6.41) and (6.42) if the pole is given in modulus and argument form.

$$|\lambda| = e^{-T_0 \zeta \omega_n} \tag{6.41}$$

$$\angle\lambda = T_0 \omega_n \sqrt{1-\zeta^2} = T_0 \omega_d \tag{6.42}$$

The desired pole-values for the pole placement controller are initially chosen as in Table 6.12, with corresponding damping and bandwidth.

Pole	Damping ratio [-]	Bandwidth [Rad/s]
0.9	1	10.54
0.9	1	10.54
0.6	1	51.08

Table 6.12 Values for selected poles

The bandwidth of the system is found to be down to 2.3 in chapter 3.5.1, this is lower than the bandwidth selected here, this might become a problem because the increase in bandwidth would cause a large control effort. If the bandwidth should be decreased the desired pole location should be moved closer to 1 in the Z-plane. The risk of having poles near 1 is that if the estimation is incorrect, this could cause the systems poles to be moved outside the unit circle, which would make an unstable system. The problem is to find balance between the risk of having an unstable system due to actuator saturation, or due to poles moving outside the unit circle. The poles listed in Table 6.12 is thought to be a compromise between these two evils.

It is shown how the pole placement controller is designed and implemented in Simulink and values for the wanted poles have been selected. The next step is to test the controller by means of simulations to test is whether it is suitable for implementation in the test bench. The test method is described in the introduction to this chapter.

6.6 Simulation Test of Pole Placement Controller

The test of the PP-controller will happen in three stages, the same as the APID and as detailed in the start of this chapter.

The first stage tests whether the PP controller performs acceptable when fed ideal model parameters. The second stage tests if the controller performs acceptable when fed estimated parameters from the PEA algorithm. The third stage is like stage 2 except noise is introduced in the system.

All simulation tests are based on a time varying LTV model which emulates the actual web winder. The simulations are also made using excitation signals to get better parameter estimates from the PEA.

6.6.1 Stage 1

In this stage the controller will be tested with the ideal system parameters as input to the calculation of control parameters. Fig. 6.30 show the dancer position during initial reference step up.

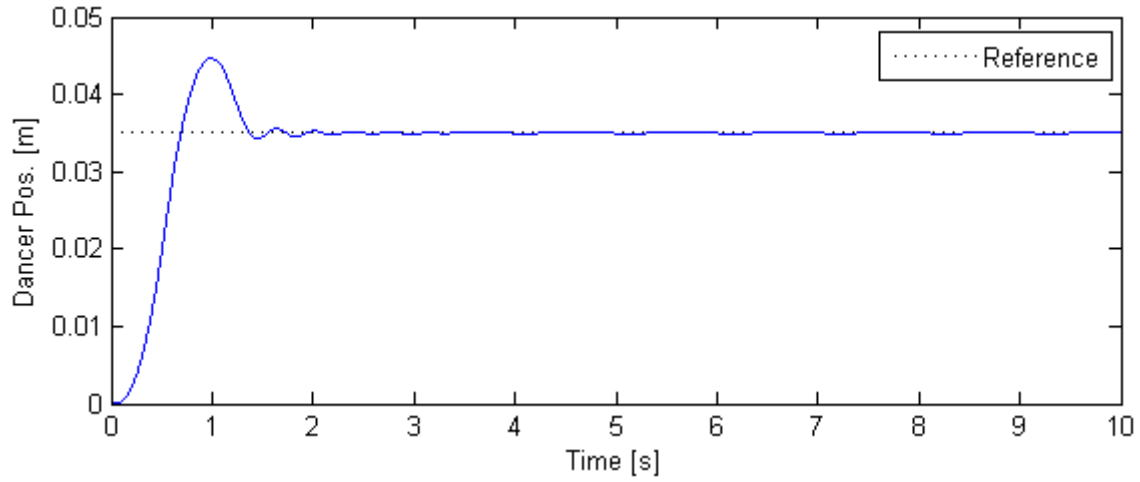

Fig. 6.49 The first 10 seconds of the step response

The step has an amplitude of 0.035 m at t=0. The results are quantified in terms of overshoot, settling time, rise time and steady state error in Table 6.13.

	Value
Overshoot [mm]	9.5
Settling time [s]	1.3
Rise time [s]	0.69
Steady state error [mm]	0

Table 6.13 The characteristic for the first stage

Table 6.13 shows the result for the first 10 s. As time progresses the behavior of the LTV system changes. To examine the controllers ability to keep the reference during changing model behavior Fig. 6.18 is made. Fig. 6.18 shows the systems output over a longer span of time.

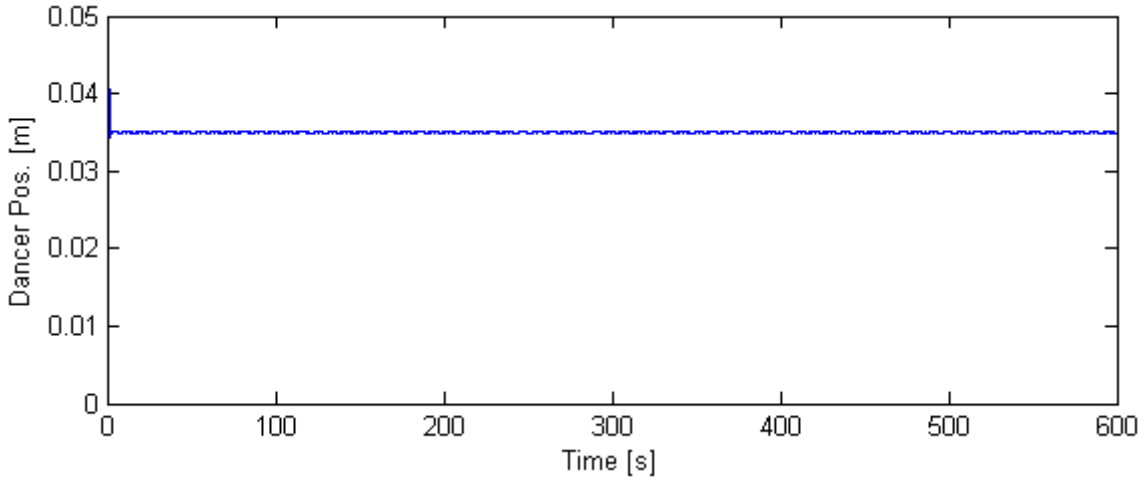

Fig. 6.50 A close up of around the reference in the hole period

Fig. 6.18 shows a slightly oscillating response. The maximum error is though within $^{+}/_{-}$1 %.This is less than the 5 % for the APID controller. Fig. 6.18 shows the control signal to the plant. It can be seen, that the control effort is small as the case for the APID controller were.

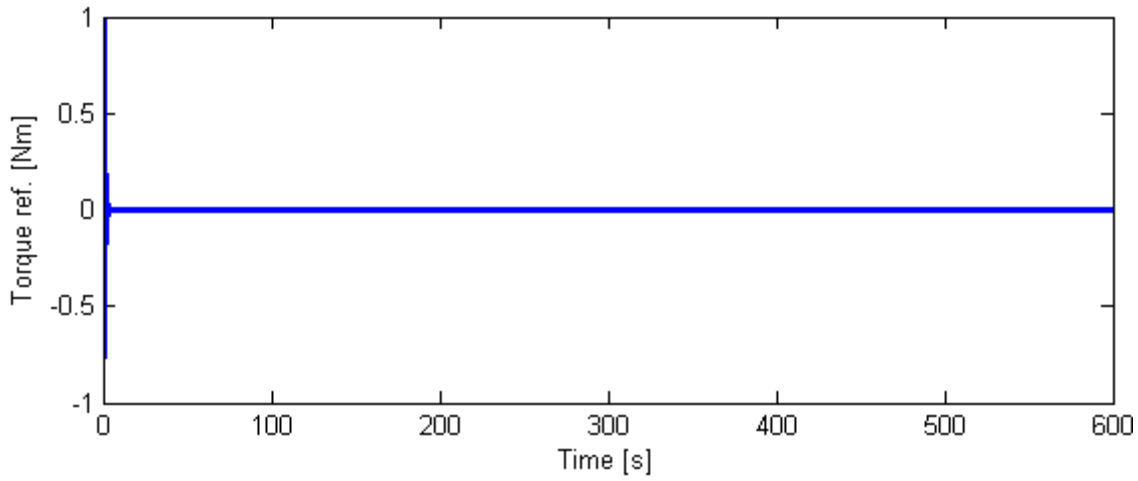

Fig. 6.51 The torque reference from the controller to the plant

Fig. 6.19 show the controller only has to do a large control effort in the beginning, hereafter the level descends fast to the level shown in Fig. 6.20

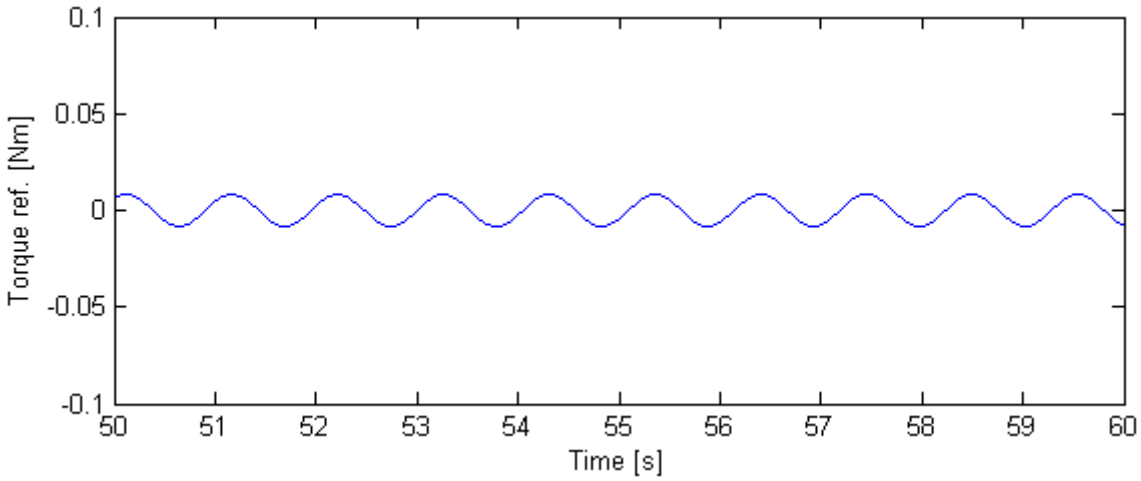

Fig. 6.52 The torque reference from the controller in the interval from 50 to the 60 s.

The injected sinusoidal excitation signal has an amplitude of 0.02 Nm, this is more than the amplitude of the torque signal in Fig. 6.20. This indicates that the controller is compensating for the added excitation signal. This might be a problem since the excitation signal is added to improve the PEAs estimates.

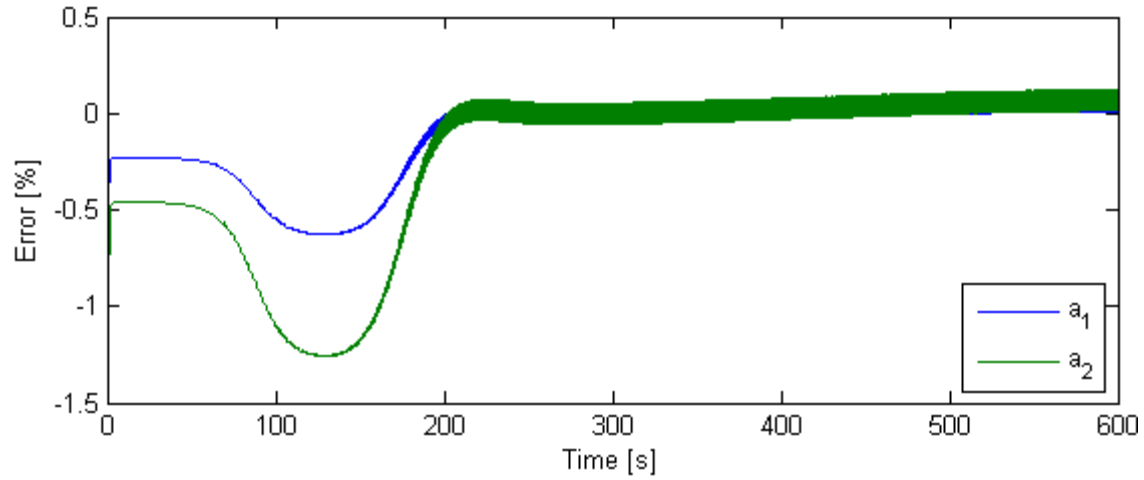

Fig. 6.53 The estimations error of a_1 and a_2

It can be seen from Fig. 6.21, that the system with this controller implemented is able to estimate for a_1 and a_2 within tolerances of 1.5% of the ideal values. This is not the case for b_1 and b_2 as it can be seen from Fig. 6.22.

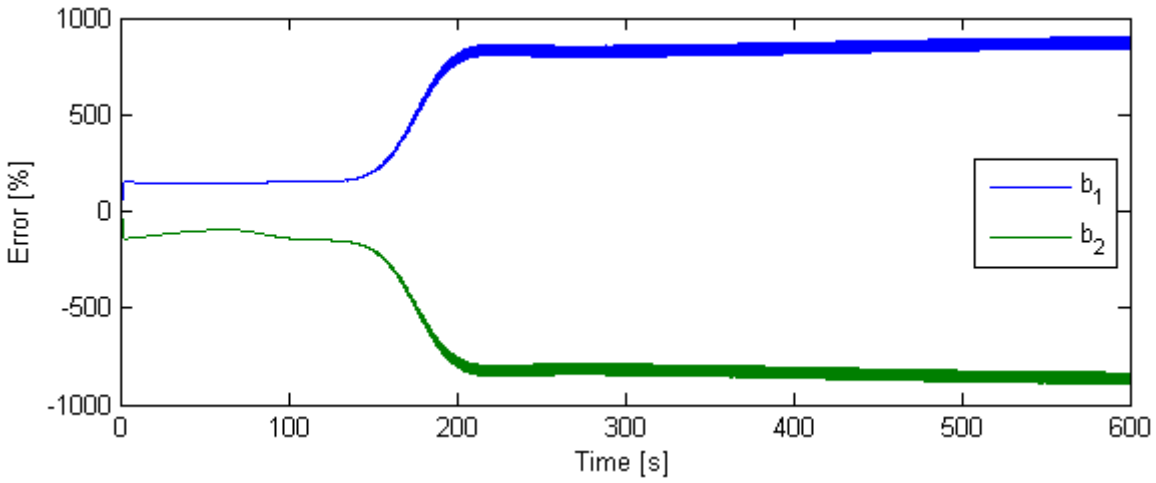

Fig. 6.54 The estimation of b_1 and b_2 for the whole period

Fig. 6.22 shows b_1- and b_2-errors of approx. 800 %, after 150 s, this indicates that the estimation algorithm might be disturbed by the addition of this controller.

This simulation indicates that the PP controller is able to keep the position output within 1 % of the reference, assumed the PP controller is fed ideal system parameters. Simulation also indicates that the PEA is disturbed by the controller, since the estimates are very inaccurate. But this does not necessary make the estimation wrong as discussed in the simulation test of the APID controller.

6.6.2 Stage 2

In this stage the controller will be tested by using the LVT-model as plant, as in stage 1. The controller is in this stage fed the estimated θ-parameters instead of the ideal.

This is to show that the system is able to control the system even when it does not use the ideal parameters. This also closes the estimation loop between the PEA and the PP controller, and makes it possible to assess whether the two blocks have positive or negative influence on each other.

Fig. 6.55 shows the initial start up where the reference is set to 0.035 m and the dancer is starting in d=0. The parameter estimation is starting from its initial guesses.

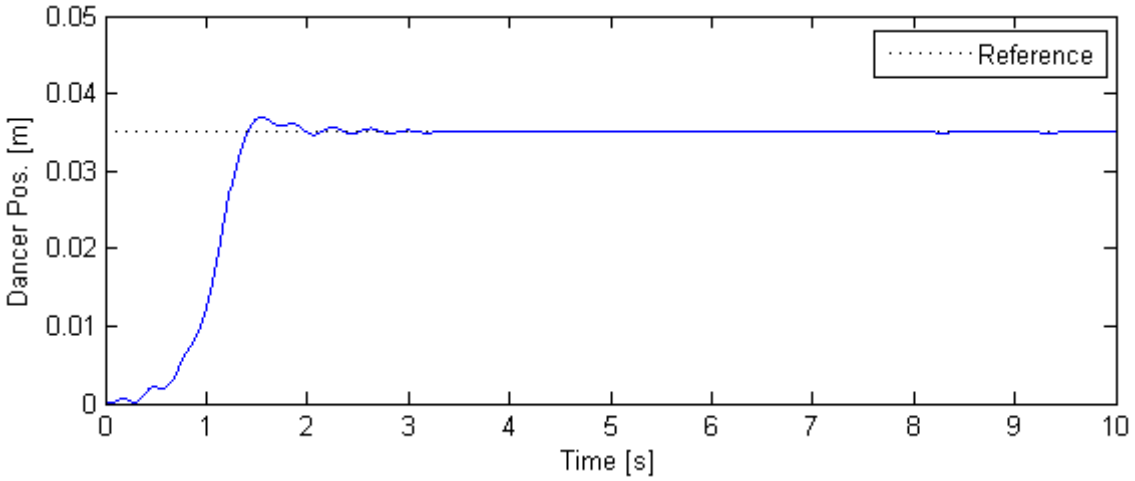

Fig. 6.55 The first 10 seconds of the step response

The start shows shows a small over shoot but at relative long rise time compared to the APID. The results for the start up simulation is shown in Table 6.14.

	Value
Overshoot [mm]	-1.91
Settling time [s]	1.59
Rise time [s]	1.4
Steady state error	0

Table 6.14 The characteristic for the second stage

Fig. 6.18 shows the rest of the controllers ability to keep the reference throughout the rest of the simulation.

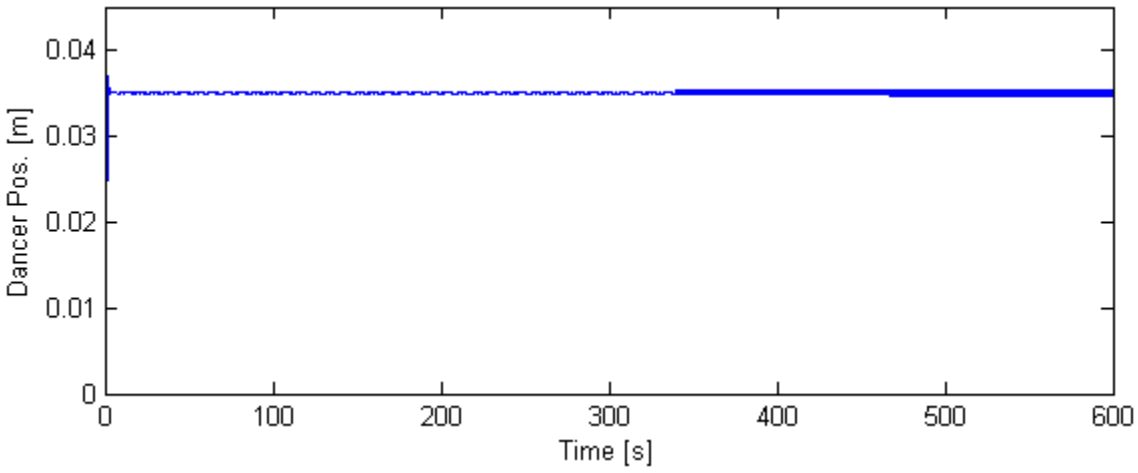

Fig. 6.56 Dancer position throughout stage 2

Fig. 6.28 show the dancer is oscillating as in stage 1 but the amplitude is rising through the simulation. But the dancer is still within 1 % of the reference from 3 s and to the end of the simulation.

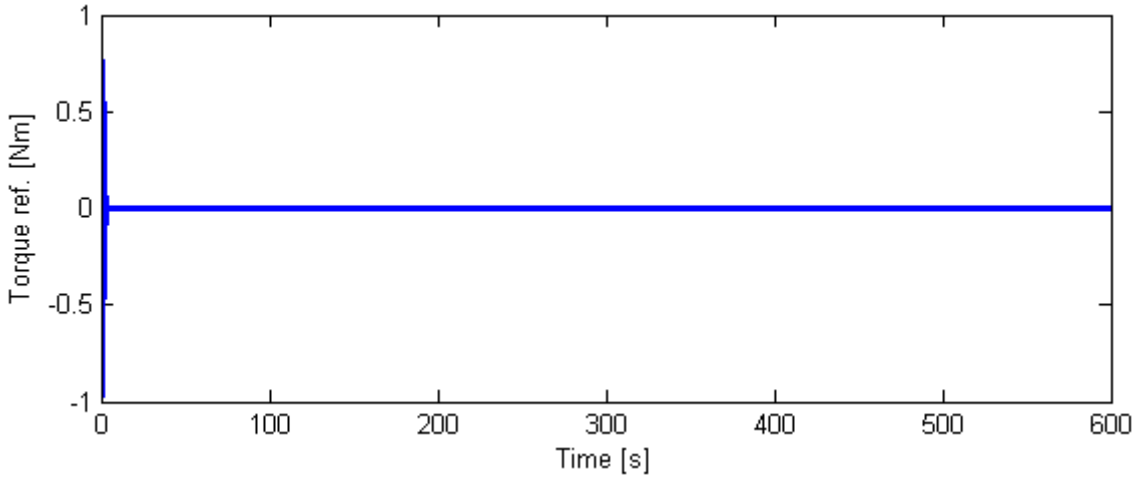

Fig. 6.57 The torque reference from the controller

Fig. 6.29 show that the control effort is small throughout the test, except for the start. Fig. 6.30 show a portion of the torque signal. This test shows that the PP controller as in stage 1 is reducing the disturbance from the excitation signal.

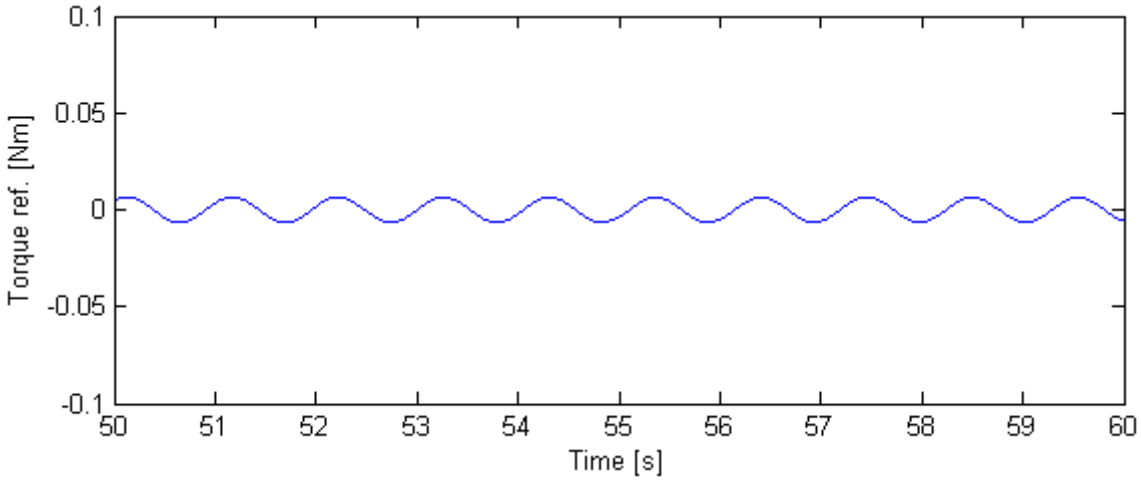

Fig. 6.58 The torque reference from the controller in the interval from 50 to 60 s.

in Fig. 6.31 show the error in percentage between the ideal a-parameters and the estimated parameters from this simulation.

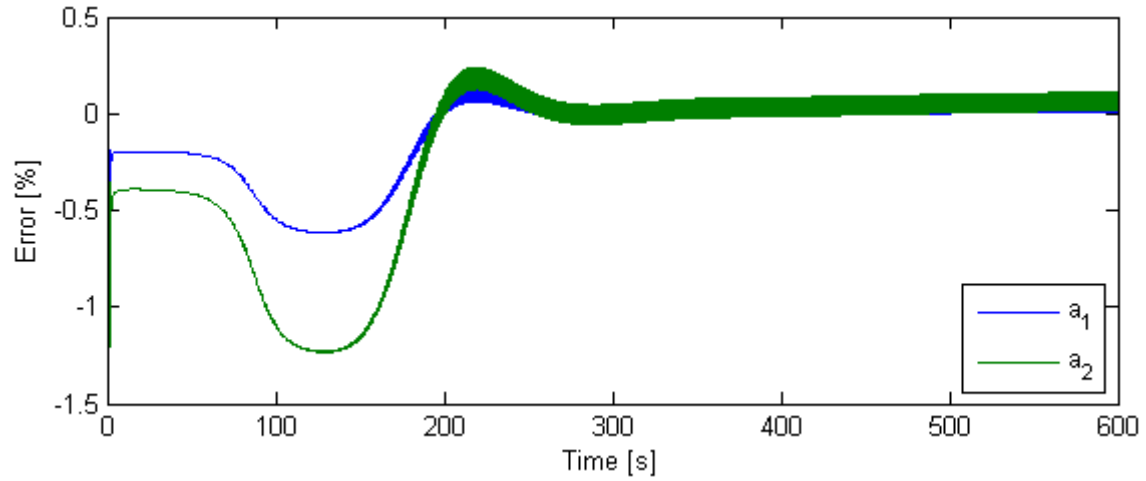

Fig. 6.59 The estimations error of a_1 and a_2

The a_1- and a_2-errors from Fig. 6.31 is alike the estimated values from stage 1, in both cases the a-parameters deviate up to 1.3% before the values drops to around $^{+}/_{-}$ 0.1%.

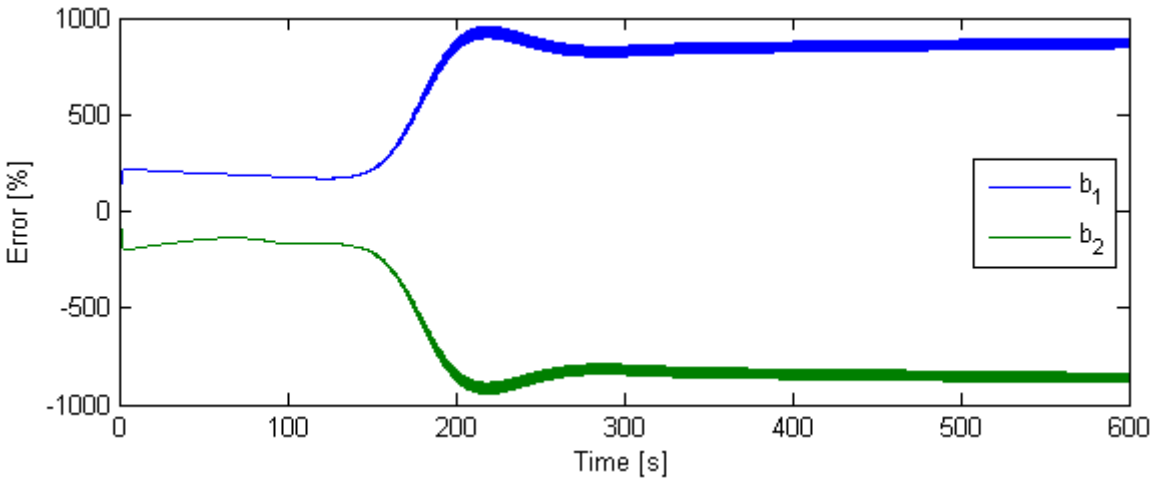

Fig. 6.60 The estimations error of b_1 and b_2

Fig. 6.32 compare the estimation of the parameters b_1 and b_2 with the ideal parameters. The comparison shows the same tendencies as in stage 1, where the parameters reaches a level of around 800 % over and under the correct value.

The inaccuracy in the parameter estimation is accepted because of the controllers' ability to keep the position deviation beneath 1% during the simulation. Deviating estimates not necessary mean a bad controller performance as discussed in stage 1. This test has shown that the PP-controller in simulations can control the output acceptable when fed estimated system parameters.

6.6.3 Stage 3

This test is essentially like stage 2 except for the addition of measurement noise in the simulation. This test will show the PP-controllers performance when noise is disturbing the feedback signal and the PEA. The test method is in detail described in the start of this chapter.

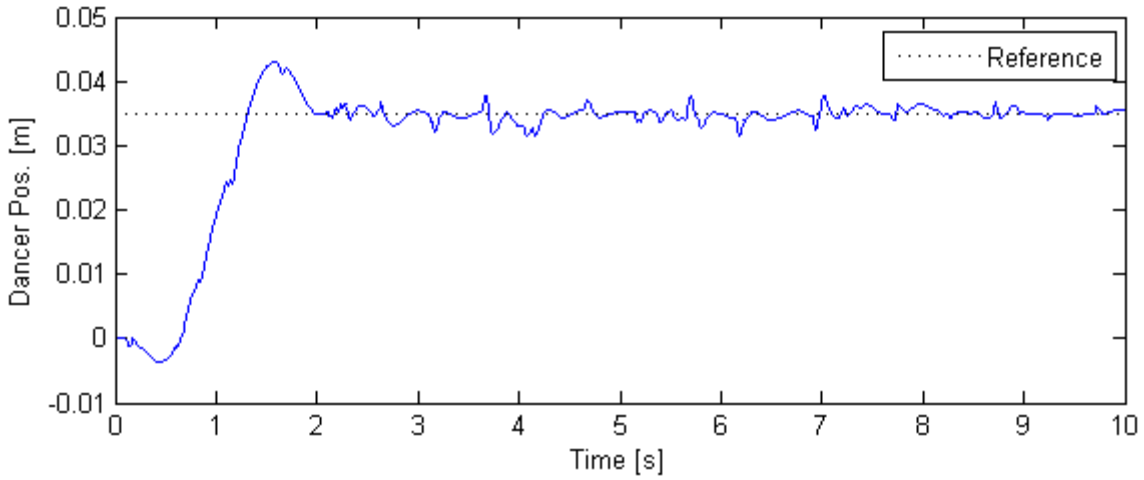

Fig. 6.61 The first 10 s of the step response

Fig. 6.35 shows the systems response in the first 10 s of the simulation. The response is compared to stage 2 more fluctuating, due to the added noise. But the output is kept close to the reference after 2 seconds, despite the addition of noise.

	Value
Overshoot [mm]	7.9
Settling time [s]	>10
Rise time [s]	1.31
Steady state error	0

Table 6.15 The characteristic for the third stage

As for the APID controller tests 3rd stage, it is not possible to determine a settling time because the position movements are larger than the tolerance selected to determine the settling time. Fig. 6.36 is made to examine the controllers ability to control the systems output when the model changes behavior.

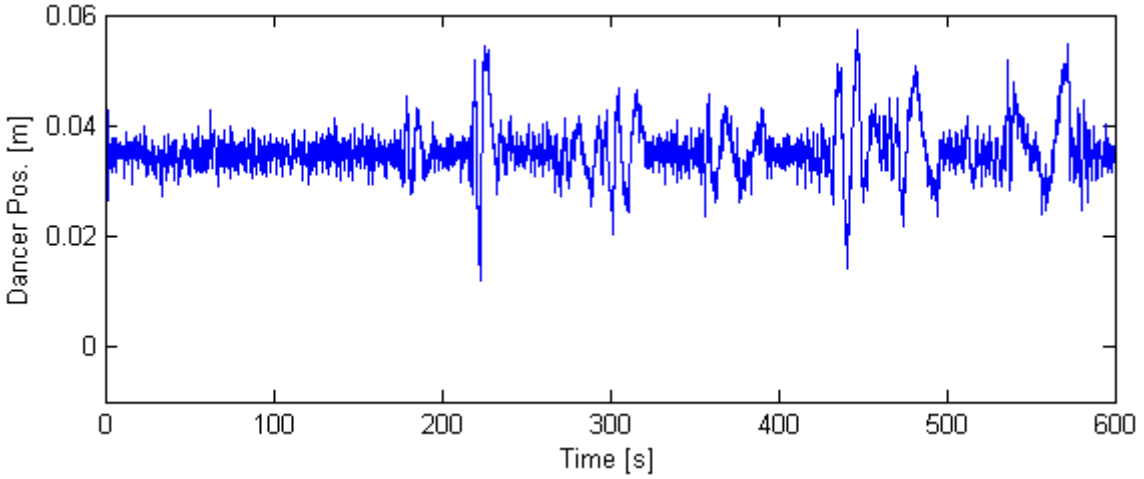

Fig. 6.62 The whole signal of the first 30 s of the step response

Fig. 6.36 shows periods e.g. around 190 s, 220 s and 430 s where the position is relative more unstable than the rest of the simulation. The APID controller was also unstable Around 190 s. but the other unstable sections have no relation to previous observations.

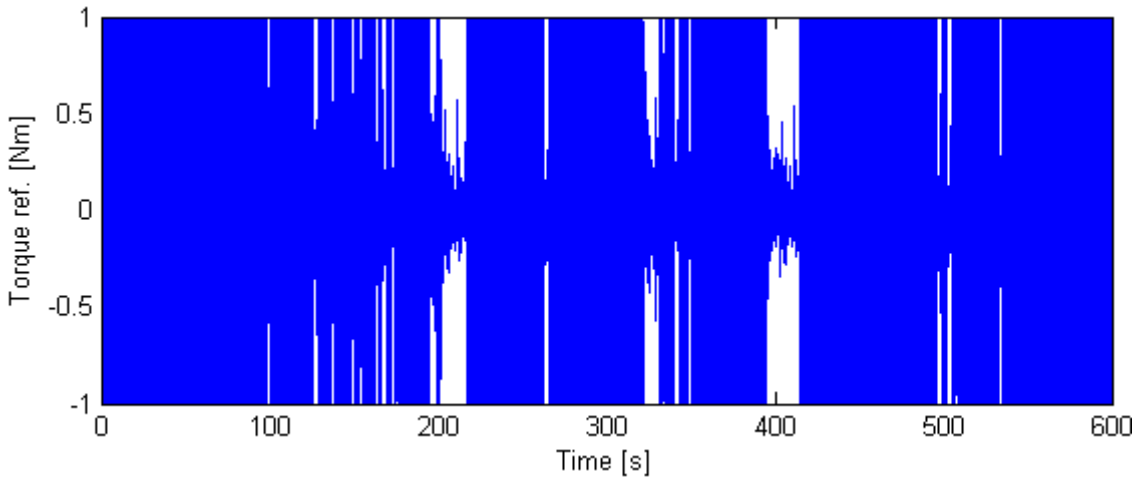

Fig. 6.63 The torque reference from the controller

Fig. 6.38 shows the torque signal to the plant. It can be seen that opposed to stage 1 and 2, the torque demanded cycles between the limits through almost the entire simulation. This is not a good thing because it indicates actuator saturation if the system experiences significant noise. This makes the system unable to cope with possible disturbances.

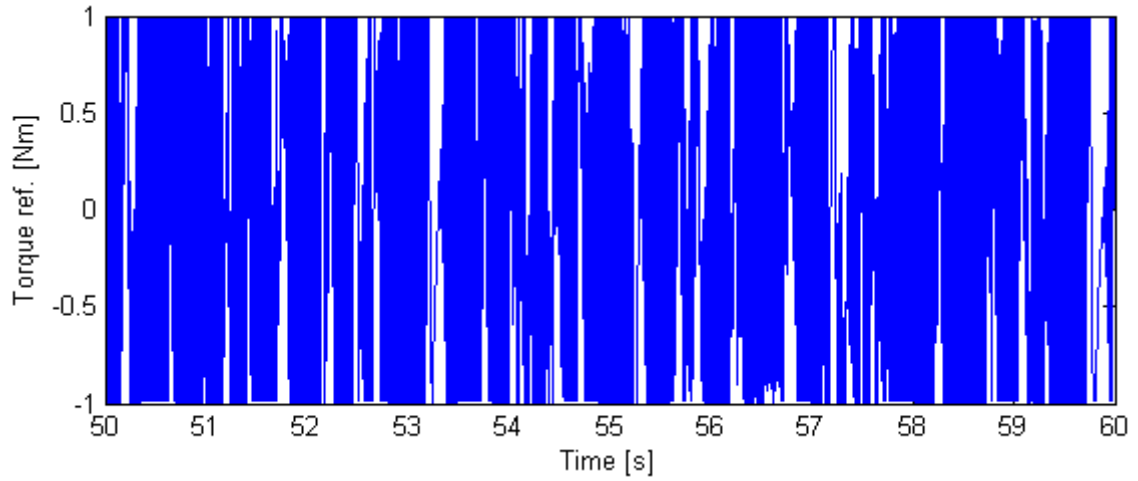

Fig. 6.64 The torque reference from the controller in the interval from the 50 to the 60 s.

The saturation in Fig. 6.39 becomes easier to analyze with the last second enlarged as shown on Fig. 6.65.

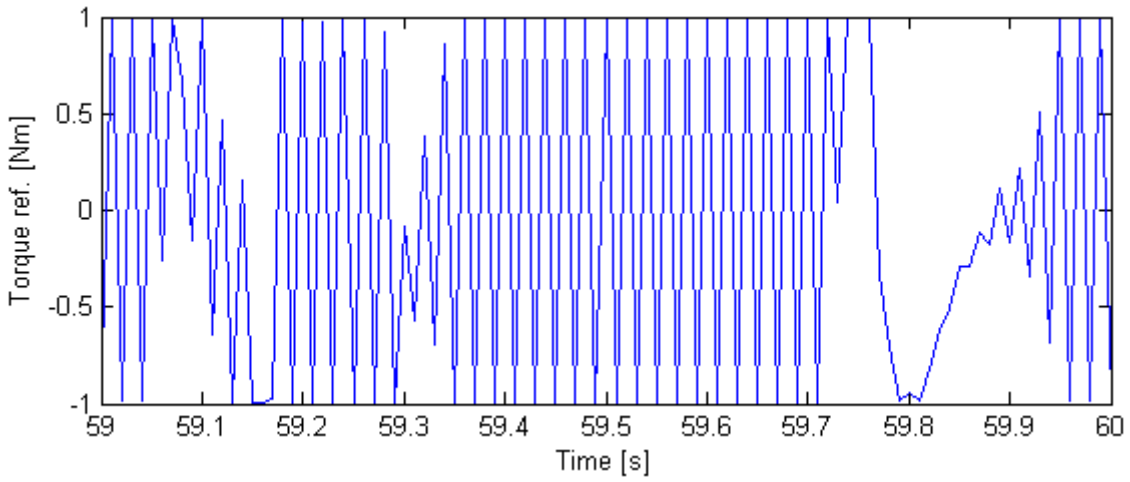

Fig. 6.65 The torque reference from the controller in the interval from the 59 to 60 s.

It can be seen from Fig. 6.65 that torque signal reaches the limitations almost every sample time. Table 6.16 contains a account of the saturation problem.

Modes	Number of times in each mode
Upper saturation	36
No saturation	27
Lower saturation	37

Table 6.16 Number of times in saturation.

Table 6.16 shows the system is in saturation 73 % of the time examined. This is not a desired controller behavior; it would be preferable to have a lower value for longer periods instead of having saturation all the time.

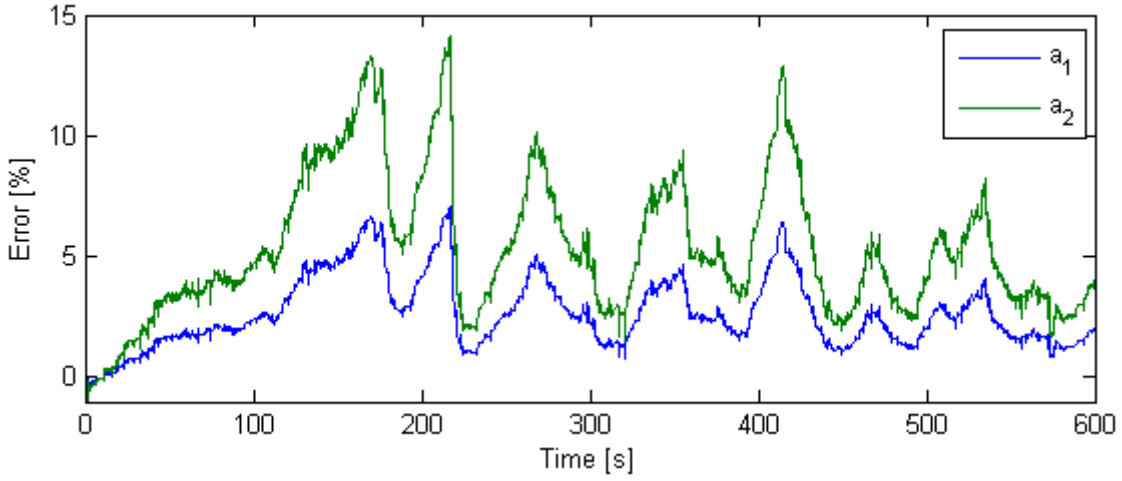

Fig. 6.66 The estimations error of a_1 and a_2

Fig. 6.40 compare the estimation of a_1- and a_2-parameters against the ideal values throughout the experiment. The estimation has deviations of maximum 14 % for a_2, and a maximum of 7% for a_1. There is no level where system holds a steady value, the error is changing all the time. The deviations are also larger than in stage 2. Compared with stage 3 for the APID controller, the errors are more oscillating but are having approx. the same average value.

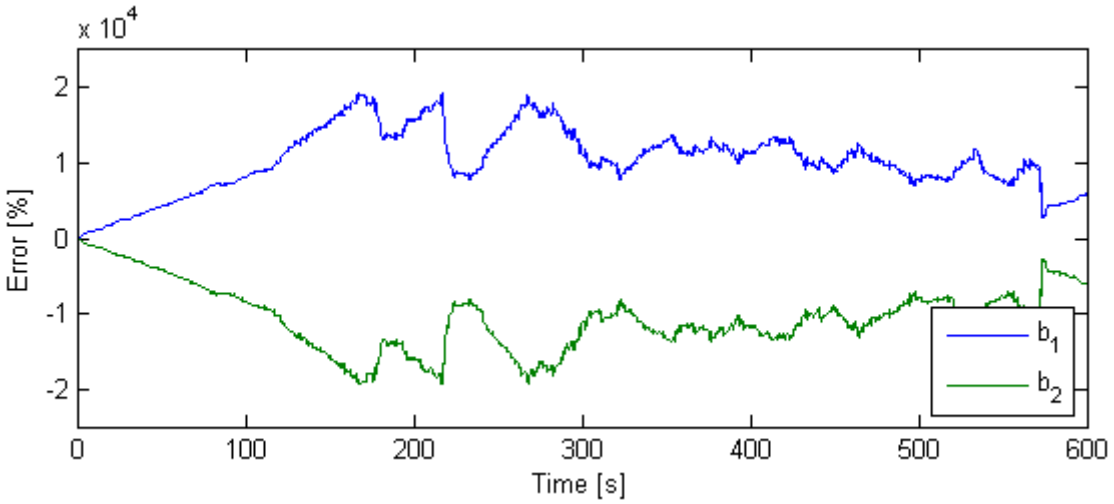

Fig. 6.67 The error of b_1 and b_2

The estimation of b_1 and b_2 in Fig. 6.67 has a large percentage error with many smaller peaks. The errors never drop to the level of stage 1 and 2, which was the case for the APID controller. As in the estimation of a_1 and a_2, the estimation never settles at a specific percentage error, but is changing all the time.

This test shows that the PP-controller has a plausible behavior, but saturation occurs when noise is introduced to the system. The noise makes the actuator cycle between its limits while creating large deviations in the position output.

6.6.4 Summary of PP-controller Simulations

The characteristics of the PP-controllers step responses for the 3 different stages are shown in Table 6.11.

	Stage 1	Stage 2	Stage 3
Overshoot [mm]	9.5	1.91	7.9
Settling time [s]	1.3	1.59	>10
Rise time [s]	0.69	1.40	1.31
Steady state error [mm]	0	0	0

Table 6.17 The characteristic for the 3 step responses

From Table 6.11 the controller gives reasonable result in all 3 stages. The over shoot for stage 2 and 3 are smaller than the large peaks experienced with the APID-controller. The settling time is also reduced, if stage 3 is left out in both cases, as either the PP- or APID-controller settles in stage 3 tests. The rise time is also improved in both stage 2 and stage 3 tests.

But the PP-controller suffers from saturation problems through the simulations when noise is introduced. Stage 3 did also show sections where the system became relative unstable. Based on these observations good performance cannot be anticipated from this controller.

6.7 Summary of Controller Design

This chapter has found four controllers based on different methods and approaches. The first two controllers are static PID-controllers. One manually tuned (PID1) and one tuned on basis of the nonlinear model with added measurement noise (PID2).

The last two controllers are adaptive controllers which change controller behavior based on estimated model parameters. The first adaptive controller is the *adaptive PID-controller* (APID), derived using a discrete PID structure and tuned using Ziegler-Nichols method. The last adaptive controller is the *adaptive pole placement controller* (PP), derived on basis of the discrete plant model and continuously updated.

The two adaptive controllers have been through extensive testing to evaluate its performance in combination with the PEA and noise. Through this testing it was observed that, even though the PEA does not find the anticipated system parameters, its solution does still represent the systems behavior acceptable.

The APID controller was found to have poor initial performance. This controller does relay on good initial system estimates. If these are not available it should first be used when the estimates are good. The controller is able to keep the reference within acceptable values as the system changes behavior, but the noise simulations reveals a vibrating output.

The PP-controller was found to have good initial performance and has fast settle time and reduced overshoot compared to the APID-controller. The simulation test showed good ability to keep the desired reference, better than the APID-controller. But when noise is introduced to the system, its performance is reduced and the output is deviating more than with the APID. Sections of relative unstable behavior are observed.

On basis of this analysis it is chosen to implement all four regulators, even though the PP-controller shows poor performance. This is chosen to examine if the anticipated behavior is realized, and to compare the actual performance.

7. Controller Comparison

In this chapter the 4 different controllers, PID1, PID2, APID and PP, are implemented on the test bench and their performance is described.

The performance is tested by changing the speed of the unwinder. This is equivalent to changing V_1 which acts as a disturbance.

7.1.1 Disturbance Planning

The disturbances are planned as a function of the winded paper length. This is shown in Table 7.1.

Winded paper [m]	50-60	70-80	90-100	110-120	130-140	150-160
Step size[RPM]	50	150	450	450	450	450

Table 7.1 Step size on speed reference at different paper length

The step size on the speed reference to the unwinder motor is made with consideration of the speed limit on the winder motor.

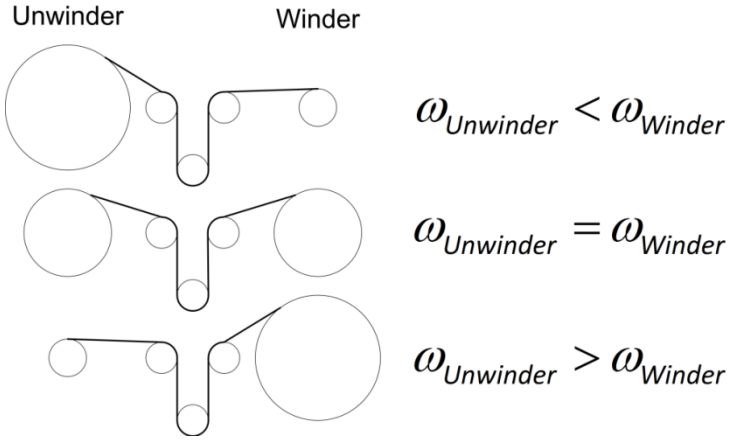

Fig. 7.1 Speed dependencies and roll diameter

From Fig. 7.1 it is seen that at the start and end of the winding process the speed difference between the winding motors are quite large.

Therefore the unwinder is initially ramped up from 100 to 500 RPM. The ramping takes 160 seconds because of a chosen slope of 2.5 RPM per second.

The speed reference to the unwinder motor during the entire winding process is shown in Fig. 7.2.

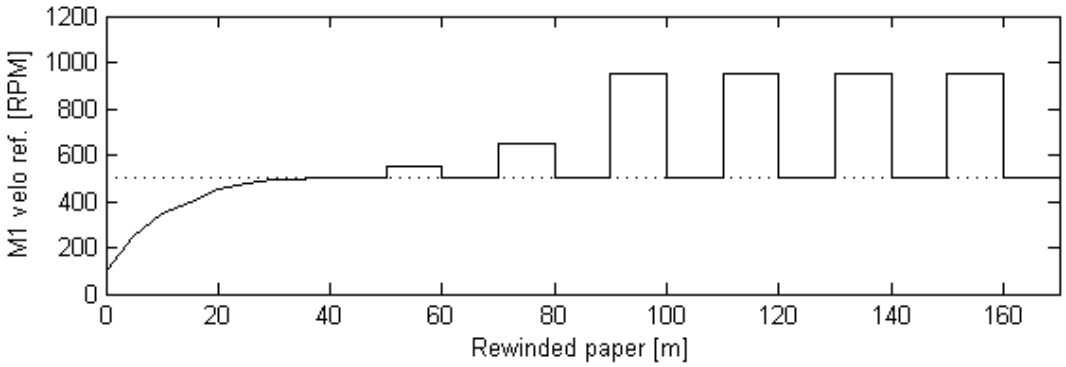

Fig. 7.2 Speed reference to unwinder motor during entire winding process

The unwinder motors speed response is limited by a speed ramp limit built in the VLT. This ramp limit is 1400 RPM per second.

7.1.2 Performance Criteria

In the following 4 definition are made for evaluating the performance of the controllers. The definitions are based on the dancer response from a disturbance. They do not necessarily have the exact some meaning as the conventional interpretation but are defined as shown in Fig. 7.3 and explained below.

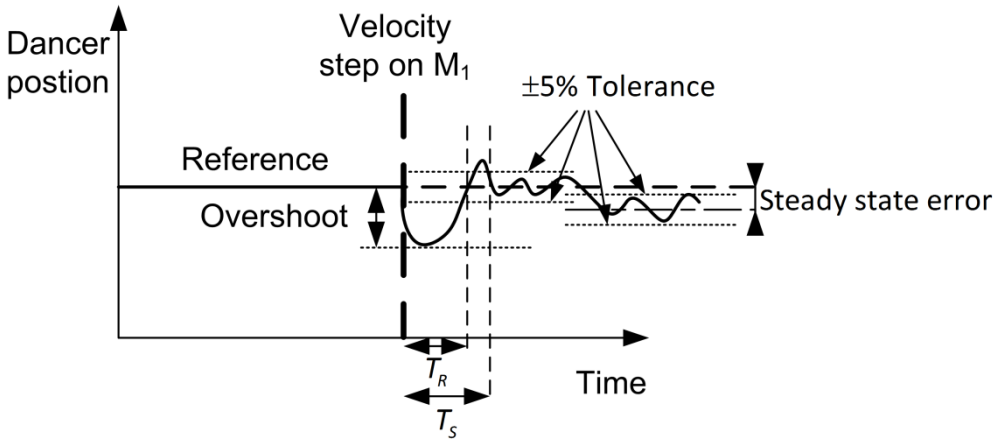

Fig. 7.3 The response to a step in unwinder speed

The explanation of the definitions is given in Table 7.1.

Name	Explaination
Overshot	Maximum deviation from the reference
Settling time, T_s	Time for the dancer returning to the reference
Rise time, T_R	Time for the dancer settling within the tolerance band
Steady state error	Steady state deviation from reference

Tabel 1 Performance definitions

It should be noted that the overshoot is measured with sign e.g. overshoot in Fig. 7.3 will have a negative value. The steady state error is defined as the deviation from the reference if the dancer position keeps within $^{+}/_{-}$ 5% given value.

7.2 Manual tuned PID

First an overview of the entire winding process is presented and afterwards a more detailed presentation of the performance is done.

In the following the data is presented in respect to time. The relation between time and web length is shown in Table 7.2.

	First test		Second test	
Web length	Step up	Step down	Step up	Step down
50-60 m	198.9 s	225.6 s	195.8 s	223.3 s
70-80 m	256.3 s	280.8 s	252.7 s	277.1 s
90-100 m	314.2 s	332.8 s	310.3 s	328.8 s
110-120 m	369.8 s	390.7 s	365.4 s	386.2 s
130-140 m	432.8 s	457.2 s	427.8 s	451.8 s
150-160 m	507.6 s	537.9 s	501.7 s	531.4 s

Table 7.2 Relation between time and web length

Two tests are done. Fig. 7.4 shows that the winding motor response is similar for both tests. Therefore only plots are shown of one of the tests.

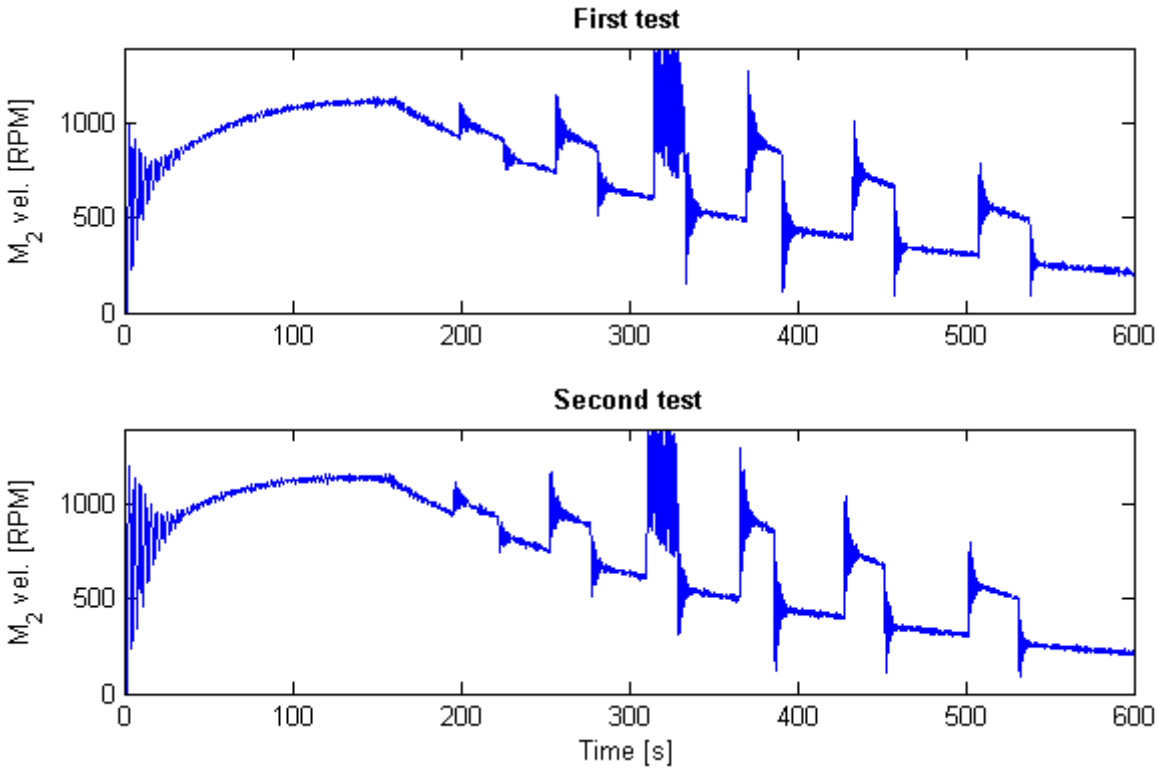

Fig. 7.4 Angular velocity of the winder motor

The unwinder speed reference and the dancer movement are shown in Fig. 7.5.

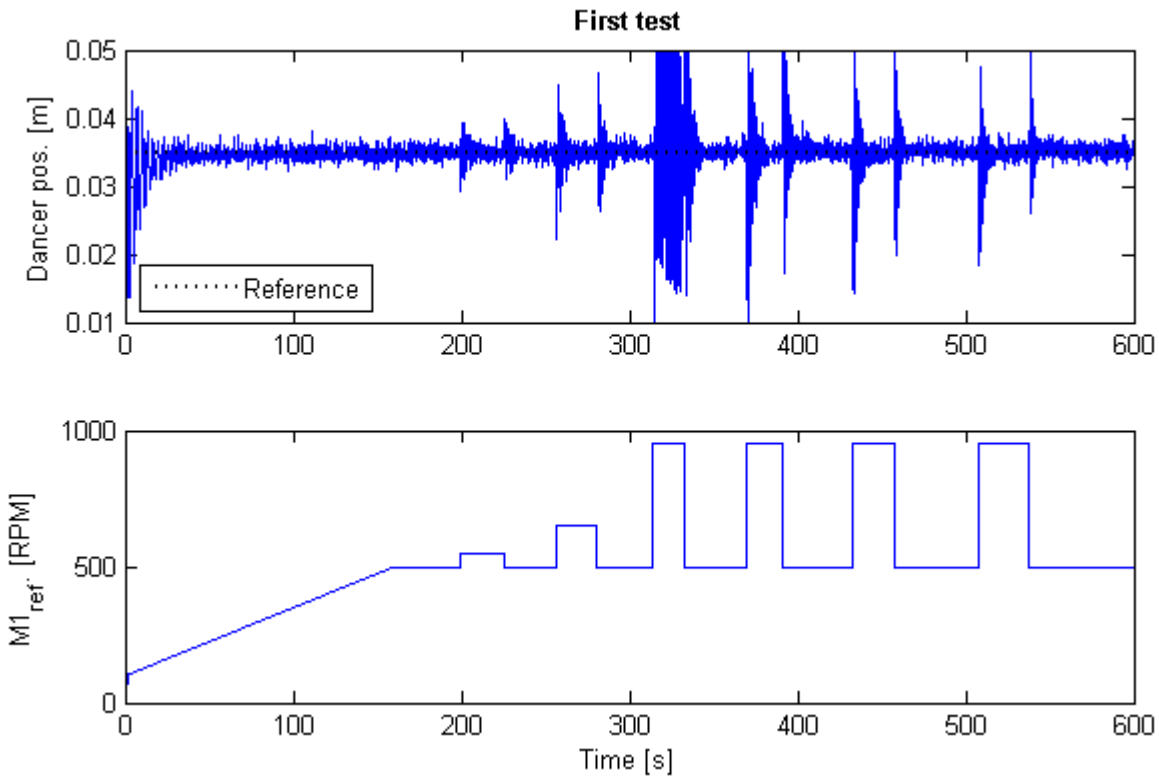

Fig. 7.5 The top graph shows the dancer position, the bottom graph shows the speed reference to the unwinder motor

The winder motor the dancer becomes oscillatory at the third step up as shown in Fig. 7.5. This is because of the speed limit on 1400 RPM on the winder and no anti wind up on this controller.

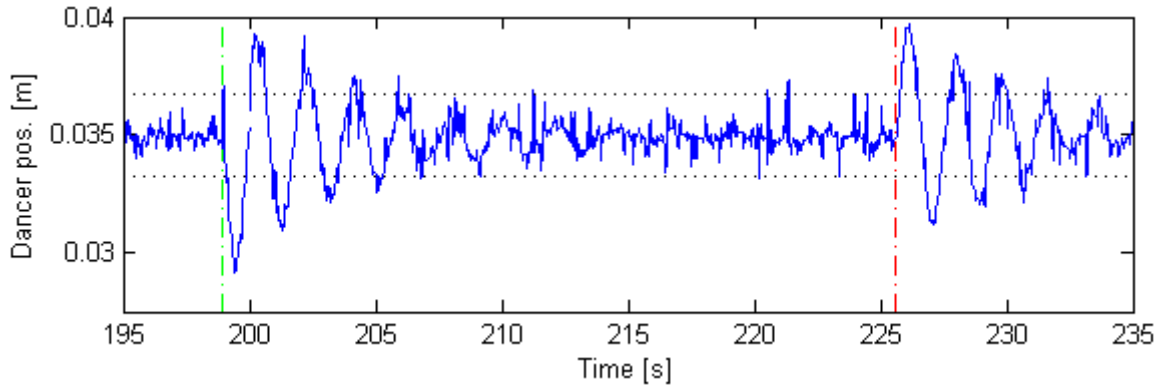

Fig. 7.6 Dancer position for the first test with disturbance at 50 m and 60 m

In Fig. 7.24 the Dancer position is shown for the first step and step down of the disturbance. The green vertical line implies a step up in speed reference and the red vertical line implies a step down. The horizontal lines imply the tolerance band.

In Fig. 7.24 it is seen that the dancer is constantly oscillating. However the amplitude of the oscillation falls to the same as before the disturbance after approximately 15 seconds.

The performance for the first disturbance is presented in Table 7.2

	First test		Second test	
	Step up	Step down	Step up	Step down
Overshoot [mm]	-5.8	4.7	-6.4	4.8
Settling time [s]	7.9	6.1	7.6	5
Rise time [s]	1.1	1	1.1	1
Steady state error [mm]	0	0	0	0

Table 7.3 Performance for disturbances at 50 m and 60 m

The response from the second disturbance is seen in Fig. 7.7.

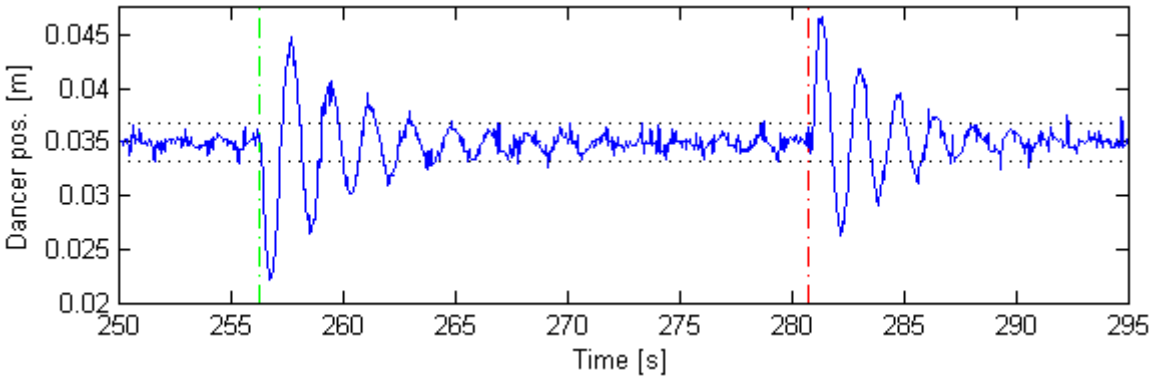

Fig. 7.7 Dancer position for the first test with disturbance at 70 m and 90 m

Comparing the second and first disturbance same tendencies in the dancer response is observed. However a larger disturbance step causes greater amplitudes.

	First test		Second test	
	Step up	Step down	Step up	Step down
Overshoot [mm]	-12.65	11.28	-12.9	12.5
Settling time [s]	9.6	3.9	13	7.6
Rise time [s]	1	1	1	1
Steady state error [mm]	0	0	0	0

Table 7.4 Performance for disturbances at 70 m and 80 m

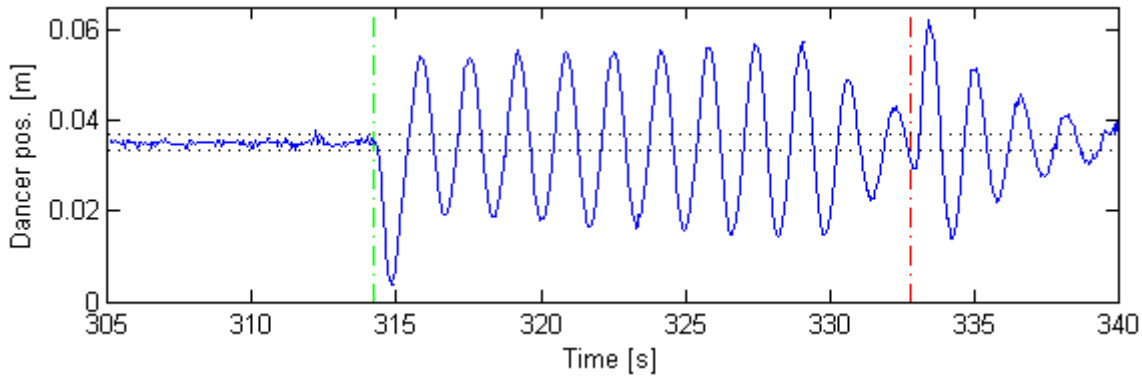

Fig. 7.8 Dancer position for the first test with disturbance at 90 m and 100 m

In Fig. 7.26 the dancer is unable to return within the tolerance band between the two steps. However the dancer is able to settle after more paper is winded.

	First test		Second test	
	Step up	Step down	Step up	Step down
Overshoot [mm]	-29.6	27.14	-31.0	16.0
Settling time [s]	>18	9.6	>18	7.5
Rise time [s]	1.2	1.1	1.2	1
Steady state error [mm]	-	0	-	0

Table 7.5 Performance for disturbances at 90 m and 100 m

The performance at the rest of the disturbances is presented in Table 7.6 to Table 7.8. In appendix I the plots of the dancer position are shown.

	First test		Second test	
	Step up	Step down	Step up	Step down
Overshoot [mm]	-26.0	23.6	-27.0	23.6
Settling time [s]	11.7	7.5	9.7	9.6
Rise time [s]	1	1	1	0.9
Steady state error [mm]	0	0	0	0

Table 7.6 Performance for disturbances at 110 m and 120 m

	First test		Second test	
	Step up	Step down	Step up	Step down
Overshoot [mm]	-20.5	20.8	-21.8	19.0
Settling time [s]	10.7	6.6	8.2	7.7
Rise time [s]	1	0.9	1	1
Steady state error [mm]	0	0	0	0

Table 7.7 Performance for disturbances at 130 m and 140 m

	First test		Second test	
	Step up	Step down	Step up	Step down
Overshoot [mm]	-16.7	14.7	-17.5	14.3
Settling time [s]	9	4.8	6.4	7.3
Rise time [s]	1	0.9	0.9	1
Steady state error [mm]	0	0	0	0

Table 7.8 Performance for disturbances at 150 m and 160 m

Larger overshot and settling time is experienced when the disturbance is step up compared to step down.

The PID controller has a relative long settling time compared to the rise time. This could properly be improved with knowledge about the plant.

7.3 Model based PID

First an overview of the entire winding process is presented and afterwards a more detailed presentation of the performance is done.

In the following the data is presented in respect to time. The relation between time and web length is shown in Table 7.2.

	First test		Second test	
Web length	Step up	Step down	Step up	Step down
50-60 m	198.2	224.6	198.8	225.4
70-80 m	254.9	279.3	255.9	280.5
90-100 m	312.4	330.8	313	332.4
110-120 m	367.5	388.2	369.2	390.1
130-140 m	429.9	454	432.1	456.4
150-160 m	503.7	533.4	506.9	537.1

Table 7.9 Relation between time and web length

Two tests are done. Fig. 7.21 shows that the winding motor response is similar for both tests. Therefore only plots are shown of one of the tests.

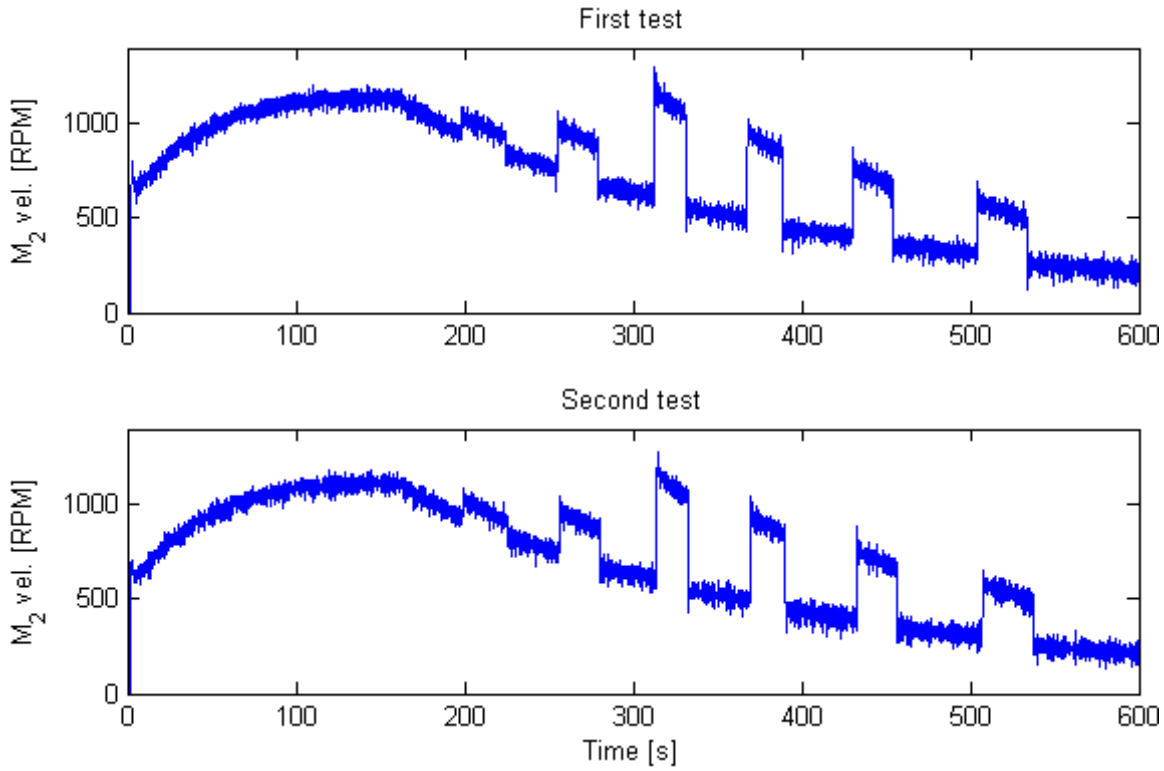

Fig. 7.9 Angular velocity of the winder motor

Comparing Fig. 7.21 with Fig. 7.4 it is seen in that between the disturbances the model based PID controller causes the angular velocity of the winder motor to oscillate more than the manual tuned PID.

This tendency is also seen when by comparing the following plots of the dancer position with plots of the dancer position from section 7.2.

The unwinder speed reference and the dancer movement are shown in Fig. 7.5.

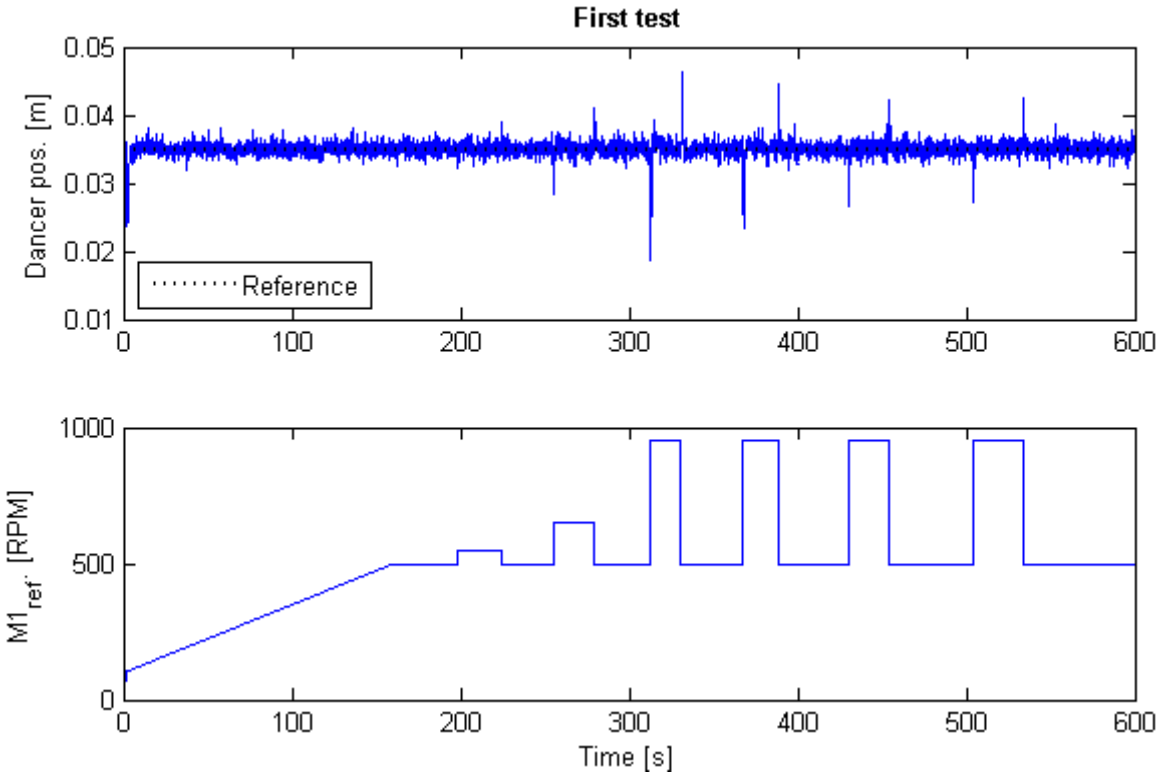

Fig. 7.10 The top graph shows the dancer position, the bottom graph shows the speed reference to the unwinder motor

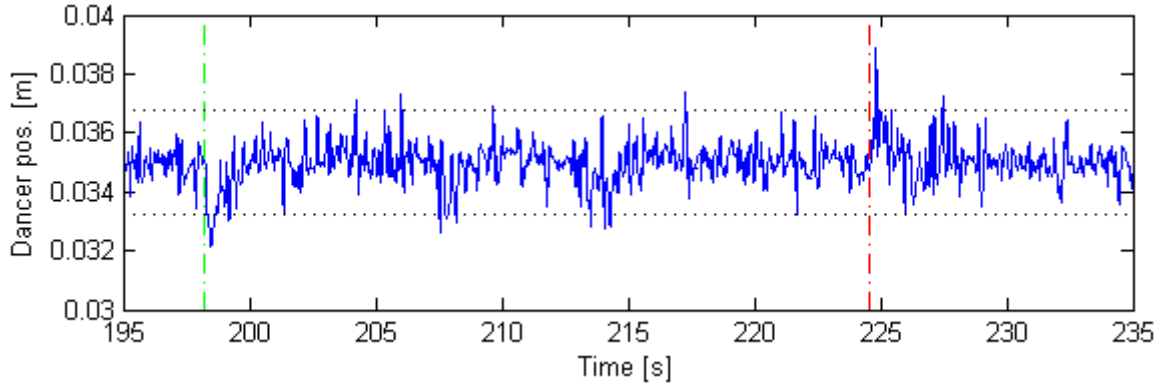

Fig. 7.11 Dancer position for the first test with disturbance at 50 m and 60 m

In Fig. 7.24 it is seen that the dancer position quickly returns back to the tolerance band after the disturbance as also the performance expresses in Table 7.10. The effects of the disturbance are almost nondetectable.

	First test		Second test	
	Step up	Step down	Step up	Step down
Overshoot [mm]	-2.8	3.83	-2.4	2.8
Settling time [s]	1	0.3	0.6	3.1
Rise time [s]	0.6	0.7	0.7	0.9
Steady state error [mm]	0	0	0	0

Table 7.10 Performance for disturbances at 50 m and 60 m

In Table 7.5 it is seen that there is a relatively large difference between the first and second step down. But this is properly caused by the noise.

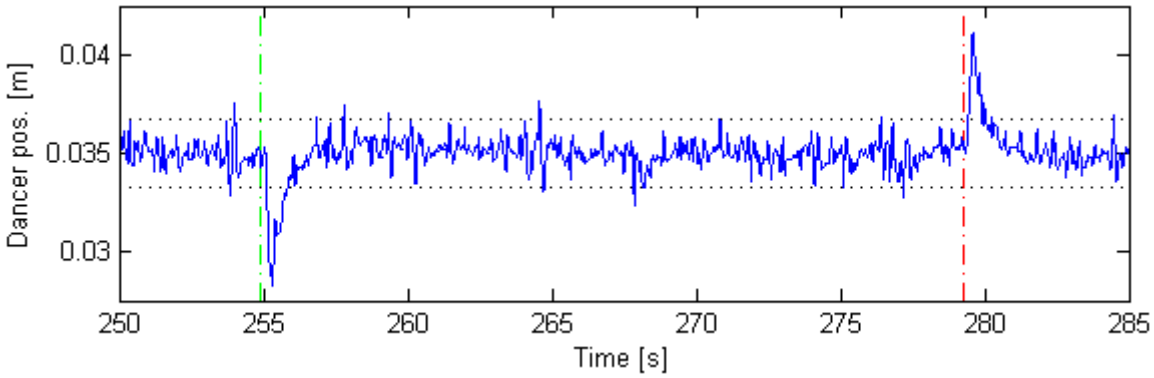

Fig. 7.12 Dancer position for the first test with disturbance at 70 m and 80 m

At the second disturbance the dancer position also returns quickly to the tolerance band. This time the impact of the disturbance is easier to detect from the noise.

	First test		Second test	
	Step up	Step down	Step up	Step down
Overshoot [mm]	-6.6	6.1	-7.4	6.0
Settling time [s]	1.9	0.9	3.5	5.2
Rise time [s]	1.8	1.5	1.5	1.1
Steady state error [mm]	0	0	0	0

Table 7.11 Performance for disturbances at 70 m and 80 m

From Table 7.24 it is seen that the settling time is quite larger in the second test compared to the first.

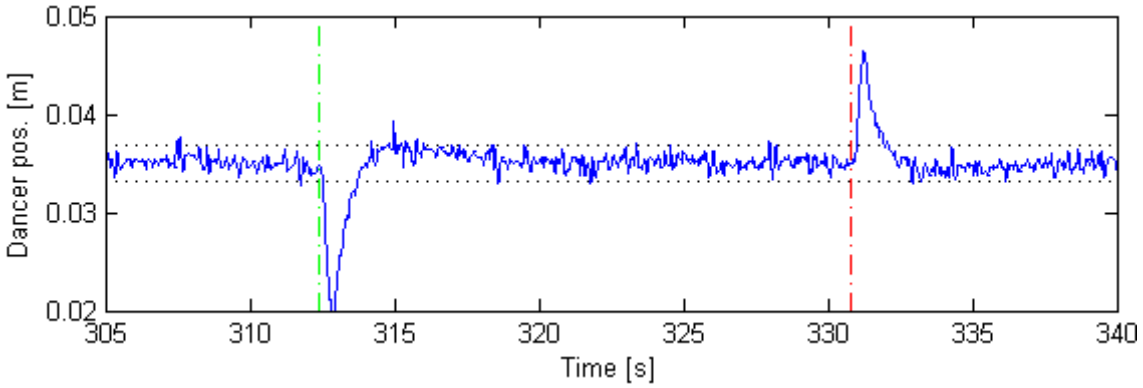

Fig. 7.13 Dancer position for the first test with disturbance at 90 m and 100 m

In Fig. 7.26 it is seen that the step up disturbance gives larger overshot than step down.

	First test		Second test	
	Step up	Step down	Step up	Step down
Overshoot [mm]	-15.4	11.3	-12.9	11.7
Settling time [s]	4.7	2.5	3.6	1.2
Rise time [s]	1.7	1.6	2.5	1.7
Steady state error [mm]	0	0	0	0

Table 7.12 Performance for disturbances at 90 m and 100 m

The performance at the rest of the disturbances is presented in Table 7.13 to Table 7.8. In appendix I the plots of the dancer position are shown.

	First test		Second test	
	Step up	Step down	Step up	Step down
Overshoot [mm]	-11.5	9.2	-10.9	9.2
Settling time [s]	3.9	1.1	4.8	1.5
Rise time [s]	1.8	1.8	1.4	1.9

Table 7.13 Performance for disturbances at 110 m and 120 m

	First test		Second test	
	Step up	Step down	Step up	Step down
Overshoot [mm]	-8.2	6.9	-10.0	7.6
Settling time [s]	1.3	1.7	1.7	3.8
Rise time [s]	1.5	1.8	1.5	1.7
Steady state error [mm]	0	0	0	0

Table 7.14 Performance for disturbances at 130 m and 140 m

	First test		Second test	
	Step up	Step down	Step up	Step down
Overshoot [mm]	-7.4	7.6	-7.4	5.7
Settling time [s]	4.8	1.5	1.1	3.3
Rise time [s]	1.6	0.6	1.5	1.7
Steady state error [mm]	0	0	0	0

Table 7.15 Performance for disturbances at 150 m and 160 m

The model based PID has proven better performance than the manual tuned PID. Less overshot, settling time and rise time is achieved at all disturbances.

7.4 Adaptive PID-controller

To shown the performance of the APID controller there is conducted 3 tests. The reason for the third test is because the first and second test has bad correlation. In the first test the controller is only able to handle the first disturbance. At the next disturbance the winder paper speed falls too far back of the unwinded paper speed and the test have to be aborted. Same thing happens in the next test at the fourth disturbance. The third test is able to complete the entire winding process.

In the following the data is presented in respect to time. The relation between time and web length is shown in Table 7.22.

	The first test		The second		The third test	
	Rising edge	Falling edge	Rising edge	Falling edge	Rising edge	Falling edge
50-60 m	197.8 s	232.1 s	200.7 s	227.5 s	200 s	227.6 s
70-80 m	262.8 s	-	258.3 s	282.9 s	258.3 s	283 s
90-100 m	-	-	316.3 s	334.9 s	316.3 s	335 s
110-120 m	-	-	372 s	-	372.1 s	393.1 s
130-140 m	-	-	-	-	435.3 s	459.5 s
150-160 m	-	-	-	-	510.9 s	543.9 s

Table 7.16 Relation between time and web length

In Fig. 7.21 the winder motor respones for all three test are shown.

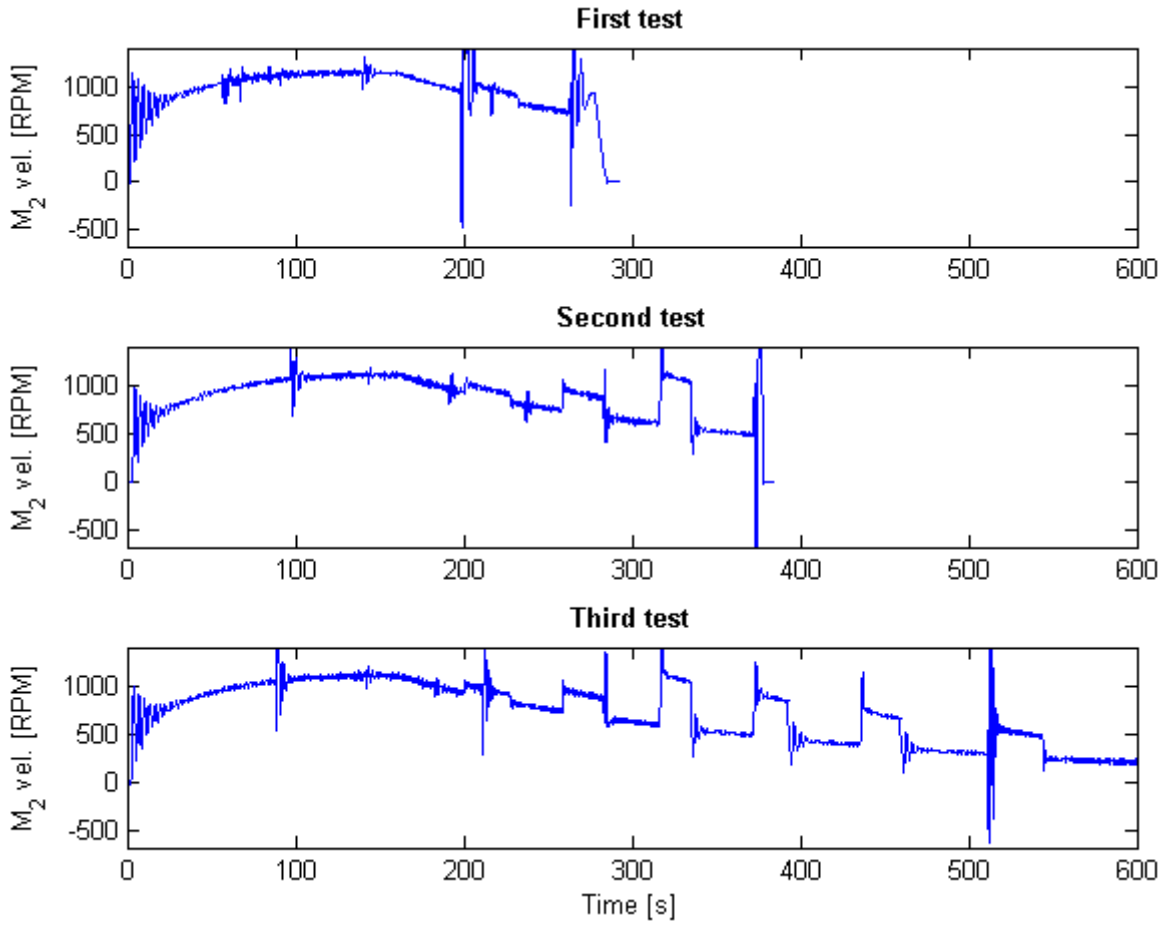

Fig. 7.14 Angular velocity of the winder motor

It is seen in Fig. 7.21 that the second and third test has approximately the same behavior at the 2nd and 3rd disturbance.

It is shown in Table 7.17 at what time instance the adaptive controller is activated.

	First test	Second test	Third test
Time [s]	56.21	96.85	88.06

Table 7.17 The time of the engagement of the adaptive controller

The reason for activating the controller at these time instances is that the controller requires better parameters than the estimation has initially found.

It is seen that when the APID is activated the dancer position becomes unstable for a short period this is shown in Fig. 7.22.

The overall response of the dancer to the changes in web speed can be seen in Fig. 7.22.

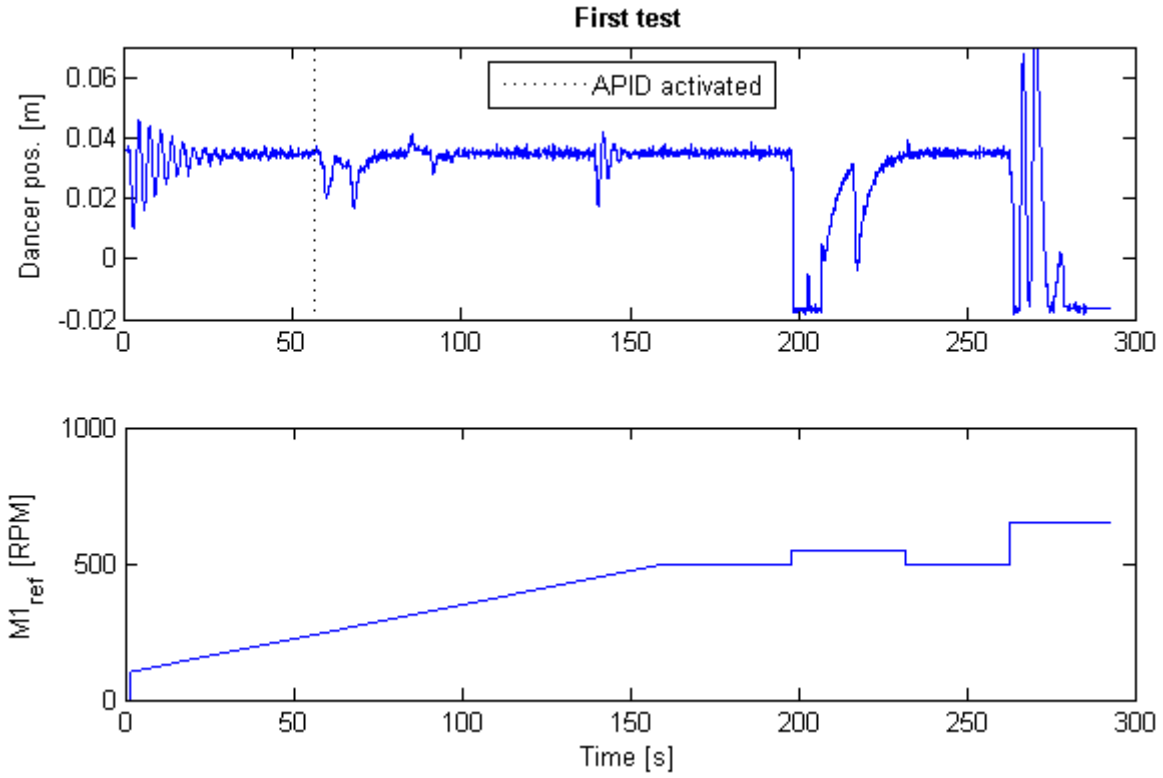

Fig. 7.15 The top graph shows the dancer position, the bottom graph shows the speed reference to the unwinder motor

In Fig. 7.22 it is seen that the dancer in the first step reaches the lower limitation of dancer which means that the paper is not tighten when it is winded. It is seen that after a few seconds the winder begin to tighten the paper e.g. move the dancer . When the 2nd step in the test emerges the CDWW is not able to tighten the paper and there is a buildup of paper between the two reels. The same problem emerged in the second test but first at the 4th disturbance.

The third test completes an entire reel and therefore only the dancer response from this test is presented in this section. The dancer response from the first and second test is found in appendix I.

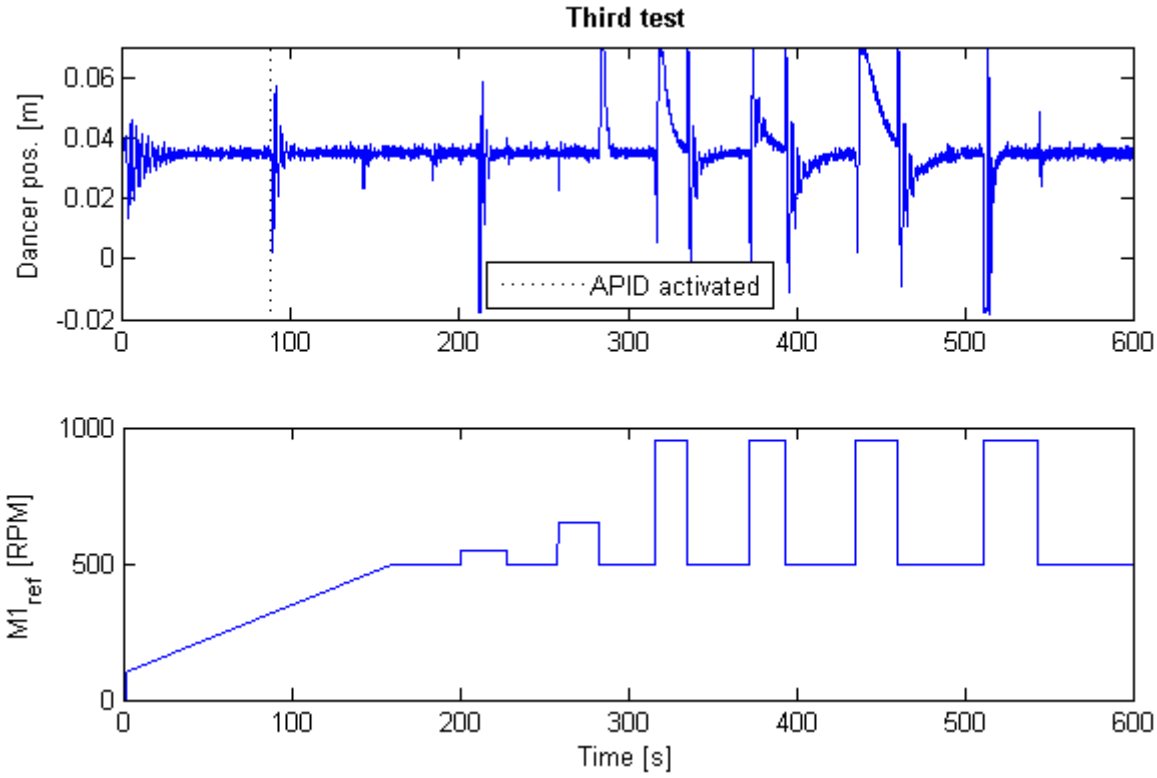

Fig. 7.16 Dancer position and speed reference to unwinder motor

The dancer response of the first disturbance is shown in Fig. 7.24.

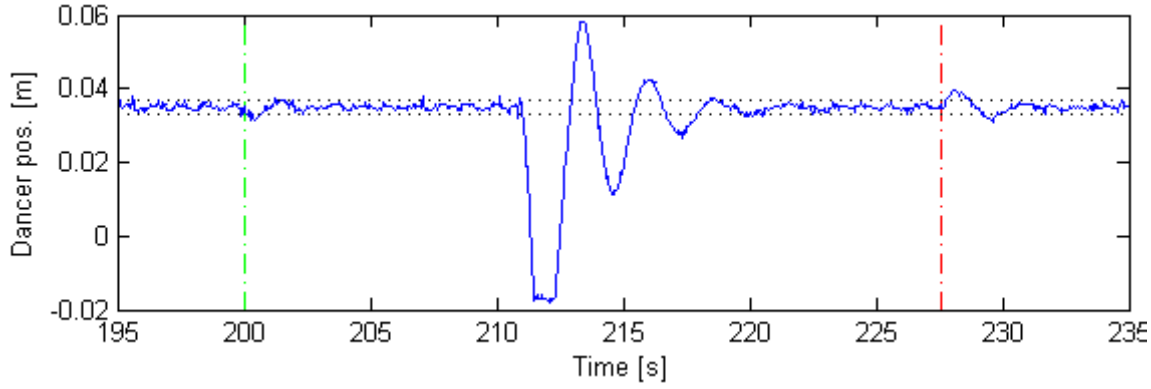

Fig. 7.17 Dancer position for the first test with disturbance at 50 m and 60 m

In Fig. 7.24 it is seen that the first disturbance has only little affect on the dancer response near the step up and step down. This is similar to the model based PID. But between the steps the dancer suddenly starts an oscillation. The dancer settles though shortly afterwards.

This could be either that the disturbance affects the parameter estimation or because of lack of excitation.

The performance at the first disturbance is seen in Table 7.23 for all three tests with APID.

	First test		Second test		Third test	
	Step up	Step down	Step up	Step down	Step up	Step down
Overshoot [mm]	-51.2	3.6	-5.2	3.7	-3.5	4.6
Settling time [s]	>35	0.8	2.8	3.8	2.4	2.4
Rise time [s]	33.2	1.2	4.9	1.4	0.8	1.4
Steady state error [mm]	-	0	0	0	0	0

Table 7.18 Performance for disturbances at 50 m and 60 m

It is seen in Table 7.23 that there is a large difference between the overshoot of the three tests. The settling time in the first test is more than 35 seconds because the dancer is not settled between step up and step down.

The dancer response from the second disturbance is Fig. 7.12.

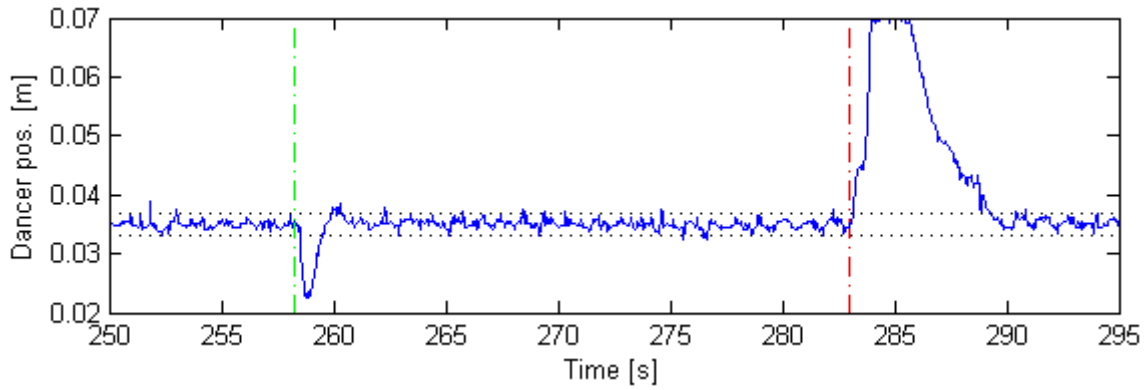

Fig. 7.18 T Dancer position for the first test with disturbance at 70 m and 90 m

In Fig. 7.12 it is seen that the dancer response at step up is similar to the model based dancer response at the same disturbance. The dancer response at step down reaches its limit. The dancer is at its maximum position in a period of 1.5 s. This could burst the paper.

The performance at the second disturbance is seen in Table 7.19.

	First test		Second test		Third test	
	Step up	Step down	Step up	Step down	Step up	Step down
Overshoot [mm]	-51.2	-	-13.3	33.5	-12.37	34.7
Settling time [s]	-	-	7.6	8.7	2.2	7.9
Rise time [s]	-	-	1.6	4	1.5	6.9
Steady state error [mm]	-	-	0	0	0	0

Table 7.19 Performance for disturbances at 70 m and 80 m

The first test has a large overshoot and is aborted because of paper build up. The second and third test both has a large overshoot at step up and step down. The sizes of the overshoots are approximately the same. There is though a divergence between the settling times at step down.

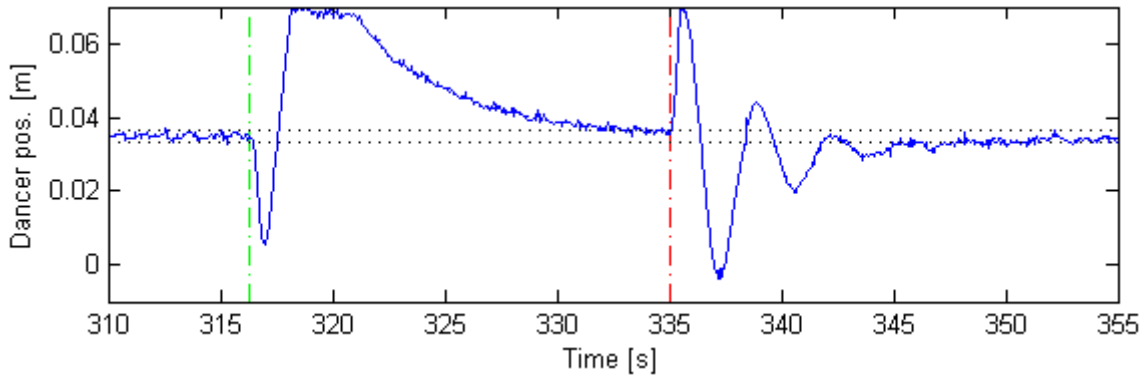

Fig. 7.19 Dancer position for the first test with disturbance at 90 m and 100 m

Fig. 7.19 shows the dancer response of the third disturbance. It is seen that the dancer reaches the maximum limit a few seconds after the step up has occurred. It stays at the limit for 3 s. The response after step down reaches the minimum limit of the dancer but returns to the tolerance limit faster than at step up.

	First test		Second test		Third test	
	Step up	Step down	Step up	Step down	Step up	Step down
Overshoot [mm]	-	-	33.8	36.1	34.2	-38.1
Settling time [s]	-	-	14.3	16.7	17.7	18.2
Rise time [s]	-	-	1.2	1.4	1.6	1.4
Steady state error [mm]	-	-	0	0	0	0

Table 7.20 Performance for disturbances at 90 m and 100 m

The performance at the third disturbance is shown in Table 7.20 Performance for disturbances at 90 m and 100 m. At the disturbances described above the overshoot is negative at step up and positive at step down. But at the third disturbance this is opposite. This is also the last step the second test is able to manage before paper builds up in.

The reason that the step down in the third test is able to reach a larger negative than positive value is because the limitations of the dancer allow larger movement below 35 mm than above. This is because the 0 of the dancer position is measured from a point where the spring in the system is tightened, because of this, it is possible for the dancer also to have negative values.

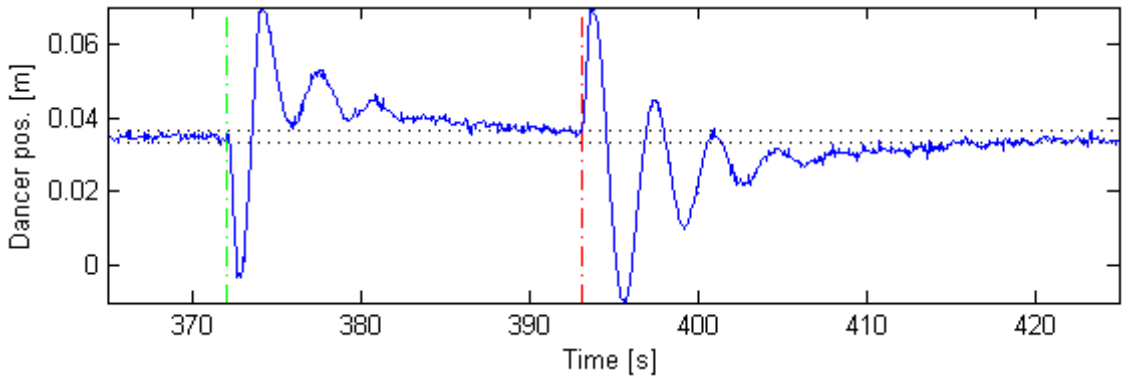

Fig. 7.20 Disturbances at 110 m and 120 m

The dancer response from the fourth disturbance is shown in Fig. 7.20. The dancer never comes within the 5 % of the reference after the step up therefore it is not possible to determine the settling time.

At step up of the fourth disturbance in the second step the dancer moves to far down and causes paper build up and the test is aborted. Therefore only the performance of the third test is shown in Table 7.21.

Third test	110-120 m		130-140 m		150-160 m	
	Step up	Step down	Step up	Step down	Step up	Step down
Overshoot [mm]	-37.62	-45	35.3	-43.7	-52	13.4
Settling time [s]	>21	30.1	>24	35.8	10.8	4
Rise time [s]	1.5	1.5	1.5	1.9	2.8	1.1
Steady state error [mm]	-	0	-	0	0	0

Table 7.21 Performance for disturbances at 110 m and 160 m

From Table 7.21 it is seen that the dancer response has large overshoots at the last three disturbances. The dancer never settles between step up and step down at the fourth and fifth disturbance. However the settling time is drastically reduced in the last step.

There are problems with the consistency of the three tests with the APID. The first test could only handle the smallest disturbance before the experiment was aborted. The second test could only handle the three first disturbances and in the third test could complete the entire winding process.

The test of the adaptive PID controller shows that there are uncertainties concerning the stability of the controller. This could be because of lack of excitation.

7.5 Pole Placement Controller

The pole placement controller is implemented in dSpace and this section shows how it performs on the actual web winder system. The controller is tested two times to test its consistency. Each test is conducted as described in this chapter's introduction. As the unwinder velocity steps are a function of time, the different steps are quantified in terms of time in Table 7.22.

Paper length	The first test		The second test	
	Rising edge	Falling edge	Rising edge	Falling edge
50-60	212.9	239.9	200.9	227.4
70-80	270.7	295.3	258.1	282.6
90-100	328.6	347.5	315.9	334.4
110-120	384.6	405.6	371.1	391.9
130-140	448.2	472.8	433.8	458.1
150-160	524.1	554.9	508.3	538.4

Table 7.22 The point in time of rising and falling edge in the two tests

Fig. 7.21 shows the angular velocity of the winder motor during the experiments. it is seen that the behavior of the two experiments are very alike.

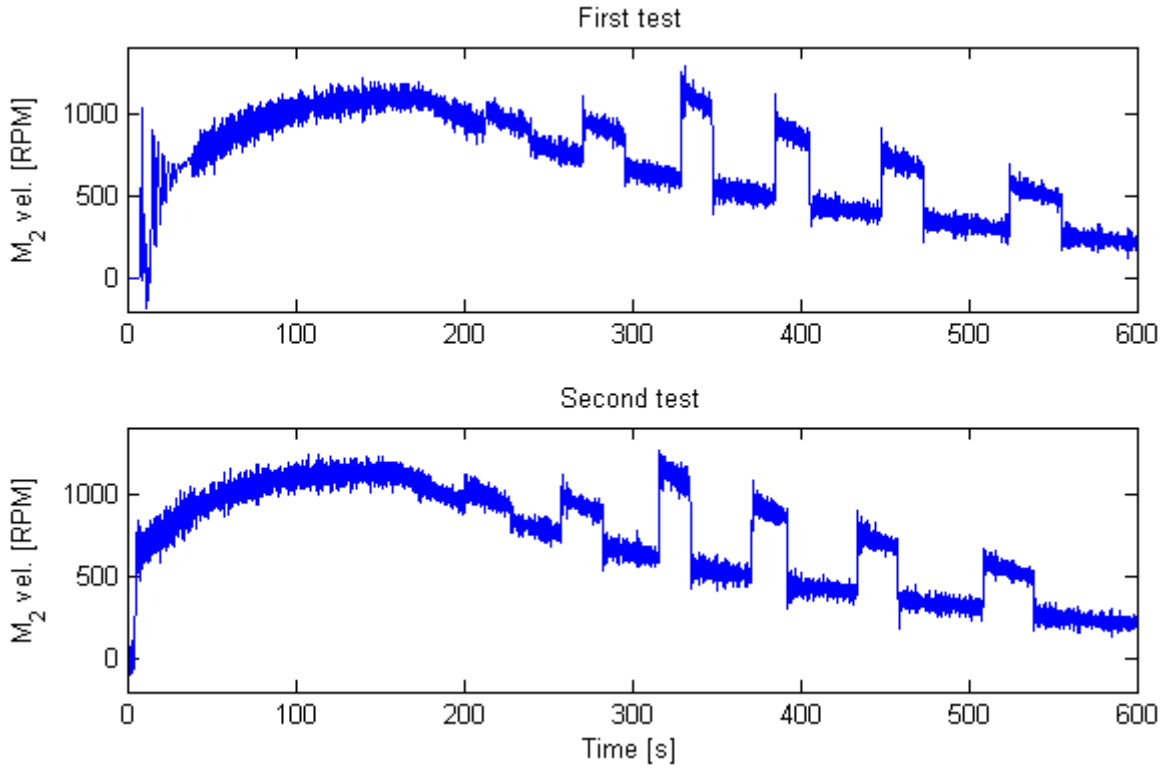

Fig. 7.21 The angular velocity of the winder motor

It can be seen that the motor in both cases is kept within the systems limitation of 1400 RPM. It is also seen that even though the velocity of the unwinder motor is kept constant the velocity of the winder is decreasing. This is obviously a function of the changing unwinder radius. It is also seen in Fig. 7.21 that the velocity is oscillating which is a result of the controller continuously trying to keep the output close to the reference.

The general response of the system to the changes in web speed can be seen in Fig. 7.22, the reference is 0.035 m in both cases. Fig. 7.22 shows the dancers position throughout the experiment, and the corresponding steps in unwinder speed reference.

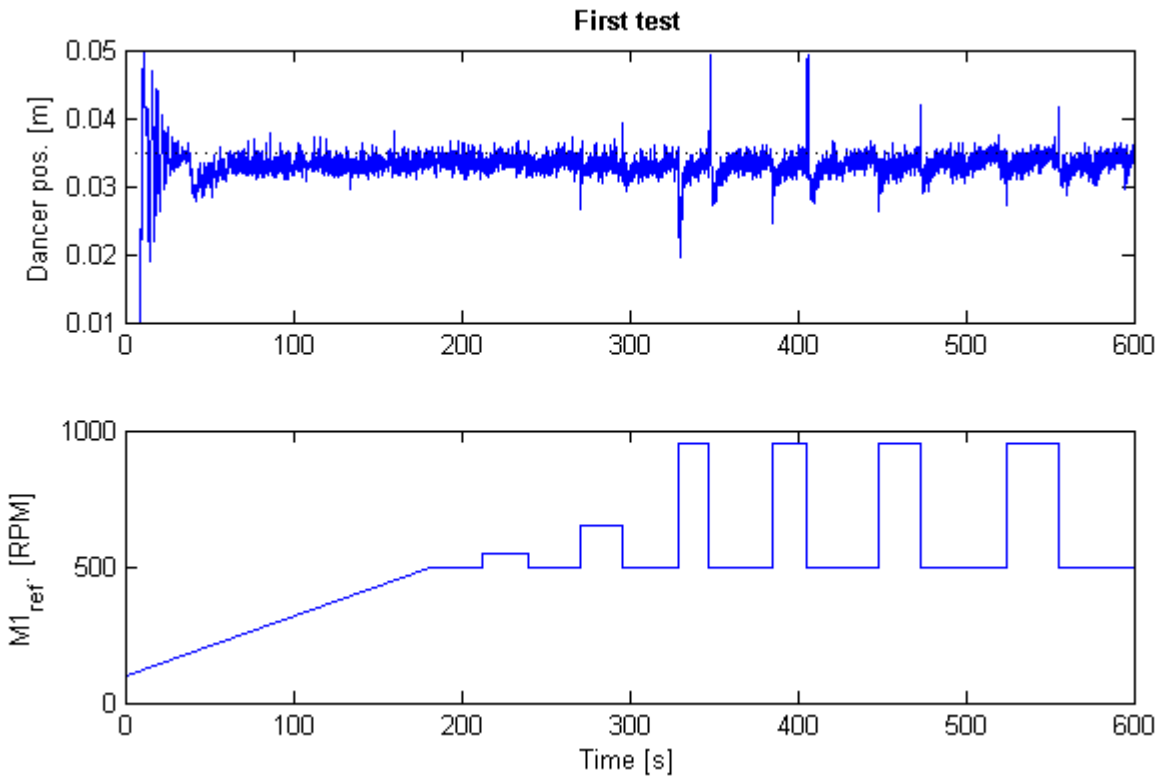

Fig. 7.22 The top graph shows the dancer position, the bottom graph shows the speed reference to the unwinder motor

In the first test the PP-controller is first applied after 40 s, this is the reason for the large deviation in the beginning. In the second test the PP-controller is engaged at the beginning of the experiment. In both cases successful. This behavior is supported by the simulation test in chapter 6.6 which also showed the PP-controller being able to start up by itself.

Only the dancer position from the first tests is shown Fig. 7.22. It can be seen that the position is kept at a fairly constant level until the third step up. It never reaches a constant level hereafter, every time there is disturbance the dancer position quickly returns to the vicinity of the reference and then slowly approaches the reference. There are peaks in the position where the speed reference is changed for the unwinder motor. The peaks go under the reference when unwinder speed steps up. And opposite when the unwinder speed is stepped down.

The simulation test chapter 6.6 showed risk of actuator saturation when using the pole placement controller, this phenomena is examined in Fig. 7.23 where the controller output can be seen.

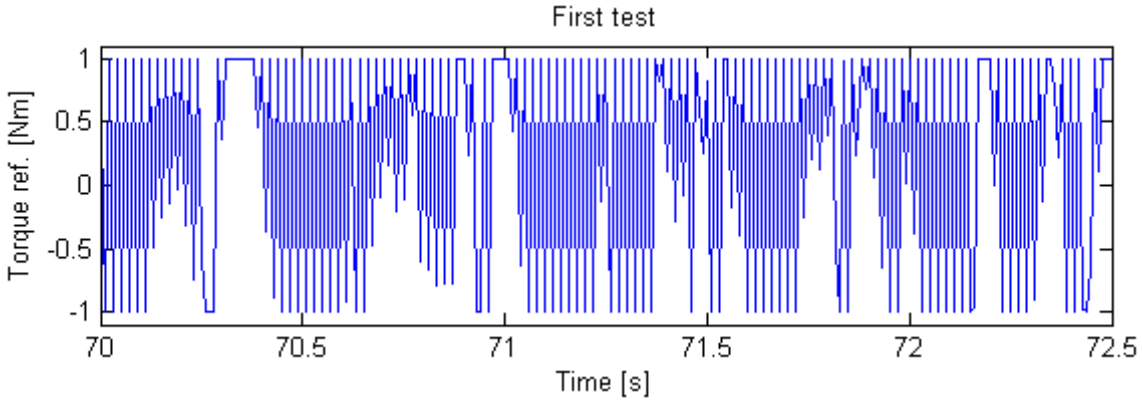

Fig. 7.23 The torque reference to the VTL

The behavior of the rest of the experiment is alike the torque reference shown in Fig. 7.23. The controller is often in either positive or negative saturation. This changes for each sample period and controller output never finds a steady state. The reason to this high amount of saturation is properly because the poles are placed with a bandwidth of 10 rad/s. A better result could, according to the theory in (Ogata, 1995), be accomplished by selecting a pole smaller than 10 rad/s. This would give a smaller increase in bandwidth and hence the control effort would be reduced.

Even though the controller has problems with the saturation, it is still described how it is performing. The first step up in the first test is shown in Fig. 7.24, the vertical green line indicates the step up in unwinder motor velocity, the vertical red line indicates the step down. The horizontal dotted black lines are the $^{+}/_{-}$ 5% tolerances for the system.

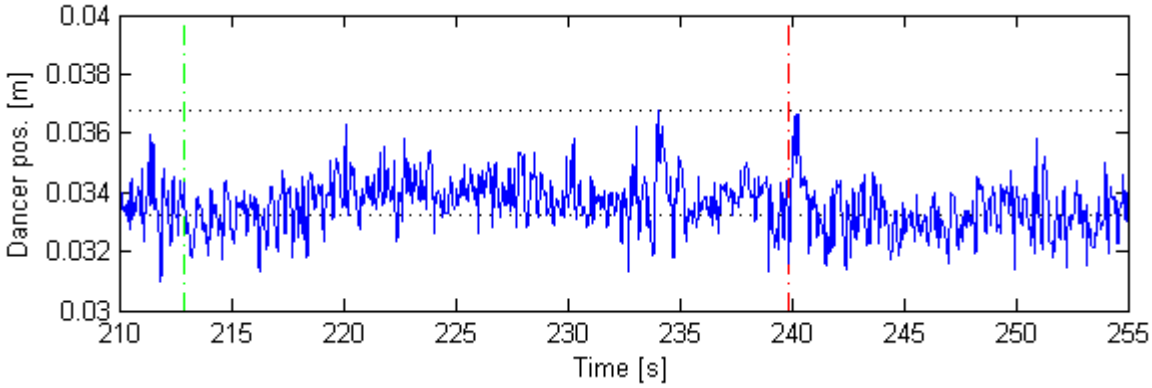

Fig. 7.24 Dancer position for the first test with disturbance at 50 m and 60 m

From Fig. 7.24 it can be seen that the first step have very little effect. The change in dancer position is not bigger than what the rest of the vibrations in signal. The system never comes within the tolerances of 5 %. The rise time of the system is very different in the two tests. This can be observed from Table 7.23, which shows the performance of the first disturbance.

	First test		Second test	
	Step up	Step down	Step up	Step down
Overshoot [mm]	-3.6	-3.6	-4.4	-4.5
Settling time [s]	>27	>31	>27	>31
Rise time [s]	6.5	11.3	0.3	0.3
Steady state error [mm]	2	2	2	2

Table 7.23 Performance with disturbance(1) at 50 m and 60 m

The size of the settling time cannot be determined before the next step appears. Fig. 7.25 shows the dancer movement when the second disturbance occurs at 70 m and steps down again at 80 m.

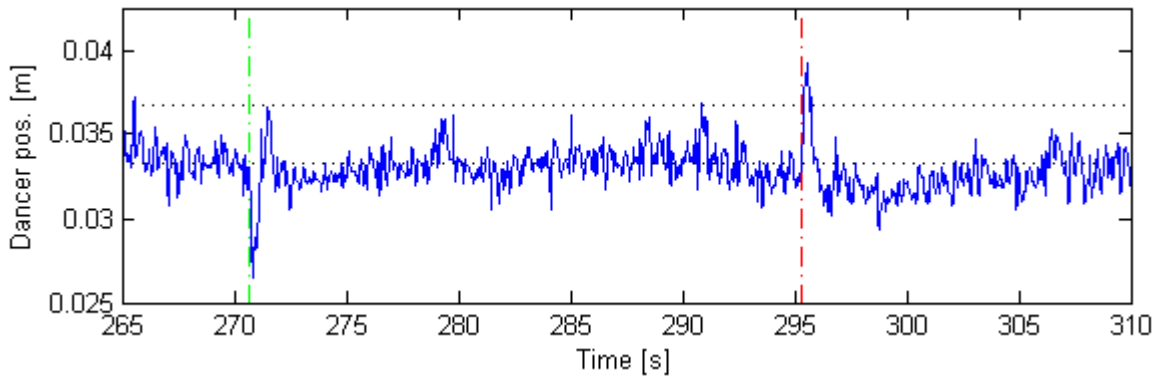

Fig. 7.25 Dancer position for the first test with disturbance at 70 m and 80 m

In this step is both the effect of the step up and the step down visible. The increase in angular velocity of the unwinder, allows the dancer to fall suddenly before the winder motor tightens the paper again. The opposite is happening when unwinder is stepped down. Here the dancer raises due to the sudden slowing of the paper which is getting too tight. The measured parameters is seen in Table 7.24.

	First test		Second test	
	Step up	Step down	Step up	Step down
Overshoot [mm]	-8.3	-5.61	-6.9	-5.3
Settling time [s]	>25	>33	>24	>33
Rise time [s]	8.3	0.5	3.4	0.5
Steady state error [mm]	-	-	-	-

Table 7.24 Performance with disturbance(2) at 70 m and 80 m

From Table 7.24 it it is seen that the rise time of the step down case is the same for both tests. The size of the overshoot in the two step downs are approximately the same, but the overshoot at the step up in the first test is 1.4 mm larger. It is not possible to determine if there is a steady state error because the system is not found settled.

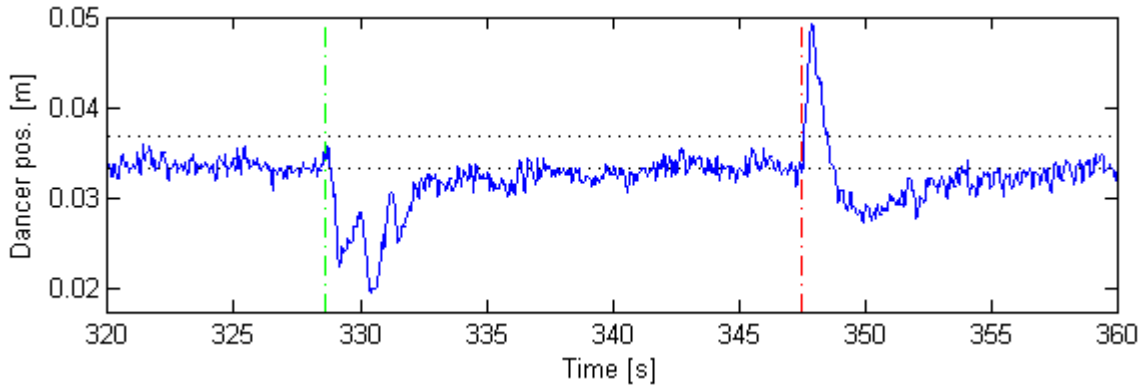

Fig. 7.26 Dancer position for the first test with disturbance at 90 m and 100 m

Fig. 7.26 show the third disturbance at 90 m and until 100 m. it is notable that the overshoot after the step up is higher than the overshoot after the step down. This is also shown in Table 7.25.

	First test		Second test	
	Rising step	Falling step	Rising step	Falling step
Overshoot [mm]	-15.2	14	-17.3	13.4
Settling time [s]	>19	>37	>19	>37
Rise time [s]	14	1	11.8	1.2
Steady state error [mm]	-	-	-	-

Table 7.25 The Performance with disturbance(3) at 90 m and 100 m

The largest overshoot in the entire experiment is at the third disturbance. Here is over shoots of above 15 mm present. The system is still having problem with reaching its reference of 35 mm. The settling time of the system is again found to be larger than the time interval between two steps.

The graphs for the 4^{th}, 5^{th} and 6^{th} steps are shown in Appendix I, as the controller displays similar behavior for the rest of the steps. The result of the analysis is though shown in Table 7.26 to Table 7.28.

	First test		Second test	
	Rising step	Falling step	Rising step	Falling step
Overshoot [mm]	-10.3	14.3	-11.1	12.8
Settling time [s]	>21	>43	>20	>42
Rise time [s]	7.4	1.2	14.7	1.2
Steady state error [mm]	-	-	-	-

Table 7.26 Performance with disturbance(4) at 110 m and 120 m

Table 7.26 shows a similar behavior between the two tests, as the overshoots in the two tests have similar sizes. But the rise time at step up are almost doubled from the first test to the second.

	First test		Second test	
	Rising step	Falling step	Rising step	Falling step
Overshoot [mm]	-8.5	7	-7.9	9.24
Settling time [s]	>24	>52	20	>50
Rise time [s]	3.7	0.6	6	0.8
Steady state error [mm]	-	-	0	-

Table 7.27 Performance with disturbance(5) at 130 m and 140 m

Opposite to the previous steps, does the 5th step have highest rise times at its rising edges instead of its falling edges. It should be noted is that the system in the second test comes within the tolerances i.e. and has a settling time.

	First test		Second test	
	Rising step	Falling step	Rising step	Falling step
Overshoot [mm]	-7.6	5	-7.3	6.3
Settling time [s]	>30	7.1	24.4	>52
Rise time [s]	6.6	1	7.1	0.7
Steady state error [mm]	-	-	0	-

Table 7.28 Performance with disturbance(6) at 150 m and 160 m

The rise time in the 6th step, shown in Table 7.28, has similar behavior in both two tests. In this step it is only the second test that is able to meet the requirements of having a 0 mm steady state error.

Both test shows that the sizes of the systems overshoot have decreased during the last four steps. This is in agreement with chapter 3.5.1 that showed an increase in radius would result in an increased damping ratio, and thereby reduced the tendency to overshoot.

The pole placement controller is through these experiments shown able to work in praxis. It is implemented and it is shown that it is able to control the reference through these experiments. It is also shown that the PP-controller is able to start the web winder from the beginning of the tests unlike the APID-controller which needed good estimates before being able to control satisfactory. It is also seen that the controller in praxis behaves much as anticipated from the simulation in chapter 6.6.

But the experiment also shows that the controller is unable to keep the dancer within 5% of reference, with the exception of two cases. The result of the controller test could be improved by selecting, poles with a smaller bandwidth, which should reduce the saturation problem. It was found that the system with the pole placement controller generally has a long settling time. But it is shown that the designed controller is able to control the web winder system.

7.6 Summary of Controller Comparison

The manual tuned PID controller results in a dancer response with large overshoot and long settling time when subjected to a disturbance. This is naturally not desirable but the controller is able to maintain the dancer at its reference position during an entire winding process when no disturbance is applied.

Better performance is experienced with the model based PID controller. This controller gives a dancer response with small overshot and short settling time when subjected to a disturbance. On the test bench this controller obtains the best performance.

The adaptive PID controller causes dancer responses with the largest overshoot and is responsible for occasional breakdown. However the controller also shows occasional better performance than the manual tuned PID. But this controller type seems to be very sensitive to deviation between correct system parameters and estimated parameters.

The next best performance on the test bench is achieved with the adaptive pole placement controller. This controller results in similar overshot and oscillation as the model based PID. However the dancer position settles just below the tolerance band of 5 % and the controller output is often at the set saturation limits.

The comparison shows that the adaptive pole placement controller is capable of starting the web winder from stand still and is also capable of keeping suppressing the disturbances. This shows that adaptive control is possible to implement on the web winder but the performance is poor, as a better performance than the model based PID was anticipated. The noise in the system is again found to disturb the adaptive controller algorithms, as indicated in the simulation tests.

8. Conclusion

The objective of this project is to utilize adaptive control to control the tension of the web material in a center driven web winder. The web winder system is found to have large changes its system parameters during the winding process. An adaptive pole placement control algorithms is therefore introduced and through simulations and experiments found working on the test bench. But its performance would be greatly improved by reduction of the systems measurement noise.

The project started by deriving a model of the web winder system to investigate how the machines physical changes affect the models response. Three models in total are derived; a nonlinear model, a linear model and a simplified model. The nonlinear and the linear model are validated through experiments and simulation. The simplified model is found valid by means of argumentation.

A parameter variation is conducted to show the effects of the models uncertainties and to show the effect of the changing parameters during the winding process. It is found that the bandwidth of the system increases 600% as the radius of the winder reel is changed between its minimum and maximum value. The damping ratio is doubled during this variation. The other parameters influence is found insignificant in comparison. This implies that if a fixed controller is to be used; it would not achieve ideal performance through the entire winding.

To be able to observe the changes in system parameters during the winding process, a parameter estimation is introduced. The recursive least square algorithm is selected as being suited and the equations for the algorithm is described. The parameter estimation via recursive least square are tested in various stages to investigate the algorithms ability to estimate correctly.

During the design phase of the parameter estimation it was found that a scaling of 1000 to the output of the system and into the parameter estimation, had an significant effect of the estimation accuracy of the b_1- and b_2-parameters.

Measurement noise in the dancer signal has proven a significant factor in the system and is found to significant disturb the parameter estimation algorithm and the controllers performance.

Several filters are implemented in the system to reduce the effects of the noise problem. A 6 Hz second order low pass filter is implemented on the dancer signal, and two 2 Hz second order low pass filters are implemented on the estimation algorithms input signals. The specific filter frequencies are determined empirical through several experiments.

It is found that the dynamic behavior of the estimated parameters needs to be evaluated to determine if the found solution is valid. As the parameter estimation algorithm might find alternate solutions.

Four different controllers are designed in this thesis; a manual tuned PID controller, a model based PID controller, an adaptive controller and a pole placement controller. The controllers are simulated in different stages, with the exception of the manual tuned PID controller.

The result of the simulation test shows that the model based PID-controller tuned by means of the nonlinear model in a conservative operation point has a overshoot of 15 mm and a settling time of 5 s.

The simulation of the adaptive PID controller showed that the system has problems with controlling the system when the estimated parameters are far from the correct value. The simulation of the pole placement controller showed that it has problems with achieving the reference value within 5 %. This could be related to noise from the measurement of the dancer position or the often output of the controller at saturation limit.

The controllers are tested in the web winder system by means of a specified unwinder velocity reference with known steps to emulate disturbances. The overshoot, settling time, rise time and steady state error are compared for 4 controllers. It is found that the best controller is the model based PID controller. But a close second is the PP-controller which shows similar performance. The PP-controller is shown able to initialize the web winder from stand still and is able to cope with large disturbances. Unfortunately it lacks the model based PID-controller ability to have zero steady state error. The adaptive controllers suffer primary from bad system estimation due to the large noise present in the system.

Thus it is shown how the web winder system can be modeled and how it can be controlled. It is possible to make a PID controller that is able to regulate the system through an entire winding process based on a nonlinear model of the system in a worst case operation point, but this require that all the parameters in the system is known. The designed adaptive pole placement controller have the potential to simply be implemented in any given web winder system, and because of this it is of interest for further studies of adaptive control of web winder systems.

9. References

Bobál, V., Böhm, J., Fessl, J., Machácek, J. 2005. *Algorithms, Implementation and Applications.* 2005. ISBN 978-1-85233-980-7.

Bobal, Vladimir, Bohm, Josef and Prokop, Roman. 1999. Practical aspects of self-tuning controllers. *Internation journal of adative control and signal processing.* 1999, Vol. Adapt. Control Signal Process., 13.

Cheok, Ka C. POLE PLACEMENT CONTROLLER DESIGN. [Online] [Cited: 06 01, 2009.] http://personalwebs.oakland.edu/~cheok/SYS635%20AdaptiveControl/05A%20IO%20Pole%20Place%20Controller.pdf.

Franklin, Gene F., Powell, J. David and Workman, Michael. 1998. *Digital Control of Dynamic Systems.* s.l. : Addison Wesley Longman, Inc., 1998. ISBN 0-201-82054-4.

Liu, Zhijun. 1998. *A Frequency Response Based Adaptive Control for Center-Driven Web Winders.* Rockwell Automation. Mequon, Wisconsin : IEEE, 1998. Article. ISBN 0-7803-4530-4.

—. 1999. *Dynamic Analysis of Center Driven Web Winder controls.* Rockwell Automation. Mequon, WI 53092 : IEEE, 1999. Article. ISBN 0-7803-5589-X.

Ljung, L. 1999. *System identification : theory for the user .* Englewood Cliffs, N.J. : Prentice-Hall, 1999.

Ljung, Lennart and Söderström, Torsten. 1983. *Theory and Practice of Recursive Identification.* Cambridge, Massachusetts : The MIT press, 1983. ISBN 0-262-12095-X.

Ogata, Katsuhiko. 1995. *Discrete-time control systems 2nd edition.* s.l. : Prentice-Hall, Inc., 1995. ISBN 0-13-328642-8.

—. 2002. *Modern Control Engineering fourth edition.* s.l. : Prenctice-Hall, Inc, 2002. ISBN 0-13-043245-8.

University of Cambridge, Department of Engineering. Young's Modulus - Cost. *Material selection and processing.* [Online] [Cited: 06 02, 2009.] http://www-materials.eng.cam.ac.uk/mpsite/interactive_charts/stiffness-cost/NS6Chart.html.

10. Appendices and Attachments

All appendices are made by the project group to examine different aspect, support a claim or to document practical experiments which takes up too much space in the thesis.

Some appendices are due to their size located on the attached CD-rom. The appendices on CD-ROM has a corresponding reading guide here also.

Appendix A	Z-transformation of the simplified model
Appendix B	dSpace setup and anti aliasing filter
Appendix C	Critical gain via Rouths stability criteria
Appendix D	Appendix for pole placement
Appendix E	Appendix to parameter variation
Appendix F	Appendix to Linear model
Appendix G	Simulation test with different parameters
Appendix H *on CD*	Test bench experiments with PEA
Appendix I *on CD*	Test bench experiments with controllers
Appendix J	Paper length

The appendices can be found on the last pages of the thesis.

10.1 Attachments

Attachment A *on CD*	Calculation of J_m inertia From: **J. S. Larsen, P. K. Jensen**. *Adaptive control with self-tuning for center-driven web winders*, 2007.

11. Abstract

Many industries require manufacturing with a continuous long piece of material, a so-called web. An example of this is the manufacturing of our daily newspaper. Here a long string of paper is feed to a rotating printing press. The paper is often unrolled from a large reel of paper and distributed through series of rollers and winded to another reel. This leads to the thesis initial problem stated as:

What influences the control of the web winder system?

A nonlinear model is derived for the system and it is validated partly by experiments with the winder motor by itself and later by test with the entire system.

A linear model is derived on basis of the non-linear model, and it is found that the two models are in agreement. A parameter variation analysis is made on basis of the validated linear model. The result of this analysis is that the radius of the winder reel is of great importance to the dynamic behavior of the system.

A simplified model with fewer parameters is presented, to ease the task of parameter estimation in the system.

From the problem analysis it is concluded that a given controller should be able to adapt to the system due to the changes in radius. The problem is stated as:

How is it possible to utilize adaptive control for the given web winder system ?

To be able to adapt the controller to the web winders changing behavior its model parameters have to be estimated. It is chosen to use the recursive least square algorithm. The main principle of the least square algorithm is described.

To ensure that the parameter estimation have a satisfying performance it is tested by means of simulation in MATLAB Simulink. To mimic the real web winder system noise is added, when the noise is added to the simulation is concluded that filters are necessary to meet the requirements for proper estimation.

The estimations algorithm is implemented in the web winder system by means of dSpace, different excitations methods are tested and it is found that a sine signal is best suited.

Four different controllers are implemented in the system two non adaptive and two adaptive. The non adaptive controllers are both PID controller, one is based on iterative manual tuning, the other is model based. The two adaptive controllers are an adaptive PID and an adaptive pole placement controller.

The four controllers are tested through simulation and on the web winder system. Good relation between the simulations and the actual behavior is found. It is also found that the adaptive pole placement controller is able to control the web winder, the performance is though exceeded by the model based PID. The reason for this is found to be governed by the amount of measurement noise in the given system.